

In presenting this dissertation as a partial fulfillment of the requirements for an advanced degree from Emory University, I agree that the Library of the University shall make it available for inspection and circulation in accordance with its regulations, governing materials of this type. I agree that permission to copy from, or to publish, this dissertation may be granted by professor Dale E. Edmondson under whose direction it was written, or, in his absence, by the Dean of the Graduate School when such copying or publication is solely for scholarly purposes and does not involve potential financial gain. It is understood that any copying from, or publication of, this dissertation which involves potential financial gain will not be allowed without written permission.

Jin Wang

Comparative Structural and Functional Properties of
Human and Rat Monoamine Oxidases

By

Jin Wang

Doctor of Philosophy

Department of Chemistry

Dale E. Edmondson, Ph.D.
Adviser

Jay Justice, Ph.D.
Committee Member

Stefan Lutz, Ph.D.
Committee Member

Accepted:

Lisa A. Tedesco, Ph.D.
Dean of the Graduate School

Date

Comparative Structural and Functional Properties of
Human and Rat Monoamine Oxidases

By

Jin Wang

B.S., Lanzhou University, 2002

Adviser: Dale E. Edmondson, Ph.D.

An Abstract of

A dissertation submitted to the Faculty of the Graduate

School of Emory University in partial fulfillment

of the requirements for the degree of

Doctor of Philosophy

Department of Chemistry

2007

ABSTRACT

Monoamine oxidases A and B (MAO A and MAO B) are flavin-containing mitochondrial membrane-bound proteins which function in the oxidative degradation of biogenic and xenobiotic amines to their corresponding aldehydes. The crystal structures of MAOs show that human MAO A is monomeric, whereas human MAO B and rat MAO A are dimeric. Recent sequencing and modeling studies suggest a rationale for these differences in that human MAO A exhibits a selective mutation in the region close to the membrane surface and the dimer interface where Glu151 is a Lys in human MAO A but remains a Glu in human MAO B and non-human MAO A's. This dissertation describes the experiments to probe the structures of purified human MAO A and MAO B which are compared with the crystal structures solved by X-ray crystallography, as well as to investigate functional consequences of the Glu151Lys selective mutation in human MAO A. Human MAO A and MAO B were labeled with a fluorophore donor attached to the acetylenic inhibitor pargyline in the active site cavities and with thiol-reactive acceptor reagent on a cysteine either on the surface of the protein or at the end of the C-terminal helices. FRET analysis shows that the structures of both human MAO A and MAO B in detergent solution are consistent with their respective crystal structures. Furthermore, the C-terminal helices of these two enzymes are suggested to exhibit a non-linear conformation in which the ends turn back toward the membrane surface. Rat MAO A was successfully expressed in *P. pastoris* system and purified according to the modified human MAO A purification procedure. Even though these two enzymes are 90% sequence identical, different surface charges on the proteins result in different binding affinities on ion-exchange columns. An electrostatic potential study on human and rat

MAO A's shows that the distribution of negatively charged residues is greater on human MAO A than on rat MAO A, resulting in a stronger binding of human MAO A to the anion-exchange DEAE-Sepharose column. Comparisons of human wild-type MAO A, human MAO A Lys151Glu mutant and rat MAO A show that there are similar functional properties among them except thermal stability. Both human MAO A Lys151Glu mutant and rat MAO A exhibit a much higher thermal stability than does human wild-type MAO A.

Comparative Structural and Functional Properties of
Human and Rat Monoamine Oxidases

By

Jin Wang

B.S., Lanzhou University, 2002

Adviser: Dale E. Edmondson, Ph.D.

A dissertation submitted to the Faculty of the Graduate
School of Emory University in partial fulfillment
of the requirements for the degree of
Doctor of Philosophy

Department of Chemistry

2007

ACKNOWLEDGEMENTS

I would like to express my special thanks to my Ph.D. advisor, Dr. Dale Edmondson, for his valuable advice, patience and enthusiasm throughout my graduate school. His wonderful education and scientific guidance made me more precise and mature in science, which will be a treasure for my whole life.

I would also like to thank my committee members, Dr. Jay Justice and Dr. Stefan Lutz for their useful advice and guidance over the past five years.

I would like to dedicate my today's achievements to my dear parents, Yaohui Wang and Suzhen Wang as well as my husband Fuchang Yin. This dissertation would not have been possible without their unlimited love and support to encourage me throughout these years.

My final acknowledgement goes to the Edmondson lab members. It is such an unforgettable time for me being in this lab for five years. I would like to specially thank Dr. Anup Upadhyay who is an excellent working partner, and Ms. Milagros Aldeco who provided wonderful technical support in my Ph.D. research.

Table of Contents

Chapter 1 Introduction.....	1
1.1 General introduction to monoamine oxidases.....	1
1.1.1 Reactions catalyzed by MAOs and their isoforms	1
1.1.2 Tissue and cell distribution.....	2
1.2 Pharmacological significance	3
1.2.1 Substrate and inhibitor similarities and specificities	3
1.2.2 Physiological role in health and disease	6
1.2.2.1 MAO A and B in psychiatric disorders	7
1.2.2.2 MAO A and B in Parkinson's disease.....	8
1.2.2.3 MAO A and B in smoking and alcoholism	9
1.3 Molecular genetics and biochemistry	10
1.3.1 Gene cloning and location	10
1.3.2 Protein expression system.....	13
1.3.3 Covalent FAD cofactor.....	14
1.3.4 Catalytic mechanism.....	18
1.3.4.1 Aminium cation radical mechanism	19
1.3.4.2 Polar nucleophilic mechanism.....	20
1.3.4.3 Concerted nucleophilic mechanism.....	22
1.3.5 Quantitative structure-activity relationships (QSAR)	23
1.4 Structural biology.....	25
1.4.1 Human MAO B.....	26
1.4.2 Rat MAO A.....	32

1.4.3 Human MAO A	34
1.4.4 Selective mutation in human MAO A	38
1.5 Characterization of mitochondrial membrane associated monoamine oxidase	40
1.5.1 Lipid composition of mitochondria	40
1.5.2 Effect of phospholipids on functional properties of MAO	42
1.5.3 Targeting signal and membrane association of MAO	43
1.6 Dissertation objectives	44

Chapter 2 Fluorescent Probes to Investigate the Structural Properties of Human

MAO A and MAO B.....	47
2.1 Introduction.....	47
2.2 Materials and Methods.....	50
2.2.1 Materials	50
2.2.2 Creation and transformation of site-specific double mutants of MAO A and MAO B	51
2.2.3 Expression and purification of human MAO A and human MAO B double mutants	52
2.2.4 Synthesis of 5'-(N-dansyl) -cadaveryl- <i>p</i> -carboxymethylpargyline (DCP).....	52
2.2.5 Time course of wild-type MAO inhibition by DCP	52
2.2.6 Labeling of human MAO enzymes with DCP.....	54
2.2.7 Labeling of DCP-labeled human wild-type MAO A/B and double mutants with 4-dimethylaminophenylazophenyl-4'-maleimide (DABMI)	54
2.2.8 Fluorescence measurements	55

2.2.9 Fluorescence resonance energy transfer (FRET) analysis.....	57
2.2.10 Modeling of MAO C-terminal helices.....	58
2.2.11 Molecular Dynamics (MD) simulation.....	59
2.3 Results.....	60
2.3.1 Spectral characterization of DCP.....	60
2.3.2 Inhibition of MAO with DCP.....	61
2.3.3 Fluorescence quenching of DCP in MAO.....	64
2.3.4 Polarization and anisotropy of DCP in MAO.....	67
2.3.5 Distance measurements in MAO.....	68
2.4 Discussion.....	74

Chapter 3 Conformational Investigations of C-terminal Helices of Human MAO A and MAO B in Their Membrane Bound Forms	78
3.1 Introduction.....	78
3.2 Materials and Methods.....	82
3.2.1 Materials.....	82
3.2.2 Creation of human MAO A Cys266Ala/Pro525Cys and MAO B Cys5Ala/Val518Cys mutants.....	82
3.2.3 Labeling of human MAO A and MAO B double mutants with N-(1- pyrenyl)maleimide (NPM).....	82
3.2.4 Isolation of yeast mitochondria.....	83
3.2.5 Reconstitution of wild-type MAO and NPM-labeled MAO samples into yeast mitochondria.....	84

3.2.6 Fluorescence measurements	85
3.3 Results.....	86
3.3.1 Characterization of MAO insertion into yeast mitochondria	86
3.3.2 Fluorescence spectra of pyrene in MAO	91
3.3.3 Polarization and anisotropy of NPM-labeled MAO in detergent solubilized and membrane bound forms.....	93
3.3.4 Quenching of pyrene-labeled MAO A and MAO B fluorescence by iodide	94
3.3.5 Quenching of pyrene-labeled MAO A and MAO B fluorescence by spin- labeled fatty acids.....	97
3.4 Discussion.....	101
 Chapter 4 High-level Expression of Rat Monoamine Oxidase A in <i>Pichia pastoris</i>107
4.1 Introduction.....	107
4.2 Materials and Methods.....	108
4.2.1 Materials	108
4.2.2 cDNA cloning of rat MAO A	108
4.2.3 Transformation of rat MAO A gene into <i>P. pastoris</i>	109
4.2.4 Expression of rat MAO A.....	109
4.2.5 Purification of rat MAO A.....	109
4.2.6 Mass spectral analysis.....	111
4.2.7 Thermal stability.....	112
4.2.8 Steady-state kinetic studies.....	112

4.3 Results.....	113
4.3.1 Enzyme expression and purification.....	113
4.3.2 Protein characterization	114
4.3.3 MALDI-TOF/TOF-MS analysis.....	114
4.3.4 Functional characterization.....	116
4.3.5 Thermal stability.....	118
4.3.6 Catalytic properties.....	120
4.4 Discussion.....	120

**Chapter 5 Functional Comparison of Human MAO A K151E and Rat MAO A with
WT-human MAO A.....124**

5.1 Introduction.....	124
5.2 Materials and Methods.....	125
5.2.1 Materials	125
5.2.2 Creation of and transformation of human MAO A K151E	125
5.2.3 Expression and purification of human MAO A K151E	126
5.2.4 Thermal stability.....	126
5.2.5 Determination of k_{cat} , K_m and K_i	127
5.2.6 Determination of $K_m(O_2)$	127
5.2.7 Steady state kinetic measurements of <i>para</i> -substituted benzylamine analogue oxidation.....	127
5.2.8 Data analysis.....	128
5.3 Results.....	128

5.3.1 Enzyme expression and purification.....	128
5.3.2 Spectral property of human MAO A K151E.....	129
5.3.3 Thermal stability.....	129
5.3.4 Steady state kinetic properties and competitive inhibition.....	132
5.3.5 $K_m(O_2)$	132
5.3.6 Steady state kinetics of the human MAO A K151E and rat MAO A catalyzed oxidation of <i>para</i> -substituted benzylamine analogues and the effects of isotopic substitution	137
5.3.7 Effect of the <i>para</i> substituent on the rates of steady state turnover.....	139
5.3.8 Quantitative structure-activity relationships describing the binding of <i>para</i> - substituted benzylamine analogues to MAO A's	151
5.4 Discussion.....	161
5.4.1 Thermal stability and substrate/inhibitor specificities.....	161
5.4.2 Mechanistic interpretation of $K_m(O_2)$	161
5.4.3 Structure-activity relationships describing the steady-state turnover rate of human MAO A K151E mutant and rat MAO A by <i>para</i> -substituted benzylamine analogues.....	162
5.4.4 Structure-activity relationships describing the binding of <i>para</i> -substituted benzylamine analogues to human MAO A K151E mutant and rat MAO A...	164
5.4.5 Mechanistic interpretation of QSAR results.....	165
Dissertation summary.....	171
References.....	176

List of Figures

Figure 1.1 Sequence alignment of various MAOs.....	10
Figure 1.2 Structure and nomenclature of flavins and analogues.....	15
Figure 1.3 6-S-cysteinyl, 8 α -N1-histidyl-FAD.....	17
Figure 1.4 Structure of human MAO B dimer.....	27
Figure 1.5 Monomeric structure of human MAO B.....	28
Figure 1.6 Schematic representation of the pargyline binding site in human MAO B.....	29
Figure 1.7 The C-terminal transmembrane helix and the neighboring apolar sites involved in membrane binding.....	30
Figure 1.8 Models illustrating the binding modes of isatin and 1,4-diphenyl-2-butene to human MAO B.....	31
Figure 1.9 Dimeric structure of rat MAO A.....	32
Figure 1.10 LIGPLOT illustration of binding of FAD and clorgyline in rat MAO A.....	33
Figure 1.11 Comparison of the active centers of rat MAO A and human MAO B.....	34
Figure 1.12 Monomeric structure of human MAO A.....	36
Figure 1.13 Comparison of cavity-shaping loops in human MAO A, human MAO B and rat MAO A.....	37
Figure 1.14 Interface view of the dimer of “non-human” MAO A.....	38
Figure 1.15 Interface view of the predicted dimer of human MAO A.....	39
Figure 2.1 Chemical structure of DCP.....	48
Figure 2.2 Chemical structure of 4-dimethylaminophenylazophenyl-4'-maleimide (DABMI).....	50
Figure 2.3 UV-Vis spectrum of DCP in 95% ethanol.....	60

Figure 2.4 Excitation and emission spectra of DCP in 95% ethanol and in potassium phosphate buffer	61
Figure 2.5 Time course of inhibition of human wild-type MAO A and MAO B by DCP	62
Figure 2.6 UV-Vis spectra of human MAOs before and after DCP inhibition	63
Figure 2.7 SDS-PAGE gel of MAO samples exposed under UV light	64
Figure 2.8 Fluorescence spectra of DCP-inhibited MAO before and after KI quenching	65
Figure 2.9 Overlap of the absorbance spectrum of DABMI with the emission spectrum of DCP	68
Figure 2.10 Fluorescence emission spectra of free DCP, MAO-bound DCP in the absence of DABMI and in the presence of DABMI	69
Figure 2.11 DCP-docked structures of human MAO A and human MAO B.....	72
Figure 2.12 Surface potential drawing of human MAO A and human MAO B.....	76
Figure 3.1 Proposed hypotheses for the structure of human MAO B C-terminal tail	78
Figure 3.2 Structural formulas of NPM and the spin-labeled fatty acids	81
Figure 3.3 Insertion of MAO A and MAO B into yeast mitochondria without treatment of proteinase K.....	88
Figure 3.4 The effect of proteinase K on insertion of purified MAO A and MAO B into yeast mitochondria.....	88
Figure 3.5 Detection of conjugates of MAO A (A) and MAO B (B) with ubiquitin	90
Figure 3.6 Temperature-dependent insertions of purified MAO A and MAO B into isolated yeast mitochondria	90

Figure 3.7 Pyrene emission fluorescence spectra	92
Figure 3.8 Stern-Volmer plots of potassium iodide quenching pyrene-labeled MAO A and pyrene-labeled MAO B	96
Figure 3.9 Estimation of transmembrane location of MAO-bound pyrene by quenching with 5- and 12-FASL	98
Figure 3.10 Proposed structural conformation of human MAO A and human MAO B C- terminal tail in mitochondrial outer membrane	105
Figure 4.1 SDS-polyacrylamide gel electrophoresis of rat MAO A	114
Figure 4.2 MALDI-TOF/TOF-MS analysis of the trypsin digested rat MAO A expressed in <i>P. pastoris</i>	115
Figure 4.3 UV-Vis spectral changes of purified rat MAO A upon anaerobic reduction by tyramine	117
Figure 4.4 UV-Vis spectra of purified rat MAO A before and after the addition of 10-fold molar excess of clorgyline	118
Figure 4.5 Comparison of thermal stability of human MAO A and rat MAO A	119
Figure 4.6 Electrostatic features of human MAO A and rat MAO A	122
Figure 5.1 UV-Vis spectra of purified human MAO A K151E before and after the addition of 10-fold molar excess of clorgyline	129
Figure 5.2 Comparison of thermal stability of WT-human MAO A, human MAO A K151E mutant and rat MAO A	130
Figure 5.3 Steady-state kinetics for the oxidation of kynuramine by human MAO A K151E with different oxygen concentrations	135

Figure 5.4 Steady-state kinetics for the oxidation of kynuramine by rat MAO A with different oxygen concentrations.....	136
Figure 5.5 Correlation of steady state rates of human MAO A K151E turnover of α , α -[^1H] and α , α -[^2H]- <i>p</i> -substituted benzylamines with the substituent electronic parameter (σ).....	140
Figure 5.6 Correlation of steady state rates of rat MAO A turnover of α , α -[^1H] and α , α -[^2H]- <i>p</i> -substituted benzylamines with the substituent electronic parameter (σ).....	141
Figure 5.7 Comparison of correlation of steady state rates of human MAO A, human MAO A K151E, rat MAO A and human MAO B turnover with the substituent electronic parameter (σ).....	142
Figure 5.8 Correlation of steady-state rates of human MAO A K151E mutant turnover of <i>p</i> -substituted benzylamines with substituent parameters.....	145
Figure 5.9 Correlation of steady-state rates of rat MAO A turnover of <i>p</i> -substituted benzylamines with substituent parameters	149
Figure 5.10 Comparison of correlations of the binding of <i>p</i> -substituted benzylamine to human MAO A, human MAO A K151E and rat MAO A with the van der Waals volume (V_w) of the <i>para</i> substituent.....	154
Figure 5.11 Correlation of binding affinity of <i>p</i> -substituted benzylamines for human MAO A K151E with substituent parameters.....	158
Figure 5.12 Correlation of binding affinity of <i>p</i> -substituted benzylamines for rat MAO A with substituent parameters	160

Figure 5.13 Model representation of the relative conformation of <i>para</i> -substituted benzylamine analogues bound to human MAO A.....	167
Figure 5.14 Electron density map of human MAO A K151E mutant	169

List of Tables

Table 1.1 Substrates and inhibitors of MAO A and MAO B.....	4
Table 1.2 Covalent linkages of FAD or FMN in known flavoproteins	16
Table 1.3 Comparison of lipid composition of mammalian cells, plant cells and yeast....	41
Table 2.1 Oligonucleotides used for site-directed mutagenesis of human MAO A and human MAO B genes.....	51
Table 2.2 Polarization/anisotropy of DCP in different environments	67
Table 2.3 Summary of FRET distances R	71
Table 3.1 Polarization/anisotropy of NPM-labeled MAO in detergent solubilized and membrane bound forms	99
Table 3.2 Stern-Volmer quenching constants for quenching of pyrene-labeled MAO A and MAO B fluorescence by iodide and spin-labeled fatty acids.....	101
Table 4.1 Purification scheme of recombinant rat liver MAO-A expressed in <i>P. pastoris</i>	113
Table 4.2 Summary of MALDI-TOF/TOF-MS analysis of trypsin-digested rat MAO A	116
Table 4.3 Comparison of steady-state kinetic properties of the purified human and rat MAO A's	121
Table 5.1 Purification scheme of human MAO-A K151E expressed in <i>P. pastoris</i>	128
Table 5.2 Comparison of steady state kinetic properties of WT-human MAO A, human MAO A K151E and rat MAO A.....	133
Table 5.3 Comparison of competitive inhibition constants for WT-human MAO A, human MAO A K151E and rat MAO A.....	134

Table 5.4 Steady-state kinetic constants for the human MAO A K151E catalyzed oxidation of <i>p</i> -substituted benzylamine analogues	138
Table 5.5 Steady-state kinetic constants for the rat MAO A catalyzed oxidation of <i>p</i> -substituted benzylamine analogues.....	138
Table 5.6 Comparison of steady-state rates of human MAO A, human MAO A K151E and rat MAO A catalyzed oxidation of α , α -[¹ H]- <i>p</i> -substituted benzylamines and deuterium kinetic isotope effects observed with α , α -[² H]- <i>p</i> -substituted benzylamines.....	139
Table 5.7 Correlations of the steady state rate of wild-type human MAO A oxidizing <i>para</i> -substituted benzylamine (k_{cat}) with steric, electronic and hydrophobic substituent parameters.....	143
Table 5.8 Correlations of the steady state rate of human MAO A K151E oxidizing <i>para</i> -substituted benzylamine (k_{cat}) with steric, electronic and hydrophobic substituent parameters.....	144
Table 5.9 Correlations of the steady state rate of rat MAO A oxidizing <i>para</i> -substituted benzylamine (k_{cat}) with steric, electronic and hydrophobic substituent parameters	148
Table 5.10 Correction of <i>p</i> -substituted benzylamine human MAO A K151E and rat MAO A binding constants for selective binding of the deprotonated form of the amine substrate	153
Table 5.11 Correlations of the binding affinities (K_d) of deprotonated <i>para</i> -substituted benzylamine for wild-type human MAO A with steric, electronic and hydrophobic substituent parameters.....	156

Table 5.12 Correlations of the binding affinities (K_d) of deprotonated <i>para</i> -substituted benzylamine for human MAO A K151E with steric, electronic and hydrophobic substituent parameters.....	157
Table 5.13 Correlations of the binding affinities (K_d) of deprotonated <i>para</i> -substituted benzylamine for rat MAO A with steric, electronic and hydrophobic substituent parameters	159
Table 5.14 Correlations of the steady-state rates of MAO A oxidizing <i>para</i> -substituted benzylamines (k_{cat}) and the binding affinities of deprotonated <i>para</i> -substituted benzylamines (K_d) for MAO A with electronic and steric substituent parameters	163

List of Schemes

Scheme 1.1 Reaction catalyzed by monoamine oxidases	1
Scheme 1.2 Proposed mechanism for MAO inhibition by propargylamines	6
Scheme 1.3 Reaction pathway for the MAO B-catalyzed oxidation of benzylamine	18
Scheme 1.4 Proposed aminium cation radical mechanism for MAO catalysis	20
Scheme 1.5 Proposed polar nucleophilic mechanism for MAO catalysis	21
Scheme 1.6 Proposed concerted nucleophilic mechanism for MAO catalysis.....	23
Scheme 1.7 Dissociation of benzoic acid	24
Scheme 2.1 Synthetic pathway to prepare 5'-(N-dansyl) -cadaveryl- <i>p</i> - carboxymethylpargyline (DCP)	53
Scheme 5.1 Reaction pathway for the MAO A-catalyzed oxidation of kynuramine	162
Scheme 5.2 Proposed concerted polar nucleophilic mechanism for MAO A catalysis...	166

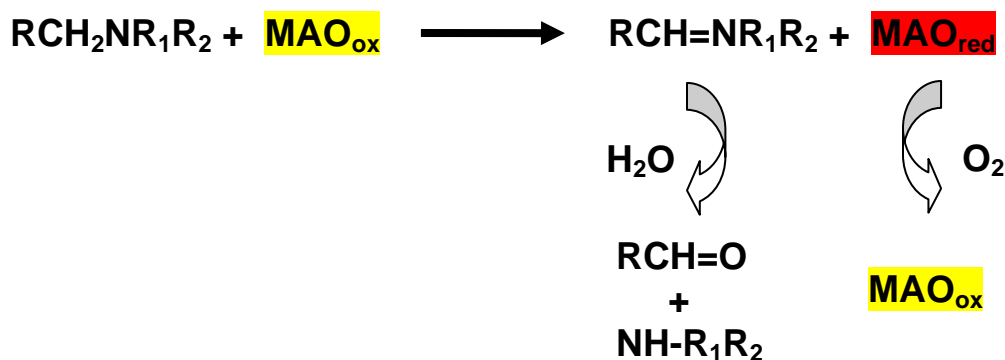
Chapter 1

Introduction

1.1 General introduction to monoamine oxidases

1.1.1 Reactions catalyzed by MAOs and their isoforms

Monoamine oxidase (MAO, E.C. 1.4.3.4) is a flavin-containing mitochondrial membrane-bound protein which functions in the oxidative degradation of biogenic and xenobiotic amines to their corresponding aldehydes (Weyler *et al.* 1990). It has been shown that, in the MAO catalytic reaction, there are two half-reactions: reduction and oxidation, and molecular O₂ serves as the electron acceptor (Edmondson *et al.* 1993). The amine substrates are first oxidized by the covalent flavin cofactor to produce an imine intermediate in the reductive half-reaction, and flavin cofactor is correspondingly reduced to the hydroquinone. The reduced flavin is then reoxidized by O₂ in oxidative half-reaction to form H₂O₂, and H₂O non-enzymatically hydrolyzes the dissociated imine product to aldehyde and NH₄⁺ (Scheme 1.1).



Scheme 1.1 Reaction catalyzed by monoamine oxidases

Monoamine oxidase has been discovered to exist as two isoforms in many tissues of humans and other mammals, termed as MAO A and MAO B (Houslay *et al.* 1976; Achee *et al.* 1977). The amino acid sequences of the two human isoforms are 70% identical with each one containing a FAD cofactor covalently attached to the conserved cysteinyl residue via an 8- α -S-thioether linkage (Walker *et al.* 1971). MAO A is a target for antidepressant drugs, while MAO B has received extensive attention as a target for neuroprotective drugs for Parkinson's disease which affects large segments of the aging population in particular (Fowler *et al.* 1980). Because of the physiological importance of MAO, a large number of inhibitors have been developed to treat various neuropsychiatric disorders (Dostert *et al.* 1989; Pletscher 1991).

1.1.2 Tissue and cell distribution

MAO exists ubiquitously in all mammals and a variety of non-mammalian sources, such as the oyster *Crassostrea angulata* (Delrio *et al.* 1982), rainbow trout (Edwards *et al.* 1986), frog (Kobayashi *et al.* 1981), sea urchin (Nicotra *et al.* 1982) *et. al.* Although MAOs in some non-mammalian sources show similar genetic properties (covalent FAD and molecular weights) compared to mammalian MAOs, they exhibit properties of both MAO A and MAO B, suggesting a single gene precursor and gene duplication on evolution to mammals.

The cellular localization of MAO A and MAO B in mammalian peripheral tissues and in the central nervous system has been identified by a variety of techniques including subcellular fractionation (Stenstrom *et al.* 1985) and immunohistochemical staining (Levitt *et al.* 1982; Westlund *et al.* 1985). Outside the nervous system, MAO A exists in

vascular tissue, liver and is differentially expressed in most tissues (Weyler *et al.* 1985; Masinirepiso *et al.* 1986). MAO B can be obtained from human platelets (Denney *et al.* 1982), and lymphocytes (Riley *et al.* 1989) and bovine kidney (Erwin *et al.* 1967; Erwin *et al.* 1967). Both MAO A and MAO B are highly coexpressed in the liver (Berry *et al.* 1994). In neuronal tissue, MAO A predominantly appears in adrenergic, noradrenergic and dopaminergic neurons (Jahng *et al.* 1997). The B form-containing neurons are believed to be responsible for the synthesis and storage of neurotransmitter serotonin (Kitahama *et al.* 1991) which occurs in serotonergic neurons. MAO B is also abundant in histaminergic neurons, astrocytes and ependymal cells (Nakamura *et al.* 1990; Ekblom *et al.* 1993). Interestingly, MAO is even observed in several non-monoaminergic neurons (Nakamura *et al.* 1990; Ekblom *et al.* 1993; Jahng *et al.* 1997; Vitalis *et al.* 2002), suggesting that the localization of MAO could be functions for neurotransmitter oxidation that we do not understand.

1.2 Pharmacological significance

1.2.1 Substrate and inhibitor similarities and specificities

Since the two isoforms of MAO share 70% sequence identity, their substrate and inhibitor specificities show both similarities and differences.

As shown in Table 1.1, MAO A oxidizes serotonin (5-hydroxytryptamine), adrenaline and noradrenaline preferentially whereas benzylamine and 2-phenethylamine are the specific substrates for MAO B (Dostert *et al.* 1989). Both A and B form oxidize tyramine and dopamine as substrates (Ocarroll *et al.* 1983).

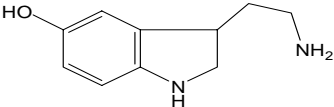
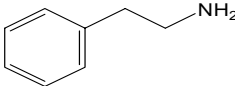
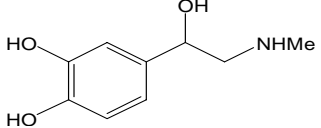
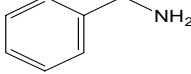
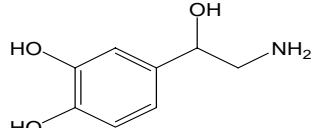
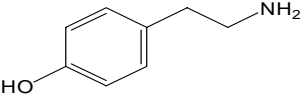
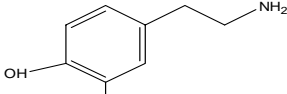
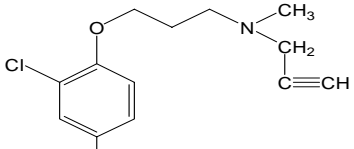
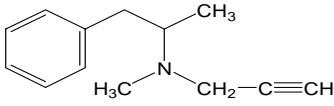
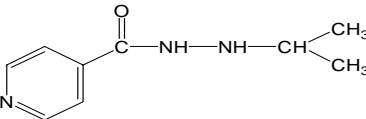
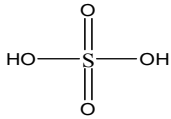

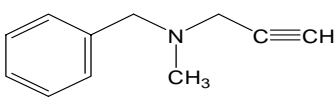
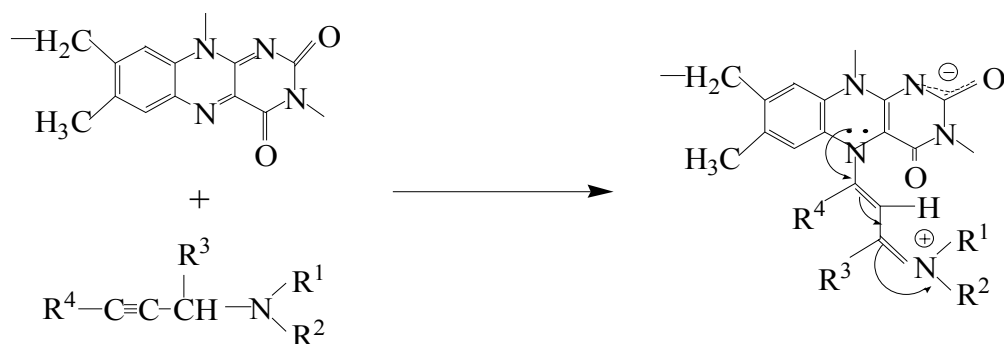
	MAO A	MAO B
Substrates	 <p>Serotonin</p>	 <p>Phenethylamine</p>
	 <p>Adrenaline</p>	 <p>Benzylamine</p>
	 <p>Noradrenaline</p>	
	 <p>Tyramine</p>	 <p>Dopamine</p>
Inhibitors	 <p>Clorgyline</p>	 <p>Deprenyl</p>
	 <p>Iproniazid</p>	 <p>Phenylzine</p>
	 <p>Tranlycypromine</p>	 <p>Propargylamine</p>

Table 1.1 Substrates and inhibitors of MAO A and MAO B

For inhibitors, clorgyline is a well known mechanism-based irreversible MAO A inhibitor first proposed by Johnston, J. P. (Swett *et al.* 1963). L- Deprenyl (selegiline), an irreversible MAO B inhibitor, has been widely used in the treatment of Parkinson disease (Wessel *et al.* 1992; Yahr 1993) with the combination of levodopa, which is shown to reduce the degradative metabolism of the dopamine generated from levodopa (Birkmayer *et al.* 1975).

Although the two isoforms of MAO are preferentially inhibited by different inhibitors, they show similar susceptibility to some inhibitors, such as iproniazid, phenylzine, tranylcypromine and propargylamines. Iproniazid, a common drug to treat tuberculosis patients, was found to produce mood elevation in patients, so this hydrazine-derived inhibitor was an initial MAO inhibitor to treat depression (Brodie *et al.* 1957). However, the latter studies indicated that this class of hydrazine-derived inhibitors (e.g. phenylzine) would cause liver toxicity and even death from hypertension on injection of food containing high tyramine level (the cheese effect) (Daneshmend *et al.* 1979), and then the direction of MAO-inhibitor development had been changed to propargylamines. It has been reported that MAO can be irreversibly inactivated by propargylamines, in which the acetylenic function being β to the nitrogen leads to formation of a covalent adduct with cofactor flavin itself covalently bound with protein (Swett *et al.* 1963). The proposed mechanism of inhibitor covalently reacted with MAO can be illustrated by the following scheme (Scheme 1.2). The basis of the inhibition is the ability of propargylamines to rearrange to allenes upon interaction with the active site of the enzyme(Abeles *et al.* 1974).



Scheme 1.2 Proposed mechanism for MAO inhibition by propargylamines

Tranlycypromine, a non-hydrazine reversible MAO inhibitor, has been used clinically to treat depression that does not respond to other types of drug therapy (Bartholomew 1962).

However, even though liver toxicity was avoided by the development of non-hydrazine inhibitors such as tranlycypromine and pargyline, combination of using MAO propargylamines-derived inhibitor and amine-rich food (such as cheese) still continued to cause the hypertensive “cheese reaction” (Anderson *et al.* 1993), since sympathetic cardiovascular activity would be potentiated with the effect of tyramine and other sympathomimetic amines.

Therefore, with the understanding of physiological and behavioural functions of MAO, in-depth studies on development of MAO-inhibitor for various conditions are necessary in the future.

1.2.2 Physiological role in health and disease

MAO regulates concentrations of important neurotransmitters in brain, such as dopamine and serotonin, as well as protects the body by oxidizing xenobiotic and dietary amines in peripheral tissues which could function as false neurotransmitters.

1.2.2.1 MAO A and B in psychiatric disorders

The studies on MAO-knockout mice have suggested that deficiency of MAO A may lead to aggressive behavior due to the elevated level of neurotransmitter serotonin and norepinephrine (Cases *et al.* 1995). Interestingly, the increase of serotonin in adult brains is much higher than that of norepinephrine. The observation of males in a Dutch family with a X-linked genetic mutation further confirmed the functional role of MAO A in neurotransmitter metabolism and behavior (Brunner *et al.* 1993). Males in this family possessing a genetic mutation, a stop codon in their MAO A genes which leads to expression of truncated and inactive enzyme, show abnormal aggressive behavior. In contrast, instead of exhibiting a behavioral disturbance, MAO B-deficient mice show increased reactivity to stress since norepinephrine and dopamine are relevant to stress response and controlled by β -phenylethylamine which is a MAO B specific substrate. In MAO B-deficient mice, the level of β -phenylethylamine is elevated and then the levels of norepinephrine and dopamine increase correspondingly (Berry *et al.* 1994). Overdegradation of the neurotransmitters dopamine and norepinephrine by increased levels (4-5 fold) of MAO B expression on aging in neuronal tissue may cause depression, a common psychiatric problem in old age (Casey 1994). It has been found that new MAO A specific inhibitors with lower side effects, such as moclobemide and brofarmomine, are effective for treatment of depression, but are not MAO B inhibitors for treatment of Parkinson's disease (Nagatsu 2004).

MAO A is assumed to be a moderating factor in the relationship between childhood maltreatment and later antisocial and violent behavior (Caspi *et al.* 2002). MAO A transcription is reduced in maltreated children who would be at higher risk for

antisocial behaviors due to the lower efficiency of degradation of neurotransmitters than normal individuals.

The studies on pathological gambling, such as DNA polymorphisms in MAO A and MAO B, have suggested that allele variants of MAO A, but not MAO B, might be associated with pathological gambling, at least in severe male gamblers (Ibanez *et al.* 2000).

1.2.2.2 MAO A and B in Parkinson's disease

Parkinson's disease is one of the common neurological disorders in that elevated level of MAO B is found (Fowler *et al.* 1980). This disease may be associated with the effect of MAO B activity by increasing the levels of toxic H₂O₂ and by bioactivating exogenous or endogenous neurotoxins which lead to degradation of dopamine-producing neurons.

Conversion of 1-methyl-4-phenyl-1,2,3,6-tetrahydropyridine (MPTP) by MAO B in glial cells to the toxic metabolite 1-methyl-4-phenylpyridine (MPP⁺) causes a Parkinson's-like syndrome since MPP⁺ selectively damages nigrostriatal dopamine-producing neurons, leading to a depletion of dopamine which functions as a neurotransmitter (Gerlach *et al.* 1996). It has been found that MAO B is required for the activation of MPTP toxicity by the fact that no damage to the dopaminergic terminals of the striatum in MAO B-deficient mice was observed after MPTP injection (Grimsby *et al.* 1997).

A number of MPTP-like compounds produced by condensation of biogenic amines with endogenous or exogenous metabolites (Naoi *et al.* 1996; Collins *et al.* 2000;

Matsubara 2000; Nagatsu 2000), such as β -carbolines and isoquinolines, have been studied to be poor substrates compared with MPTP, even though become activated by oxidized by MAO (Nagatsu 1997).

1.2.2.3 MAO A and B in smoking and alcoholism

A number of studies including whole-body PET-scans (Fowler *et al.* 1996; Fowler *et al.* 2003) have shown the link between cigarette smoke and MAO inhibition. The first evidence is inhibition of MAO activity by components in cigarette smoke in mouse skin (Essman 1977). The observed decrease of MAO activity in smokers is thought to be caused by several tobacco constituents that possess MAO-inhibitory activity. The β -carboline compound norharmane has been found to be a major inhibitor for both MAO A (Herraiz *et al.* 2005) and MAO B (May *et al.* 1991) in tobacco smoking. The β -carboline harmane is a potent inhibitor for MAO A (Herraiz *et al.* 2005) not for MAO B. The isolated benzoquinone and 2-naphthylamine from tobacco leaves exhibit very weak MAO-inhibiting property (Khalil *et al.* 2000; Hauptmann *et al.* 2001). Farnesol is also in plant leaves and is a specific inhibitor of MAO B (Khalil *et al.* 2006).

An extensive literature has reported an association between MAO activity and alcoholism (Sullivan *et al.* 1978; Devor *et al.* 1993; Faraj *et al.* 1994; Demir *et al.* 2002). In general, there are two types of alcoholism: Type I which has a low genetic susceptibility for alcoholism and is seen in both men and women, Type II which is highly heritable and only seen in males (Cloninger *et al.* 1981). No relation exists between MAO B activity and Type I alcoholism by the fact that normal MAO B levels are found in Type I alcoholism. It is not easy to clarify the association between low level MAO B activity

and Type II alcoholism since many factors may be involved in, such as personality traits, gender and race (Robinson *et al.* 1980), psychiatric disorders and medication (Fowler *et al.* 1982). Lower levels of MAO B found in Type II alcoholism may be due to personality trait which is a result of abnormal MAO levels. Moreover, most alcoholics are also smokers as well (70-90%), thus with the high concomitant tobacco use, the effect of alcoholism in MAO activity is ambiguous. So far, the clear role of alcohol in MAO activity is still not well understood.

1.3 Molecular genetics and biochemistry

1.3.1 Gene cloning and location

MAO has been found in higher eukaryotic organisms, such as mammals and fish (Edwards *et al.* 1986; Chen *et al.* 1994). To compare MAO across all investigated species, the full-length cDNA encoding MAO A or MAO B from all sources was isolated by using oligonucleotide probes and the deduced amino acid sequences were determined.

The deduced amino acid sequences of MAO from different sources have revealed that all forms of MAO are highly homologous (Abell *et al.* 2001). As shown in Figure 1.1, A form or B form of MAO across species (human, bovine, rat and mouse) exhibits high sequence homology (86-88% identity). The sequence identity between MAO A and MAO B in certain species is approximately 70%.

HumanMAOB.	1	-----MSNKCDVVVVGGGISGMAAAKLLHD
BovineMAOB.	1	-----MSNKCDVVVVGGGISGMAAAKLLHD
RatMAOB.	1	-----SNKCDVIVVGGGISGMAAAKLLHD
MouseMAOB.	1	-----MSNKSDVIVVGGGISGMAAAKLLHD
BovineMAOA.	1	-----MESLQKTS DAGMFDVVVIGGGISGLSAAKLLAE
HumanMAOA.	1	-----MENQEKASIAGHMFDDVVVIGGGISGLSAAKLLTE
RatMAOA.	1	-----MTDLEKPNLAGHMFDDVGLIGGGISGLAAAKLLSE
MouseMAOA.	1	-----MTDLEKPSITGHMFDDVVVIGGGISGLAAAKLLSE

TroutMAOB. 1 -----MTAQNIFDVIIVIGGGISGLSAAKLLKE
A. niger 1 MTSRDGYQWTPETGLTQGVPSLGVISPPPTNIEDTDDKDGPDVDVIIVIGGGYCGLTATRDITV
MAO-N.

HumanMAOB. 26 SGLNVVLEARDRVGGRTYTLRNQKVKYVDLGGSYVGPTQNRILRLAKELGLETYKVN
BovineMAOB. 26 SGLNVVLEARDRVGGRTYTLRNQKVKYVDLGGSYVGPTQNHILRLSKELGLETYKVN
RatMAOB. 25 CGLSVVLEARDVGGRTYTLRNKNVKYVDLGGSYVGPTQNRILRLAKELGLETYKVN
MouseMAOB. 26 CGLSVVLEARDRVGGRTYTLRNKNVKYVDLGGSYVGPTQNRILRLAKELGLETYKVN
BovineMAOA. 35 HEVNVVLEARDRVGGRTYTVRNEHVDYVDVGGAYVGPTQNRILRLSKQLGLETYKVN
HumanMAOA. 35 YGVSVVLEARDRVGGRTYTVRNEHVDYVDVGGAYVGPTQNRILRLSKELGIETYKVN
RatMAOA. 35 YKINVLVLEARDRVGGRTYTVRNEHVKYVDVGGAYVGPTQNRILRLSKELGIETYKVN
MouseMAOA. 35 YKINVLVLEARDRVGGRTYTVRNEHVKYVDVGGAYVGPTQNRILRLSKELGIETYKVN
TroutMAO. 28 KGLSPVLEARDRVGGRTFTVQNEQTKYVDLGGAYVGPTQNRILRLAKECGVKTIKVN
A. niger 61 AGFKTLLEARDRIGGRSWS-NIDGYPEMGGTWHVHWHQSHVWREITRYKMHNALSPSF
MAO-N.

HumanMAOB. 86 --ERLIHFVKGKSYPRFGFPFPVWNPITYLD-----HNNFWRTMDDMGREIPSDAPWKAP
BovineMAOB. 86 --ERLIHFVKGKSYPRFGFPFPVWNPITYLD-----HNNLWRTMDDMGREIPSDAPWKAP
RatMAOB. 85 --ERLIHFVKGKSYAFRFGFPFPVWNPITYLD-----YNNLWRTMDEMGEIPSDAPWKAP
MouseMAOB. 86 --ERLIHFVKGKSYAFRFGFPFPVWNPITYLD-----NNLWRTMDEMGEIPSDAPWKAP
BovineMAOA. 95 --ERLVHYVKGKTYPRFGAFPVWNP IAYLD-----YNNLWRTMDNMGEIPADAPWEAP
HumanMAOA. 95 --ERLVQYVKGKTYPRFGAFPVWNP IAYLD-----YNNLWRTIDNMGEIPTDAPWBAQ
RatMAOA. 95 --ERLVQYVKGKTYPRFGAFPVWNP IAYLD-----YNNLWRTMDEMGEIPVDAPWQAR
MouseMAOA. 95 --ERLVQYVKGKTYPRFGAFPVWNP IAYLD-----YNNLWRTMDDMGEIPVDAPWQAR
TroutMAO. 88 --ERLVHYVKGKSYPRFGFPFPVWNP IAYLD-----YNNLWRKMDMGEIIPREAPWKAP
A. niger 120 NFSRGNVNHQLRINPTTSTYMTHEAEDELLRSALHKEINVDGTINGRIVLPFPHDMFYVP
MAO-N.

HumanMAOB. 139 LAEEWDNMTMKELLDKICWTESSA--KQLATL FVNLCVTAETHEVSALWFLWYVKQCGGTT
BovineMAOB. 139 LAEQWDLMTMKELLDKICWTESS--KQLATL FVNLCVTAETHEVSALWFLWYVKQCGGTT
RatMAOB. 138 LAEEWDYMTMKELLDKICWTESS--KQLATL FVNLCVTAETHEVSALWFLWYVKQCGGTT
MouseMAOB. 139 LAEEWDYMTMKELLDKICWTKST--KQLATL FVNLCVTAETHEVSALWFLWYVKQCGGTT
BovineMAOA. 148 HAV EWDMTKMDLIEKICWTKTA--RQFASLFVNINVTSEPHEVSALWFLWYVKQCGGTT
HumanMAOA. 148 HADKWDKMTMKELIDKICWTKTA--RRFAYLFVNINVTSEPHEVSALWFLWYVKQCGGTT
RatMAOA. 148 HAQEWDMTKMDLIDKICWTKTA--REFAYLFVNINVTSEPHEVSALWFLWYVVRQCGGTA
MouseMAOA. 148 HAAEWDMTKMDLIDKICWTKTA--REFAYLFVNINVTSEPHEVSALWFLWYVVRQCGGTS
TroutMAO. 141 HAAEWDMTKQLFDKICWTESSA--RRFATL FVNINVTSEPHEVSALWFLWYVKQCGGTM
A. niger 179 EFRKYDEMSYSERIDQIRDELSSLNERSSELEAFILLCSGGTLENSSEFGFELHFWAMSGYTY
MAO-N.

HumanMAOB. 197 RIISTTNGGQERK--FVGGSGQVSEIRMDLLGDRVKLERPVIYIDQTEGENVLVETLNHEM
BovineMAOB. 197 RIFSTTNGGQERK--FVGGSGQVSEIRMDLLGDRVKLERPVIHIDQTEGENVLVETLNHEL
RatMAOB. 196 RIISTTNGGQERK--FVGGSGQVSEIRMDLLGDRVKLERPVIHIDQTEGENVVVKTLNHEI
MouseMAOB. 197 RIISTTNGGQERK--FVGGSGQVSEIRMDLLGDRVKLERPVIHIDQTEGENVIVKTLNHEI
BovineMAOA. 206 RIFSVTNGGQERK--FVGGSGQVSEIRMDLLGDRVKLRSEPVTYVDQSSBNITVETLNREL
HumanMAOA. 206 RIFSVTNGGQERK--FVGGSGQVSEIRMDLLGQVKNLHPVTHVDQSSDNIIEETLNHEH
RatMAOA. 206 RIFSVTNGGQERK--FVGGSGQVSEIRMDLLGDKVKLSSPVTYIDQTDNIIIVETLNHEH
MouseMAOA. 206 RIFSVTNGGQERK--FVGGSGQISEQIMVLLGDKVKLSSPVTYIDQTDNIIIEETLNHEH
TroutMAO. 199 RIFSTTNGGQERK--FVGGSSQISEQIMVLLGDKVKLSSPVYKIDQTEGDMVEVETLNKEBT
A. niger 239 QGCMDCLSYKFKDQGSFAFRRFWEEAAGTGRLGYVFGCPVRSVWNERDAARVTARDGRE
MAO-N.

HumanMAOB. 255 YEAKYVISAIPPTLGMKIHFNPPLPMMRNQMITRVP LGSVIKCI VYYKEBFWRKKDYCGT
BovineMAOB. 255 YEAKYVISAIPPVVLGMKIHFNPPLPMMRNQLITRVP LGSVIKSI VYYKEBFWRNMDYCGS
RatMAOB. 254 YEAKYVISAIPPVVLGMKIHFSPPLPILRNQLITRVP LGSVIKCMVYYKEBFWRKKDFCGT
MouseMAOB. 255 YEAKYVISAIPPALGMKIHFSPPLPMLRNQLISRVP LGSVIKCMVYYKEBFWRKKDFCGT
BovineMAOA. 264 YECRYVISAIPPTLTAKIHFPELPSERNQLIQRLPMGAVIKCMVYYKEAFWKKKDYCGC
HumanMAOA. 264 YECKYVINAIPTTLTAKIHFPELPAERNQLIQRLPMGAVIKCMVYYKEAFWKKKDYCGC
RatMAOA. 264 YECKYVISAIPPIITAKIHFPELPPERNLIQRLPMGAVIKCMVYYKEAFWKKKDYCGC
MouseMAOA. 264 YECKYVISAIPPVLTAKIHFPELPPERNLIQRLPMGAVIKCMVYYKEAFWKKKDYCGC
TroutMAO. 257 YKAKYVIVATPPGLNLKMHFNPELPLRNQLIHRVPMGSAIKCI VYYKENFWRKKGYCGT
A. niger 299 FAAKRLVCTIPLNVLSTIQSPALSTER---ISAMQAGHVNMC TKVHAEVDN--KDMRWS
MAO-N.

```

HumanMAOB. 315 MIIDGEEAPVAYTLDDTKPFGNYAAIMGFILAHKARKLARLTKEERLKKLCELYAKVLGS
BovineMAOB. 315 MIEEGEEAPVAYALDDTKPDGSPAIITGFILAHKARKLARLTKEERLKKLCDLYAKVLGS
RatMAOB. 314 MVIEGEEAPIAYTLDDTKPDAGCAAIMGFILAHKARKLVRLTKEERLRKLCELYAKVLNS
MouseMAOB. 315 MVIEGEEAPIAYTLDDTKPDGTAAAIMGFILAHKARKLVRLTKEERLRKLCELYAKVLNS
BovineMAOA. 324 MIEDEEAPISITLDDTKPDGSLPAIMGFILARKADRLAKVHKDIRKRKICERYAKVLGS
HumanMAOA. 324 MIEDEEAPISITLDDTKPDGSLPAIMGFILARKADRLAKLHKDIRKRKICELYAKVLGS
RatMAOA. 324 MIEDEEAPISITLDDTKPDGSLPAIMGFILARKADRLAKLHKDIRKRKICELYAKVLGS
MouseMAOA. 324 MIEDEEAPISITLDDTKPDGSPAIMGFILARKAERLAKLHKDIRKRKICELYAKVLGS
TroutMAO. 317 MVIEEEEAPICLTLDDTKPDGTVPAIMGFILARKCRKLCGLTKEERKKRICEIYSRVLGS
A. niger 354 TGIAYPFNKLCYALGDGTTTPAGNTHLVCFGT DANHIQPDDEDVRETLKAVGQLAPGTFVKG
MAO-N.

HumanMAOB. 375 LEALHPVHYEKNWCCEQYSGGCYTYFPPGILTQYGRVLRQPVDRIYFAGTETATHWSG
BovineMAOB. 375 QEALHPVHYEKNWCCEQYSGGCYTSYFPPGIMTQYGRVLRQPVGRIYFAGTETATHWSG
RatMAOB. 374 QEALQPVHYEKNWCCEQYSGGCYTAYFPPGILTQYGRVLRQPVGKIFFAGTETASHWSG
MouseMAOB. 375 QEALQPVHYEKNWCCEQYSGGCYTYFPPGILSYGRVLRQPVGKIFFAGTETASHWSG
BovineMAOA. 384 QEALHPVHYEKNWCCEQYSGGCYTAYFPPGIMTQYGRVLRQPVGRIYFAGTETATWSG
HumanMAOA. 384 QEALHPVHYEKNWCCEQYSGGCYTAYFPPGIMTQYGRVLRQPVGRIYFAGTETATKWSG
RatMAOA. 384 QEALYPVHYEKNWCCEQYSGGCYTAYFPPGIMTQYGRVLRQPVGRIYFAGTETATQWSG
MouseMAOA. 384 QEALSPVHYEKNWCCEQYSGGCYTAYFPPGIMTYGRVLRQPVGRIYFAGTETATQWSG
TroutMAO. 377 QEALHPVHYEKNWCCEQYSGGCYTAYFPPGILTQYGRVLRQPVGRIYFAGTETATEWSG
A. niger 414 RLVFH-----NWVKDEFKAGAWFFSRP-GMVSECLQGLREKHRGVVFANSDWALGNRS
MAO-N.

HumanMAOB. 435 YMEGAVEAGERAAREILHAMGKIPEDIWQSEPESSVDVPAQPITTTFLERHLPSVPGLLR
BovineMAOB. 435 YMEGAVEAGERAAREILHAMGKIPEDIWLPPEPESVDVPAKPITTTFLQRHLPSVPGLLK
RatMAOB. 434 YMEGAVEAGERAAREILHAI GKIPEDIWQPEPESVDVPAKPITNTFLERHLPSVPGLLK
MouseMAOB. 435 YMEGAVEAGERAAREILHAI GKIPEDIWQPEPESLDVPAKPITSTFLERHLPSVPGLLK
BovineMAOA. 444 YMEGAVEAGERAAREVLNGLKLSAKDIWQPEPEADVPAVEITPSEWERNLPSVSGLLK
HumanMAOA. 444 YMEGAVEAGERAAREVLNGLKLVTEKDIWQPEPEKDVPAVEITHTFWERNLPSVSGLLK
RatMAOA. 444 YMEGAVEAGERAAREVLNGLKVAKKDIWQPEPEKDVPAVEITHTFLERNLPSVPGLLK
MouseMAOA. 444 YMEGAVEAGERAAREVLNGLKVAKKDIWQPEPEKDVPAVEITHTFLERNLPSVPGLLK
TroutMAO. 437 YMEGAVEAGERAAREVLYEMGRIPQSQI WQTEPESEVVPALPFVTTFWERNLPSVGGFVN
A. niger 466 FIDGALIECTRAARVLEELGTRKREVKARL-----
MAO-N.

HumanMAOB. 495 LIGLTTIF SATALGFLAHKRGLLVRV
BovineMAOB. 495 LIGLTTIF SATALGFLAHKRGLLVRV
RatMAOB. 494 LIGLTTIF SATALGFLAHKRGLFVRF
MouseMAOB. 495 LFGLTTIF SATALGFLAHKRGLFVHF
BovineMAOA. 504 IVGFSTSI TALWFVMYRFLLSRS--
HumanMAOA. 504 IIGFSTSV TALGFVLYKYKLLPRS--
RatMAOA. 504 ITGVSTSV ALLCFVLYKIKKLPCLPC---
MouseMAOA. 504 ITGFSTSV ALLCFVLYKFKQPOS---
TroutMAO. 497 FLAASVLSVATAAGMLAYOKGLLTRS
A. niger -----
MAO-N.

```

Figure 1.1 Sequence alignment of various MAOs

The location of MAO A and B genes has been determined to be in close proximity on the X-chromosome using somatic cell mouse/human hybrid lines (Pintar *et al.* 1981; Kochersperger *et al.* 1986). The fact that both genes exhibit identical exon-intron organization but different promoter organization explains the difference of the two isoforms of MAO in their tissue-specific expression and functions (Shih *et al.* 2004).

1.3.2 Protein expression system

Since MAO A and MAO B are functionally distinct due to their different affinities to the various substrates and inhibitors, their genetic and biochemical properties should be investigated separately. In many cases, the MAO isoforms are colocalized in a certain tissue and not easily isolated from one another. Although some tissues contain only one form of MAO, such as human placenta for MAO A or human platelets for MAO B, very limited amounts of purified enzymes can be obtained. Moreover, isolating MAO directly from the tissue would not allow site-directed mutagenesis to be applied to study the functional role of residues involved in enzyme catalysis.

With the improvement of molecular biology, the appearance of recombinant DNA has facilitated expression of mammalian proteins in non-mammalian expression system, such as bacteria and yeast. In particular, yeast expression systems, such as *Saccharomyces cerevisiae* (Muller *et al.* 1998) and *Pichia pastoris* (Higgins *et al.* 1998; Cregg *et al.* 2000), offer several advantages in that the growth of yeast is fast and inexpensive, and yeast cells have the machinery for post-translational modifications. In recent years, the methylotrophic yeast *Pichia pastoris* has been developed as an excellent host for the large-scale expression of proteins from different sources, since this expression system possesses strong constitutive promoter (GAP promoter), strong inducible promoter (alcohol oxidase promoter) and high levels of expression.

In our laboratory, human liver recombinant MAO B was first successfully expressed in *P. pastoris* and (Newton-Vinson *et al.* 2000), compared to *Saccharomyces cerevisiae*, *Pichia pastoris* displays several advantages in expression of human MAO A: higher protein yield, more pronounced thermal stability and no C-terminal proteolysis of

the serine residue (Li *et al.* 2002). Therefore, with the success of expression of human MAO in *P. pastoris* (Newton-Vinson *et al.* 2000; Li *et al.* 2002), we have expressed both human and rat wild-type MAO A and B or mutant enzymes separately in *P. pastoris* for further catalytic and structural studies.

1.3.3 Covalent FAD cofactor

Flavin is widespread in organisms and involved in a variety of biological reactions (Ghisla *et al.* 1989). As shown in Figure 1.2, the core structure of the flavin molecule is the isoalloxazine ring which is the combination of xylene (the A ring), pyrazine (the B ring) and pyrimidine (the C ring). Flavin molecules vary with the different side chains at the position 10 on isoalloxazine ring. For example, riboflavin, also known as vitamin B₂, is composed of isoalloxazine ring and D-ribityl side-chain. With the assistance of ATP, riboflavin serves as an integral component for the synthesis of two flavin coenzymes: FMN (flavin mononucleotide) and FAD (flavin-adenine dinucleotide) which is the conjugation of FMN and AMP (adenosine monophosphate). These two flavin coenzymes exist in a number of flavoproteins through either non-covalent bonding to the protein or through covalent linkage to a residue side chain (Mewies *et al.* 1998). So far, the molecular significance of covalent linkage of flavin coenzymes to proteins is still elusive. The known flavoproteins containing covalently linked FMN or FAD are summarized in Table 1.2.

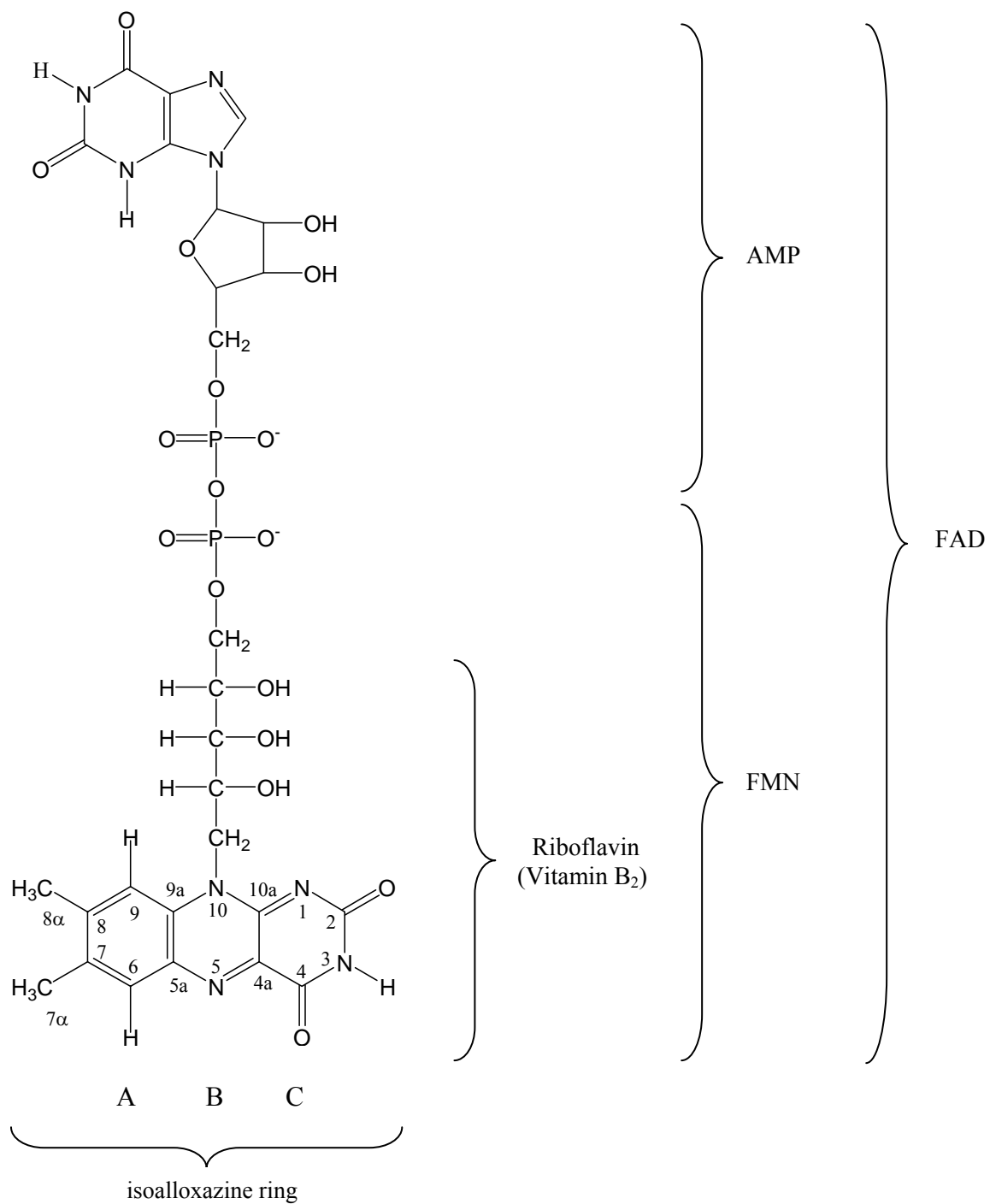


Figure 1.2 Structure and nomenclature of flavins and analogues.

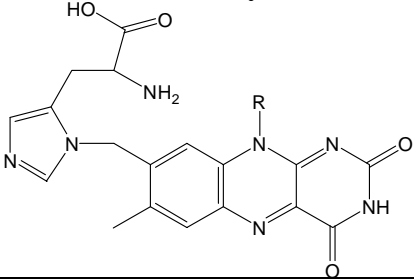
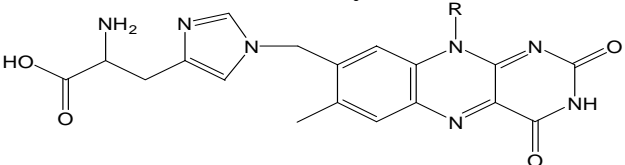
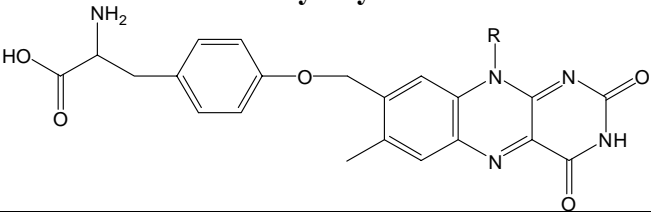
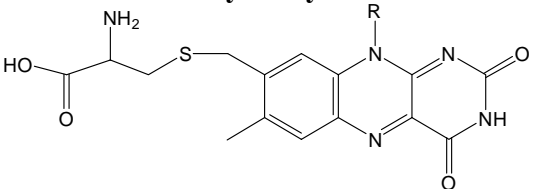
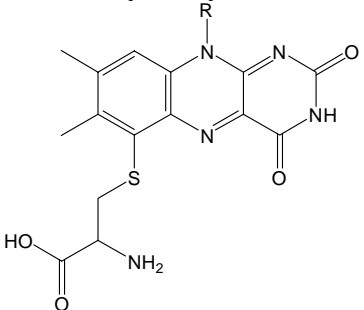
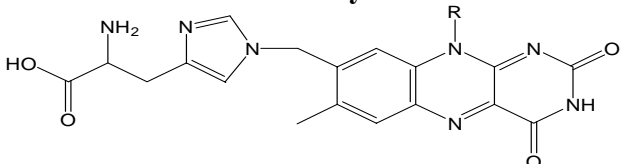
Covalent linkage	Enzyme
<p>8α-N1-Histidyl-FAD</p> 	<p>Some cholesterol oxidase D-Cyclopiazonate oxidocyclase L-Galactonolactone oxidase L-Gulonolactone oxidase Thiamine dehydrogenase</p>
<p>8α-N3-Histidyl-FAD</p> 	<p>Choline oxidase Dimethylglycine dehydrogenase Fumarate reductase Sarcosine dehydrogenase Vanillyl-alcohol oxidase</p>
<p>8α-O-Tyrosyl-FAD</p> 	<p><i>p</i>-Cresol methylhydroxylase 4-Ethylphenol methylenehydroxylase</p>
<p>8α-S-Cysteinyl-FAD</p> 	<p>Monoamine oxidase Flavocytochrome <i>c</i> sulfite dehydrogenase</p>
<p>6-S-Cysteinyl-FMN</p> 	<p>Dimethylamine dehydrogenase Trimethylamine dehydrogenase</p>
<p>8α-N3-Histidyl-FMN</p> 	<p>Sarcosine oxidase Succinate dehydrogenase choline dehydrogenase some cholesterol oxidases</p>

Table 1.2 Covalent linkages of FAD or FMN in known flavoproteins

In isoalloxazine ring, electron-rich xylene moiety and electron-deficient pyrimidine moiety are linked by pyrazine ring to undergo many chemical reactions. Particularly, due to electrophilic character, the N(5) and C(4a) position on pyrazine ring are involved in reversible formation of adducts with nucleophiles. Flavin is known as a biological redox catalyst which undergoes reversible one- and two-electron oxidation-reduction reactions (Ghisla *et al.* 1989).

Besides these known covalent linkages of FAD or FMN, a novel flavinylation of 6-S-cysteinyl, 8 α -N1-histidyl FAD has been found in the crystal structure of glucooligosaccharide oxidase (Huang *et al.* 2005). As shown in Figure 1.3, the FAD cofactor is cross-linked to the enzyme via C⁶ atom and the 8 α -methyl group of the isoalloxazine ring with Cys¹³⁰ and His⁷⁰, respectively.

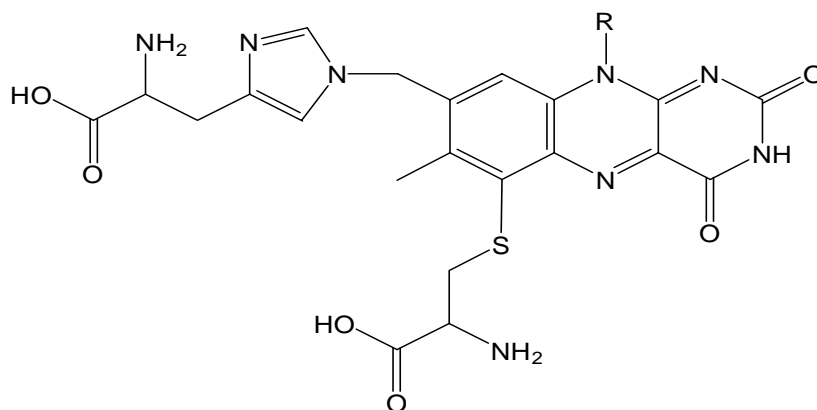
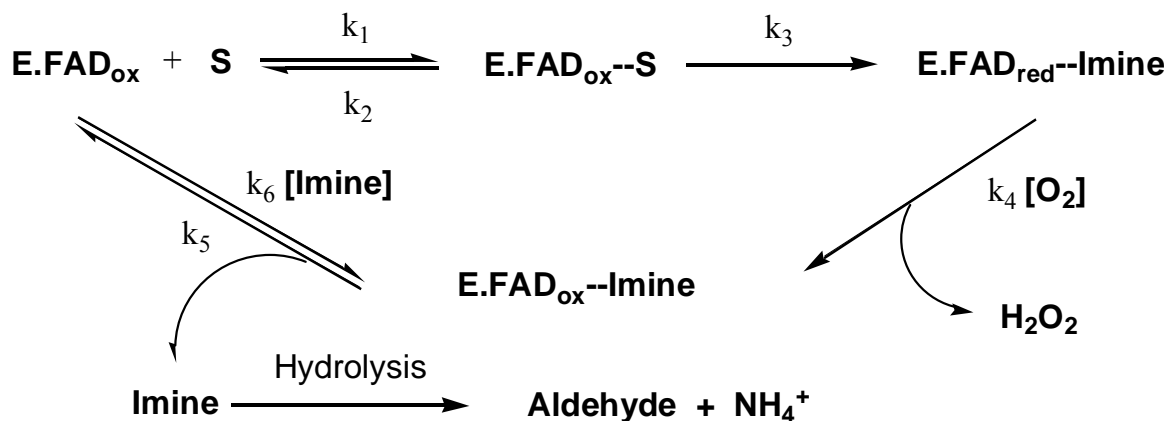


Figure 1.3 6-S-cysteinyl, 8 α -N1-histidyl-FAD

In the case of monoamine oxidase, the UV/Vis absorption spectrum displays absorption peaks at 380 and 450 nm, respectively, resulting from the oxidized form of flavin in which the isoalloxazine chromophore is at the lowest transition (Yue *et al.* 1993).

1.3.4 Catalytic mechanism

Due to the important role of monoamine oxidases in the oxidation of amine neurotransmitters, there are a quite number of literatures on understanding of the catalytic mechanism of monoamine oxidases. Since MAO A is highly homologous with MAO B, it is assumed that both MAO A and MAO B follow the similar chemical mechanisms. The mechanistic pathway for MAO B-catalyzed oxidation of benzylamine supported by considerable amounts of kinetic evidence (Husain *et al.* 1982; Pearce *et al.* 1985; Edmondson *et al.* 1993) is shown in Scheme 1.3 (Ramsay 1991): flavin in oxidation state is reduced by amine substrate to produce reduced enzyme-imine complex; the reduced enzyme-imine complex subsequently is reoxidized by oxygen with subsequent formation of H₂O₂ and the imine product dissociates from the enzyme followed by hydrolysis.



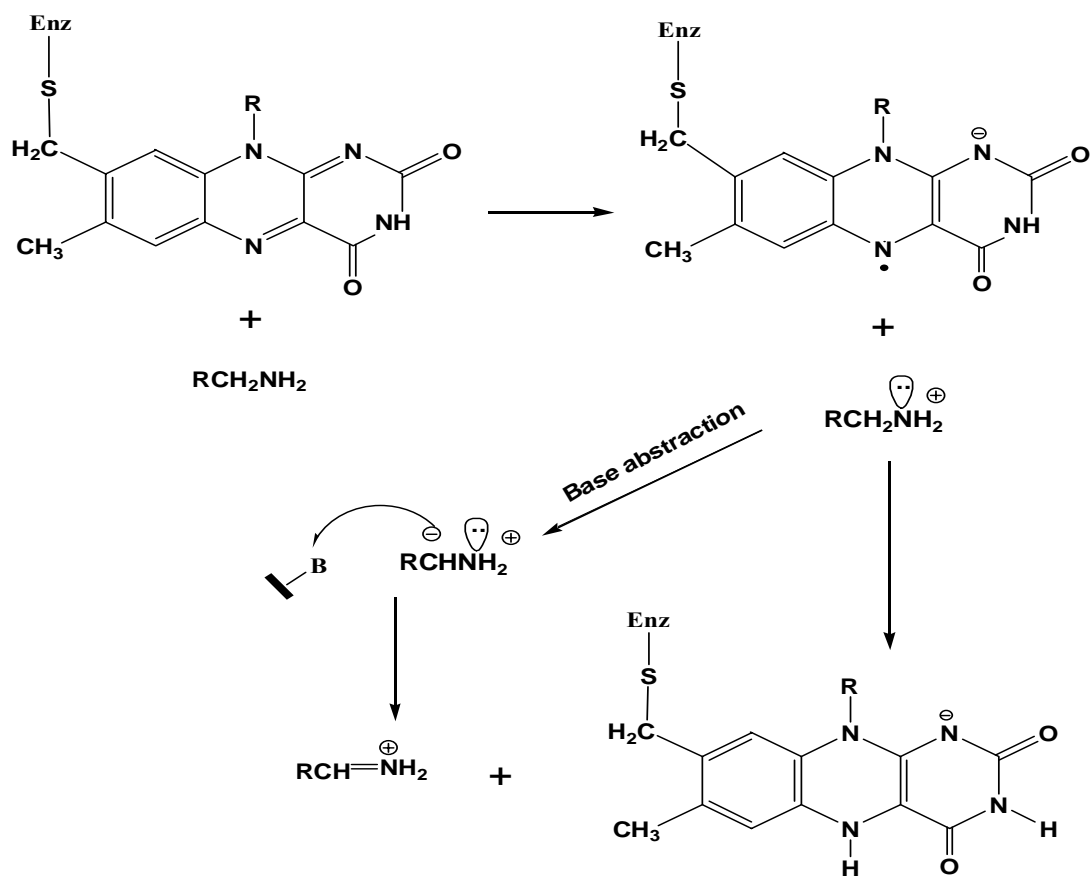
Scheme 1.3 Reaction pathway for the MAO B-catalyzed oxidation of benzylamine

Mechanistic studies on MAO catalysis were not feasible until the success of purifying enzyme from specific tissue (Salach 1979; Salach *et al.* 1981; Weyler *et al.* 1985). Furthermore, the application of recombinant MAO expressed in yeast system

(Weyler *et al.* 1990; Li *et al.* 2002) facilitated development of study on the catalytic mechanism of monoamine oxidase.

1.3.4.1 Aminium cation radical mechanism

In 1980, Silverman and colleagues originally proposed the mechanism of monoamine oxidase B catalysis by electrochemical oxidation of *N*-cyclopropyl benzylamine (Scheme 1.4) (Silverman *et al.* 1980). According to this mechanism, an aminium cation radical intermediate and flavin semiquinone are formed via an initial single-electron transfer (SET) from the amine nitrogen to the oxidized flavin cofactor, followed by α -CH deprotonation and radical migration to the α -carbon of the substrate; subsequently the second SET occurs either directly to the flavin radical or via an amino acid residue to form the resultant products imine and flavin hydroquinone. However, the major problem regarding the validity of aminium cation radical mechanism is the unfavorable redox potentials for the one-electron-transfer step (Walker *et al.* 1994). Moreover, no experimental data, such as detectable EPR signal of a transient flavin semiquinone, is available to support the aminium cation radical mechanism. Thus, more direct and valid data are required to critically investigate aminium cation radical mechanism.

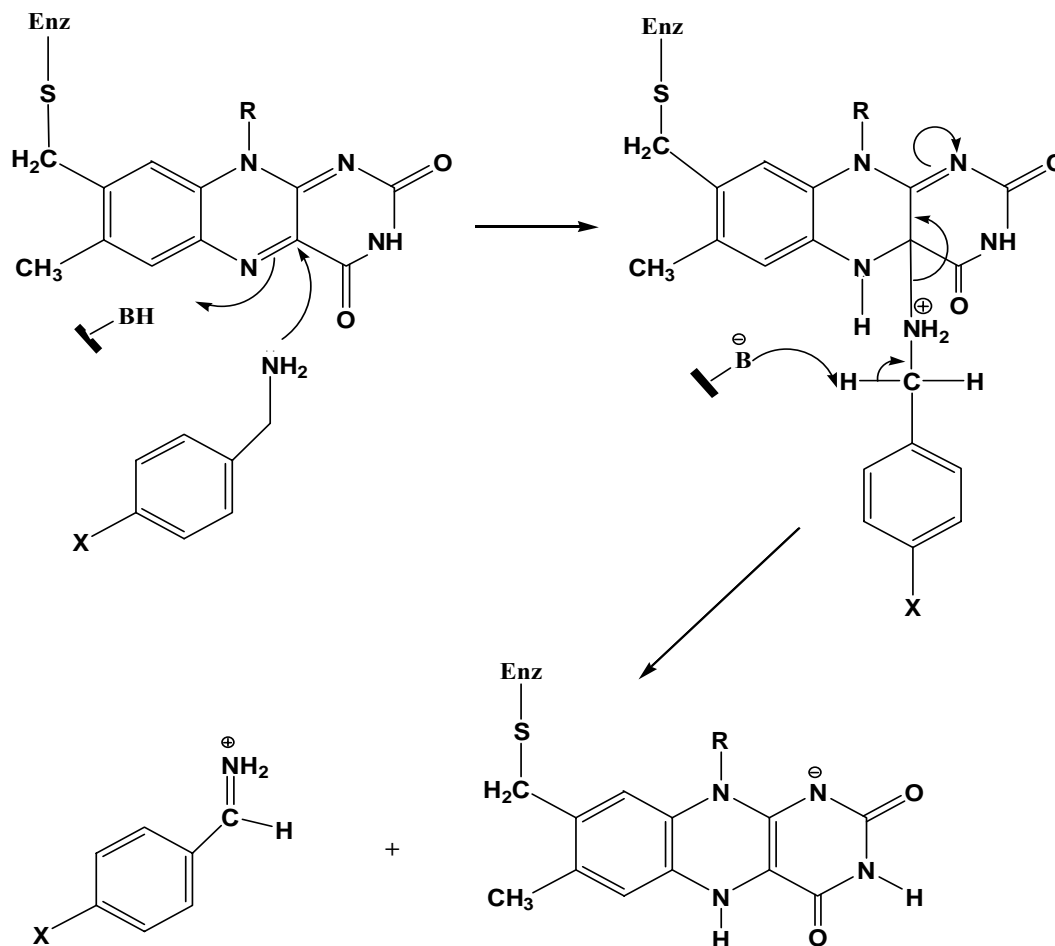


Scheme 1.4 Proposed aminium cation radical mechanism for MAO catalysis

1.3.4.2 Polar nucleophilic mechanism

A polar nucleophilic mechanism, as shown in Scheme 1.5, was originally proposed by Hamilton (Brown *et al.* 1970): the deprotonated amine attacks the flavin 4a position to form an amine-flavin 4a adduct; with assistance of an amino acid residue serving as a base at the active site on the enzyme, a proton is abstracted from α -carbon of amine-flavin 4a adduct, followed by the formation of the protonated imine product which is released from the reduced flavin. Even though oxidative deamination of benzylamine in the presence of N(3)-methylflavin was observed in model system work of Mariano

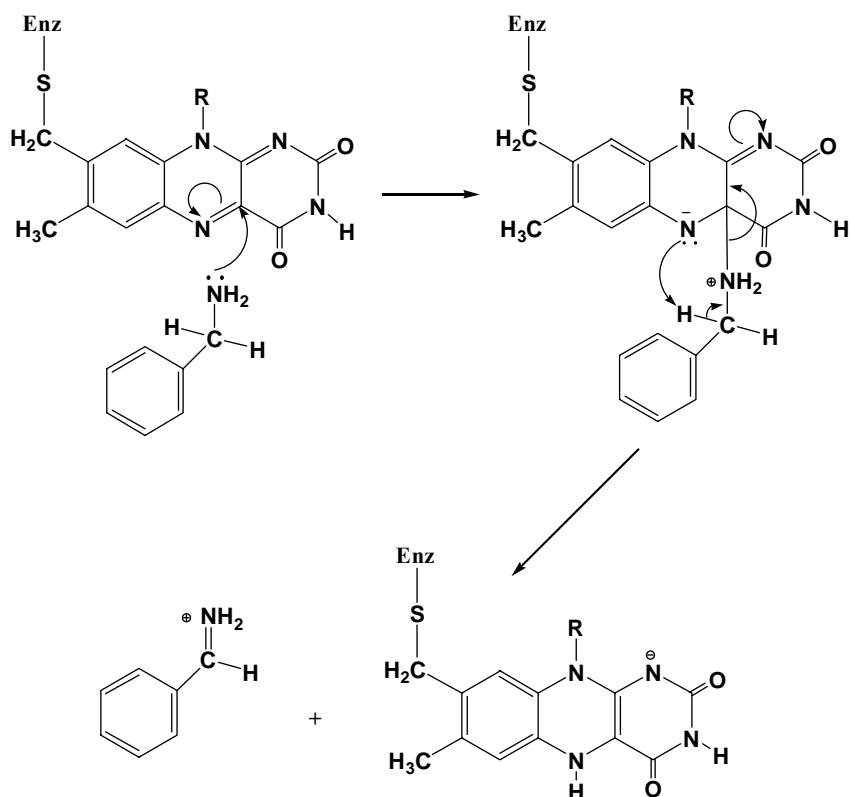
(Kim *et al.* 1993), the more direct evidence obtained from high-resolution crystal structure of MAO B shows no appropriate basic amino acid at the active site is not in agreement with the original polar nucleophilic mechanism (Binda *et al.* 2002). Moreover, no spectroscopically detectable flavin 4a adduct was observed (Walker *et al.* 1994).



Scheme 1.5 Proposed polar nucleophilic mechanism for MAO catalysis

1.3.4.3 Concerted nucleophilic mechanism

On the basis of polar nucleophilic mechanism, Edmondson and colleagues proposed a concerted nucleophilic mechanism for MAO catalysis as shown in Scheme 1.6 (Miller *et al.* 1999): the formation of an amine-flavin-C4a adduct results in the transformation of the N(5) to a very basic site ($\text{pK}_a \sim 25$), the proton from α -carbon of amine substrate is then abstracted by the nitrogen at 5 position of the flavin ring with subsequent formation of the protonated imine product released from the reduced flavin. There are several experimental lines of evidence available to support concerted nucleophilic mechanism. The major one is quantitative structure-activity relationships (QSAR) on a series of *para*-substituted benzylamine analogs, showing that electron-withdrawing *para* substituents increase the limiting rate of α -C-H bond cleavage for MAO A catalysis (Miller *et al.* 1999). Moreover, observed large kinetic isotope effects on the rate of flavin reduction by all amine substrates and the formation of the protonated imine product suggest that α -C-H bond cleavage is rate-limiting step (Miller *et al.* 1999). The similar pK_a of nitrogen at flavin 5 position to that of benzyl proton (~ 30) (Bordwell *et al.* 1992) further supports that N(5) plays a role in proton abstraction in a concerted manner. Therefore, this concerted nucleophilic mechanism is consistent with most existing models and enzymatic mechanistic data.

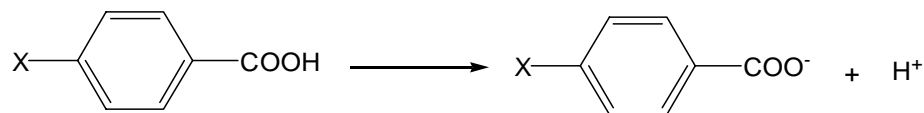


Scheme 1.6 Proposed concerted nucleophilic mechanism for MAO catalysis

1.3.5 Quantitative structure-activity relationships (QSAR)

Quantitative structure-activity relationships (QSAR) are useful approaches to study the correlation between structural properties and activities of compound, providing an understanding of the effect of structure on activity. Nowadays, QSAR studies have been widely applied in many fields, such as drug design and environmental risk assessment.

The early QSAR study was the correlation between electronic properties of organic acid (benzoic acid) and bases with their equilibrium constants and reactivity (Scheme 1.7) which was initially developed by Louis Hammett (Hammett 1935).



Scheme 1.7 **Dissociation of benzoic acid**

The linear relation of the equilibrium constants for the ionization of benzoic acid was found according to Hammett equation (Equation 1.1):

$$\log k_X = \rho\sigma + \log k_H \quad \text{Equation 1.1}$$

where k_x is either an equilibrium constant or a rate constant of substituted compound, k_H is corresponding equilibrium constant for the parent, unsubstituted compound, ρ , the slope of the line, reflects the sensitivity of such a reaction to the electronic effect of the substituents X and σ represents the relative strength of the electron-withdrawing or electron-donating properties of the substituents.

Even though the Hammett equation is a milestone in investigating organic and biochemical reaction mechanisms, there are certain limitations to the application of the Hammett equation. In biological systems, the electronic effect of substituents can be masked by other contributions to provide meaningful QSAR. The Hansch equation, a modification of Hammett equation, has developed a variety of parameters as descriptor of the structural properties of compounds (Equation 1.2) (Hansch *et al.* 1995).

$$\log k(\text{or } K_d) = \rho(\sigma) + A(\pi) + B(V_w)(\text{or } E_s) + C \quad \text{Equation 1.2}$$

in which, k is rate constant reflecting rate of product formation or enzyme turnover, K_d is dissociation constant describing the substrate dissociation constant from all complexes

prior to the isotope-sensitive step, σ is electron donating or withdrawing properties of the substituent, π is lipophilicity of the substituent, V_w is van der Waals volume and E_s is Taft steric parameter representing the steric effect affecting intramolecular and intermolecular hindrance to the reaction or binding.

Multi component analysis is required to determine the contribution of each parameter in Equation 1.2. Based on the assumption that the data has a Gaussian distribution, the F value is utilized to evaluate how good the data fits to the regression analysis (Equation 1.3):

$$F_{1,n} = (n - 2) \frac{r^2}{1 - r^2} \quad \text{Equation 1.3}$$

where r^2 is regression coefficient. In general, a higher F value indicates a better fit.

1.4 Structural biology

Although MAO has been of interest to scientific research and been widely investigated by a variety of genetic, biochemical approaches in the past decades, its pronounced functional role in neurological disorders has not been fully understood which directly affects the design of MAO inhibitors. With the improvement of physical techniques, X-ray crystallography has become a very powerful means to determine the three-dimensional structure of a protein which is valuable for drug design and new potential therapeutic indications.

Among all the deposited crystal structures in protein data bank, the majority of structures are soluble proteins, and only a few 3-D structure of membrane proteins have been solved. As one member of membrane proteins, MAO appears their intrinsic

difficulties, such as purity of protein and solubility in detergent. Moreover, sufficient quantity of protein is also a key factor for crystallization. The use of the efficient *Pichia* protein expression system in our laboratory overcame these limitations. So far, we have solved the crystal structures of human MAO A and MAO B with the collaboration with Mattevi (Binda *et al.* 2002; De Colibus *et al.* 2005), and the structure of rat MAO A was solved by Ito *et al.* (2004).

1.4.1 Human MAO B

The crystal structure of human MAO B complexed with pargyline was initially solved at 3.0 Å resolution by X-ray crystallography using two crystal forms in 2002 (Binda *et al.* 2002). The overall structure reveals a dimeric enzyme with the C-terminal hydrophobic α -helix in each monomer anchored into the phospholipid bilayer (Figure 1.4). The surface area responsible for dimer formation is $\sim 2,095 \text{ \AA}^2$ and accounts for 15% of the total surface area of one human MAO B monomer.

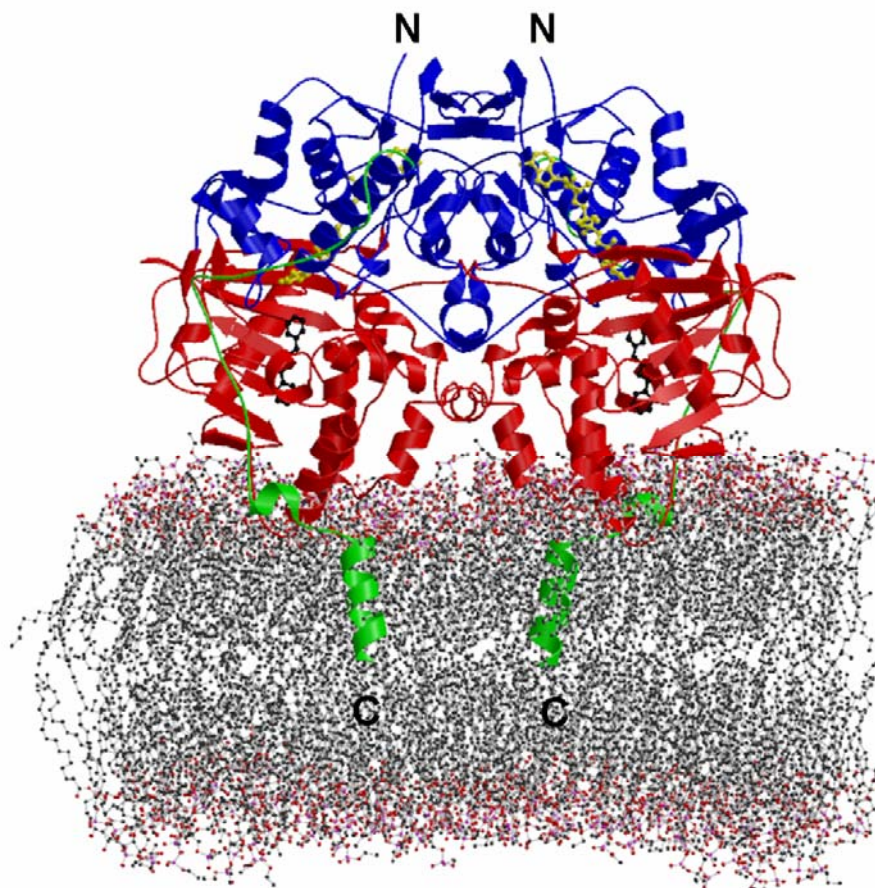


Figure 1.4 Structure of human MAO B dimer. Each monomer consists of three domains: FAD binding domain (in blue), substrate/inhibitor-binding domain (in red) and membrane-binding domain (in green). Flavin cofactor is in yellow.

MAO B contains two cavities termed the “entrance” cavity and the “substrate” cavity, which constitute the substrate path from the protein surface to the covalent flavin (Figure 1.5). The flat substrate cavity nearest the flavin with a volume of 420 \AA^3 is surrounded by aromatic and aliphatic amino acids. The hydrophobic “entrance cavity” with volume of 290 \AA^3 is situated between the active site and the protein surface, and it is shielded from solvent by loop 99-112. This loop is believed to affect the substrate and inhibitor specificities of MAO since its movement would control access of substrates or

inhibitors to the entrance cavity. Residues Phe168, Leu171, Ile199 and Tyr326 serve as a “gate” between the entrance and substrate cavities for the diffusion of substrates.

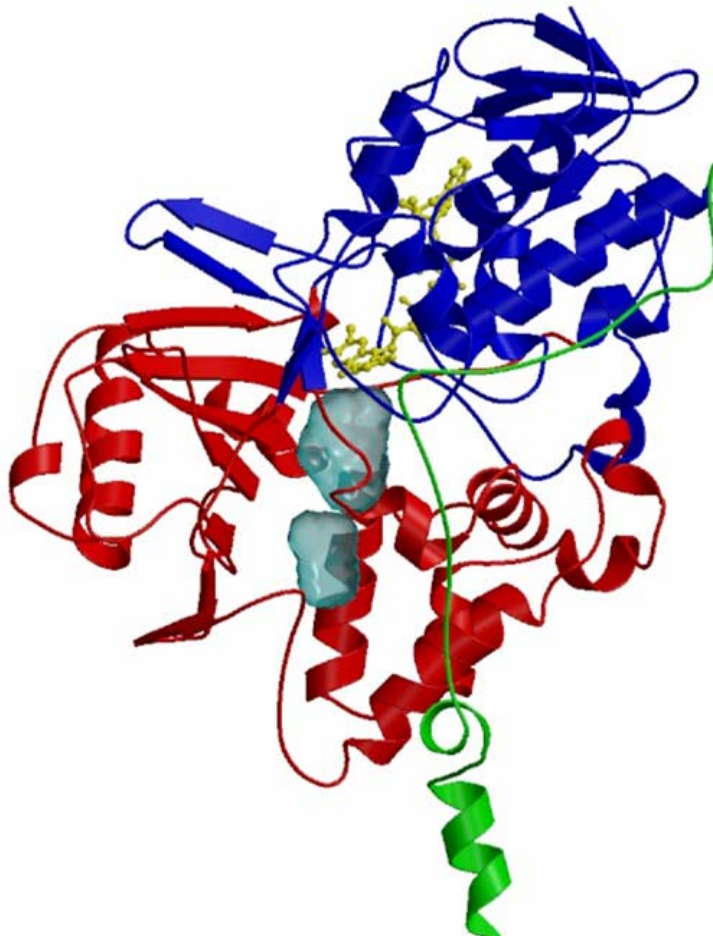


Figure 1.5 Monomeric structure of human MAO B. Human MAO B contains the dipartite cavities (in cyan): substrate cavity (420 \AA^3) adjacent to flavin cofactor, entrance cavity (290 \AA^3) facing the membrane surface.

Additionally, the structure of MAO B in complex with an inhibitor provides insights into the mode of inhibition: pargyline, a specific inhibitor of MAO B, covalently binds to the N5 atom on the *re* side of the flavin (Figure 1.6).

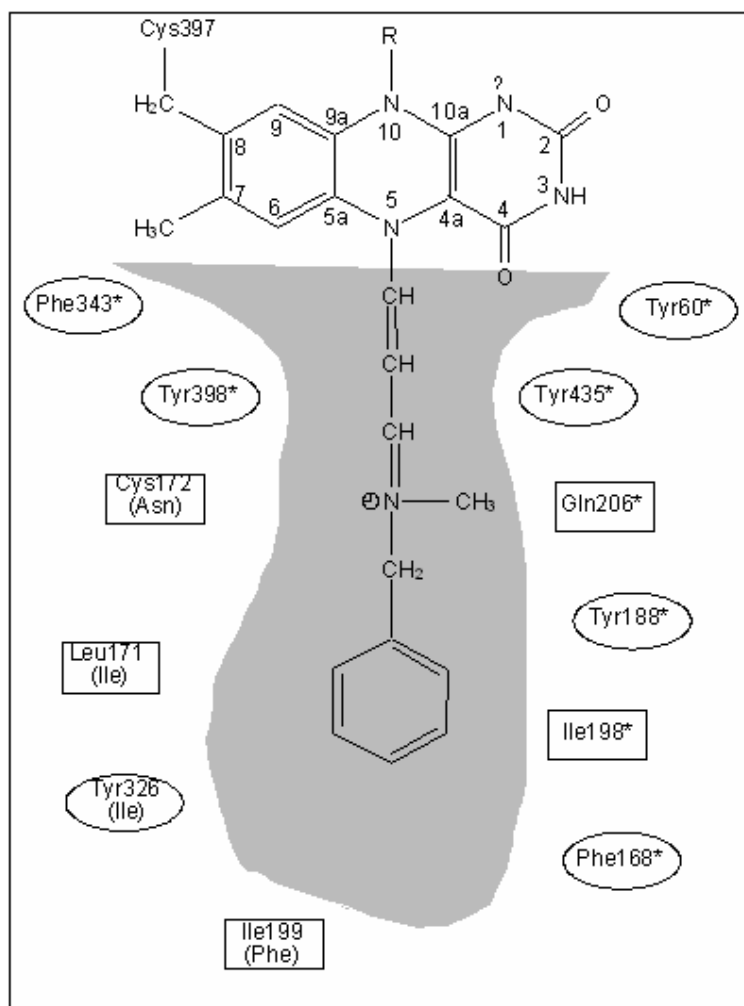


Figure 1.6 Schematic representation of the pargyline binding site in human MAO B. MAO B residues that are conserved in human MAOA are indicated by an asterisk. For nonconserved amino acids, the replacement side chains of MAOA are in parentheses. Aromatic side chains are enclosed in ellipsoidal frames. Other residues are in rectangular boxes. The atoms of the flavin ring are numbered. (Binda *et al.* 2002)

Residues 460-520 on the C-terminus form a membrane binding region. As shown in Figure 1.7, the structure of the C-terminal helix is only solved to position 500, and the last 20 amino acids are missing in the structure, due to the flexibility of these residues leading to this region disordered in the electron density map. The residues 489-500 are thought to be a transmembrane helix and 501-520 is predicted to extend the C-terminal helix to span the membrane. All these hydrophobic residues on the C-terminal helix may facilitate its insertion into the phospholipid bilayer.

A series of truncated human MAO B mutants, at amino acid position 511, 504, 498, 492, 486, 481, 476, 467, 417 and 387, respectively, have been studied (Rebrin *et al.* 2001). These truncations did not abolish the attachment of human MAO B to the membrane, indicating that although the C-terminal transmembrane helix plays an important role in interaction between MAO and membrane, other parts of the sequence may also be involved.

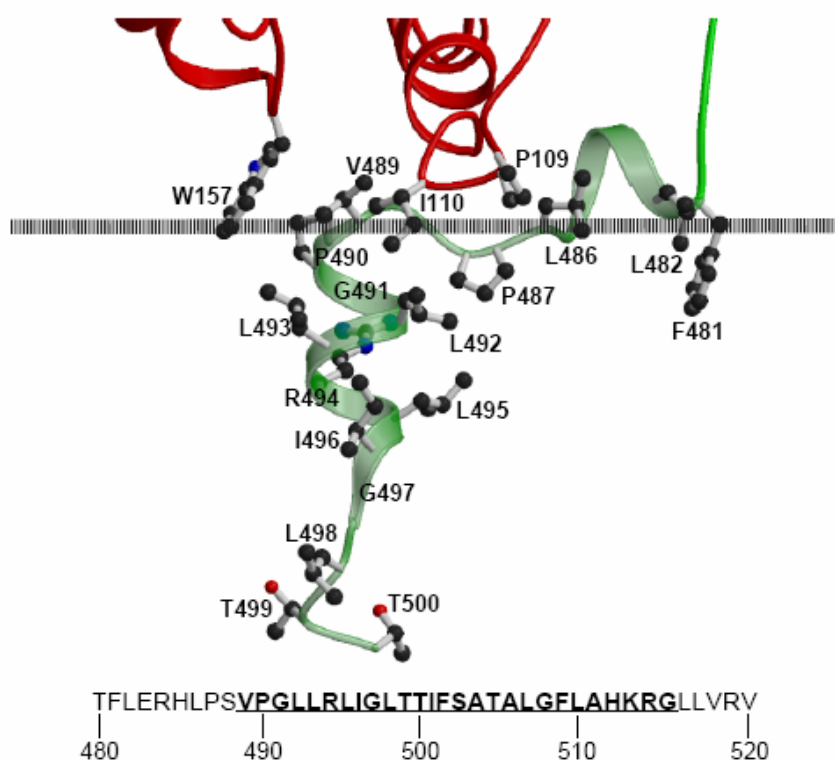


Figure 1.7 The C-terminal transmembrane helix (in semi transparent green) and the neighboring apolar sites involved in membrane binding (in red). Carbon atoms are in black, nitrogen atoms are in blue and oxygen atoms are in red. The gray line indicates the upper boundary of the membrane. Residues 489-515 are predicted to form the transmembrane helix. The last 20 residues (511-520) are not involved in the crystal structure due to not well-defined pattern in electron density map (Binda *et al.* 2002).

The recent crystal structures of human MAO B in complex with several reversible noncovalent inhibitors, such as 1,4-diphenyl-2-butene and isatin have been solved to 1.6 Å (Binda *et al.* 2003; Binda *et al.* 2004). Interestingly, the two cavities, entrance cavity

and substrate cavity observed in isatin-inhibited human MAO B (Figure 1.8 A), are fused into one single cavity when MAO B is in complex with 1,4-diphenyl-2-butene (Figure 1.8, B). Residue Ile199 is proposed to play a critical role in gating the separation of the two cavities by changing its conformation. Site-directed studies on Ile199 further suggest that the mutation of Ile199 to Phe does not show the “open/closed” conformation as observed with Ile199, and Ile199 in human MAO B is responsible for the binding of human MAO B-selective reversible inhibitors such as 1,4-diphenyl-2-butene, farnesol or chlorostyrylcaffeine (Hubalek *et al.* 2005).

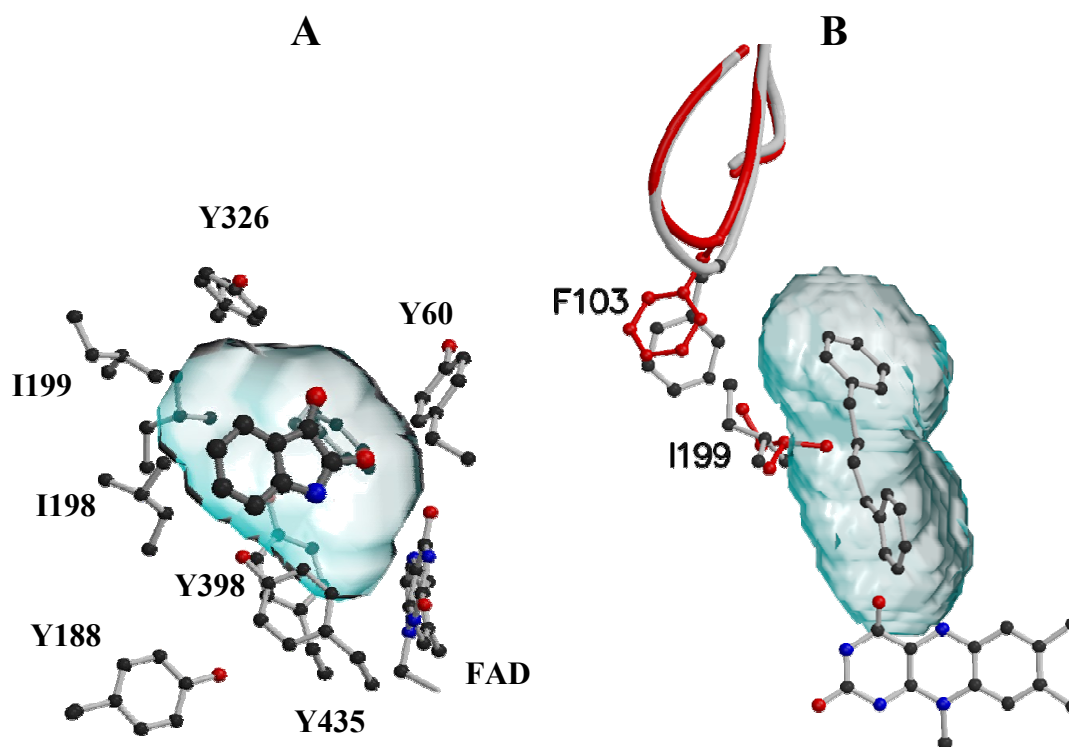


Figure 1.8 Models illustrating the binding modes of isatin (A) and 1,4-diphenyl-2-butene (B) to human MAO B. The surface of the solvent inaccessible substrate-binding cavity is semi-transparent. In isatin binding mode, Ile-199 adopts a “closed” conformation. In 1,4-diphenyl-2-butene-binding mode, Ile-199 (in black) adopts an “open” conformation. In panel B, it is noted that the side chains of Phe103 and Ile-199 (in red, “closed” conformation) of isatin-complexed MAO B are superimposed to 1,4-diphenyl-2-butene-complexed MAO B structure.

1.4.2 Rat MAO A

Before the structure of human MAO A, the crystal structure of rat MAO complexed with clorgyline was solved at 3.2 Å by Ito *et al.* (2004), suggesting that rat MAO A is dimeric (Figure 1.9) even though it packs in a tetrameric formation in the crystal.

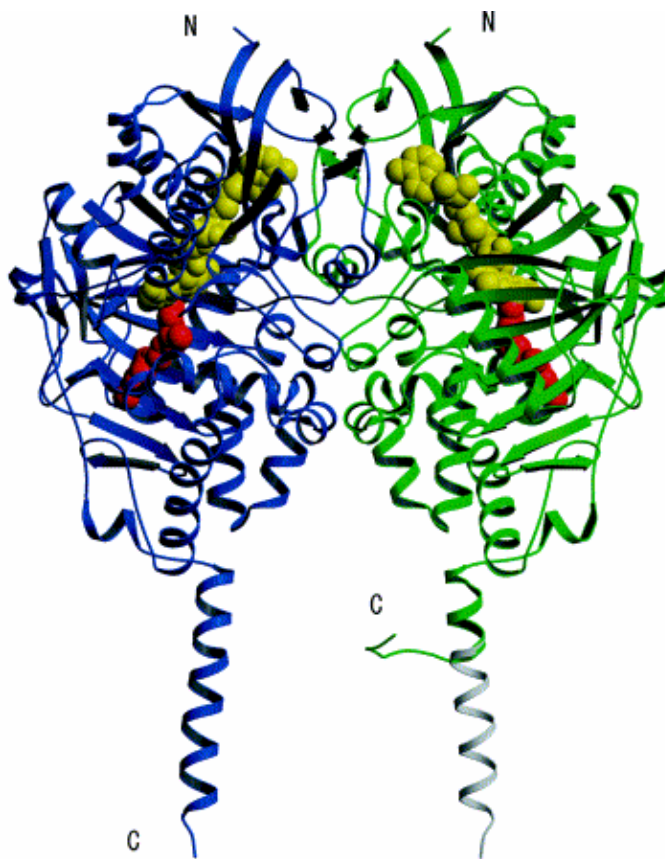


Figure 1.9 Dimeric structure of rat MAO A. FAD cofactor and inhibitor clorgyline, shown as a space-filling model, are in yellow and in red, respectively. The letters N and C represent N-terminus and C-terminus, respectively. The helix in grey is a predicted structure. (Ma *et al.* 2004)

As shown in Figure 1.10, the hydrogen bonding and hydrophobic interactions between FAD cofactor and MAO A protein are believed to stabilize the structures of MAO proteins. Moreover, in the clorgyline-binding site formed by the isoalloxazine rings of FAD and a couple of aromatic residues within MAO A, besides a covalent bond

between clorgyline and FAD, several hydrogen bonding and hydrophobic interactions also play an important role in stabilizing inhibitor binding.

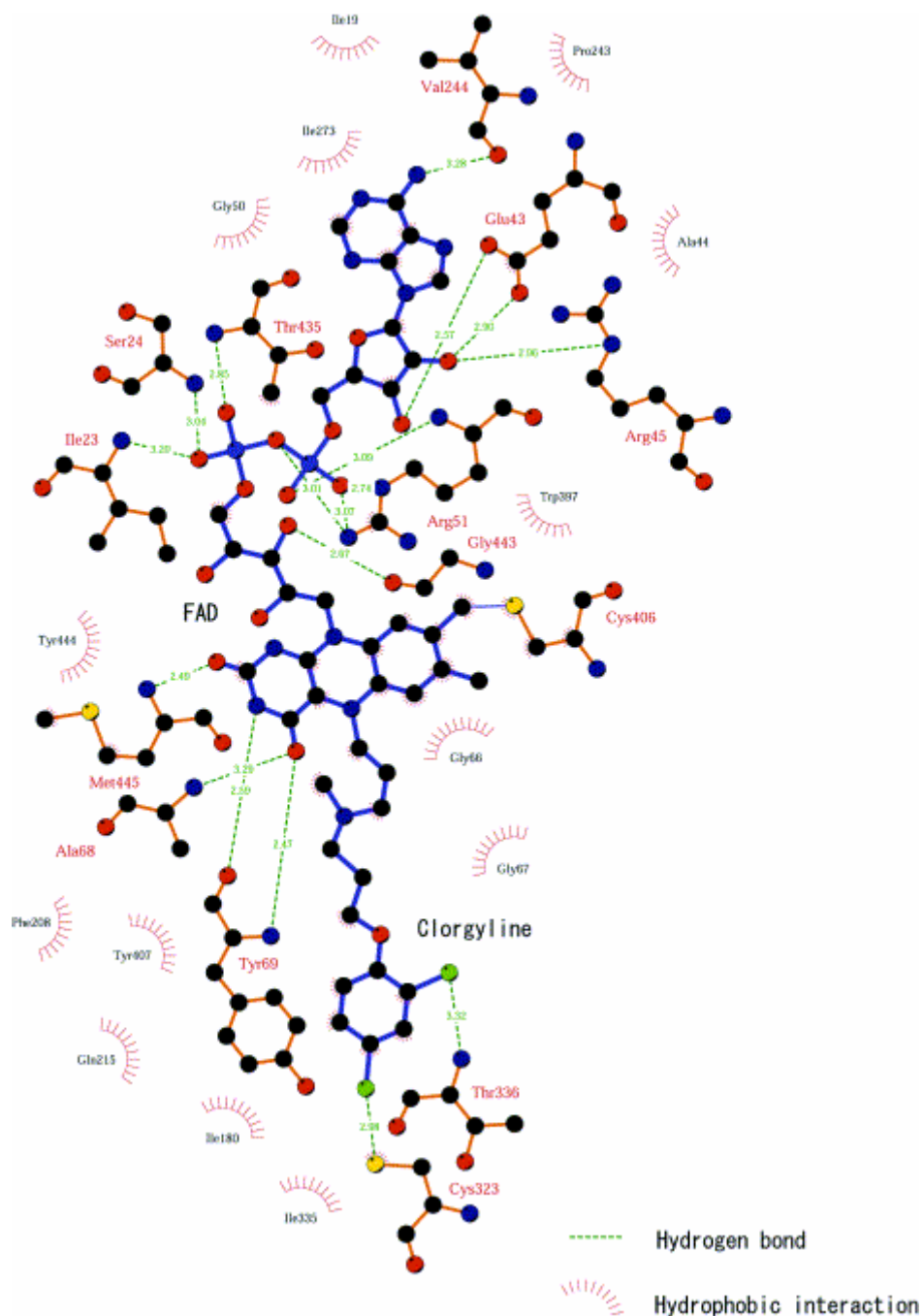


Figure 1.10 LIGPLOT (Wallace *et al.* 1995) illustration of binding of FAD and clorgyline in rat MAO A. The dashed lines represent hydrogen bonds (the distances indicated in angstroms) between FAD and rat MAO A. The residues involved in hydrophobic interactions are shown. (Ma *et al.* 2004)

The superimposed structures of rat MAO A and human MAO B (Figure 1.11) explained why clorgyline is a specific inhibitor for MAO A by the fact that residue Tyr326 in MAO B is in the position of the benzene ring of clorgyline bound to MAO A.

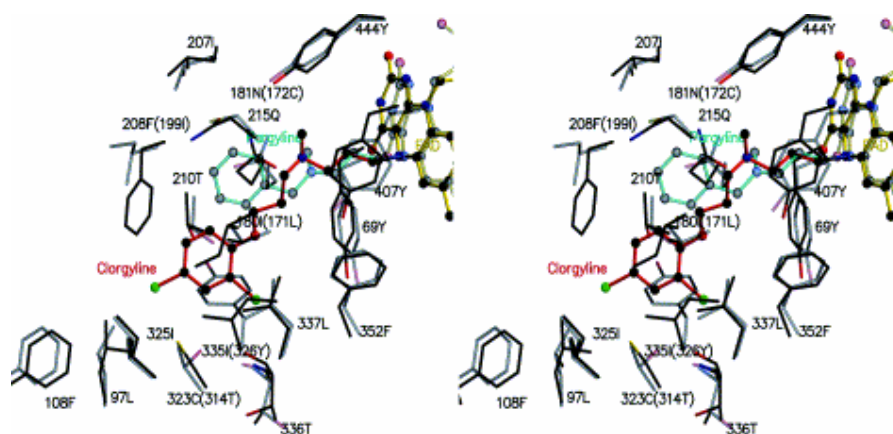


Figure 1.11 Comparison of the active centers of rat MAO A and human MAO B. The C^α atoms of residues 309 to 499 in rat MAO A were fitted to those of residues between 300 and 490 in human MAO B. Residues of MAO protein are labeled according to rat MAO A; the residues differing in human MAO B are labeled in parentheses. The residues of MAO proteins are in black, while FAD is symbolized in yellow ball and stick. Clorgyline bound to rat MAO A is shown in red ball and stick. Pargyline bound to human MAO B is shown in cyan ball and stick. All elements of human MAO B are shown as semi-transparent. (Ma *et al.* 2004)

Due to the low resolution of rat MAO A crystal structure, not much detailed conclusions can be drawn on rat MAO A. The structures at higher resolution are needed in the future.

1.4.3 Human MAO A

Even though human MAO A has 90% sequence identity with rat MAO A and 70% sequence identity with human MAO B, unlike these latter MAO proteins, human MAO A is crystallized as a monomer (3.0 Å) with a unique active site and loop conformation (De Colibus *et al.* 2005).

Two crystal forms of human MAO A with clorgyline grown under identical conditions were analyzed to determine its structure. The solved 506 residues in crystal form II instead of 464 in crystal form I make it possible to visualize the first turns of the C-terminal membrane-bound helix. As shown in Figure 1.12, human MAO A, unlike human MAO B which contains dipartite cavities, consists of a single hydrophobic cavity of 550 Å³ lined by 5 aromatic and 11 aliphatic residues. However, the “aromatic cage” of these two enzymes formed by the covalent FAD cofactor and the two tyrosines in the active sites are identical, in agreement with the fact that both enzymes follow the same catalytic mechanism (Edmondson *et al.* 2004).

Interestingly, the cavity-shaping loop consisting of residues 210-216 within human MAO A shows a quite different conformation from that of human MAO B and rat MAO A (Figure 1.13). The loop in human MAO A (Figure 1.13 A) seems to be more extended, whereas the loop in human MAO B (Figure 1.13 B) is like a coil. In addition, with comparison of the cavity-shaping loop between human and rat MAO A's, despite the identical amino acid sequences in the active sites of these two enzymes, their loop conformations are apparently different. In fact, the conformation of cavity-shaping loop in rat MAO A (Figure 1.13 C) is more similar to the homologous loop in human MAO B. Together with these observations, it is possible that oligomeric state of enzyme would affect the conformation of this loop since both rat MAO A and human MAO B are dimers whereas human MAO A is monomeric. Moreover, the conformation of this loop would affect substrate and inhibitor specificities of MAO proteins since it plays a role as a gate in controlling access of substrates and inhibitors.

In general, the structural differences between human MAO A and rat MAO A, such as oligomeric state and the conformation of the cavity-shaping loop, raise the question that whether the rat is a suitable model for MAO drug development in the human. In this dissertation, functional properties of human MAO A and rat MAO A were compared and some interesting differences between these two enzymes are observed and presented (Chapter 4 and Chapter 5).



Figure 1.12 Monomeric structure of human MAO A. Human MAO A consists of three domains: FAD binding domain in blue (residues 13-88), substrate/inhibitor-binding domain in red (residues 89-219 and 295-399) and membrane-binding domain in green (residues 463-506). Flavin cofactor is in yellow. Unlike human MAO B, human MAO A contains a single hydrophobic cavity indicated in cyan (550 \AA^3). Residues 1-12, 111-115 and 507-527 are not visible in the electron density map. The dashed line connects residues 110-116.

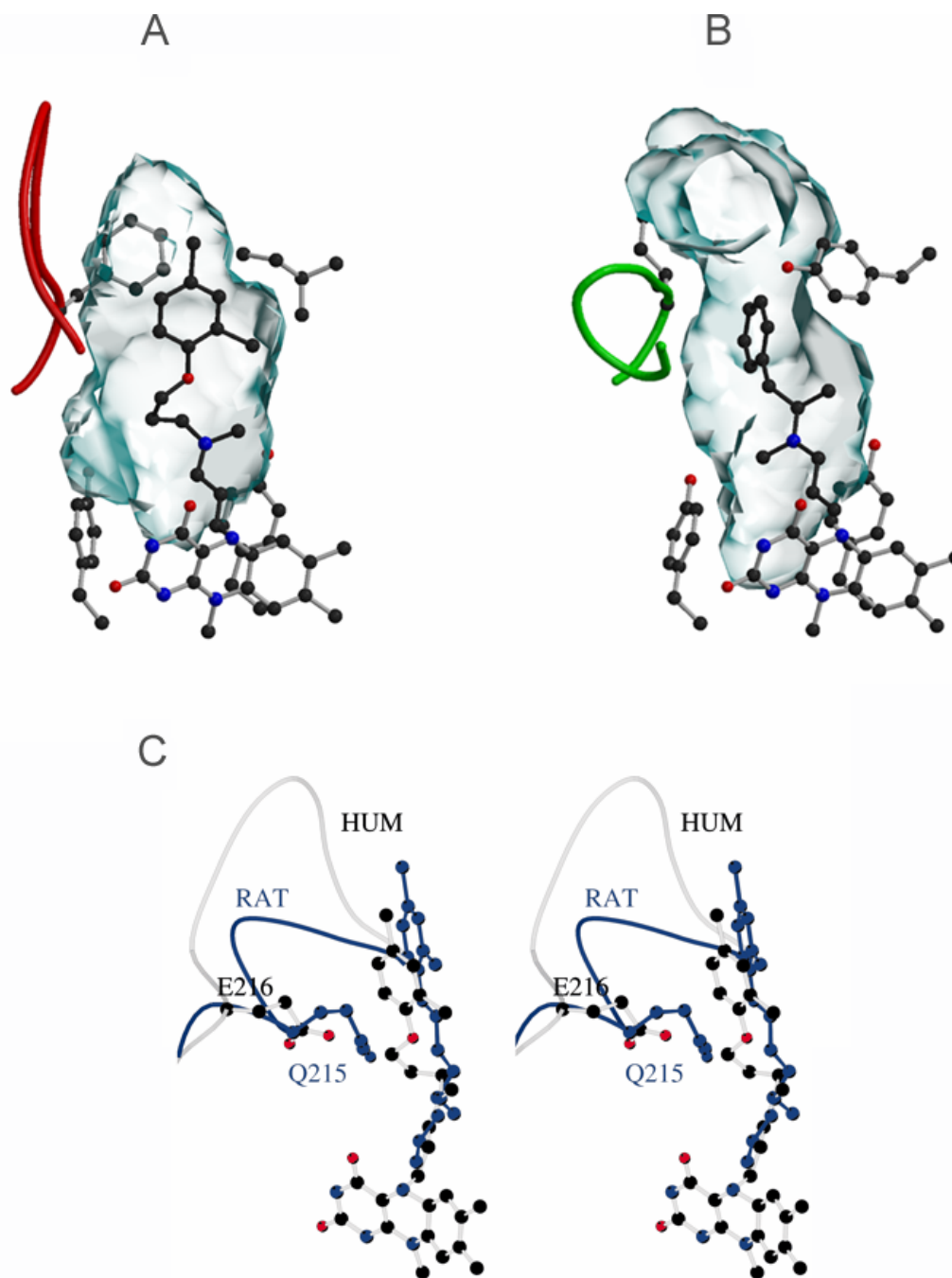
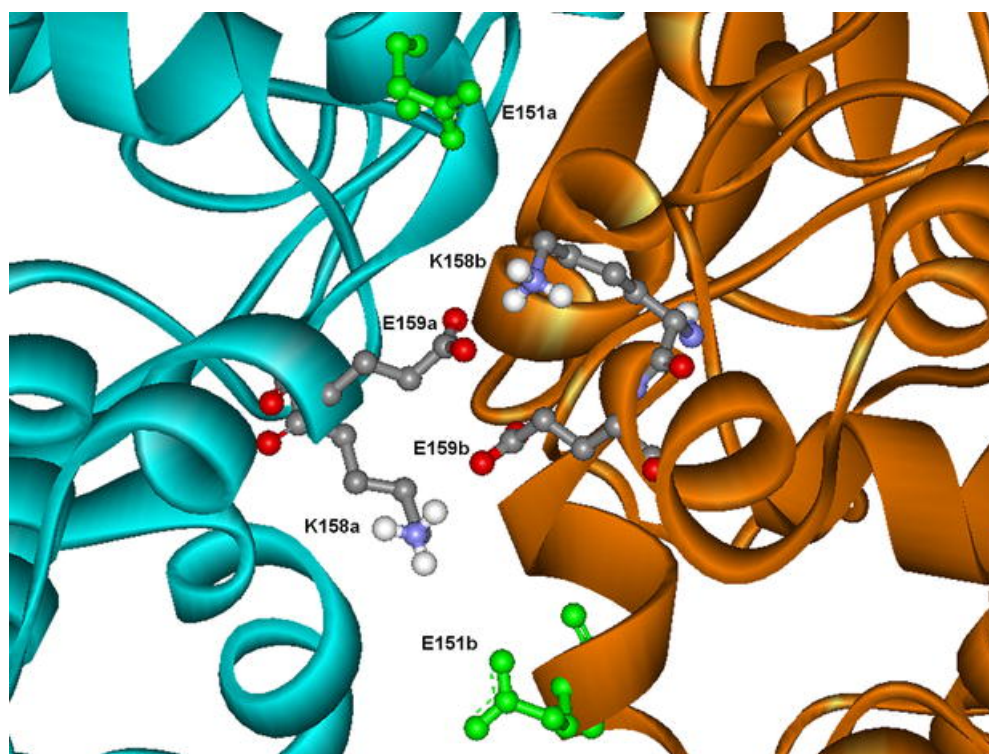


Figure 1.13

Comparison of cavity-shaping loops in human MAO A, human MAO B and rat MAO A. FAD cofactor and the bound inhibitor are shown in ball-stick mode. (A) The loop structure of human MAO A indicated in red. The substrate and inhibitor cavity is shown as a semitransparent cyan surface. (B) The loop structure of human MAO A indicated in green. (C) Superposed structure of human MAO A and rat MAO A using the C^α atoms of the two MAO A structures. Atoms of human MAO A are in grey and atoms of rat MAO A are in blue. (De Colibus *et al.* 2005)

1.4.4 Selective mutation in human MAO A

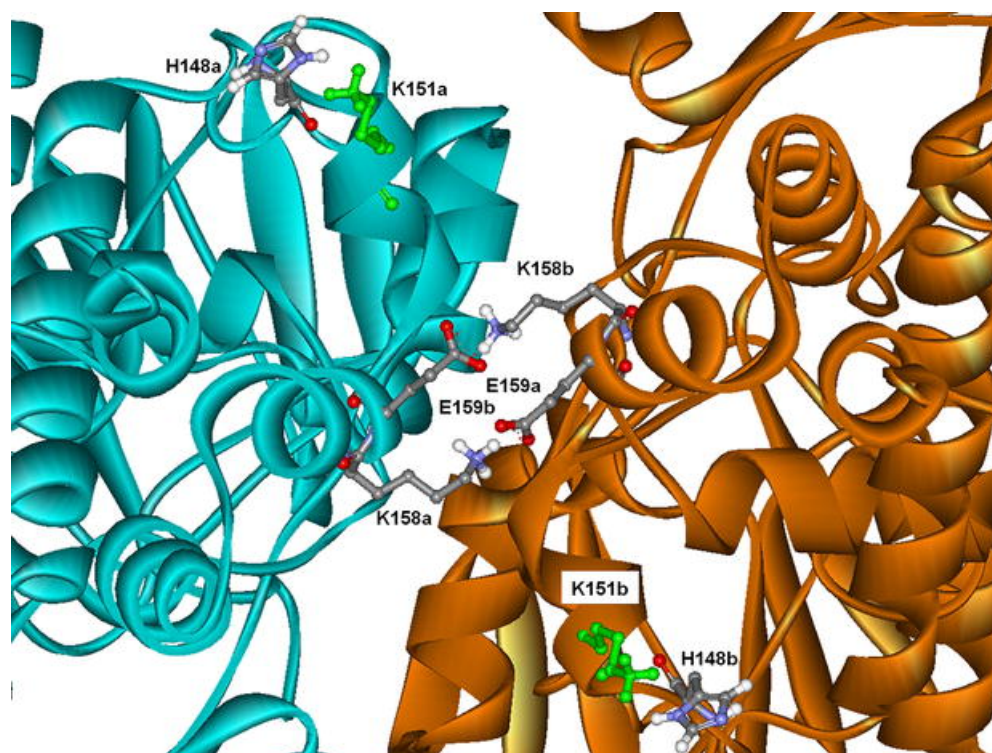
Based on a population genetic analysis of human and other mammalian MAO proteins (including non-human primates), Andrés and colleagues proposed that an exclusive residue mutation exists in human MAO A (Glu151Lys). In other mammalian MAO A's and human MAO B's, there is a conserved glutamate at the corresponding position (Andrés *et al.* 2004). Based on this sequence difference and on modeling studies, Andrés *et al.* proposed human MAO A is monomeric due to this mutation. This modeling study would explain the fact that both human MAO B and rat MAO A are crystallized as dimers whereas human MAO A is a monomer in crystalline form. As shown in Figure 1.14, the amino acid glutamate 151 in non-human MAO A's (142 in MAO B's) is



From Andrés *et al.* (2004).

Figure 1.14 Interface view of the dimer of “non-human” MAO A. Monomer a is in cyan blue and monomer b is in orange. Side-chain atoms of residues Glu151, Lys158 and Glu159 in both monomers are shown in ball-stick mode, in which Lys158 and Glu159 are in grey while Glu151 is in light green.

thought to be involved in dimerization of both monomers (monomer *a* and *b*) via stabilizing two salt bridges formed by Glu159a-Lys158b and Lys158a-Glu159b. In contrast, the presence of Lys at position 151 in human MAO A (Figure 1.15) destabilizes the attraction between Glu159a and Lys158b due to a repulsive interaction of Lys151a with Lys158b. Besides the structural comparison, the calculation of electrostatic energy between two monomers also shows the change of Glu to Lys in human MAO A results in a increase of 73.8 kJ/mol, suggesting this human exclusive selection mutation might reduce stabilization of the MAO A dimer.



From Andrés *et. al.* (2004).

Figure 1.15 Interface view of the predicted dimer of human MAO A. The residue at position 151 is lysine in light green.

Therefore, on the basis of the modeling study, experimental data, such as site-directed mutagenesis on human MAOs and steady-state kinetic analysis, are needed to

verify the prediction of selective mutation in human MAO A gene affecting dimerization of the protein. The functional consequences of human MAO A Lys151Glu mutant are detailedly discussed in Chapter 5 of this dissertation.

1.5 Characterization of mitochondrial membrane associated monoamine oxidase

1.5.1 Lipid composition of mitochondria

A double membrane system (outer membrane and inner membrane) of mitochondria contains lipids and proteins. It has been known that, rather than directly synthesized in mitochondria, most mitochondrial lipids are imported from their site of synthesis, such as the endoplasmic reticulum for eukaryotic cells, to mitochondria (Daum *et al.* 1997). With respect to lipid composition, mitochondria from mammals are similar to that from plant and eukaryotic microorganisms. As shown in Table 1.3, phosphatidylcholine and phosphatidylethanolamine are major phospholipids (~80% of total phospholipids). The level of cardiolipin in inner mitochondrial membrane (IMM), is much higher than in outer mitochondrial membrane (OMM), whereas phosphatidylinositol in IMM is lower than in OMM.

It has been found that aging (Chan *et al.* 1970; Vorbeck *et al.* 1982), diet (Filipowicz *et al.* 1983) and temperature (Mak *et al.* 1983) may affect the composition of lipids.

	Mammalian cells (Rat liver)		Plant cells (Cauliflower)		Yeast (<i>S. cerevisiae</i>)	
	IMM	OMM	IMM	OMM	IMM	OMM
Phospholipid (mg/mg protein)	0.20	0.45	0.41	0.63	0.15	0.91
Sterol (mg/mg protein)	<0.01	0.04	0.03	0.08	0.03	<0.01
	% of total phospholipids					
Phosphatidylcholine	40	54	42	47	38	45
Phosphatidylethanolamine	34	29	38	27	30	23
Phosphatidylinositol	5	13	5	23	8	21
Phosphatidylserine	3	2	--	--	2	3
Cardiolipin	18	<1	15	3	20	6
Phosphatidic acid	--	1	--	--	2	2

Table 1.3 Comparison of lipid composition of mammalian cells, plant cells and yeast.

1.5.2 Effect of phospholipids on functional properties of MAO

Mitochondrial lipids are not only structural elements, but also they significantly affect and regulate functions of proteins in their membranous environments. A number of experimental studies on lipid-protein interactions have demonstrated that the physical state of the lipids in the membrane played a crucial role in the activity of membrane-bound proteins (Lee 1977; Jost 1980; Quinn 1990). Moreover, the theoretical simulations further suggested that lipid-protein interactions of integral membrane proteins are involved in stability and function of such proteins (Feller 2000; Heimburg 2000; Deol *et al.* 2004).

Using purified intact rat brain mitochondria with integrated spin-labeled stearic acids, an early electron spin resonance (ESR) study (Huang 1980) has suggested that the lipid-protein interactions would regulate the functional states of MAO: the functional properties of MAO A was not affected by the fluidity properties of the membrane lipids, whereas the nature of MAO A showed an strong dependence on physical state of the bulk membrane lipids. Huang and colleagues performed a series of phospholipase treatments on purified rat brain mitochondria and found that the loss of an intact gross bilayer by the treatment of phospholipase A dramatically decreased the activities of both MAO A and MAO B, indicating that this intact bilayer structure is required to maintain MAO functional since both enzymes are integral membrane proteins (Huang *et al.* 1980). Interestingly, in the case of phospholipase C digestion, MAO A was inactivated whereas MAO B was intact and activated; phospholipase D slightly inactivated MAO A but significantly decreased activity of MAO B. Further reconstitution studies indicate that high concentration of phospholipids (phosphatidylinositol and phosphatidylserine, but not

phosphatidylethanolamine) could recover the enzymatic activity of MAO in the case of unincorporated phospholipase removed (Navarrowelch *et al.* 1982). These observations suggested that the functional state of MAO A is dependent upon the fluidity of the hydrophobic region of membrane, and ionic and polar characteristics of the surface layer of the membrane plays an important role in modulating MAO B functions.

1.5.3 Targeting signal and membrane association of MAO

In 1992, Ito *et al.* proposed that mitochondrial targeting sequence for rat liver MAO B is located within the 29 C-terminal amino acids by the observations that deletion of 28 amino acid residues at the C-terminus abolished the targeting of the enzyme to membrane, whereas deletion of 55 amino acids in the amino-terminal had no effect on the mitochondrial anchoring of rat MAO B (Mitoma *et al.* 1992). This finding is consistent with the structure of MAO that this enzyme does not contain the typical residues at the N-terminus responsible for the targeting and anchoring (Shore *et al.* 1995). The C-terminal truncated mutant of human MAO B further confirmed the important role of C-terminus in mitochondrial attachment (Rebrin *et al.* 2001). On the other hand, the function and insertion of MAO A were not influenced by the deletion of C-terminal 24 amino acids (Weyler 1994), suggesting that C-termini of MAO A and MAO B follow different targeting and insertion mechanism.

In all known crystal structure of MAOs, the last several residues are not solved due to their flexibility so that they are disordered in the crystals. The conformation of these residues in the membrane is still elusive. In our laboratory, biochemical labeling approach has been used and it provided insight into the membrane portion of C-terminal

α -helix, whether the terminus of the transmembrane helix traverses the outer mitochondrial membrane or turns back toward the surface of membrane (Chapter 3).

1.6 Dissertation objectives

Monoamine oxidase A and B (MAO A and MAO B) are flavoproteins and play an important role in the degradation of neurotransmitter as well as metabolism of biogenic and xenobiotic amines. Although these two mitochondrial membrane bound proteins have been extensively studied for decades including structural breakthroughs on human MAO A, human MAO B and rat MAO A (Binda *et al.* 2002; Ma *et al.* 2004; De Colibus *et al.* 2005), some aspects of structural and functional properties are still elusive. The main objectives of this dissertation involve the corresponding structural studies on human MAO A and MAO B, as well as comparison of functional consequences between human and rat MAO A's.

The first objective is, using fluorescence resonance energy transfer (FRET) technique, to investigate and to compare the structural properties of human MAO A and MAO B in solubilized form with their corresponding crystal structures. A comprehensive study of the reactivity of thiol groups with N-ethylmaleimide in our laboratory has shown that, if MAO is inhibited by its inhibitor, only the cysteine on the surface of the protein (Cys266 in human MAO A and Cys5 in human MAO B) would react with thiol reactive reagent, whereas other cysteines buried in interior of protein would not (Hubalek *et al.* 2003). Therefore, this property allows us to determine the distance between the chromophore in the active site and the top of the enzyme by FRET. Moreover, mutant forms of human MAO A and MAO B in which the reactive thiol groups at Cys266 (MAO

A) and Cys5 (MAO B) were replaced by Ala and thiol groups are now positioned near the end of the C-terminal helix at Pro525 (MAO A) and Val518 (MAO B). These mutants permit distance determinations between the chromophore in the active site cavity and the end of their respective C-terminal helices.

The second objective is to investigate the conformation of the end of C-terminal helices of human MAO A and MAO B in membrane bound form. The last several residues at C-terminal helices of MAOs in solved crystal structures (residues 507-527 in MAO A and residues 501-520 in MAO B) are not visible in electron density maps, thus it is still not known whether their C-terminal transmembrane helices traverse the outer mitochondrial membrane or turn back toward the surface of membrane. Chapter 3 describes fluorescence quenching experiments utilized in membrane system to answer this question. The cysteines on the C-terminal helices of Cys266Ala/Pro525Cys MAO A mutant and Cys5Ala/Val518Cys MAO B mutant, the same mutants as in FRET analysis, were labeled by a thiol reactive fluorescent reagent. In order to rule out non-specific labeling in membrane system, Cys525 of clorgyline-inhibited MAO A and Cys518 of pargyline-inhibited-MAO B in detergent solubilized form were selectively labeled with fluorophore, respectively, followed by reconstituted into membrane. Fluorescence quenching technique provides insight into the conformation of C-terminal helices of both human MAO A and MAO B.

In our laboratory, recombinant human liver MAO A and MAO B have been successfully expressed and purified in *P. pastoris* (Newton-Vinson *et al.* 2000; Li *et al.* 2002), providing copious amount of purified enzymes for structural and mechanistic studies. Although Ma *et al.* (Ma *et al.* 2004) have expressed His-tagged full-length rat

MAO A in *Saccharomyces cerevisiae*, the yield of purified protein is not as high as *Pichia pastoris* expression system used for human MAO A and MAO B. The third objective is, taking advantage of success on human MAO A and MAO B, to improve expression and purification level of rat MAO A. As will be documented in this dissertation, the *P. pastoris* expression system is superior to the *S. cerevisiae* expression system of rat MAO A. Moreover, a slightly different purification procedure of rat MAO A rather than human MAO A suggests that these two enzymes have some structural differences.

The fourth objective to investigate the functional properties of human MAO A, human MAO A Lys151Glu mutant and rat MAO A. Thermal stability profiles provide information about structural stability. Detailed kinetics data using various substrates and competitive inhibitors demonstrate the functional relationship among these enzymes. A series of *p*-substituted benzylamine analogues were used to investigate structure and activity relationship in human MAO A, human MAO A Lys151Glu mutant and rat MAO A. The observed large isotope effects suggest these enzymes follow α -C-H bond cleavage mechanism. The QSAR correlations of the dissociation constants (rate constants) provide insight into the structure of MAO A substrate-binding site.

Chapter 2

Fluorescent Probes to Investigate the Structural Properties of Human MAO A and MAO B

2.1 Introduction

The 3-D structures of human MAO A and MAO B have been solved by X-ray crystallography (Binda *et al.* 2002; De Colibus *et al.* 2005). However, crystal data only reveal the structural properties of MAOs in crystalline form, and may not reflect the dynamic conformations of MAOs in their native states. Moreover, as stated in Chapter 1, the conformations of the C-termini of human MAO A and B (residues 507-527 in MAO A and residues 501-520 in MAO B) are still unknown since these residues are not well defined in electron density maps. Therefore, it would be valuable to investigate the overall architectures of MAOs in their biological system, as well as the conformation of C-terminal transmembrane helix, whether it is flexible in solubilized form. In this chapter, biochemical approaches, such as fluorescence resonance energy transfer, were used to provide insights into structural properties of human MAO A and B in their detergent solubilized form.

Fluorescence resonance energy transfer (FRET), a distance-dependent physical process, has been widely used in biological science, such as protein-protein interaction and molecular interactions inside living cells. The basic principle of this technique is that energy transfer occurs, if donor and acceptor are separated by a certain distance (20-60 Å) as well as the emission wavelength of excited donor overlaps the absorption spectrum of acceptor (Lakowicz 1983). With regard to MAOs, it would be of interest to determine the

overall architectures, such as entire length of the enzymes in detergent solubilized form using FRET technique. According to the solved crystal structures, the entire length of MAO (~100 Å) exceeds the measurable distances of FRET. Therefore, the active site of MAO would be a candidate as a middle point to measure distances to areas of the molecule discussed above.

MAO can be irreversibly inactivated by propargylamines, such as pargyline, in which the triple bond β to the amine nitrogen on the *re* side of the flavin forms a covalent flavocyanine adduct with cofactor (Swett *et al.* 1963). Moreover, Rando initially reported the utility of the dansyl chromophoric group (5-(dimethylamino)-1-naphthalenesulfonamido) as a probe of MAO (Rando 1977). This fluorescence probe has been extensively utilized for sensing or labeling purposes in terms of its spectroscopic properties. In this project, a dansyl group was attached to pargyline by synthesizing 5'-(N-dansyl)-cadaveryl-*p*-carboxymethylpargyline (DCP) (Figure 2.1) according to a published procedure (Rando 1977). Correspondingly, with inhibition by DCP, the active site of MAO is specifically fluorescently labeled.

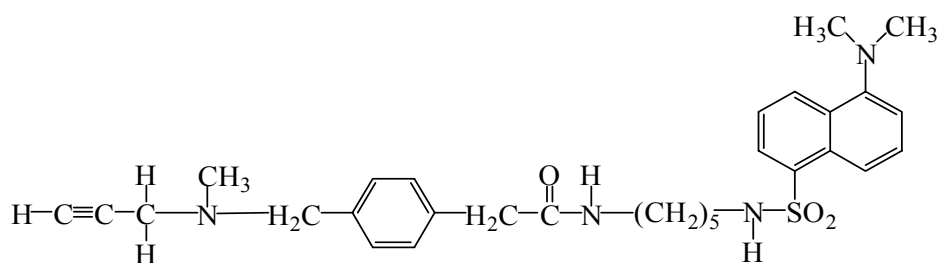


Figure 2.1 Chemical structure of DCP

Due to the reactivity of the S-H bond, a cysteine would be an appropriate target for acceptor labeling. Human MAO A and MAO B each contain 9 cysteine residues, in

which one cysteine residue (407 in MAO A and 397 in MAO B) is covalently attached in a thioether linkage to the FAD cofactor (Weyler 1989). The solved crystal structures of MAOs indicate that, except Cys266 in MAO A and Cys5 in MAO B which are situated on the surface of the protein relative to the membrane binding region, other cysteine residues are “buried” below the surface of the protein. A comprehensive study of the reactivity of thiol groups with N-ethylmaleimide in our laboratory used mass spectrometry to probe the thiol reactivity of both MAO A and MAO B in aqueous detergent solution as well as in the mitochondrial membrane. These data showed that Cys266 (MAO A) and Cys5 (MAO B) are reactive with biotinylated NEM in membrane preparations and that the level of thiol reactivity of either enzyme in detergent solutions is dependent on the temperature and the binding of acetylenic inhibitors to the active sites (Hubalek *et al.* 2003). This observation could be due to the rigidity of inhibited MAO so that sulfhydryl-reactive reagent would not be accessible to cysteines buried in interior of protein. This high level of specificity and selectivity of thiol reactivity in MAOs provides a feasible way to site-directedly label Cys266 of MAO A and Cys5 of MAO B by thiol-reactive probes, respectively. When the emission wavelength of the fluorescent probe in the active site effectively overlaps the excitation of a thiol-reactive probe, FRET will occur, and the distances between the active site and Cys266 in MAO A or Cys5 in MAO B, respectively, can be measured.

FRET can be likewise applied to determine the distance between the active site and the C-terminus of the transmembrane helix of MAO in the same manner. Because there is no cysteine on C-termini of MAO A and MAO B, Pro525 of MAO A and Val518 of MAO B were substituted with cysteine, respectively. It is noted that Cys266 (MAO A)

and Cys5 (MAO B) on the top surface of the molecule were mutated to alanine to rule out their interference with specific labeling on the C-termini of MAO A and B by thiol-reactive probes. As a result, mutant Pro525Cys-Cys266Ala of MAO A and Val518Cys-Cys5Ala of MAO B were generated for FRET measurements.

The fluorescent probe 4-dimethylaminophenylazophenyl-4'-maleimide (DABMI) (Figure 2.2), a thiol reactive reagent, was used as an acceptor in FRET analysis.

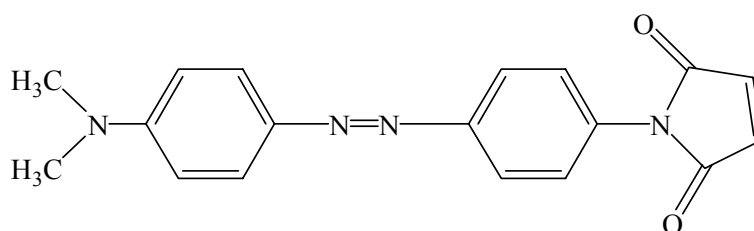


Figure 2.2 Chemical structure of 4-dimethylaminophenylazophenyl-4'-maleimide (DABMI)

Therefore, combination of the distances from the active site to the surface of MAO and to the C-terminus of the transmembrane helix of MAO would provide insights into whether these two proteins exhibit similar structures in their detergent solubilized forms as in their crystalline forms determined by X-ray crystallography.

2.2 Materials and Methods

2.2.1 Materials

Dansylcadaverine and *p*-bromomethylphenylacetic acid were purchased from Sigma. Reduced Triton X-100 and N-methylpropargylamine were from Fluka. 4-dimethylaminophenylazophenyl-4'-maleimide (DABMI) was from Molecular Probes. Unless noted, all other chemicals were purchased from Fisher.

2.2.2 Creation and transformation of site-specific double mutants of MAO A and MAO B

All site-specific double mutants of human MAO A and MAO B were created using QuikChange XL Site-Directed Mutagenesis Kit (STRATAGENE). The mutagenic primers used in this study are listed in Table 2.1. The PCR amplifications and the subsequent cloning steps were carried out according to the manufacturer's instruction.

The constructs of human MAO A C266A/P525C in pPIC3.5K vector and human MAO B C5A/V518C in pPIC3.5K vector were linearized with *Sal* I and *Sac* I, respectively, to target integration at the AOXI locus in the *Pichia* genome. The spheroplast transformation of the mutated MAO genes into the yeast strain KM71 was performed by the method described previously (Li *et al.* 2002).

Desired mutation		Primer sequence
MAO A	Cys-266→Ala	5'-C CAT GAA CAT TAT GAG <u>GCC</u> AAA TAC GTA ATT AAT GCG-3'
	Pro-525→Cys	5'-TAC AAA TAC AAG CTC CTG <u>TGC</u> CGG TCT TGA
MAO B	Cys-5→Ala	5'-ATG AGC AAC AAA <u>GCC</u> GAC GTG GTC GTG GTG-3'
	Val-518→Cys	5'-GCC CAC AAA AGG GGG CTA CTT <u>TGT</u> AGA GTC TAA-3'

Table 2.1 Oligonucleotides used for site-directed mutagenesis of human MAO A and human MAO B genes

2.2.3 Expression and purification of human MAO A and human MAO B

double mutants

All mutants were overexpressed in the methylotrophic yeast *Pichia pastoris* and purified as described previously (Newton-Vinson *et al.* 2000; Li *et al.* 2002). The purified mutant proteins were stored in 50 mM potassium phosphate (pH 7.2) containing 20% glycerol and 0.8% (w/v) β -octyl-glucopyranoside.

2.2.4 Synthesis of 5'-(N-dansyl)-cadaveryl-*p*-carboxymethylpargyline (DCP)

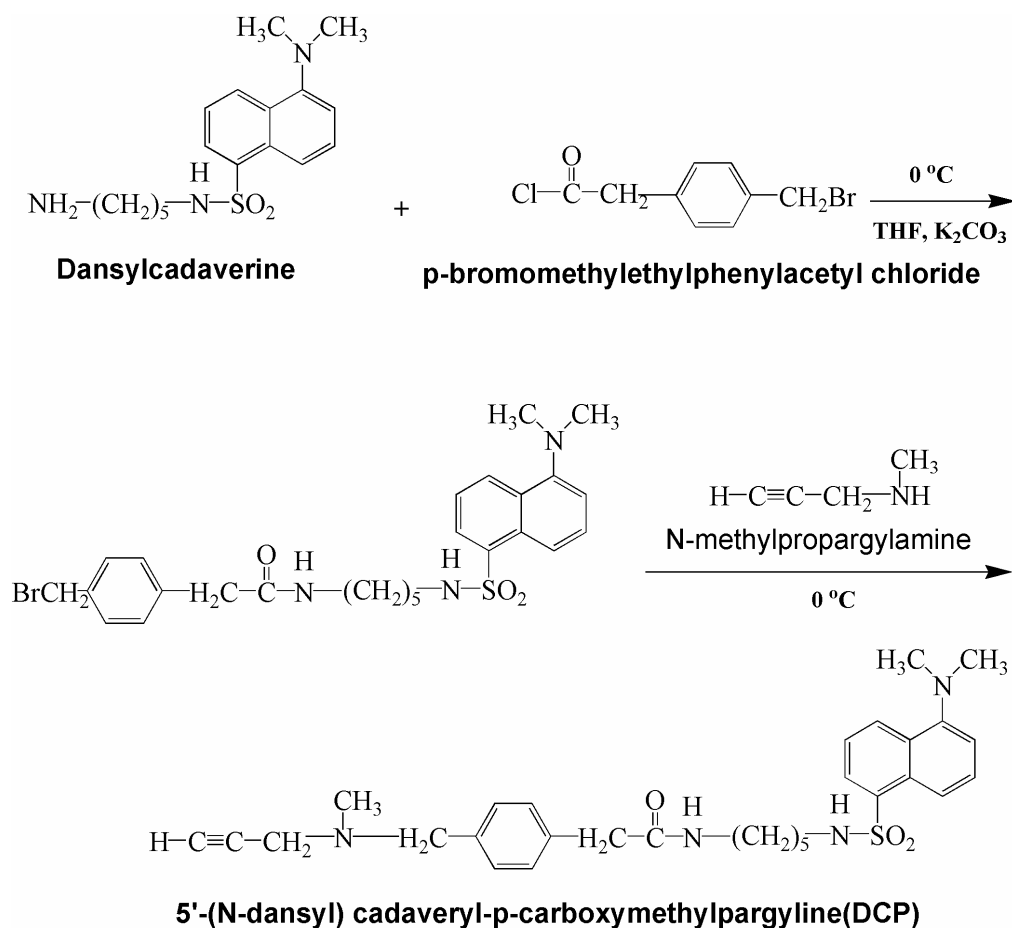
5'-(N-Dansyl)-cadaveryl-*p*-carboxymethylpargyline (DCP) was synthesized as described by Rando (Rando 1977). *p*-Bromomethylphenylacetyl chloride was prepared by thionyl chloride treatment of *p*-bromomethylphenylacetic acid. The overall synthesis pathway is summarized in Scheme 2.1.

The DCP was purified by thin-layer chromatography on the plates that is coated silica gel 60 W plates without fluorescent indicators. After purification of the crude product, a single migrating fluorescent band was observed in a 5% (v/v) methanol-chloroform solvent with $R_f = 0.46$. The NMR spectrum ($CDCl_3$) of DCP showed a quartet (benz-H) at 8.4 δ , a multiplet (naph-H) at 7.3 δ , a singlet (benz-CH₂-N) at 3.5 δ and a triplet (H-C \equiv C) at 2.2 δ . Low-resolution FAB-LSIMS data showed a single mass peak with $m/z = 535.4$ ($M + 1H^+$), consistent with the molecular weight of DCP (534.3).

2.2.5 Time course of wild-type MAO inhibition by DCP

Human wild-type MAO A and MAO B (5 μ M) were incubated with a 20-fold excess DCP at 15°C in the dark. For MAO A, at certain time intervals, 10 μ L aliquots

were removed and immediately added to 1 ml of 1 mM kynuramine in assay buffer (50 mM potassium phosphate, 0.5% reduced Triton X-100, pH 7.5) incubated at 25°C. The rate of oxidation of kynuramine was followed spectrophotometrically by monitoring the formation of product 4-hydroxyquinone with characteristic absorption at 316 nm. The measurement condition of MAO B was similar to that of MAO A, except that the substrate was benzylamine (3 mM) and the product was benzaldehyde with characteristic absorption at 250 nm.



Scheme 2.1 Synthetic pathway to prepare 5'-(N-dansyl)-cadaveryl-*p*-carboxymethylpargyline (DCP)

2.2.6 Labeling of human MAO enzymes with DCP

The purified human wild-type MAO A and MAO A C266A/P525C (~20 μ M) in 25 mM potassium phosphate containing 20% glycerol and 0.8% (w/v) β -octyl-glucopyranoside (OGP) were incubated with 20 fold excess DCP (~400 μ M) at 4°C on a rotating wheel (10-20 r.p.m.) in the dark. The inhibition of wild-type MAO B and MAO B C5A/V518C was carried out in a similar way at room temperature. Aliquots were removed and subjected to activity assay (kynuramine as substrate for MAO A's, benzylamine as substrate for MAO B's) over time until the inhibition was complete. The unreacted DCP was removed by anion exchange chromatography using a DEAE SepharoseTM Fast Flow (Amersham Biosciences, Uppsala, Sweden) column for MAO A's or Bio-Rad MacroPrep® High-Q column (Bio Rad Laboratories, Hercules, CA) for MAO B's. The column was equilibrated with 25 mM potassium phosphate containing 20% glycerol and 0.8% OGP (pH 7.2). After uploading the DCP-labeled sample, the column was washed with 20 column volumes of the same buffer as used for equilibrating column. The protein was eluted from the column using 200 mM potassium phosphate containing 20% glycerol and 0.8% OGP (pH 7.2). The eluted fractions were collected, concentrated and stored in 50 mM potassium phosphate with 20% glycerol, 0.8% OGP (pH 7.2).

2.2.7 Labeling of DCP-labeled human wild-type MAO A/B and double

mutants with 4-dimethylaminophenylazophenyl-4'-maleimide (DABMI)

The DCP-inhibited MAO samples were labeled with 20:1 molar excess DABMI at 4°C with rotating overnight in the dark. Due to limited solubility of DABMI in aqueous

solution, the concentrated stock solution of DABMI was prepared in dimethyl sulfoxide and diluted into the protein solution so that the volume of the organic solvent was below 0.6% of the total aqueous solution volume. Since some DABMI label was not dissolved in the protein solution, the undissolved label was removed by centrifugation and followed by anion exchange chromatography as described in 2.2.7 to remove excess DABMI.

2.2.8 Fluorescence measurements

Steady state fluorescence measurements were conducted on an AMINCO-Bowman Series 2 luminescence spectrometer with a continuous wave 150 W Xenon lamp. The excitation wavelength was 345 nm and emission wavelength was 495 nm.

Polarization spectra and anisotropy measurements were performed in the same spectrofluorometer with polarizers in the excitation and emission ports. With the same excitation wavelength (345 nm) and emission wavelength (495 nm), all values were calculated by the software module of the fluorimeter according to the following equation:

$$Polarization(P) = \frac{I_{//} - I_{\perp}}{I_{//} + I_{\perp}} \quad \text{Equation 2.1}$$

$$Anisotropy(r) = \frac{I_{//} - I_{\perp}}{I_{//} + 2I_{\perp}} \quad \text{Equation 2.2}$$

where $I_{//}$ and I_{\perp} are the intensities observed parallel and perpendicular, respectively, to the axis of the vertically polarized excitation light. All polarization and anisotropy values are the averages of ten measurements.

For fluorescence quenching, in principle, there are two types of quenching, dynamic quenching which occurs when the excited fluorophore encounters quencher and then returns to the ground state without emission of a photon, static quenching in which a nonfluorescent complex is formed between the fluorophore and the quencher (Lakowicz 1983).

Dynamic quenching of fluorescence is described by the Stern-Volmer equation:

$$F_0 / F = 1 + K_D [Q] \quad \text{Equation 2.3}$$

where F_0 and F are the fluorescence intensities in the absence and the presence of quencher, respectively. K_D is the Stern-Volmer quenching constant and $[Q]$ is the concentration of quencher.

Equation describing static quenching, similar to dynamic quenching, is as follows:

$$F_0 / F = 1 + K_S [Q] \quad \text{Equation 2.4}$$

It is noted that K_s here is the association constant which is given by

$$K_S = \frac{[F - Q]}{[F][Q]} \quad \text{Equation 2.5}$$

in which, $[F-Q]$ is the concentration of the nonfluorescent complex and $[F]$ is the concentration of uncomplexed fluorophore.

In this work, the DCP-labeled human MAO A and human MAO B samples (~10 μ M) were quenched by the addition of aliquots of a freshly prepared KI (6 M).

2.2.9 Fluorescence resonance energy transfer (FRET) analysis

According to the theory of Förster energy transfer (Stryer 1978), the singlet-singlet energy transfer occurs via a resonance interaction of the dipole pair between the donor and acceptor. In this study, DCP was the energy donor and DABMI was the energy acceptor. Since DABMI is a non-fluorescent acceptor, energy transfer efficiency of the donor in the presence of acceptor was followed by the donor quenching method.

The fluorescent spectra of the protein samples in the absence and the presence of acceptor were recorded at different protein concentrations. To keep the system consistent, all fluorescent spectra were normalized according to the protein concentrations. The protein concentration was determined by using the molar absorption coefficient of flavocyanine adduct at 410 nm ($23,400 \text{ M}^{-1} \text{ cm}^{-1}$).

The donor-acceptor distance, R , can be calculated by the following equation:

$$R = R_0[(1 - E) / E]^{1/6} \quad \text{Equation 2.6}$$

where E is the measured efficiency of energy transfer, R_0 is the Förster distance which is the critical distance for 50% energy transfer. E is related to the intensity of donor fluorescence in the absence (F_D) and the presence of acceptor (F_{DA}), which can be calculated by

$$E = 1 - (F_{DA} / F_D) \quad \text{Equation 2.7}$$

R_0 is given by

$$R_0^6 = (8.79 \times 10^{23} [k^2 n^{-4} Q_D J(\lambda)]) \quad (\text{in } \text{Å}^6) \quad \text{Equation 2.8}$$

in which, κ^2 is the orientation factor which is typically assumed equal to 2/3 if donor or acceptor exhibits isotropic motion, n is the refractive index of the medium separating

donor and acceptor and for protein solution, n is assumed equal to 1.36. Q_D is the quantum yield of the donor and is determined by

$$Q_D = \frac{F_{DA} - F_{free}}{F_D - F_{free}} \quad \text{Equation 2.9}$$

where F_{free} is the intensity of donor fluorescence itself without bound protein. $J(\lambda)$ is the spectral overlap integral ($M^{-1} \text{ cm}^1$) defined in

$$J(\lambda) = \frac{\int_0^{\infty} F_D(\lambda) \varepsilon_A(\lambda) \lambda^4 d\lambda}{\int_0^{\infty} F_D(\lambda) d\lambda} \quad \text{Equation 2.10}$$

where $F_D(\lambda)$ is the fluorescence emission spectrum of the donor and $\varepsilon_A(\lambda)$ is the absorption spectrum of the acceptor ($M^{-1} \text{ cm}^{-1}$) as a function of wavelength λ (cm). For the dipole pair of dansyl group and DABMI, $J(\lambda)$ is equal to $7.15 \times 10^{-14} M^{-1} \text{ cm}^{-1}$ (Barden *et al.* 1987).

2.2.10 Modeling of MAO C-terminal helices

The last several residues that are not visible in electron density maps of the human MAO A (507-527 residues) and MAO B (500-520 residues) crystal structures were built up by using program O (Jones *et al.* 1991). Basically, 5 N-terminal residues of a 20-residue helix which was generated from the protein structure were superimposed with existing portion of the C-terminal helix in the crystal structures (503-507 in human MAO A and 496-500 in human MAO B), respectively. Finally, these residues in the 20-residue helix were mutated to their corresponding sequences in the proteins.

2.2.11 Molecular Dynamics (MD) simulation

Molecular Dynamics (MD) simulation was performed to predict the structure of MAO with DCP. The crystal structures of human MAO A with clorgyline (PDB ID: 2BXS) and human MAO B with pargyline (PDB ID: 1GOS) used in this simulation contain the predicted C-terminal helices generated by using program O. The GROMACS (Van der Spoel *et al.* 2005) MD simulation package on a Linux cluster with two 2.6 GHz AMD Opteron dual-core processor was used to carry out all the simulations. The protein simulation utilized the GROMOS96 43a1 forcefield with additional parameters of FAD (Ryckaert *et al.* 1977) and DCP from ab initio calculations. The DCP ligand was manually placed inside the active site cavity of the protein to substitute their original ligands (clorgyline in human MAO A and pargyline in human MAO B), respectively, and simple point charge (SPC) water (Berendsen *et al.* 1981) molecules were also added to the system. A 2 nanosecond MD simulation was performed at 312 K and 1 bar, followed by the steepest decent energy minimization procedure. Bond lengths were constrained with the SHAKE algorithm, allowing a 2 femtosecond timestep. The Berenderson scheme was used to control both the temperature and pressure with constant of 0.1 and 1.0 picosecond, respectively. The Particle Mesh Ewald (PME) method (Darden *et al.* 1993) was used to treat the electrostatic interactions.

2.3 Results

2.3.1 Spectral characterization of DCP

The spectral properties of DCP were determined by UV-Vis and fluorescence spectroscopy, respectively. In UV-Vis spectrum of DCP (Figure 2.3), there are two absorption peaks, 250 nm and 345 nm, respectively. The corresponding fluorescence spectra of DCP are shown in Figure 2.4. The fluorescence spectrum of the dansyl group is known to be solvent-sensitive. Emission of DCP in 95% ethanol is at 515 nm (solid line), whereas in highly polar solvents such as phosphate buffer, DCP yielded “red-shift” spectra with a much lower intensity (~14 fold lower) (dashed line).

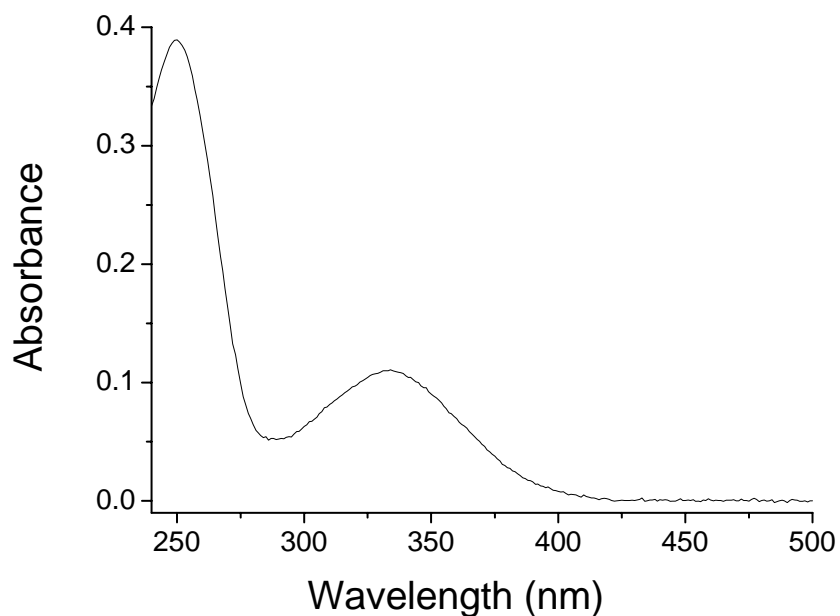


Figure 2.3 UV-Vis spectrum of DCP in 95% ethanol.

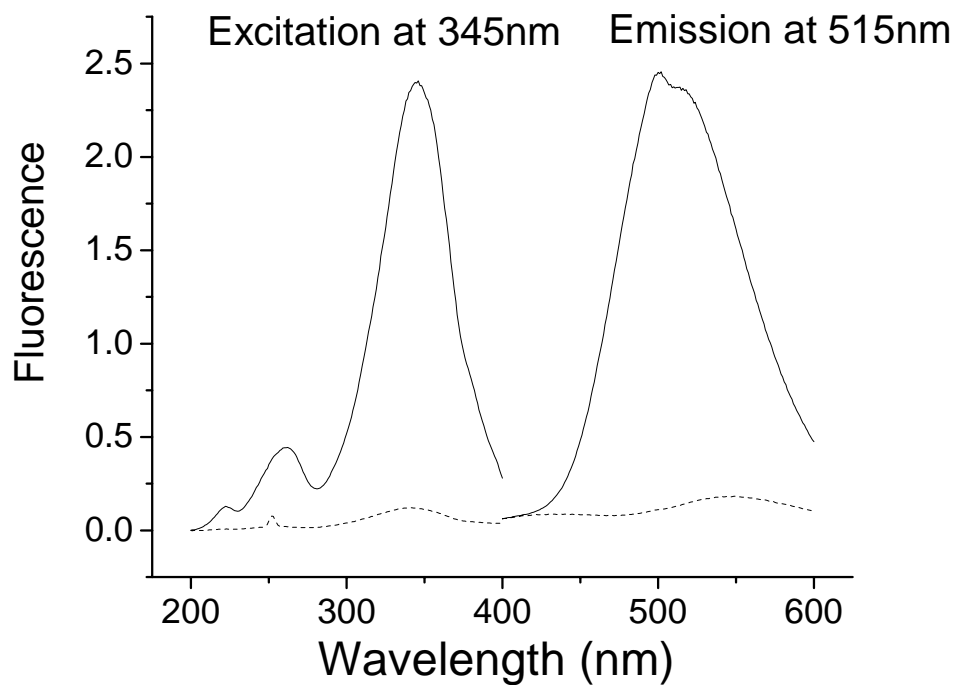


Figure 2.4 Excitation and emission spectra of DCP in 95% ethanol (—) and in potassium phosphate buffer (----), respectively.

2.3.2 Inhibition of MAO with DCP

Human MAO A (5 μ M) or human MAO B (5 μ M) was incubated with 100 μ M of DCP at 15°C, respectively. As shown in Figure 2.5, with an increase in incubation time, both enzymes lost activities. Human MAO A was fully inhibited by DCP within 450 minutes, whereas human MAO B lost its activity within 4 days.

After complete inhibition of MAO A and MAO B by DCP, excess DCP was removed by ion-exchange chromatography. Formation of the flavocyanine adduct was observed by the appearance of the characteristic absorption at 413 nm, suggesting that DCP was covalently bound to MAO A and to MAO B, respectively (Figure 2.6 A and B).

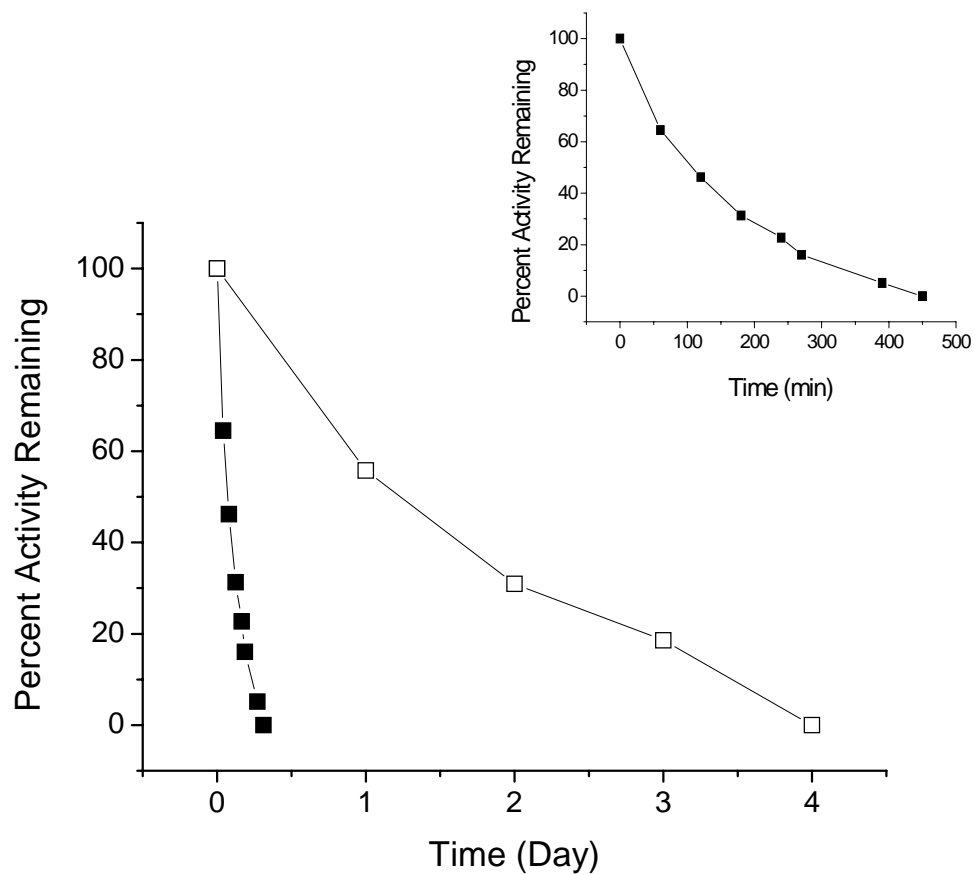
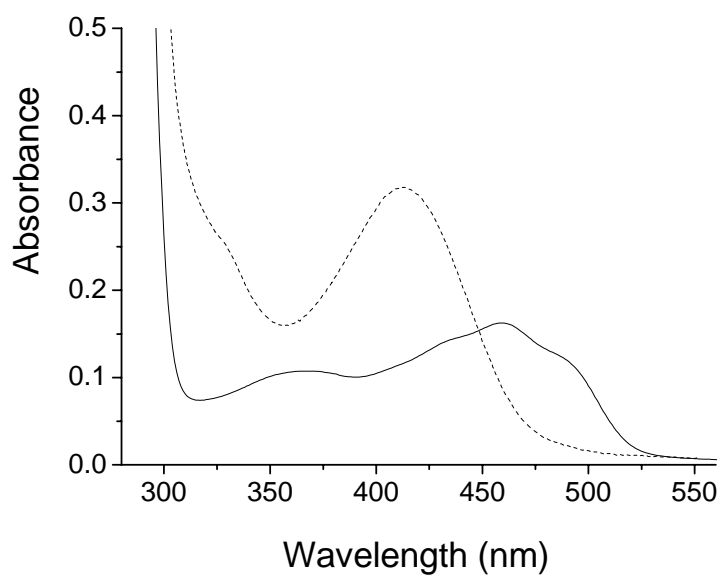


Figure 2.5 Time course of inhibition of human wild-type MAO A (■) and MAO B (□) by DCP. Inset: Time course of inhibition of human MAO A by DCP in minute scale.

(A) Human MAO A



(B) Human MAO B

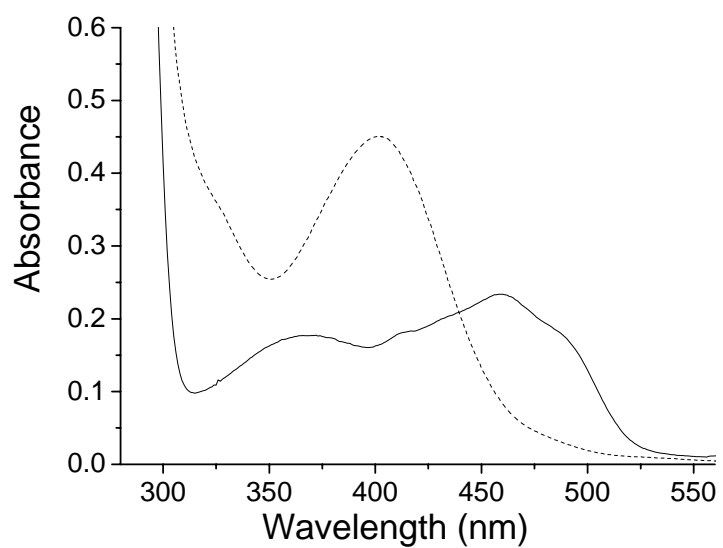


Figure 2.6 UV-Vis spectra of human MAOs before(—) and after (----) DCP inhibition

SDS-PAGE gel further confirmed that DCP is covalently bound to MAO (Figure 2.7). Both MAO A and MAO B show very faint fluorescence background bands (lane 1 and lane 4). No strong fluorescence bands were observed for clorgyline-inhibited MAO A and pargyline-inhibited MAO B with addition of DCP (lane 3 and lane 6). These observations might be due to the fluorescence of covalently bound flavin. DCP-inhibited MAO samples showed much stronger fluorescence intensity (lane 2 and lane 5).

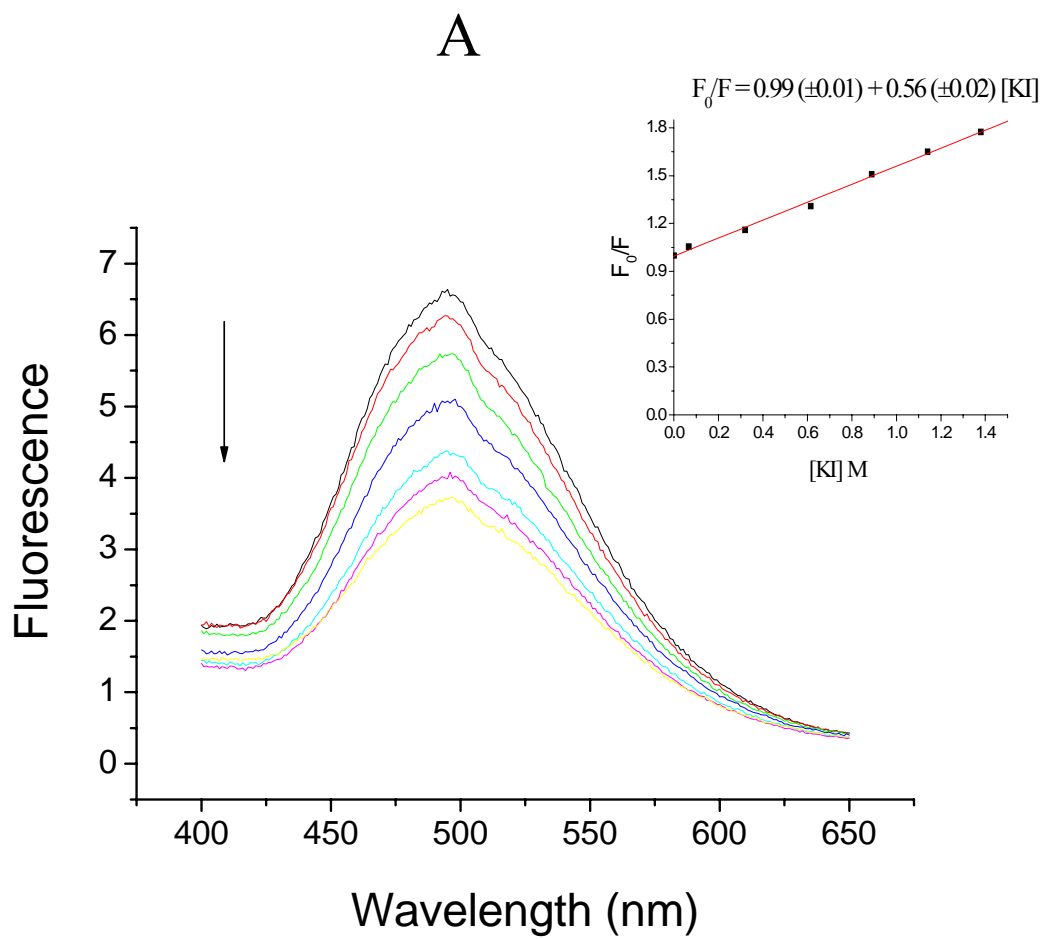


Figure 2.7 SDS-PAGE gel of MAO samples exposed under UV light. (1) human MAO A, (2) DCP-inhibited MAO A, (3) clorgyline-inhibited MAO A with DCP (1:1), (4) human MAO B, (5) DCP-inhibited MAO B, and (6) pargyline-inhibited MAO B with DCP (1:1).

2.3.3 Fluorescence quenching of DCP in MAO

To access whether DCP in MAO A and MAO B exhibits different solvent exposure, iodide quenching experiments, in which emission spectra were monitored from 400 to 600 nm at excitation of 345 nm, were performed to determine the relative accessibilities of dansyl groups to the quencher in MAO A and in MAO B. An important quenching feature of I^- is that I^- cannot penetrate into the interior of the proteins (Lakowicz 1983), so the internal flavin and tryptophans are not expected to be quenched by I^- . Fluorescence quenching data of DCP-inhibited MAO A and DCP-inhibited MAO B by I^- are shown in Figure 2.8. The linear Stern-Volmer plots indicate that a single fluorophore population is present. This single class of fluorophore is a dansyl group instead of two tryptophans in

MAO because the excitation wavelength of tryptophan is 285 nm, not 345 nm, as well as bound dansyl groups are exposed to bulk solvent.



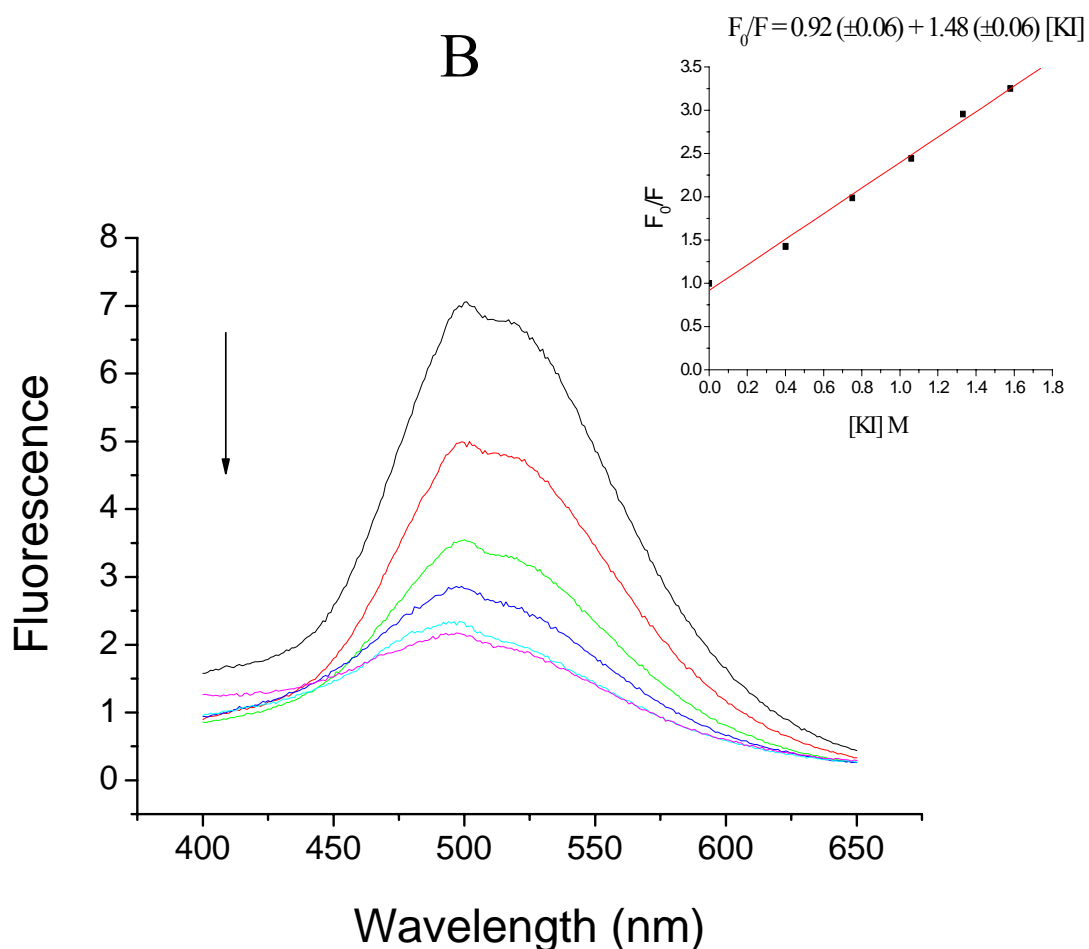


Figure 2.8 Fluorescence spectra of DCP-inhibited MAO before and after KI quenching. (A) Emission spectra of DCP-inhibited MAO A quenched by KI. KI concentrations (M) (from up to down): 0, 0.066, 0.32, 0.615, 0.889, 1.14, 1.38 (B) Emission spectra of DCP-inhibited MAO B quenched by KI. KI concentrations (M) (from up to down): 0, 0.4, 0.75, 1.06, 1.33, 1.57
Insets: The Stern-Volmer plots for the iodide quenching.

The lower accessibility of dansyl group in DCP-inhibited MAO A ($K_q = 0.56 \text{ M}^{-1}$) to the quencher I^- was observed. For DCP-inhibited MAO B ($K_q = 1.48 \text{ M}^{-1}$), the dansyl group accessibility to the aqueous environment was enhanced. These observations would reveal that environments of DCP located in these two enzymes are different.

2.3.4 Polarization and anisotropy of DCP in MAO

Concerning the motion of dansyl group, when DCP is covalently or noncovalently bound to MAO A or MAO B, the macromolecule and the attached label rotate as a unit, therefore the rotational freedom of the dansyl group should become markedly hindered, which can be evaluated by polarization and anisotropy parameters. The emission anisotropy kinetics of the dansyl fluorescence (Table 2.2) showed that polarization and anisotropy values of both DCP-inhibited MAO A and DCP-inhibited MAO B are much greater than that of free DCP, showing that bound DCP has a mobility that is significantly decreased by the enzymes. Moreover, the greater polarization/anisotropy data of MAO B with DCP than that of MAO A with DCP under the same condition indicates that the dansyl group in MAO B is less mobile than in MAO A.

In principle, polarization values for an isotropic solution must be $-0.33 \leq P \leq 0.5$, and anisotropy values are $-0.2 \leq r \leq 0.4$ (Lakowicz 1983). Moreover, according to the estimation of rotational correlation time of MAO dimer in detergent micelles, P_0 and r_0 values (the values observed for the same fluorophore in vitrified solution) are ~ 0.5 and ~ 0.4 , respectively. Therefore, for both MAO A with DCP and MAO B with DCP, their polarization and anisotropy values are close to upper limits, suggesting mobility of DCP is highly restricted in the enzymes.

	Polarization	Anisotropy
DCP	0.081 ± 0.001	0.055 ± 0.001
MAO A with DCP	0.249 ± 0.003	0.181 ± 0.003
MAO B with DCP	0.334 ± 0.002	0.250 ± 0.002

Table 2.2 Polarization/anisotropy of DCP in different environments

2.3.5 Distance measurements in MAO

As shown in Figure 2.9, the absorption spectrum of DABMI acceptor, exhibiting a maximum at 447 nm, overlaps well with the emission spectrum of DCP. The overlap integral for DCP-DABMI pair is $7.15 \times 10^{14} \text{ M}^{-1} \text{ cm}^{-1}$ (Barden *et al.* 1987).

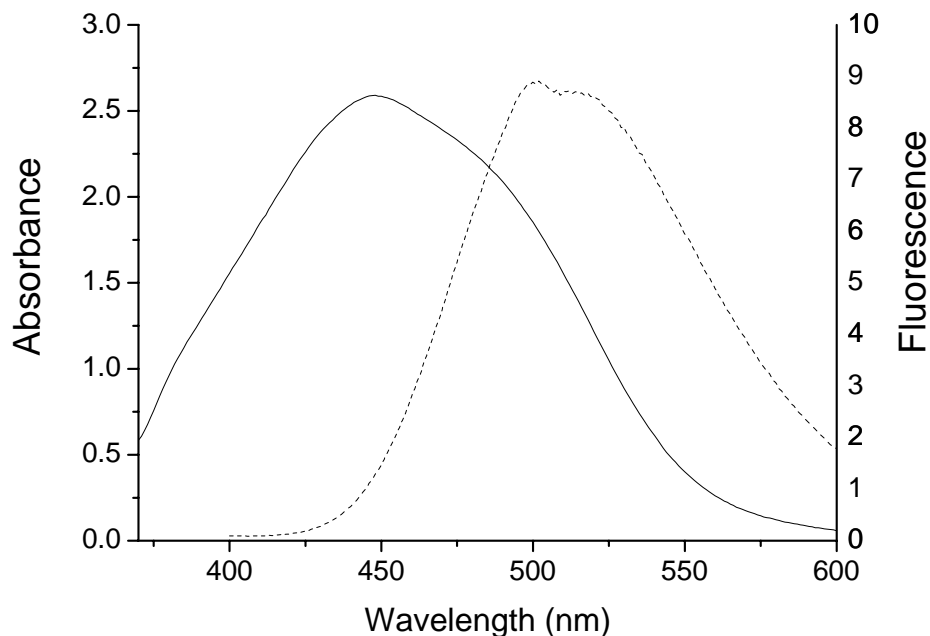
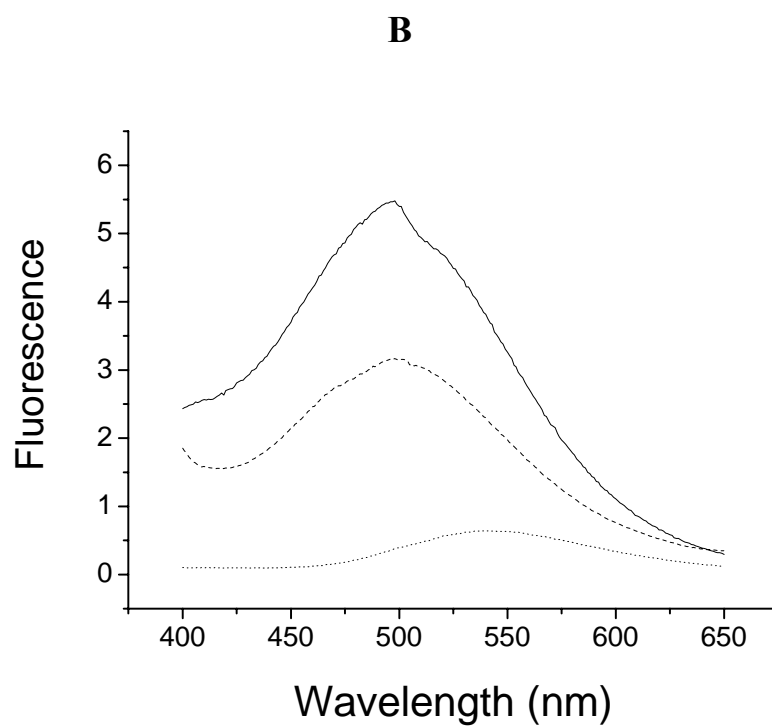
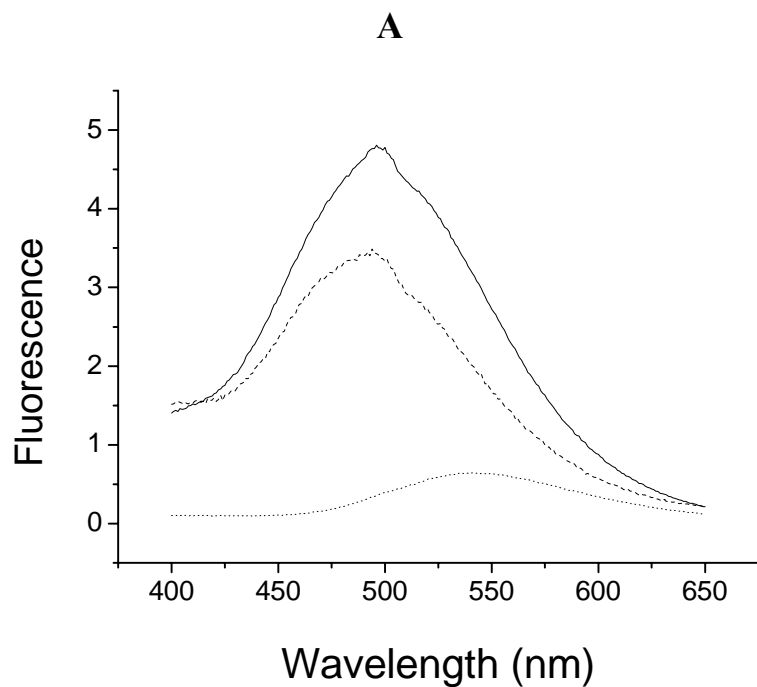


Figure 2.9 **Overlap of the absorbance spectrum of DABMI at 447 nm (—) with the emission spectrum of DCP at 495 nm (---). DABMI and DCP were in 50 mM potassium phosphate (pH 7.2)**

Since DABMI is a non-fluorescent acceptor, FRET analysis was performed by measuring the decrease in the fluorescence of the donor DCP. The fluorescence intensity depends upon the concentration of the fluorophore in sample solution, thus DCP concentrations in different samples (in the absence and the presence of DABMI) have to be adjusted for further FRET analysis. According to stoichiometry of MAO to DCP (1: 1), protein concentrations can be used to estimate the concentration of DCP in protein

samples. Protein concentration were determined using characteristic absorption of flavocyanine adduct at 411 nm ($\epsilon = 23,400 \text{ M}^{-1} \text{ cm}^{-1}$).



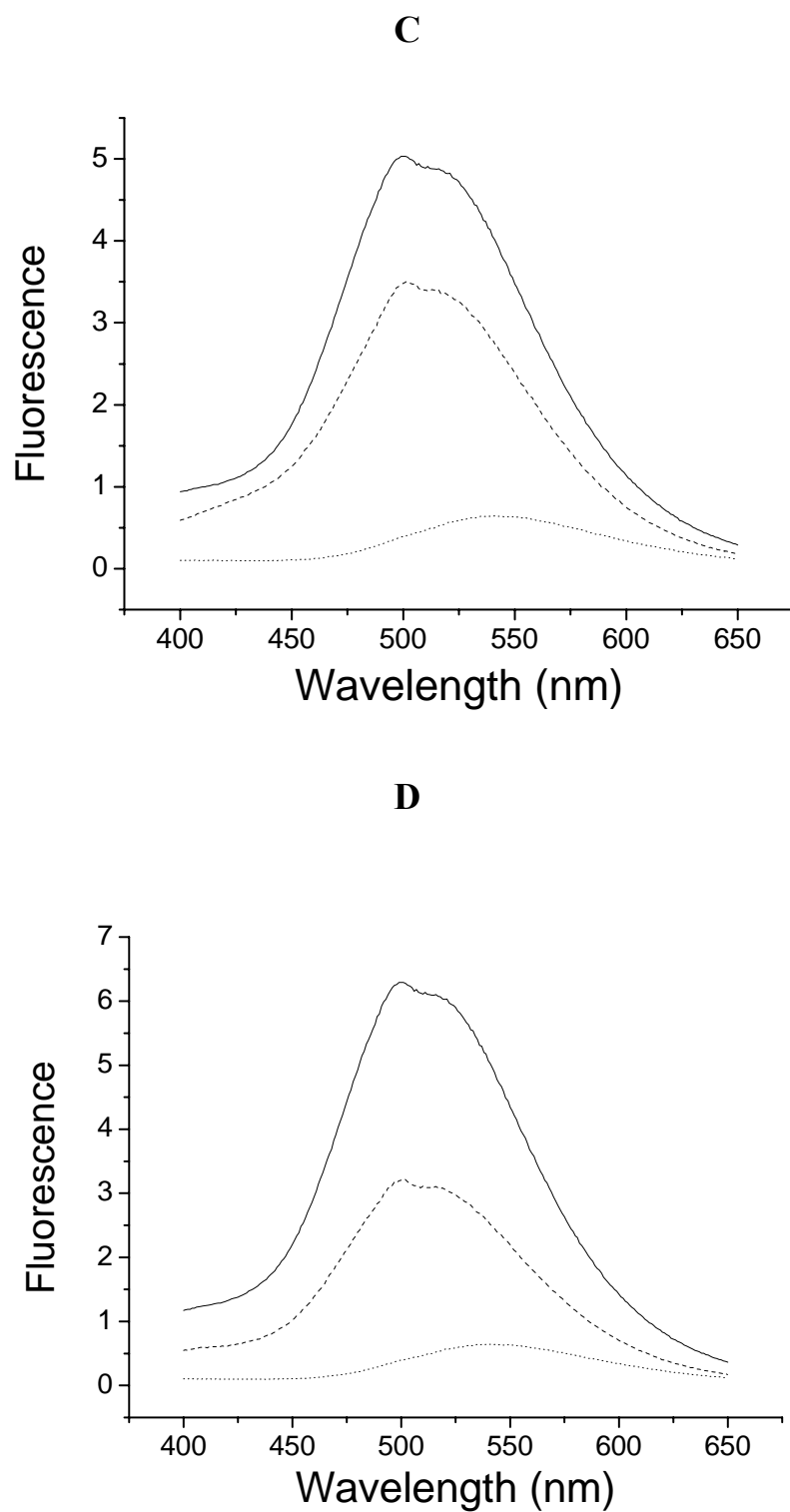


Figure 2.10

Fluorescence emission spectra of 10 μM of free DCP (.....), 10 μM of bound DCP in the absence of DABMI (—) and in the presence of DABMI (----), in (A) human wild-type MAO A, (B) human MAO A Cys266Ala-Pro525Cys mutant, (C) human wild-type MAO B and (D) human MAO B Cys5Ala-Val518Cys mutant, respectively. Concentrations of enzyme samples were normalized to 10 μM according to the absorbance of enzyme at 411 nm (stoichiometry of MAO to DCP is 1:1).

Figure 2.10 shows the fluorescence emission spectra of DCP in the absence and the presence of DABMI on MAO. The significant decrease in fluorescence intensity of DCP in the presence of DABMI was observed, indicating Förster resonance energy transfer occurred from DCP to DABMI on MAO. It is noted that the emission spectra of DCP bound to MAO blue shifted ~40 nm relative to that of free DCP, suggesting the environment change of DCP in protein.

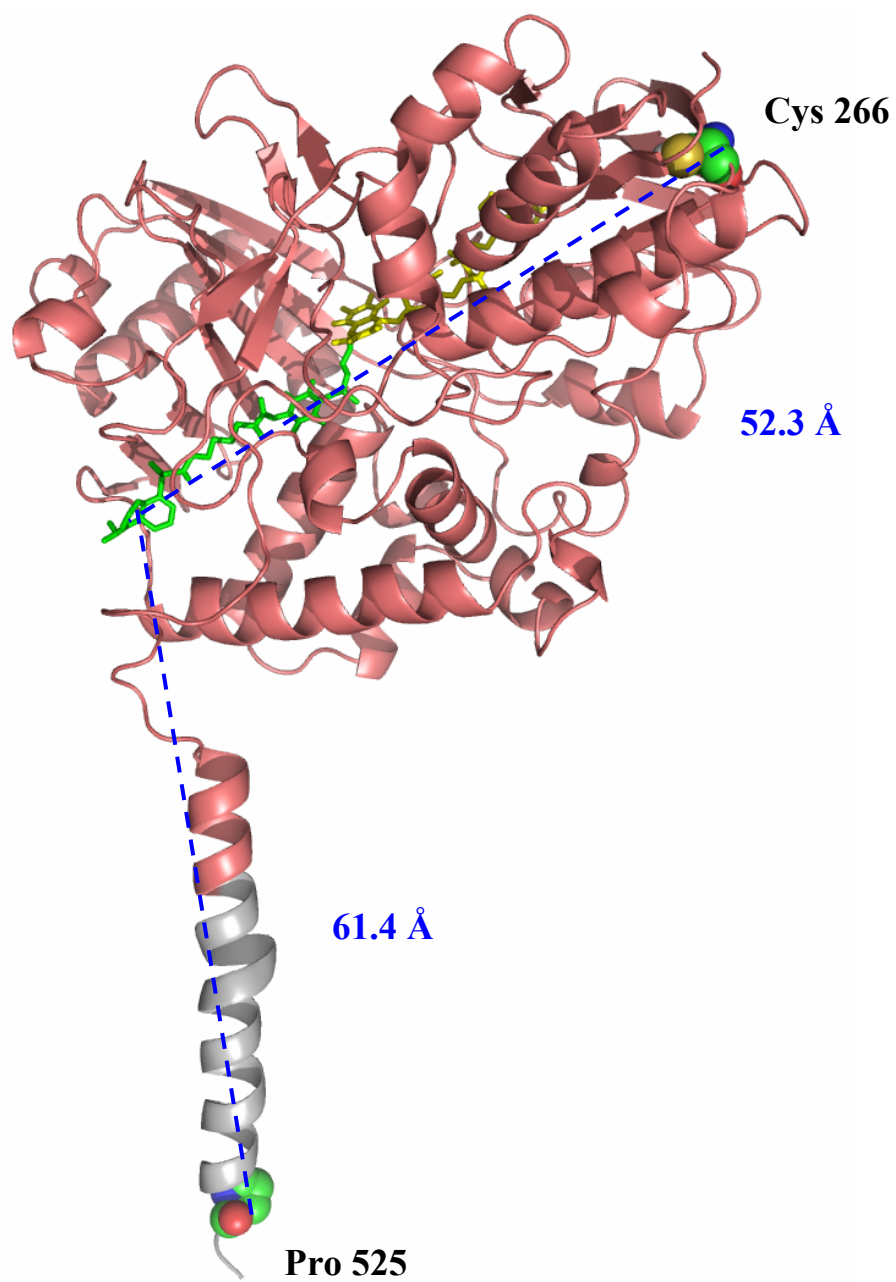
According to the Equation 2.6 stated in Material and Methods, the distances are calculated and summarized in Table 2.3.

	Human MAO A		Human MAO B	
	Upper half	Lower half	Upper half	Lower half
	(R_A^U)	(R_A^L)	(R_B^U)	(R_B^L)
E	0.276	0.421	0.302	0.489
Q_D	0.676	0.523	0.654	0.456
R₀ (Å)	45.0	43.1	44.7	42.1
FRET distance (R, Å)	52.9	45.4	51.4	42.4
Predicted distance (R', Å)	52.3	61.4	52.5	55.4

Table 2.3 Summary of FRET distances R.
R's are the distances measured from the crystal structures.

To better understand the relationship of the MAO structures in detergent solubilized form and in crystalline form, the distances in the crystal structures were

A



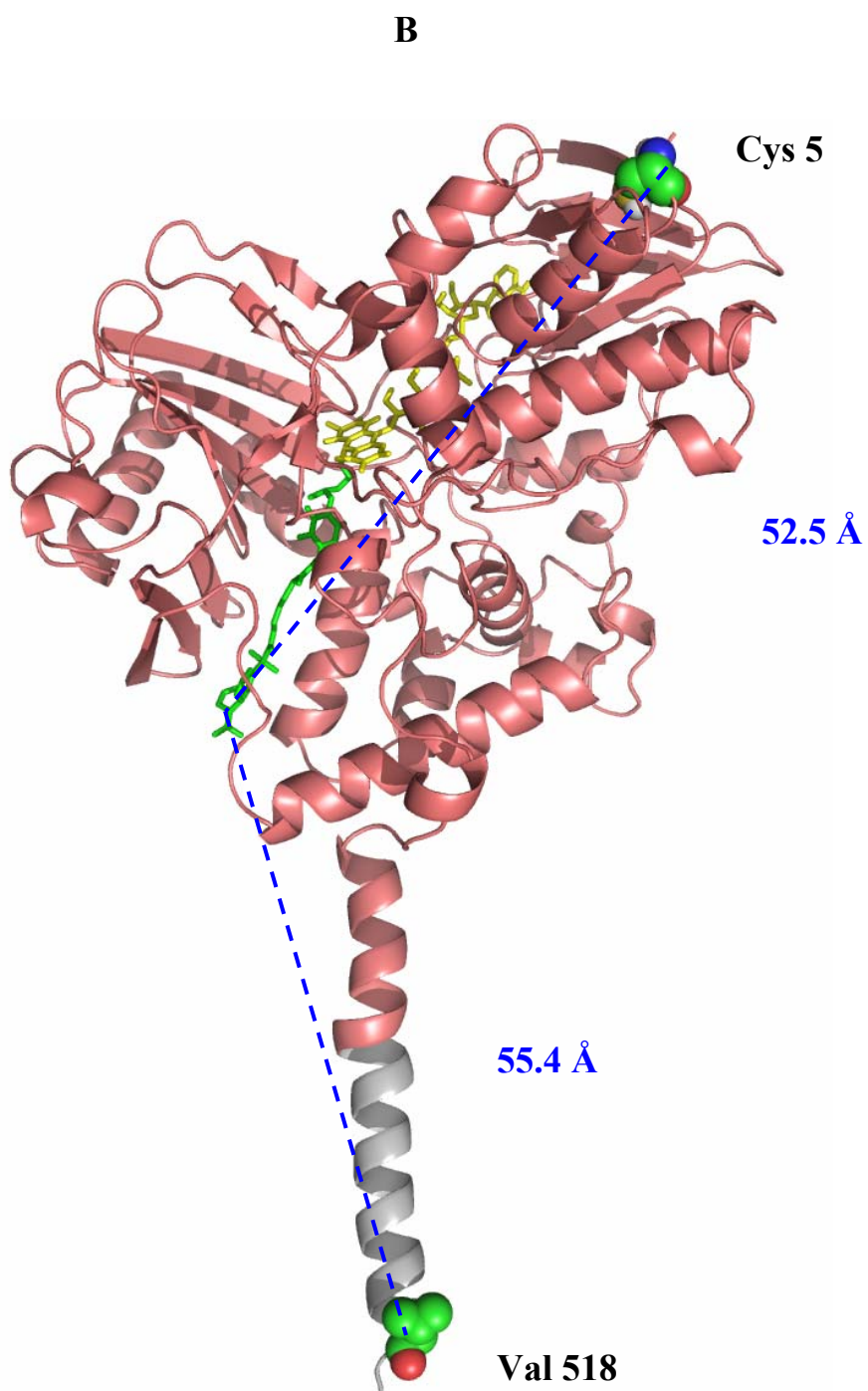


Figure 2.11 DCP-docked structures of human MAO A (A) and human MAO B (B). FAD and DCP drawn in ball and stick mode are in yellow and in green, respectively. The grey colored region is a predicted structure. The distances shown by dashed line are in angstroms. Residues involved in distance measurement are indicated in sphere mode.

measured as well. Since the conformation of last several residues (including residue 525 in human MAO A and 518 in human MAO B) on C-terminal helices of human MAO A and human MAO B are not solved in the crystal structures and DCP-complexed MAO structures are not available, the structures of C-terminal helices were modeled using Program O and DCP was then docked into the active site cavity of the known crystal structures with predicted C-terminal structure using molecular dynamics simulation. The DCP docked structures of human MAO A and human MAO B are shown in Figure 2.11 (A) and (B), respectively. The dansyl ring of DCP in human MAO A is more exposed outside the active site cavity than that in human MAO B. The distances between DCP and Cys266 (R_A^U) and between DCP and Pro525Cys (R_A^L) in human MAO A, as well as the distances between DCP and Cys5 (R_B^U) and between DCP and Val518Cys (R_B^L) in human MAO B, are measured in the modeled structures and listed in Table 2.3.

With comparison of the distances in detergent solubilized form (R) and in crystalline form (R'), the distances R_A^U and R_B^U obtained from FRET are well consistent with that from crystal data (53 Å and 51 Å, respectively), whereas the experimentally determined distances R_A^L and R_B^L are shorter than that from the crystal structure with the modeled C-terminal helices.

2.4 Discussion

Since DCP is a modified pargyline analog, it covalently binds to the flavin cofactor of MAO to form flavocyanyne adduct with a maximal absorption at 411 nm. During the inhibition of MAO with DCP, the A form shows a different behavior than the B form. Even though pargyline is a MAO B specific inhibitor, MAO A was inhibited by

DCP much faster than MAOB. This observation might be explained by their structural differences. The active site cavity of MAO A is shorter and wider than that of MAO B, making DCP more accessible to the substrate/inhibitor-binding domain of MAO A. Moreover, as shown in DCP-docked MAO structures (Figure 2.11), the fluorophore on DCP is exposed outside the active site cavities in both MAO A and MAO B, and it seems to be more mobile in MAO A than in MAO B. This assumption is further supported by polarization and anisotropy measurements, showing that dansyl chromophore is more restricted in MAO B than in MAO A.

Since Γ^- is a negatively charged quencher, the positive environment would facilitate the quenching efficiency. As shown in Figure 2.11, the dansyl ring on DCP sticks out of the active site cavities of either MAO A or MAO B, thus the nature of the charged residues in front of the entrance of active site cavities would affect the quenching efficiency of Γ^- . Surface potential structures of MAOs (Figure 2.12) show that, in MAO B, a sufficient amount of positively charged residues are in front of the entrance cavity, making Γ^- more accessible to the fluorophore. In contrast, most area in front of the entrance of the active site cavity in MAO A is covered by neutral residues and some negatively charged residues, and weak attraction or even repulsive interaction would impair the interaction between Γ^- and dansyl ring. Therefore, different surface potentials in MAO A and in MAO B affect the quenching efficiency of Γ^- , and DCP is quenched more efficiently in MAO B than in MAO A.

Yguerabide has pointed out that decrease in the polarity of the environment of a fluorescent probe-like dansyl group increases its fluorescence efficiency and decreases the wavelength of its maximum emission (Yguerabide 1972). The active site cavities of

MAO A and MAO B are surrounded by aromatic and aliphatic amino acids and show strong hydrophobic properties. Consequently, as can be seen in Figure 2.10, a more apolar environment results in the increase of fluorescence intensity as well as the “blue-shift” of the peaks of DCP in both MAO A and MAO B.

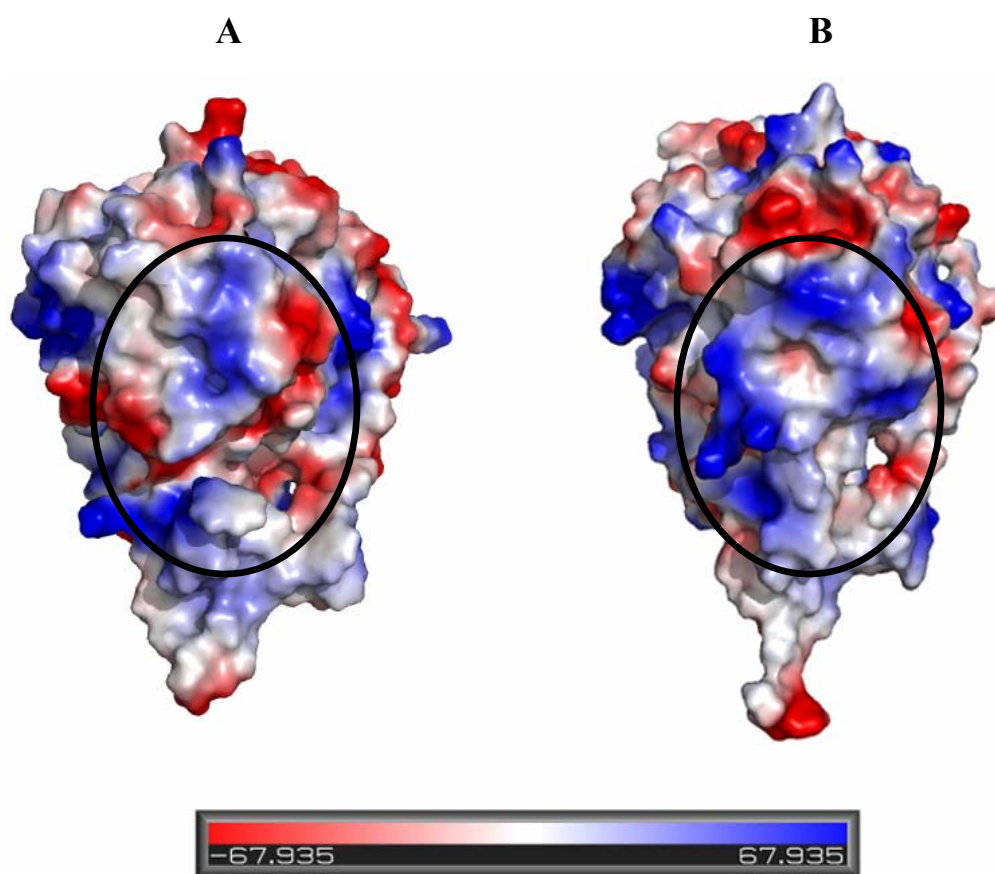


Figure 2.12 Surface potential drawing of human MAO A (A) and human MAO B (B). This figure was generated by anti-clockwise rotating the structures in Figure 2.11 90° along the vertical axis, and the orientation of the structures faces the entrance of active site cavity. Ovals mark the region consisting of the residues in front of the entrance cavity. The figures were prepared with the program Pymol (DeLano Scientific, San Carlos, CA). Electrostatic potential is colored from negative potential (red) to positive potential (blue). Neutral potential is shown in white.

As stated in Chapter 1, the crystal structures of the last several residues on C-termini in human MAO A (residues 507-527) and human MAO B (residues 501-520) are not solved, the predicted helices were modeled by program O, assuming the C-terminal

helix is in a continuing and straight manner (Figure 2.11). The experimentally determined distances between DCP and the N-terminus of the protein in MAO A (R_A^U) and MAO B (R_B^U) are consistent with the distances measured from the known crystal structures, indicating that FAD binding domain and substrate/inhibitor-binding domain of the protein structures in their detergent solubilized forms are similar to those in their respective crystal forms. However, the distances (R_A^L and R_B^L) obtained between DCP and the end of C-terminal helices are shorter than that measured from the crystal structures with the modeled C-terminal helices. It can be explained by the assumption proposed by Binda *et al.* (Binda *et al.* 2004) that, instead of traversing the outer mitochondrial membrane, C-terminal helix is interrupted and turns back to the membrane surface. In Chapter 3, the conformation of C-terminal helices in human MAO A and MAO B will be discussed.

Chapter 3

Conformational Investigations of C-terminal Helices of Human MAO A and MAO B in Their Membrane Bound Forms

3.1 Introduction

The 3-D structures of human MAO A and MAO B have been solved by X-ray crystallography (Binda *et al.* 2002; De Colibus *et al.* 2005). However, the conformations of the end of C-terminal helices (residues 507-527 in MAO A and residues 501-520 in MAO B) are still unknown since these residues are not well defined in electron density maps. In the outer mitochondrial membrane, these disordered residues are predicted to either turn back toward the surface of membrane (Figure 3.1, left panel) or traverse the outer mitochondrial membrane (Figure 3.1, right panel) (Binda *et al.* 2004).

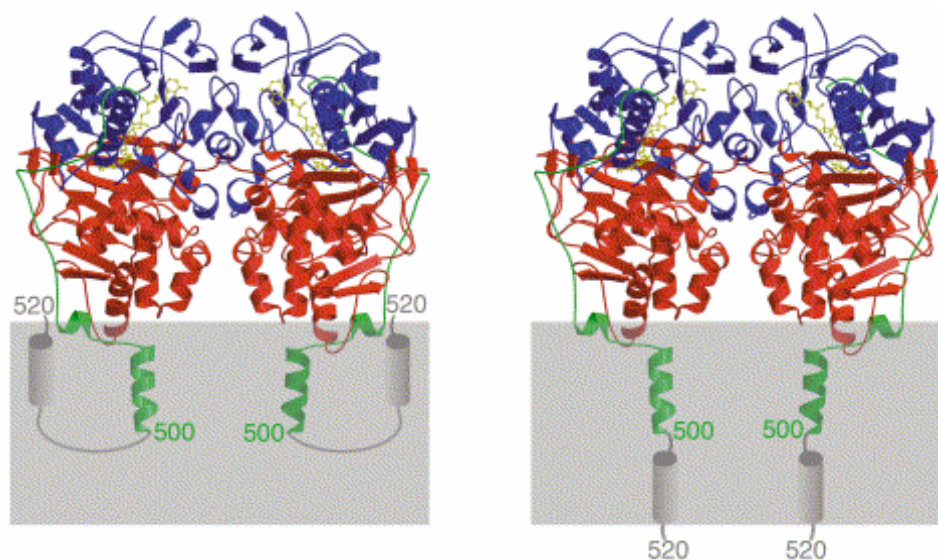


Figure 3.1 Proposed hypotheses for the structure of human MAO B C-terminal tail (residues 500-520). The gray square represents the membrane, while the two possible conformations of the C-terminal part are depicted as gray cylinders. In the left panel, the helix is suggested to be interrupted, with the polypeptides chain turning back with the C-terminus positioned on the same side of the membrane with respect to the main body of the protein. In the right panel, the helix spans the entire bilayer. (Binda *et al.* 2004)

In the present work, the spatial relationship between membrane-embedded C-terminal helices of MAOs and the membrane bilayer was studied using fluorescence spectroscopy.

Due to the reactivity of S-H bond, a cysteine was chosen for fluorescence labeling. However, there are no cysteine residues on the C-terminal helices of both human MAO A and MAO B. In order to apply thiol reactive fluorescent reagent, cysteine residues were introduced at the Phe525 site in human MAO A and the Val518 site in human MAO B which are on the ends of their C-terminal tails, respectively. It should be noted that Cys266 (MAO A) and Cys5 (MAO B) on the top surface of the protein were mutated to Ala to rule out their interference with specific labeling on the transmembrane helix by thiol-reactive probes. Previous studies have shown that only the cysteine residues exposed outside of the inhibited MAO can be labeled by thiol reactive reagent (Hubalek *et al.* 2003). Therefore, with the mutation of the cysteine residues on the top surface of the protein to alanines, the introduced cysteines on the C-terminus by site-directed mutagenesis are the only cysteine residues exposed in detergent solution, and they would be specifically labeled by thiol reactive fluorescent reagent.

Since the aim of this work is to investigate the conformation of C-terminal helices of human MAO A and MAO B in their membrane bound forms, the fluorophore-labeled C-termini have to be anchored into the outer mitochondrial membrane. However, due to the possibility of undesirable non-specific labeling of other cysteine-containing membrane protein, the cysteines on C-terminal helices of human MAO A and MAO B cannot be specifically labeled in natural membrane bound form. An alternative approach to selectively label these cysteines with fluorophores would be labeling the detergent

solubilized protein followed by reconstitution into membrane. McCauley *et al.* have successfully incorporated newly synthesized MAO into rat liver mitochondria (Zhuang *et al.* 1988; Zhuang *et al.* 1992). This approach was applied to insertion of purified detergent solubilized MAO into yeast mitochondria in this work.

N-(1-Pyrenyl)maleimide (Figure 3.2 A), a fluorescence probe specific for sulfhydryls in a hydrophobic environment, has been widely used in studies of physical properties of lipids of biological membranes (Galla *et al.* 1980; Melnick *et al.* 1981; Zachariasse *et al.* 1982) since its pyrene group has a high affinity for lipids and a long excited state lifetime ($\sim 10^{-7}$ sec) which makes this probe highly sensitive to quenching (Chong *et al.* 1985). For pyrene labels, spin-labeled fatty acids are common paramagnetic quenchers to investigate the location of fluorophore with respect to the membrane surface. The quenching efficiency of spin-labeled fatty acids is dependent on the position of the nitroxide radical group in the fatty acid chain, and the penetration depth for the doxyl group with nitroxide has been studied by the EPR isotropic splitting factor (Gaffney *et al.* 1974) and permeability measurements of the spin label reducing reagent, ascorbate (Schreiermuccillo *et al.* 1976). Moreover, paramagnetic quenching might provide information about the distance between nitroxide radicals and the fluorophores since this type of quenching requires $\sim 4-6$ Å interaction distances (Green *et al.* 1973). Therefore, the fatty acids bearing nitroxide groups at different positions have been extensively used to serve as molecular rulers to locate the depth of membrane-embedded fluorophores.

In this work, the cysteine residues on the C-termini of MAO A and MAO B were labeled with N-(1-pyrenyl)maleimide, and spin-labeled fatty acids, such as 5-doxylstearic acid (5-FASL) and 12-doxylstearic acid (12-FASL) (Figure 3.2 B and C, respectively),

were used to quench the extrinsic fluorescence of a pyrene moiety attached to the end of C-terminal helices of MAO which has been reconstituted into yeast mitochondria. With different position of nitroxide radicals on fatty acids, fluorescence quenching techniques provide insight into the conformation of C-terminal helices in human MAO A and MAO B in their membrane bound forms.

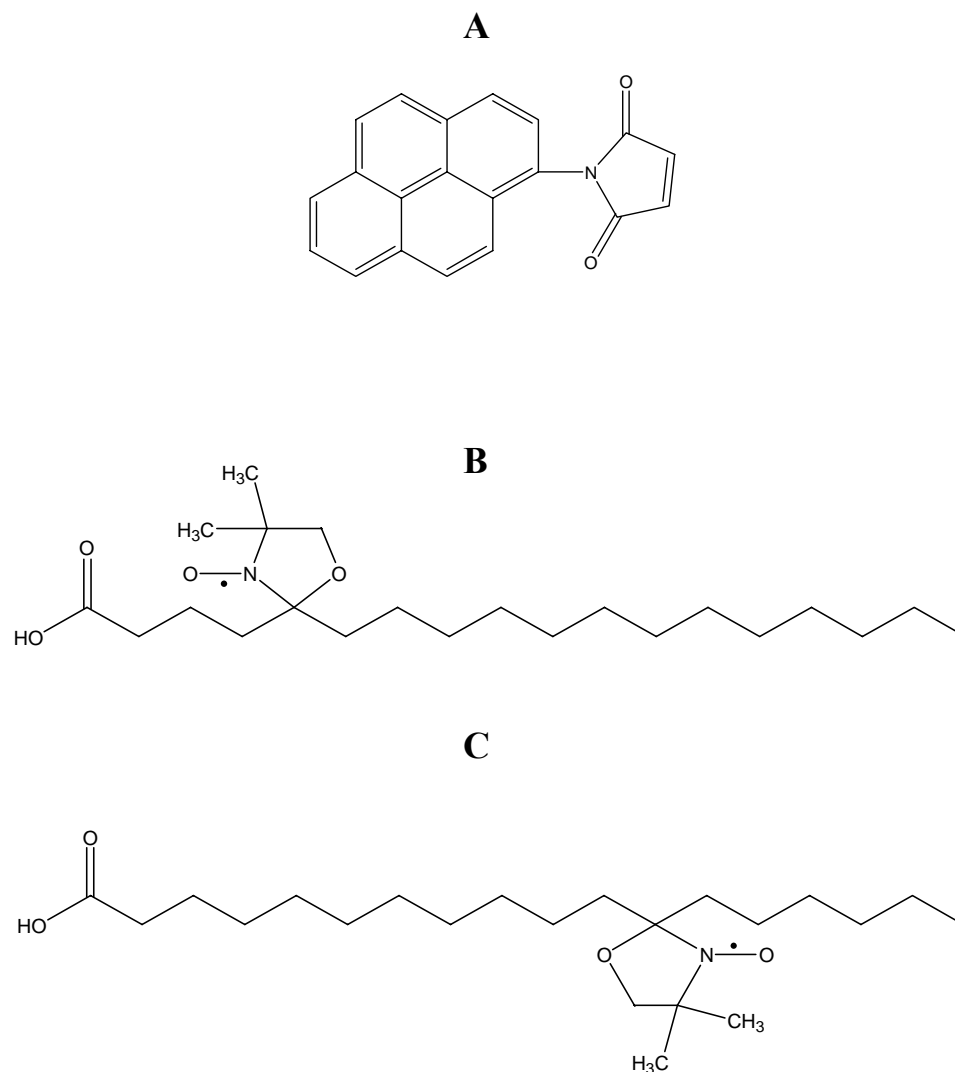


Figure 3.2 Structural formulas of NPM and the spin-labeled fatty acids used in this study. (A) N-(1-pyrenyl)maleimide (B) 5-doxyloystearic acid (5-FASL) (C) 12-doxyloystearic acid (12-FASL)

3.2 Materials and Methods

3.2.1 Materials

Magnesium chloride, potassium chloride, dithiothreitol (DTT), sucrose, HEPES, adenosine triphosphate (ATP), creatine phosphate, creatine phosphokinase, potassium iodide, Tris-HCl, glycerol, ethylenediamine tetraacetic acid (EDTA), potassium hydroxide, mannitol, bovine serum albumin, phenylmethylsulfonyl fluoride (PMSF), Tris.SO₄, N-(1-pyrenyl)maleimide (NPM) and 5'-spin-labeled fatty acid (5-FASL) were purchased from Sigma-Aldrich Chemical Co.. 12'-spin-labeled fatty acid (12-FASL) was from Toronto Research Chemicals, Inc..

3.2.2 Creation of human MAO A Cys266Ala/Pro525Cys and MAO B Cys5Ala/Val518Cys mutants

Refer to all procedures stated in Materials and Methods of Chapter 2

3.2.3 Labeling of human MAO A and MAO B double mutants with N-(1-pyrenyl)maleimide (NPM)

The human MAO A and MAO B mutants were inhibited by their inhibitors, clorgyline and pargyline, respectively. The inhibited enzymes were labeled with a 20:1 molar excess NPM at 4°C with rotating overnight in the dark. Due to limited solubility of NPM in aqueous solution, the concentrated stock solution of NPM (20 mM) was prepared in dimethyl sulfoxide and diluted into the protein solution so that the volume of the organic solvent was below 0.6% of the total aqueous solution volume. Since some unreacted NPM was not dissolved in the protein solution, the modified NPM-MAO

solutions were centrifuged for 10 min at 9,000 rpm to pellet NPM aggregates and followed by anion exchange chromatography as described in 2.2.7 of Chapter 2 to remove excess NPM.

3.2.4 Isolation of yeast mitochondria

Yeast cells were cultivated to OD_{600} of 1-2, harvested by centrifugation ($4,400 \times g$, 5 min at room temperature) and washed once with distilled H_2O . The cell pellets were resuspended to 0.5 g, wet weight/ml in 100 mM Tris. SO_4 (pH 9.4) with 10 mM DTT and then incubated for 15 min at $30^\circ C$ with moderate shaking. After centrifugation at $3000 \times g$ for 5 min, the cell pellets were washed with 1.2 M sorbitol and then resuspended in 1.2 M sorbitol, 20 mM potassium phosphate (pH 7.4 with KOH) to give 0.15 g of cell wet weight/ml. To digest the cell wall, Zymolyase 5000 was added to a concentration of 3 mg/g of cell wet weight and the suspension was incubated at $30^\circ C$ with gentle shaking. Percent of spheroplast formation was followed as follows: $[(OD_{max} - OD_{min}) / OD_{max}] \times 100$, where, $OD_{max} = OD_{600}$ before adding (or immediately after adding) Zymolyase, and OD_{min} is OD_{600} at any time after adding Zymolyase. (Usually it takes 30-60 min to form 90% spheroplasts). When all the cells had been converted to spheroplasts, they were isolated by centrifugation ($3,000 \times g$, 5 min, $4^\circ C$) followed by washing twice with 1.2 M sorbitol. All subsequent steps should be performed at $0-4^\circ C$. The pellets were resuspended in homogenization buffer (0.6 M mannitol, 10 mM Tris-Cl (pH 7.4), 0.2% (w/v) bovine serum albumin, 1 mM EDTA, 1 mM phenylmethylsulfonyl fluoride (PMSF) to a concentration of 0.15 g of spheroplasts (wet weight)/ml. After chilling on ice for 20-30 min, the spheroplasts were homogenized by 10-15 strokes in a tight fitting Dounce

homogenizer. The homogenate was diluted with one volume of homogenization buffer and centrifuged for 5 min at $2,000 \times g$. The supernatant was saved and the pellet was rehomogenized and recentrifuged as before. The supernatants were combined and centrifuged ($17,400 \times g$, 12 min, 4°C). The sedimented mitochondria were resuspended in SEM buffer (10 mM MOPS/KOH, 250 mM sucrose, 1 mM EDTA, pH 7.4) and centrifuged again ($2,000 \times g$, 5 min, 4°C) to remove any residual cell debris. The supernatant was recentrifuged at $17,400 \times g$ for 12 min (4°C). Finally mitochondria were washed twice with SEM buffer and resuspended in a small volume of SEM buffer, frozen in liquid nitrogen and stored at -80°C for further use.

3.2.5 Reconstitution of wild-type MAO and NPM-labeled MAO samples into yeast mitochondria

Freshly isolated mitochondria (400 μg) in 200 μl import buffer (10 mM MOPS, 5 mM MgCl_2 , 80 mM KCl, 250 mM sucrose, 5% fatty acid free BSA, pH 7.2 with KOH) with ATP-generating system (4 mM ATP, 10 mM creatine phosphate, 4 $\mu\text{g}/\text{ml}$ creatine phosphokinase) and 200 ng/ml ubiquitin was incubated with 60 μl of 20 μM wild-type MAO or NPM-labeled MAO double mutants at 15°C for 2 hours followed by application of 10 $\mu\text{g}/\text{ml}$ proteinase K for 15 min on ice. The protease was inhibited with 2 mM phenylmethylsulfonyl fluoride (PMSF). The protein sample was centrifuged at 12,000g for 20 min. The pellets were washed two times with SEM buffer (250 mM sucrose, 1 mM EDTA and 10 mM MOPS, pH 7.2) and then resuspended in 20 μl SEM buffer. The reconstituted wild-type MAO samples (MAO A and MAO B) in mitochondrion were subjected to activity assays and western blot to determine their levels of insertion.

3.2.6 Fluorescence measurements

Steady state fluorescence measurements were conducted on an AMINCO-Bowman Series 2 luminescence spectrometer with a continuous wave 150 W Xenon lamp.

Polarization spectra and anisotropies measurements were performed in the same spectrofluorometer with polarizers in the excitation and emission ports. With the same excitation wavelength (345 nm) and emission wavelength (376 nm), all values were calculated by the software module of the fluorimeter according to the following equation:

$$Polarization(P) = \frac{I_{//} - I_{\perp}}{I_{//} + I_{\perp}}$$

$$Anisotropy(r) = \frac{I_{//} - I_{\perp}}{I_{//} + 2I_{\perp}}$$

where $I_{//}$ and I_{\perp} are the intensities observed parallel and perpendicular, respectively, to the axis of the vertically polarized excitation light. All polarization and anisotropy values are the averages of ten measurements.

For fluorescence quenching, spin-labeled fatty acid (5-FASL or 12-FASL) from a stock ethanolic solution was directly added into the pyrene-labeled protein solution. After incubation at room temperature for 30 min, fluorescence intensity measurements were carried out. Excitation wavelength was 345 nm and emission wavelength was 376 nm. Excitation and emission slit widths were 4 nm.

The fluorescence of pyrene-labeled human MAO A and human MAO B mutants (~10 μ M) were quenched by freshly prepared 6 M solution of KI.

3.3 Results

3.3.1 Characterization of MAO insertion into yeast mitochondria

The aim of this work is to investigate the conformation of C-terminal helices of MAO in membrane bound form based on site-directed labeling a cysteine residue at C-terminal helices with fluorophores. However, this labeling method is not well-suited for studying proteins associated with naturally occurring biological membranes due to the possibility of undesirable non-specific labeling of other cysteine-containing membrane proteins, when they are present in native membranes. Therefore, alternative approach used in this work is that the protein is specifically labeled by fluorescence probe in its detergent solubilized form and then reconstituted into isolated yeast mitochondria.

A number of years ago, McCauley's laboratory successfully inserted newly synthesized bovine MAO A and MAO B that are expressed in a reticulocyte lysate translation system into isolated rat liver mitochondria (Zhuang *et al.* 1988; Zhuang *et al.* 1992). Moreover, both ATP and ubiquitin were found to be required to achieve protein insertion into mitochondria in a proteinase K-resistant form. In this work, we revived this approach and applied it to insertion of the purified detergent solubilized MAO into isolated yeast mitochondria. The importance of ATP and ubiquitin in insertion process was also evaluated.

Since previous work concerning insertion of MAO into mitochondria was carried out in translation mixture and both ATP and ubiquitin were present in the reticulocyte lysate, the depletion of ATP and ubiquitin was achieved by addition of apyrase and IgG purified from antisera against ubiquitin, respectively (Zhuang *et al.* 1989; Zhuang *et al.* 1992). In the work presented in this dissertation, instead of newly synthesized enzyme,

the detergent solubilized MAO needs to be inserted into yeast mitochondria, so there is no endogenous ATP and ubiquitin to affect the evaluation of importance of these two components and they can be readily removed by omitting them in the reaction buffer. Aliquots of purified MAO A or MAO B were incubated with isolated yeast mitochondria for 2 hours at 15°C with different combinations of import buffer, ATP and ubiquitin, and then subjected to western blot analysis. As can be seen in Figure 3.3, depletion of import buffer, ATP or ubiquitin had no apparent effect on the “binding” of both MAO A and MAO B to the mitochondria. The reason to use the term “binding” is that it is still not known whether the protein is appropriately inserted into mitochondria or randomly associated with mitochondria. Therefore, it is critical to ensure the location of MAO after importing. Since the endogenous monoamine oxidase activities of rat liver mitochondria can be protected by the outer membrane from treatment with proteinase K (Weiss *et al.* 1979), proteinase K could be used to test whether the protein is appropriately inserted into mitochondria, rather than bound in some artifactual process. As shown in lane 1 and lane 2 of Figure 3.4, respectively, there is no endogenous monoamine oxidase in the yeast mitochondria that was used for insertion experiments, and membrane bound MAOs are proteinase K resistant. In the case of MAO insertion into yeast mitochondria, with the treatment of proteinase K, the depletion of either ATP or ubiquitin completely prevented insertion of MAO into yeast mitochondria (lane 3-5 in Figure 3.4). On the other hand, the depletion of import buffer affected the insertion of MAO (lane 6 in Figure 3.4). With assist of import buffer, ATP and ubiquitin, MAO was properly inserted into yeast mitochondria in a proteinase K-resistant form (lane 7 in Figure 3.4). These observations suggest that both ATP and ubiquitin are also required for insertion of purified MAO into

yeast mitochondria. Moreover, import buffer is essential component for protein insertion judged by its sensitivity to proteinase K.

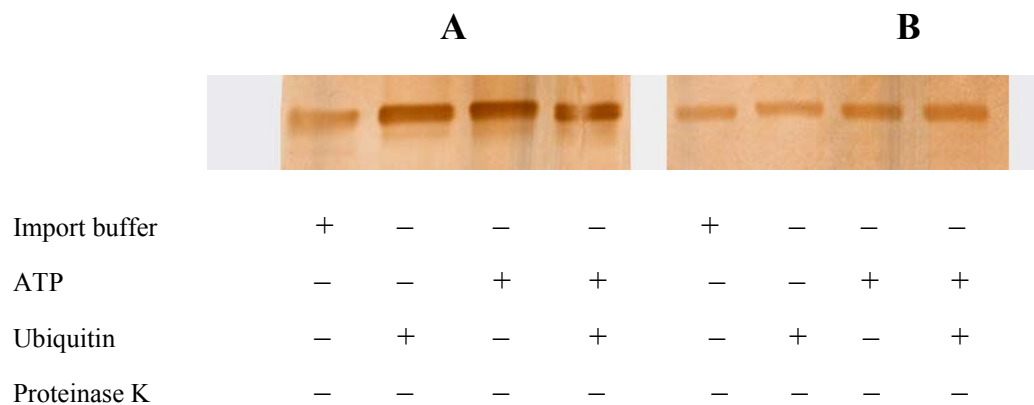
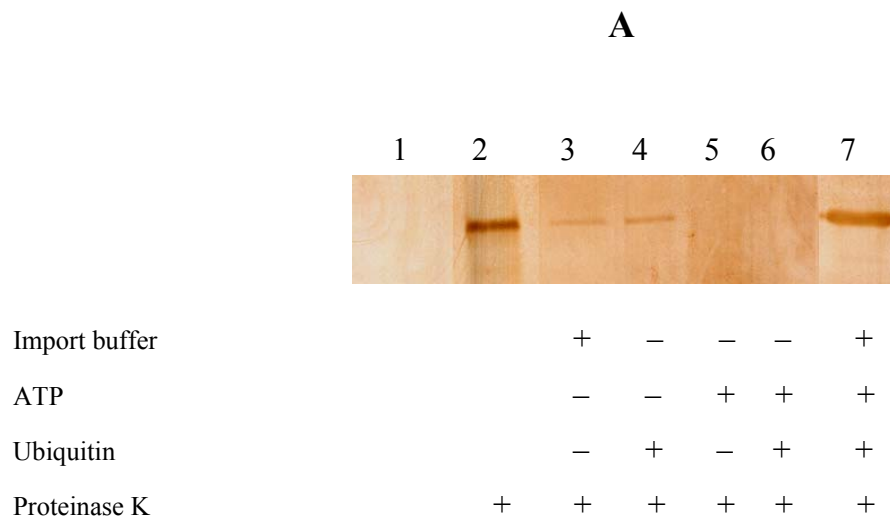


Figure 3.3 Insertion of MAO A (A) and MAO B (B) into yeast mitochondria without treatment of proteinase K. Yeast mitochondria (400 μ g) were incubated at 15°C for 2 hours under the conditions for the insertion reaction described under “Materials and Methods”. When indicated, import buffer, ATP and ubiquitin were removed, respectively, by omitting from the reaction mixture.



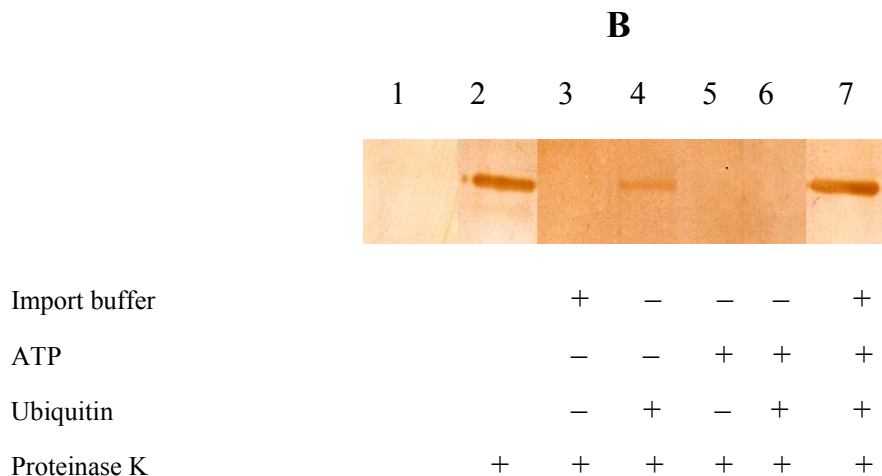


Figure 3.4 The effect of proteinase K on insertion of purified MAO A (A) and MAO B (B) into yeast mitochondria. Lane 1: yeast mitochondria. Lane 2: human MAO A or B in membrane bound form. Lane 3-7: Insertion of MAO A or B into yeast mitochondria under different conditions. Yeast mitochondria (400 μ g) were incubated at 15°C for 2 hours under the conditions for the insertion reaction as described in “Materials and Methods”. The mixtures were chilled and incubated with 10 μ g/ml proteinase K for 15 min on ice before the mitochondria were isolated from the mixtures. The proteolytic reaction was terminated with 2 mM PMSF. Mitochondria were isolated and analyzed by western blot using antisera raised against human MAO A. When indicated, import buffer, ATP and ubiquitin were removed, respectively, by omitting from the reaction mixture.

In the hypothetical model of MAO insertion, McCauley proposed that when newly synthesized MAO binds to the outer membrane, ubiquitin and ATP are required for subsequent insertion and ubiquitin would form conjugates with protein (Zhuang *et al.* 1992). However, the formation of MAO-ubiquitin conjugates was not observed since McCauley *et al.* could not isolate soluble MAO-ubiquitin conjugate from the reticulocyte lysate with antibody against either protein. In this work, the purified MAO is inserted into yeast mitochondria, so no other contaminants would affect the detection of ubiquitin. To further investigate whether MAO-ubiquitin conjugates are formed, mouse monoclonal IgG₁ against ubiquitin was applied to detect the existence of ubiquitin when MAO was inserted into yeast mitochondria. As can be seen from Figure 3.5, with treatment of

proteinase K, a strong protein band is shown between 40 kDa and 81 kDa (the size of MAO is 60 kDa and ubiquitin is 8.5 kDa), suggesting ubiquitin-MAO conjugates are formed after insertion.

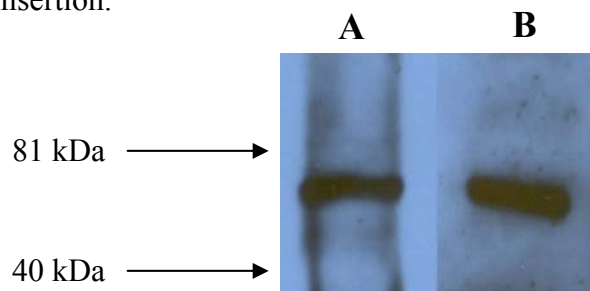
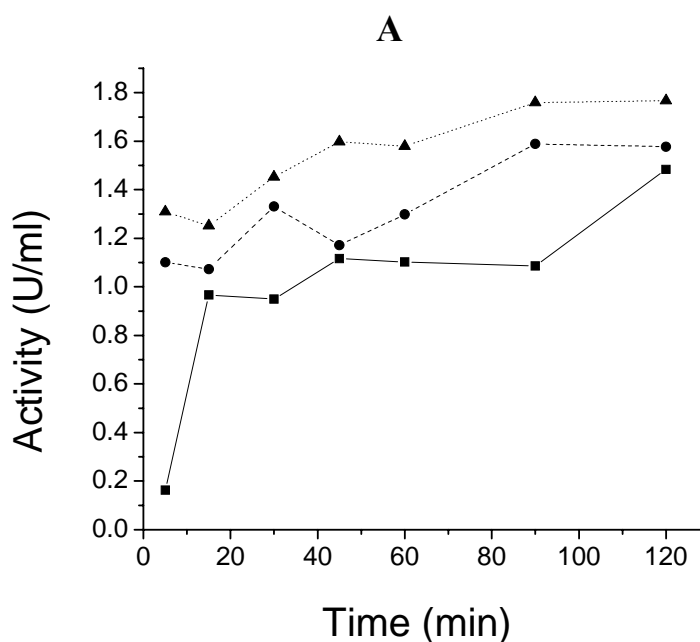


Figure 3.5 Detection of conjugates of MAO A (A) and MAO B (B) with ubiquitin. The blots were developed using an ECL western blotting detection kit (Amersham Pharmacia Biotech, Little Chalfont, Buckinghamshire, UK)

With successful insertion method, the efficiency of MAO importing into yeast mitochondria was investigated at three different temperatures: 0°C, 15°C and 25°C. As shown in Figure 3.6, the increase of the incubation temperature accelerated the insertion efficiency of both MAO A and MAO B into yeast mitochondria, indicating temperature would be a factor of affecting protein insertion.



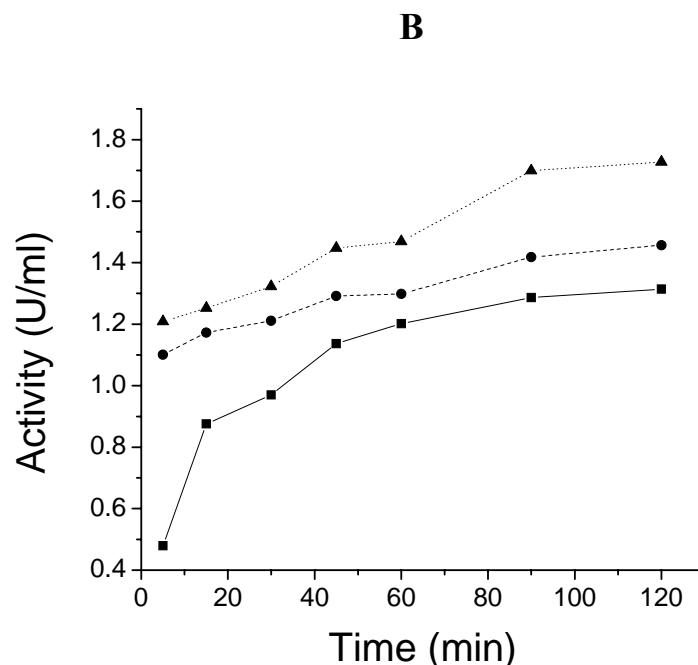


Figure 3.6 Temperature-dependent insertions of purified MAO A (A) and MAO B (B) into isolated yeast mitochondria. Yeast mitochondria (400 μ g) were incubated with 10 μ M enzymes for 2 hours at 0°C (—■), 15°C (- - ●) and 25°C (.....▲), respectively, under the conditions for the insertion reaction as described in “Materials and Methods”. Every 20 or 30 min, aliquots of reaction mixture were removed and immediately centrifuged at 12,000g for 20 min. The pellets were washed two times with SEM buffer and resuspended in 10 μ l SEM buffer followed by activity assay. Kynuramine (1mM) in assay buffer (50 mM potassium phosphate, pH 7.5) was used as MAO A substrate to measure activity of the inserted MAO A. The rate of oxidation of kynuramine was followed spectrophotometrically by monitoring the formation of product 4-hydroxyquinone with characteristic absorption at 316 nm. The activity measurement condition of MAO B was similar to that of MAO A, except that the substrate was benzylamine (3 mM) and the product was benzaldehyde with characteristic absorption at 250 nm.

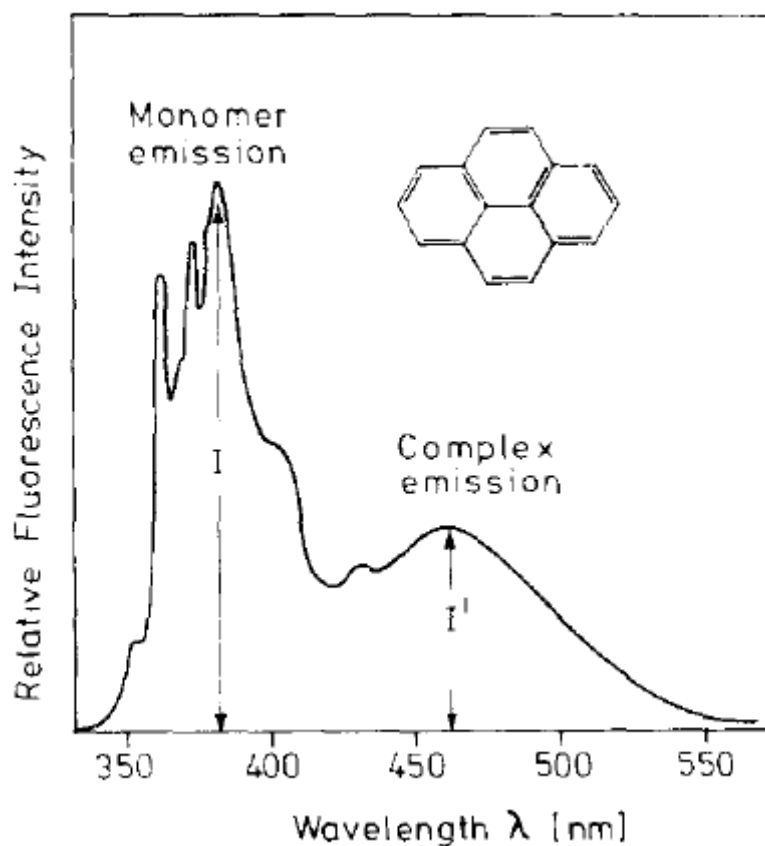
3.3.2 Fluorescence spectra of pyrene in MAO

According to insertion method described above, pyrene-labeled human MAO and B double mutants were reconstituted into isolated yeast mitochondria, and their spectral properties were characterized.

It has been reported that when hydrophobic probe pyrene is excited at 345 nm, the fluorescence spectra of this fluorophore in lipid membranes exhibit a superposition of the

monomer (structured band in the region 370-400 nm) and the excimer (excited pyrene dimers, wide structureless band with $\lambda_{\text{max}} = 465-480$ nm) (Figure 3.7 A) (Galla *et al.* 1974). As can be seen in Figure 3.7 (B), with the excitation wavelength at 345 nm, the fluorescence spectra of pyrene-labeled MAO A either in detergent solubilized form (solid line) or being reconstituted into yeast mitochondria (dashed line) consist of only pyrenyl monomer emission, and there is no emission of the excimer at 465 nm. The fluorescence spectra of pyrene-labeled MAO B in both forms are very similar to that of MAO A (not shown). These observations will be discussed below.

A



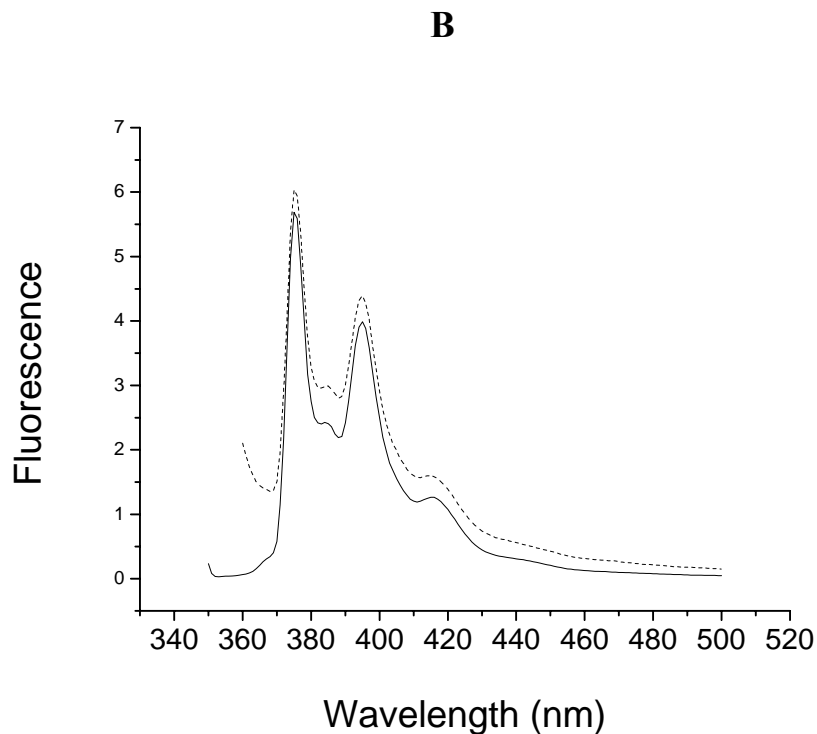


Figure 3.7 Pyrene emission fluorescence spectra. (A) Fluorescence spectrum of pyrene embedded in dipalmitoyllecithin bilayers (Galla *et al.* 1974). (B) Fluorescence spectra of pyrene with MAO A in detergent solubilized form (—) and in membrane bound form (- -), respectively.

3.3.3 Polarization and anisotropy of NPM-labeled MAO in detergent solubilized and membrane bound forms

Fluorescence polarization and anisotropy are the useful techniques to evaluate the motion of protein of interest when fluorophores are attached to the protein. In this work, the emission anisotropy kinetics of the pyrene fluorescence (Table 3.1) show that polarization and anisotropy values of both NPM-labeled MAO A and MAO B are greater than that of free NPM, suggesting that mobility of bound NPM is significantly decreased by enzyme. Moreover, polarization and anisotropy values of both NPM-labeled MAO A and MAO B in membrane bound form are much greater (~3 fold) than that in detergent

solubilized form, suggesting that pyrene-labeled C-terminal helix is more mobile in detergent solution than in the mitochondria membrane. These observations are agreement with the known crystal structures (Binda *et al.* 2002; De Colibus *et al.* 2005), in which, due to their flexibility, the C-terminal helices of both MAO A and MAO B are not visible in the electron density maps. When C-terminal helices are inserted into the mitochondria membrane, the motion of these helices is greatly hindered by lipid bilayer, resulting in the increase of polarization and anisotropy of pyrene fluorescence.

		Polarization	Anisotropy
Free NPM		0.007 ± 0.003	0.005 ± 0.002
NPM-labeled MAO A	in detergent solubilized form	0.110 ± 0.001	0.076 ± 0.001
	in membrane bound form	0.279 ± 0.002	0.205 ± 0.002
NPM-labeled MAO B	in detergent solubilized form	0.107 ± 0.003	0.074 ± 0.002
	in membrane bound form	0.296 ± 0.001	0.218 ± 0.001

Table 3.1 Polarization/anisotropy of NPM-labeled MAO in detergent solubilized and membrane bound forms.

3.3.4 Quenching of pyrene-labeled MAO A and MAO B fluorescence by iodide

To determine if the pyrene-labeled residues are buried in mitochondria membrane, iodide quenching was applied in the absence and presence of the lipid bilayer. The solid

lines in Figure 3.8 A and B show that, when pyrene-labeled MAOs are in solubilized detergent micelles, the fluorescence of pyrene is dramatically quenched by iodide. In contrast, in the mitochondrial outer membrane (Figure 3.8 A and B, dashed lines), the iodide quenching efficiency is much lower. The Stern-Volmer quenching constants derived from Figure 3.8 are summarized in Table 3.2.

The study of Γ quenching pyrene in lecithin bilayers has shown that the reaction rate of Γ with pyrene is very slow, $<10^{-8} \text{ M}^{-1} \text{ s}^{-1}$ (Barber *et al.* 1976). It might be ascribed to the reluctance of Γ to leave the aqueous phase and to enter the apolar region where the fluorophores reside in. Likewise, if pyrene labeled C-terminus of MAO is located in membrane bilayer, separating from the aqueous phase by the head group of phospholipid, Γ residing in the aqueous phase would not readily penetrate these lipid regions and interact with pyrene fluorophore. Therefore, the observations that quenching efficiency of Γ with pyrene in membrane bilayer is much lower than in aqueous solution suggest that, the pyrene-labeled residue on the C-terminus of MAO is buried in the hydrophobic region of the mitochondrial outer membranes.

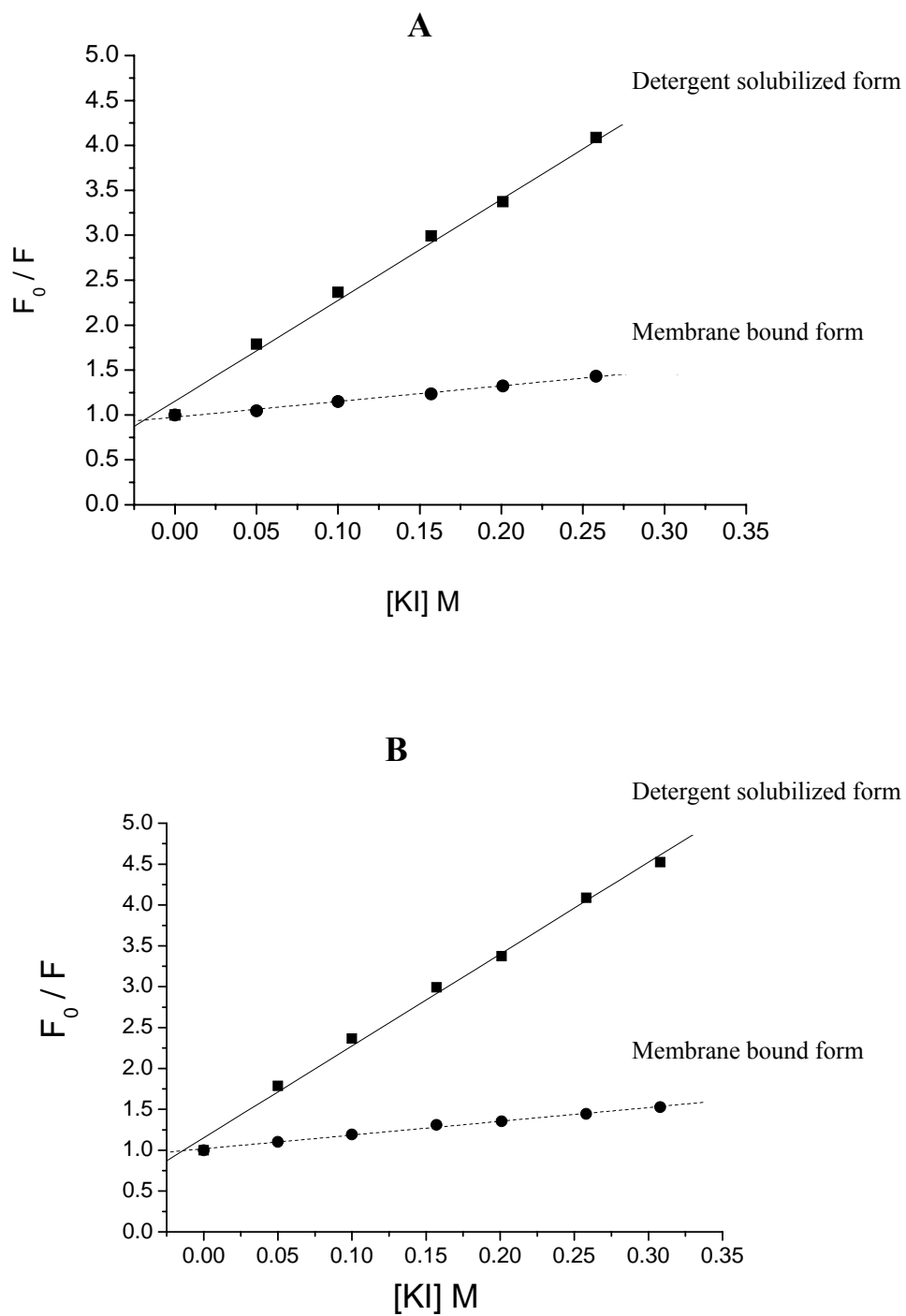


Figure 3.8

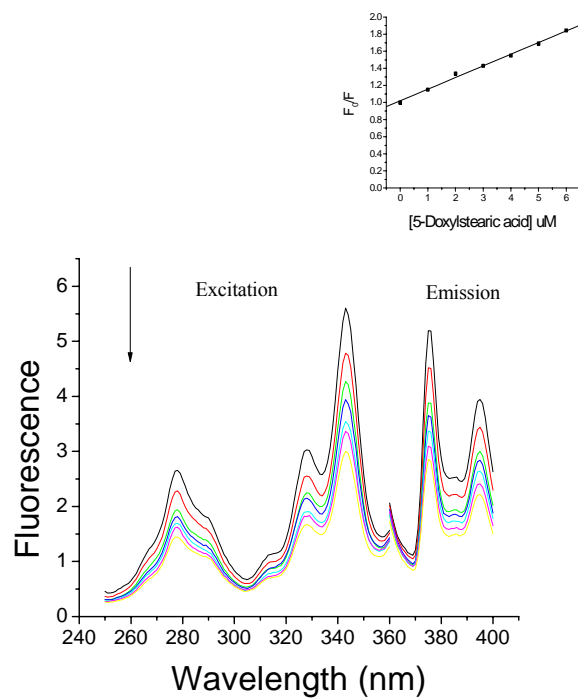
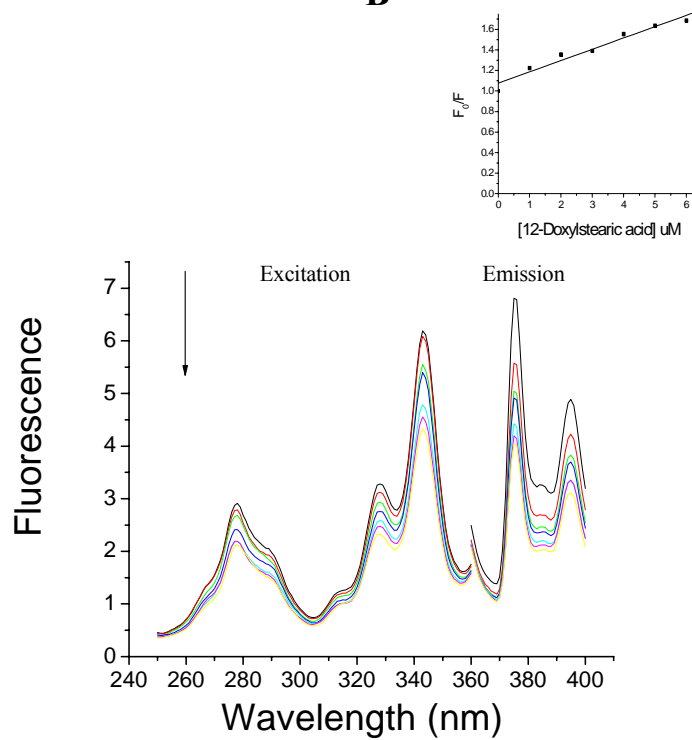
Stern-Volmer plots of potassium iodide quenching pyrene-labeled MAO A (A) and pyrene-labeled MAO B (B). Solid lines represent pyrene-labeled MAO A and B in solubilized forms. Dashed lines represent pyrene-labeled MAO A and B in membrane bound forms.

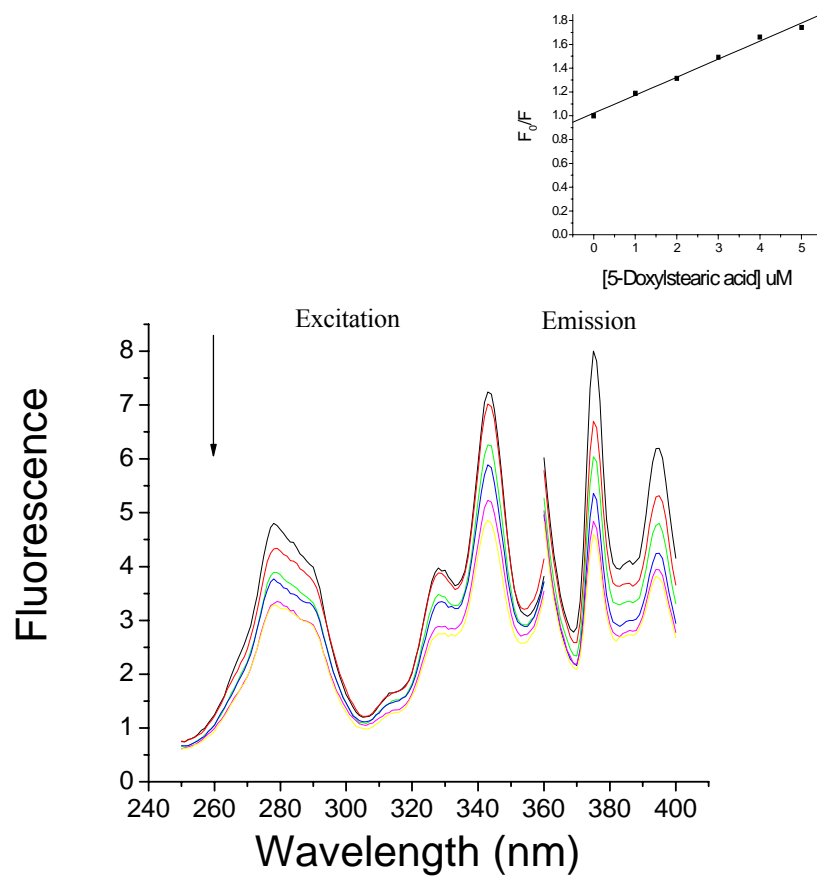
3.3.5 Quenching of pyrene-labeled MAO A and MAO B fluorescence by spin-labeled fatty acids

The spatial relationship of pyrene-labeled C-terminal helix with respect to the membrane bilayer was studied by paramagnetic quenching with two different spin labeled fatty acids that have been frequently used to determine the position of fluorophore-labeled residue in lipid bilayer membrane.

In this study, spin-labeled stearic acids with the nitroxide group at positions 5 and 12 along the fatty acyl chain (5-FASL and 12-FASL, respectively) were used to quench the extrinsic fluorescence of pyrene-labeled MAO A and B that are reconstituted into yeast mitochondria, and the quenching profiles are shown in Figure 3.9. The decrease in fluorescence intensity by spin-labeled stearic acids was monitored at 376 nm and fluorescence intensity of pyrene in the absence of quencher (black line) served as the control, F_0 . No deviation from linearity of Stern-Volmer plots (Figure 3.9 insets) is apparent, indicating the quencher is accessible to fluorophores.

In the case of MAO A reconstituted into mitochondria membrane, quenching efficiency of the 5-FASL is slightly higher than the 12-FASL (Table 3.2), indicating the end of C-terminal helix which is labeled with pyrene fluorophore might be almost located in the middle of membrane-water interface and the hydrophobic interior with a little bit proximity to membrane surface. For MAO B, the 5-FASL quenches pyrene more effectively (~2 fold) than the 12-FASL (Table 3.2), suggesting the fluorophore is located closer to the membrane-water interface.

A**B**

C

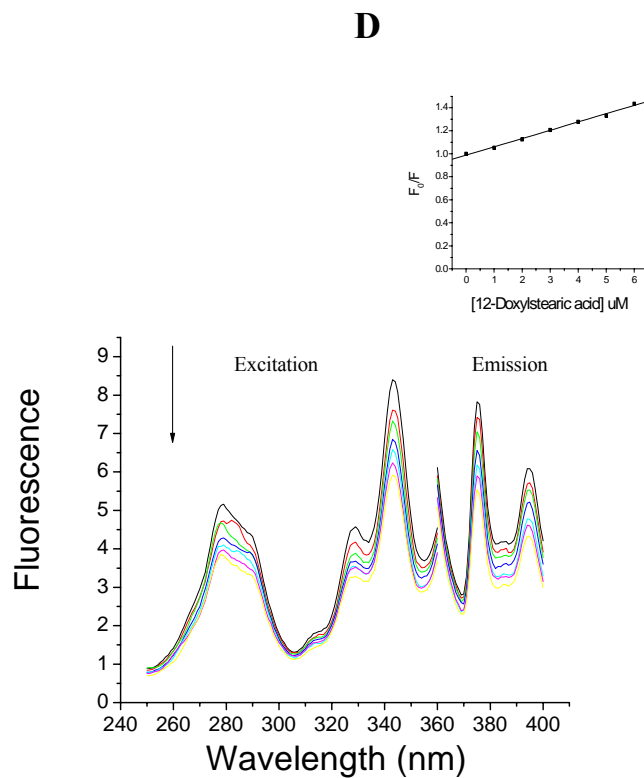


Figure 3.9

Estimation of transmembrane location of MAO-bound pyrene by quenching with 5- and 12-FASL. Shown are fluorescent spectra of pyrene-labeled MAO in membrane bound form before and after spin-labeled fatty acids quenching. (A) pyrene-labeled MAO A quenched by 5-FASL (B) pyrene-labeled MAO A quenched by 12-FASL (C) pyrene-labeled MAO B quenched by 5-FASL (D) pyrene-labeled MAO B quenched by 12-FASL. The insets show Stern-Volmer plots of F_0/F vs concentration of spin-labeled fatty acids. F_0 and F are fluorescence intensities in the absence and in the presence of quenchers, respectively. The fluorescence emission was measured at 376 nm at an excitation wavelength of 345 nm.

		MAO A	MAO B
		K_q (M^{-1})	
Iodide	(in detergent solubilized form)	12.19±0.18	11.24±0.38
	(in membrane bound form)	1.74±0.06	1.68±0.06
		K_q (μM^{-1})	
5-FASL	(in membrane bound form)	0.14±0.01	0.15±0.02
12-FASL	(in membrane bound form)	0.11±0.01	0.07±0.01

Table 3.2 Stern-Volmer quenching constants for quenching of pyrene-labeled MAO A and MAO B fluorescence by iodide and spin-labeled fatty acids.

3.4 Discussion

The work presented in this dissertation shows that purified MAO can be assembled into yeast mitochondria in the presence of ATP and ubiquitin. The hypothetical model of newly synthesized MAO insertion proposed by McCauley (Zhuang *et al.* 1992) has suggested that the requirement of ATP and ubiquitin might result in formation of ubiquitin-protein conjugate. However, there was no direct evidence for formation of such a conjugate, even though McCauley *et al.* has reported a mutant form of ubiquitin, that is not involved in ATP-dependent reaction with the ubiquitin-activating enzyme (E1), inhibited the insertion of bovine MAO B into mitochondria (Zhuang *et al.* 1989). In this work, ubiquitin-MAO conjugates have been detected by use of mouse monoclonal IgG₁ against ubiquitin, further confirming that, with assistance of ubiquitin, detergent solubilized MAO can be imported into yeast mitochondria in a proteinase K-resistant form. McCauley *et al.* speculated that ubiquitin might function like chaperones

in protein transport. However, due to the lack of further biochemical and genetic data, the mechanism that ubiquitin conjugation may be involved in protein translocation into mitochondria still remains unclear.

A typical fluorescence spectrum of pyrene is the superposition of the monomer and the excimer emission (Figure 3.7 A). Formation of excimers in fluid media is thought to be a diffusion controlled process, and the high mobility of pyrene exhibits a high excimer yield (Leonhardt *et al.* 1963; Forster 1969). Due to very low solubility of pyrene in water (10^{-6} M), pyrene in aqueous solution does not show an excimer emission at 465 nm (Figure 3.7 B, solid line). Similarly, the mobility of pyrene attached to the end of C-terminal helix of MAO is restricted in mitochondria membrane so that the emission spectra of pyrene become purely monomeric as well (Figure 3.7 B, dashed line).

It has been stated that the conformations of the end of C-terminal helix (residues 507-527 in MAO A and residues 501-520 in MAO B) are still unknown since these residues are not well defined in electron density map. It would be due to the flexibility of the C-terminal helices of MAO in crystalline form. Comparisons of polarization and anisotropy values of pyrene-labeled MAO in detergent solubilized and membrane bound form (Table 3.1) confirm this assumption. These data show that polarization and anisotropy values of both NPM-labeled MAO A and MAO B in membrane-bound form are ~3 fold greater than that in detergent solubilized form. Incorporation into the lipid bilayer results in the mobility restrictions of C-terminal helices which would be located in a certain position of mitochondria membrane. This consequence enabled us to investigate spatial disposition of C-terminal helices of MAO in membrane.

The doxyl groups of 5-FASL and 12-FASL are assumed to penetrate the membrane about 6 and 15 Å, respectively, from the head-group interface (Voges *et al.* 1987); therefore, different quenching efficiencies of these stearic acids with spin label at different positions along the fatty acyl chain provide information about the membrane-embedded fluorophores. In this work, the topography of the pyrene-labeled cysteine residues on the end of C-terminal helices of MAO with respect to the membrane was experimentally determined by differential fluorescence quenching with spin-labeled stearic acids. According to fluorescence quenching data (Table 3.2), pyrene-labeled MAOA was quenched by 5-FASL slightly greater than 12-FASL. For pyrene-labeled MAO B, the extrinsic fluorescence of pyrene was more readily accessible to quenching by 5-FASL than by 12-FASL. These observations indicate that the end of the C-terminal helix of MAO A would be almost located in the middle of the headgroup interface and the center of the bilayer with a little bit proximity to membrane surface, whereas the end of the C-terminal helix of MAO B is closer to membrane-water interface.

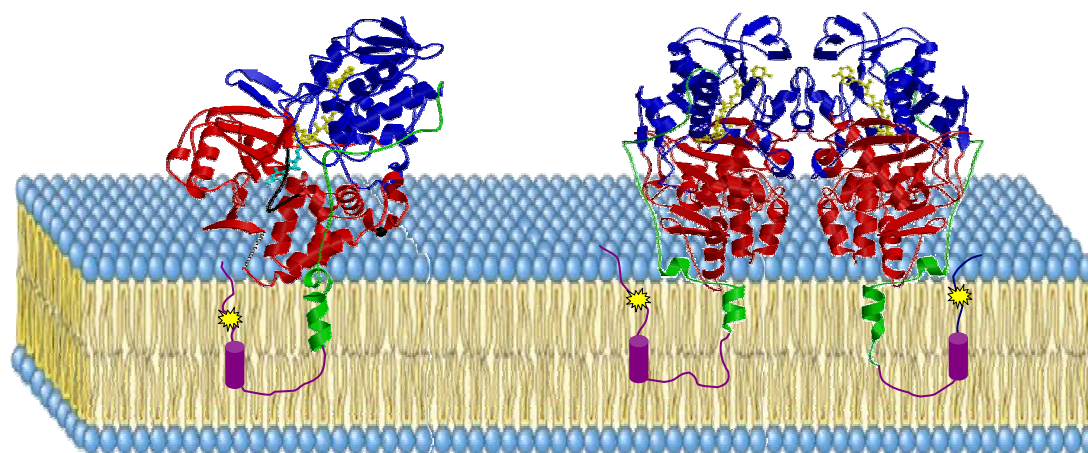
In terms of the predicted structures of C-terminal helices of MAO A and MAO B embedding in mitochondria membrane, the length of the helices would be approximately 45 and 46 Å, respectively, if they are linear. However, a reasonable thickness of mitochondrial outer membrane is ~38 Å. Being mitochondrial outer membrane proteins, if C-terminal helices of MAO span the membrane, the last several residues should be exposed on the opposite side of the membrane with respect to the main body of the protein such that iodide and 5-FASL will not be readily accessible to pyrene-labeled residue on the end of the C-terminal helix. The possible explanation for the results presented in this work, as shown in Figure 3.10, is that the last several residues in MAO

A and MAO B, rather than extending the transmembrane helix, may turn back toward the outer membrane surface. This assumption would be supported by the protein sequences. As shown in Figure 3.10, in the C-terminal helix domains that are not solved by X-ray crystallography, there are two glycine and one proline residues in human MAO A and three glycine residues in human MAO B, respectively. Glycine, which has no side chain, frequently occurs in turn regions of proteins, and proline, whose side chain forms a closed loop with the backbone, introduces a destabilizing kink in an α -helix. Thus, the existence of glycine and proline residues in C-terminal helix would lead to the breaks of α -helix, and this helix turns back to the surface of membrane, rather than traversing the outer mitochondrial membrane. Positively charged residues lysine and arginine on the C-terminus would also facilitate the location of the end of C-terminal helix close to the anionic phospholipid head groups at the membrane-water interface.

In fact, the assumption of conformation of C-terminal helices in MAO is compatible with distance measurements presented in Chapter 2. The distances obtained between DCP, a fluorophore-labeled MAO irreversible inhibitor, at the active site cavity and the end of C-terminus are shorter than that measured from the crystal structures with modeled C-terminal structures. In these modeled structures, the C-terminal helix is assumed to be linear. However, very likely, glycine and proline residues interrupt the C-terminal transmembrane helices of MAO and the polypeptide chain turns back with the C-terminus positioned on the side of membrane-water interface.

Therefore, combining the results of FRET distance measurements, fluorescence quenching data and the protein sequence analysis together, the location of C-terminus of

MAO in mitochondrial outer membrane supports the model depicted in panel A of Figure 3.1.



Human MAO A: SVSGLLKIIGFSTSVTALGFVLYKYKLLPRS
 | | |
 500 510 520

Human MAO B: VPGLLRLIGLTTIFSATALGFLAHKRGLLVRV
 | | |
 490 500 510

Figure 3.10 Proposed structural conformation of human MAO A (left panel) and human MAO B (right panel) C-terminal tail in mitochondrial outer membrane. FAD binding domain in blue (residues 13-88 in human MAO A, residues 4-79, 211-285 and 391-453 in human MAO B), substrate/inhibitor-binding domain in red (residues 89-219 and 295-399 in human MAO A, residues 80-210, 286-390 and 454-488 in human MAO B) and membrane-binding domain in green (residues 463-506 in human MAO A, residues 489-500 in human MAO B). The amino-acid sequences of the C-terminal residues of both human MAO A and human MAO B are indicated. The predicted C-terminal parts (residues 507-527 in human MAO A and residues 501-520 in human MAO B are underlined) are depicted as purple cylinders for α -helix. Yellow stars represent pyrene fluorophores which are attached to the position 525 in human MAO A and the position 518 in human MAO B, respectively.

Although human MAO A and MAO B share 70% sequence identity, their structures differ in some aspects, such as oligomeric states and active site cavities (Binda *et al.* 2002; De Colibus *et al.* 2005). Interestingly, a chimera of human MAO B in which

the C-terminus (residues 393-520) was replaced with the human MAO A C-terminus (residues 402-527) shows no catalytic activity (Chen *et al.* 1996). This observation suggests that MAO C-termini cannot be “swapped” between A and B forms and they function differently in protein folding and membrane insertion, compatible with the results of the studies of their C-terminal helices in this work.

It has been found that in rat liver mitochondrial outer membranes, the majority of phosphatidylethanolamine (PE) faces the cytosol, and phosphatidylinositol (PI) and phosphatidylserine (PS) are preferentially oriented towards the intermembrane space, whereas in mitochondrial outer membranes of yeast, PE faces the intermembrane space and PI is equally distributed across both sides of the outer membrane (Daum *et al.* 1997). The difference in transbilayer distribution of phospholipids between mammals and yeast might cause differential topologies of membrane protein in mitochondria. Therefore, it would be valuable, in the future, to investigate conformation of C-terminus of MAO in their native membranes.

One of the ongoing projects in our laboratory is to construct MAO A and MAO B into phospholipid Nanodiscs and to crystallize and determine the structures of these nanodisc complexes of MAO A and MAO B by X-ray crystallography. It would provide better insights into how MAO A and MAO B bind to the outer mitochondrial membrane.

Chapter 4

High-level Expression of Rat Monoamine Oxidase A in *Pichia pastoris*

4.1 Introduction

The pharmacologically important membrane bound flavoenzymes monoamine oxidase A (MAO A) functions in the oxidative degradation of the neurotransmitters dopamine and serotonin (Weyler *et al.* 1990). Human MAO A is found to be ~90% identical in sequence with rat MAO A with each one containing a FAD cofactor covalently attached to conserved cysteinyl residue via an 8- α -S-thioether linkage. This identity is the premise for using rat MAO A as a good model for the human enzyme in drug development studies. X-ray structural analysis on both enzymes demonstrate that human MAO A is monomeric (De Colibus *et al.* 2005) and rat MAO A dimeric (Ma *et al.* 2004). To further study the functional consequences of this difference in oligomeric form between these two enzymes, it would be valuable to develop an efficient expression system to obtain sufficient amount of functional enzyme so that their catalytic properties could be directly compared.

So far, recombinant human liver MAO A has been successfully overexpressed in the *P. pastoris* expression system and purified with a high yield (Li *et al.* 2002). Ma *et al.* have expressed His-tagged full-length rat MAO A in *Saccharomyces cerevisiae* (Ma *et al.* 2004) and purified only 10 mg of rat MAO A per liter of culture. In our laboratory, taking advantage of *P. pastoris* expression system, rat MAO A is expressed to a high level and ~500 mg of purified enzyme can be obtained from a 1-L fermentation culture.

Furthermore, during the purification procedure, the binding properties of rat MAO A to the ion-exchange column differs from that of human MAO A, suggesting that in spite of the high degree of sequence homology, human MAO A and rat MAO A exhibit different functional characteristics.

4.2 Materials and Methods

4.2.1 Materials

A rat liver cDNA library was the generous gift from Dr. Edward Morgan, Emory University, Department of Pharmacology. The plasmid (pPIC3.5K) and yeast strain KM71 were purchased from Invitrogen Corp. All media for spheroplast transformation and cell growth were prepared as described in the Invitrogen Multi-Copy *Pichia* Expression Kit manual. The antibiotic G418 was purchased from Mediatech (Herndon, VA). β -Octylglucopyranoside was from Anatrace Inc. Reduced Triton X-100 was from Fluka. All the other chemicals were purchased from Sigma-Aldrich.

4.2.2 cDNA cloning of rat MAO A

A 1581 bp cDNA sequence encoding the full-length rat MAO A was amplified by PCR using the rat liver cDNA library as the template and the following oligonucleotides as the primers: rMAOA-F: 5'-GCGGGATCCATGACGGATCTGGAGAAG-3'; rMAOA-R: 5'-CGCGAATTCTCAGCATGGGAGCTTCTTAAT-3'. Underlining in the rMAOA-F and rMAOA-R denotes the restriction sites of *Bam*HI and *Eco*RI, respectively. The isolated fragment was subcloned into *Bam*HI-*Eco*RI-digested pPIC3.5K vector.

4.2.3 Transformation of rat MAO A gene into *P. pastoris*

The pPIC3.5K/rMAO A construct was linearized with *Sal* I to target integration at the AOXI locus in the *Pichia* genome. The spheroplast transformation of rat MAO A gene into the yeast strain KM71 was performed by the method described previously (Li *et al.* 2002).

4.2.4 Expression of rat MAO A

Several G418-resistant transformants were chosen to perform shake-flask expression screening as instructed in the Invitrogen *Pichia* manual. After examination by activity assay and Western blot analysis, the colony containing highest multiple copies of the rat MAO A gene was chosen for fermentation growth and expression. Fermentation of cells expressing rat MAO A was carried out according to the protocol the same as human MAO A (Li *et al.* 2002). The cells were harvested by centrifugation at 1500×g for 10 min at 4°C. After washing with breakage buffer (50 mM sodium phosphate, 5% glycerol, 1 mM EDTA, 1 mM PMSF, pH 7.2), the cells were stored at -80°C.

4.2.5 Purification of rat MAO A

Yeast cells from a 1 liter of culture was suspended into 1 liter of breakage buffer with an equal volume of silica-zirconia beads (0.5 mm in diameter) and then broken in Biospec Beadbeater (Bartlesville, OK) with 6 cycles of 2-min beating and 5-min chilling on the ice. After separation from the glass beads by filtration through a layer of Miracloth (Calbiochem), the cell lysate was isolated from unbroken cells and large cell debris by centrifugation at 1500×g for 10 min at 4°C. The supernatant which is the cell lysate was

centrifuged at $100,000\times g$ for 25 min at 4°C to isolate the membrane fraction. The pellet was resuspended to a protein concentration of 25mg/ml in 10 mM potassium phosphate at pH 7.2 and then digested by 1 mg of phospholipase C and 6700 units of phospholipase A_2 per 500 mg of protein with 25 mM CaCl_2 . The digestion reaction was stirred at room temperature in the dark for 1 hour with the maintained at pH 7.0-7.2 by adding dilute NH_4OH . The digestion mixture was centrifuged at $100,000\times g$ for 15 min at 4°C and the pellet was resuspended into 10 mM potassium phosphate at pH 7.2 to a protein concentration of approximately 15 mg/ml. Triton X-100 was added to a final concentration of 0.5% (w/v) and the mixture was stirred at room temperature in the dark for 30 min. After centrifugation at $100,000\times g$ for 15 min at 4°C , the Triton X-100 extract was collected and uploaded onto a fast flow DEAE-Sepharose column ($25\times 600\text{mm}$) which was charged with 5 column volumes of 250 mM potassium phosphate (pH 7.2) and pre-equilibrated with 10 column volumes of 10 mM potassium phosphate containing 20% glycerol (pH 7.2). After washing with 10 column volumes of 10 mM potassium phosphate containing 20% glycerol and 1 mM PMSF (pH 7.2) to remove unbound protein, the enzyme was eluted with a linear gradient of 20 to 200 mM potassium phosphate buffer containing 20% glycerol, 30 μM DTT, 0.8% (w/v) β -octylglucopyranoside, 0.5 mM d-amphetamine and 1 mM PMSF (pH 7.2). The enzyme fraction was pooled according to $A_{280/456}$ ratios and specific activity. After concentrated to 30 μM by Amicon Ultra 30K centrifugal filter (Millipore), the salt concentration of the enzyme was adjusted to 50 mM potassium phosphate and the purified rat MAO A was stored at 4°C in 50% (v/v) glycerol.

During the purification process, 1 ml samples of cell lysate, membrane fraction phospholipase digestion, Triton X-100 extract and the purified protein were saved, respectively. The protein activities were measured as described in 4.2.8 steady state studies. The protein concentrations of all samples were determined with Biuret method, except that the purified protein for which Bearden's method was used.

4.2.6 Mass spectral analysis

The sample for MALDI-TOF/TOF-MS experiments was prepared as follows: the rat MAO A band was excised from a 2-D gel, destained by Destaining Solution (10 mM ammonium bicarbonate/50% acetonitrile/water) and dried in speed vacuum. The gel slices were treated with fresh Activated Trypsin (0.05 $\mu\text{g}/\mu\text{l}$ of trypsin in 10 mM ammonium bicarbonate/water) and Digestion Buffer (10 mM ammonium bicarbonate) and incubated at 37°C overnight. The reaction was stopped by adding 10% (v/v) trifluoroacetic acid, and the digestion mixture was removed and stored in a clean tube. Peptides were extracted from gel pieces using 150 μl of 10 mM ammonium bicarbonate/60% acetonitrile/water. All digestion mixtures were collected, concentrated and reconstituted in 10 μl of 10 mM ammonium bicarbonate/60% acetonitrile/water. The aliquots were then desalted by ZipTip_{C18} equilibrated with 0.1% trifluoroacetic acid and eluted with 70% acetonitrile/0.1% trifluoroacetic acid/water. The in-gel trypsin digested rat MAO A peptide sample was analyzed on a Bruker Daltonics Ultraflex II MALDI-TOF/TOF-MS (Billerica, MA). The matrix used for MALDI-TOF/TOF-MS was α -cyano-4-hydroxycinnamic acid. The rat MAO A peptide sample was analyzed in the positive ionization mode.

4.2.7 Thermal stability

Solutions of human MAO A (10 μ M), and rat MAO A (10 μ M) were incubated at three different temperatures: 0°C, 25°C, 30°C. The loss of enzyme activity was determined over a 2-hour period. Every 10 minutes, 5 μ L aliquots were removed for the determination of catalytic activity. For human MAO A, the rate of 1 mM kynuramine oxidation in 50 mM HEPES with 0.5% reduced Triton X-100 (pH 7.5) was monitored at 316 nm. The rate of oxidation of 1 mM *p*-(trifluoromethyl)benzylamine oxidation in 50 mM HEPES with 0.5% reduced Triton X-100 (pH 7.5) by rat MAO A to *p*-(trifluoromethyl)benzaldehyde was followed spectrophotometrically by monitoring characteristic absorption at 243 nm.

4.2.8 Steady-state kinetic studies

All rat MAO A activity assays were performed in 50 mM potassium phosphate assay buffer (pH 7.5) with 0.5% reduced Triton X-100 and the conversion of substrates was spectrophotometrically assayed using a Perkin-Elmer Lambda 2 UV-Vis spectrophotometer at 25°C. 4-CF₃-benzylamine was the substrate used for measurement of thermal stability and competitive inhibition by following the formation of the corresponding aldehyde at 243 nm ($\epsilon = 11,800 \text{ M}^{-1}\text{cm}^{-1}$). It is noted that d-amphetamine was removed by gel filtration (Sephadex G-25) before performing steady-state kinetic studies.

4.3 Results

4.3.1 Enzyme expression and purification

As described in the experimental section, rat MAO A was successfully overexpressed in *P. pastoris*. The purification scheme of rat MAO A (Table 4.1) shows that 1 liter cell culture produced 687 units of rat MAO A protein and protein with a yield of 43% was purified from the crude product. We find that rat MAO A binds less tightly to the DEAE-Sepharose column than does wild-type human MAO A since 25 mM potassium phosphate buffer, which was used for purification of wild-type human MAO A, interferes the binding of rat MAO A to the DEAE-Sepharose column. Therefore, a low salt concentration (10 mM potassium phosphate) was used for resuspending the pellets, pre-equilibrating and washing the column. It is found that rat MAO A elutes from the column earlier than human MAO A. The specific activity of purified rat MAO A (1.42 U/mg) is similar to that of human MAO A (1.7 U/mg) (Li *et al.* 2002).

Step	Total protein (mg)	Total activity (U)	Specific activity (U/mg)	Yield (%)
Cell Lysate	27010	687	0.025	100
Membrane Fraction	12464	596	0.048	87
Phospholipase Digestion	11938	472	0.040	69
Triton X-100 Extraction	2441	432	0.177	63
DEAE Sepharose Elution pool	207	294	1.42	43

Table 4.1 Purification scheme of recombinant rat liver MAO-A expressed in *P. pastoris*

4.3.2 Protein characterization

The purity of rat MAO A at the different purification steps using SDS-polyacrylamide gel is shown in Figure 4.1 a. The main bands of each lane have the same molecular weights (60 kD) which represent MAO. The purified rat MAO A is also confirmed by Western blot analysis using antisera raised against human MAO A (Figure 4.1 b). Rat MAO A expressed in *P. pastoris* contains a covalent flavin cofactor detected by an antisera specific for the covalent flavin moiety (Figure 4.1 c) (Barber *et al.* 1987).

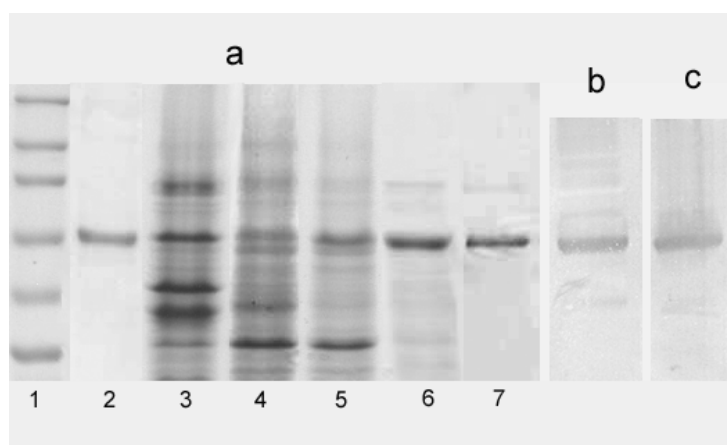


Figure 4.1 SDS-polyacrylamide gel electrophoresis of rat MAO A. (a) Coomassie-stained gel (7.5%) of rat MAO A at different purification steps: lane 1: protein standard; lane 2: wild-type human MAO A (control); lane 3: cell lysate; lane 4: membrane fraction; lane 5: phospholipase digestion; lane 6: Triton X-100 extraction; lane 7: purified rat MAO A. (b) Western blot of rat MAO A detected by antisera against MAO. (c) Western blot of rat MAO A detected by antisera against the flavin cofactor.

4.3.3 MALDI-TOF/TOF-MS analysis

In order to confirm the sequence of rat MAO A, the enzyme was digested with trypsin and analyzed by MALDI-TOF/TOF-MS. The results are shown in Figure 4.2, and the bottom panel shows the peaks with lower intensity that are not obvious in the top panel. The sizes of the labeled fragments are consistent with that of the calculated peptides of trypsin-digested rat MAO A listed in Table 4.2.

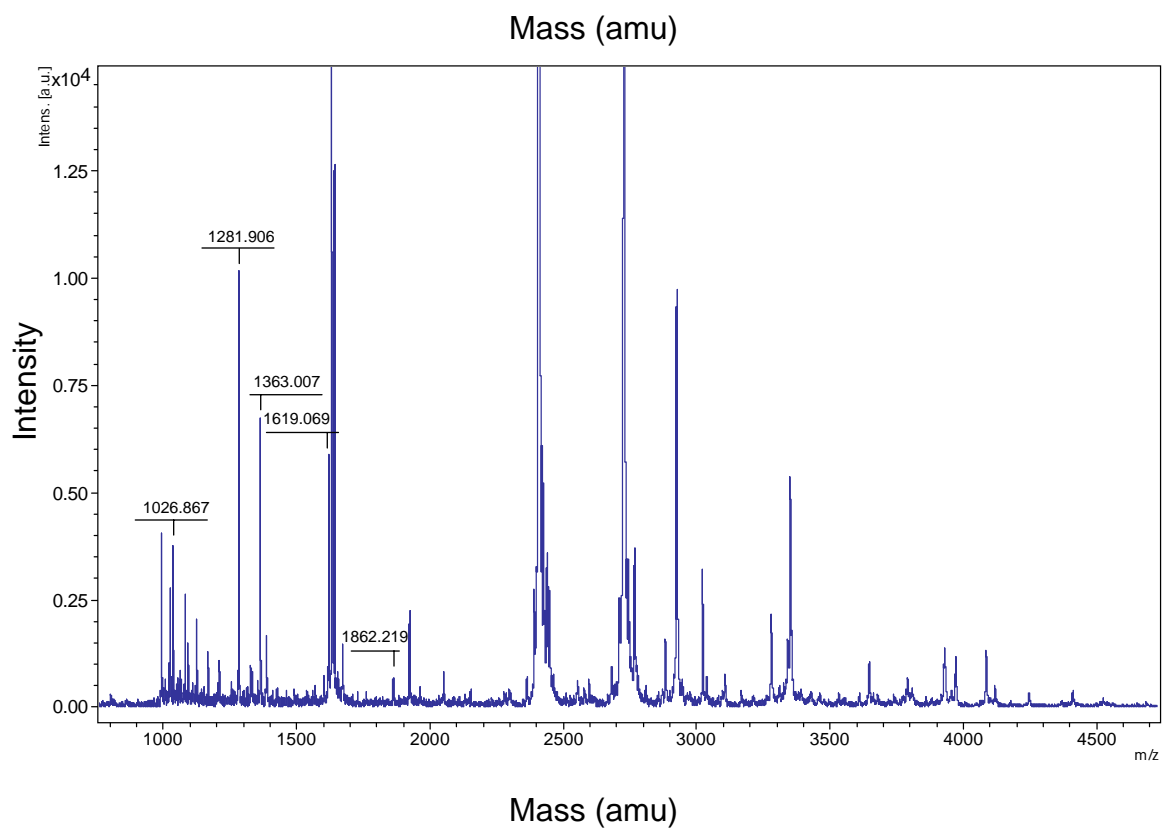
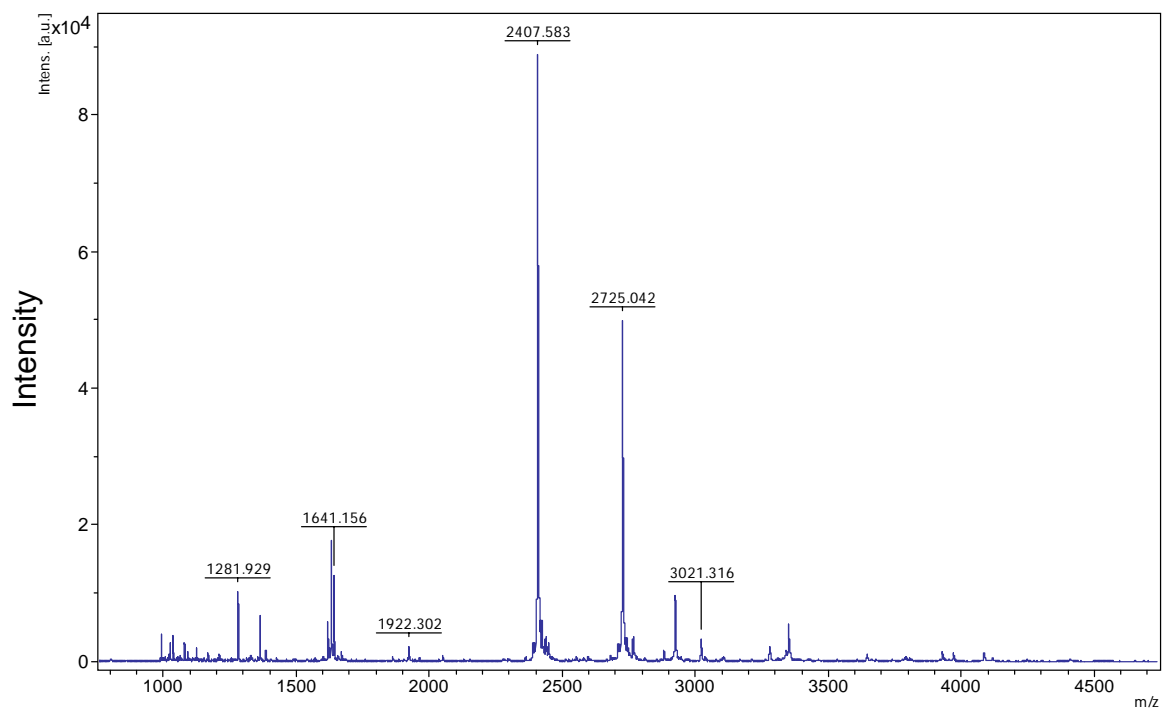


Figure 4.2 MALDI-TOF/TOF-MS analysis of the trypsin digested rat MAO A expressed in *P. pastoris*.

Position of cleavage site	Resulting peptide sequence	Observed Peptide mass (Da)	Calculated Peptide mass (Da)
45	INVLVLEAR	1026.867	1026.244
76	WVDVGGAYVGPTQNR	1619.069	1618.769
129	GAFPPVWNPLAYLDYNNLWR	2407.583	2406.728
147	EIPVDAPWQAR	1281.929	1281.434
237	FVGGSGQVSEQIMGLLGDK	1922.302	1922.183
291	IHKPELPPER	1363.007	1362.594
395	VLGSQEALYPVHYEEK	1862.219	1862.069
421	NWCEEQYSGGICYTAYFPPGIMTQYGR	3021.316	3022.331
454	IYFAGTETATQWSGYMEGAVEAGER	2725.042	2724.938
493	DVPAIEITHTFLEER	1641.156	1640.857

Table 4.2 Summary of MALDI-TOF/TOF-MS analysis of trypsin-digested rat MAO A.

4.3.4 Functional characterization

To estimate the functionality of rat MAO A after purified from *P. pastoris*, the level of anaerobic reduction of the flavin cofactor by the substrate tyramine was determined by the spectral changes of flavin absorbance (456 nm). As shown in Figure 4.3, after addition of the excess substrate tyramine, the flavin (the solid line, 1, Figure 4.3) was significantly “bleached” (the dashed line, 2, Figure 4.3). To further confirm if the flavin cofactor was completely reduced, the excess reducing reagent sodium dithionite was added to the protein solution, and only a slight further reduction of flavin cofactor was observed (the dotted line, 3, Figure 4.3). With the comparison of the spectral changes of flavin cofactor between addition of tyramine and sodium dithionite, the purified rat MAO A was estimated to be 96% functional.

As shown in Figure 4.4, addition of the acetylenic mechanism-based irreversible inhibitor clorgyline, the oxidized flavin ($\epsilon = 12,000 \text{ M}^{-1} \text{ cm}^{-1}$) of recombinant rat MAO A is stoichiometrically converted to its N(5) flavocyanine adduct ($\epsilon = 23,400 \text{ M}^{-1} \text{ cm}^{-1}$), further confirming that the purified rat MAO A is almost fully functional.

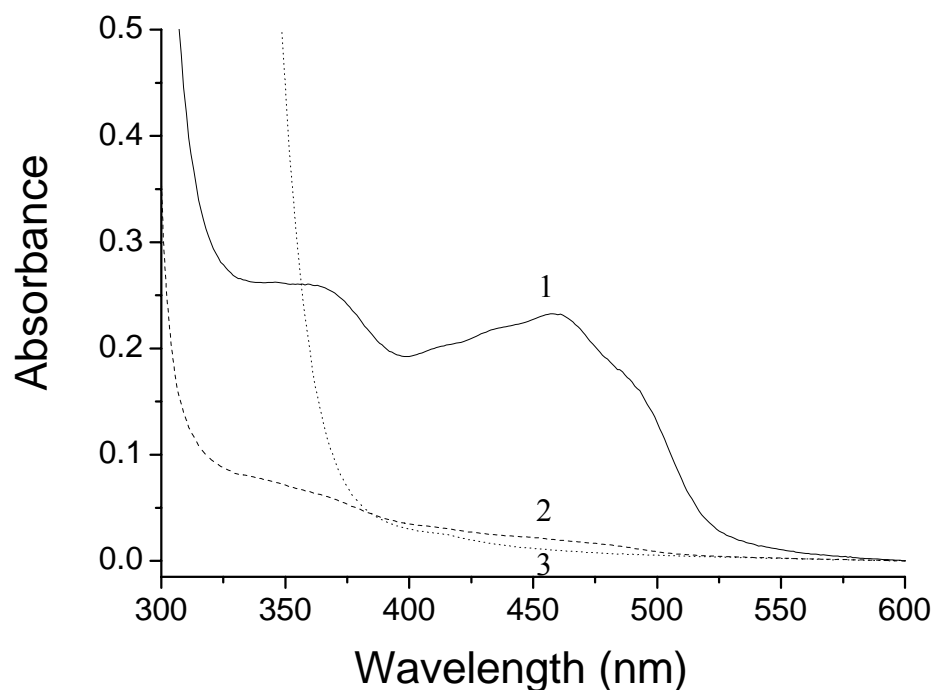


Figure 4.3 UV-Vis spectral changes of purified rat MAO A upon anaerobic reduction by tyramine in 50 mM potassium phosphate containing 20% glycerol and 0.8% (w/v) β -octylglucopyranoside. Line 1 (—) is purified rat MAO A before the addition of tyramine. Line 2 (---) is purified rat MAO A after the addition of excess tyramine. Line 3 (.....) is purified rat MAO A after the addition of a few crystals of sodium dithionite.

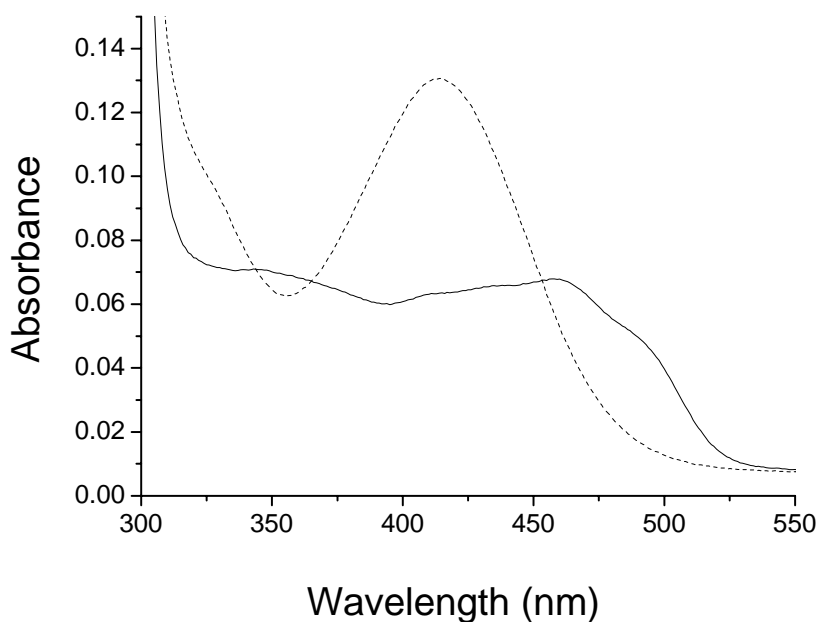


Figure 4.4 UV-Vis spectra of purified rat MAO A before (—) and after (---) the addition of 10-fold molar excess of clorgyline. The reaction was performed in 50 mM potassium phosphate buffer (pH 7.2) containing 20% glycerol and 0.8% (w/v) β -octylglucopyranoside.

4.3.5 Thermal stability

As reported previously, human MAO B, which is dimeric (Binda *et al.* 2002), exhibits a higher thermal stability than monomeric human MAO A (De Colibus *et al.* 2005). Therefore, thermal stability experiment was performed to investigate if the purified rat MAO A is thermally more stable than human MAO A. The data in Figure 4.5 show that both purified human and rat MAO A can remain fully active when incubated at temperature as high as 0°C and are stable for at least 120 minutes. At 25°C, only 10% of rat MAO A activity is lost after 120-minute incubation, whereas human MAO A loses ~60% activity. Rat MAO A still retains ~80% of enzyme activity after being incubated at 30°C for 120 minutes. In contrast, ~80% of human MAO A activity is lost at that temperature.

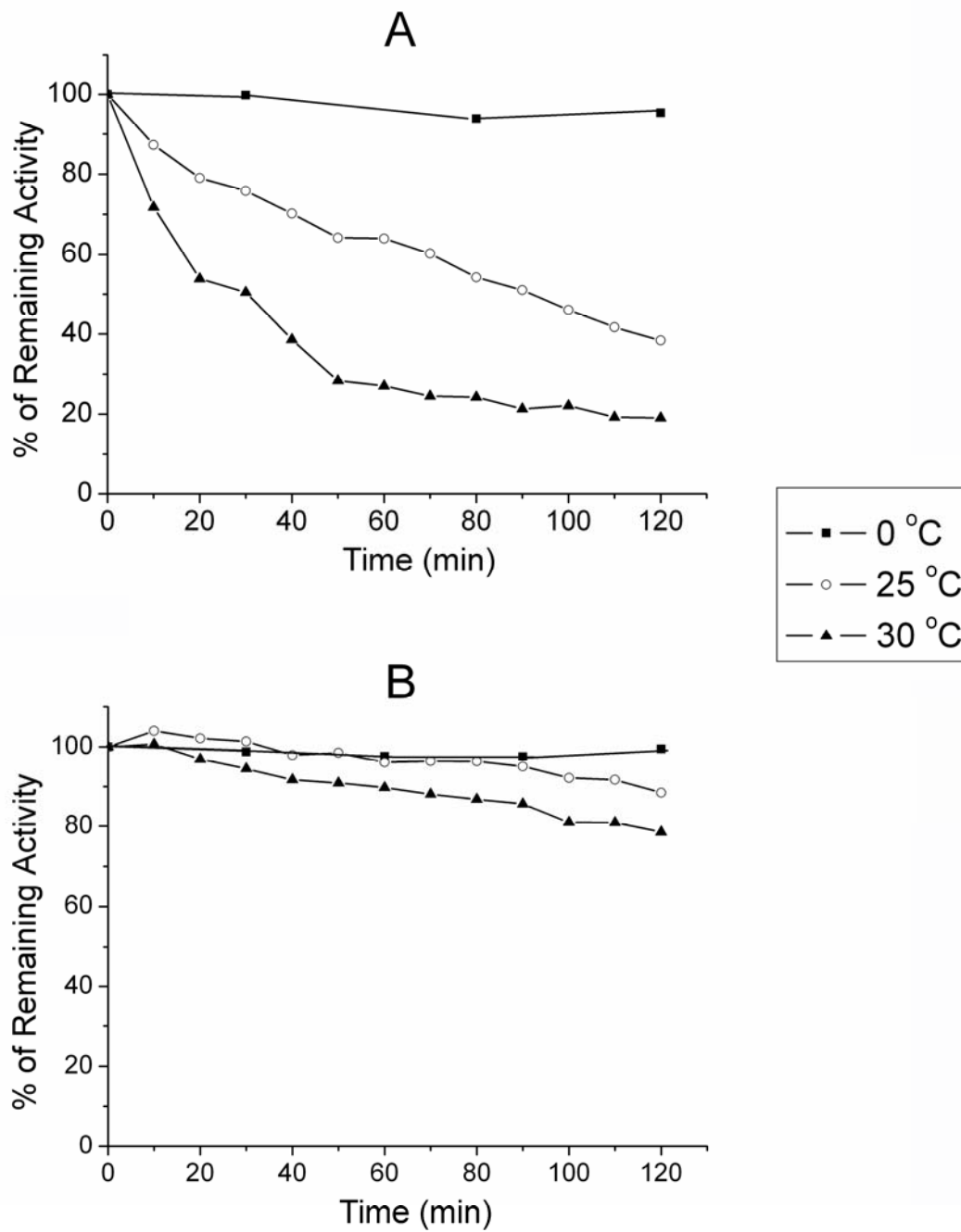


Figure 4.5 Comparison of thermal stability of human MAO A (A) and rat MAO A (B). Profiles of remaining enzyme activity versus incubation time at 0°C, 25°C and 30°C, respectively, are shown.

4.3.6 Catalytic properties

The steady-state kinetic parameters for rat MAO A compared with the published values for human MAO A are shown in Table 4.3. Rat MAO A exhibits a much higher catalytic efficiency (40-fold increase) for oxidation of benzylamine relative to human MAO A. For the substrates kynuramine and serotonin, the turn over number and K_m values of rat MAO A are not significantly different from that of human MAO A. Rat MAO A oxidizes phenylethylamine, the MAO B specific substrate, with a ~7 fold higher catalytic efficiency than does human MAO A.

The values of K_i of rat MAO A for different inhibitors, isatin, phentermine and d-amphetamine, are essentially identical with those of human MAO A.

4.4 Discussion

As shown previously with human MAO A, the multiple copies of the rat MAO A gene can be incorporated into the *Pichia* genome to facilitate the high level expression of the enzyme. As documented in this chapter, the amount of rat MAO A produced in the *Pichia* expression system is 50-fold higher than in *S. cerevisiae*, which is helpful in the future for mechanistic and structural studies.

It is of interest that, as observed in purification profile of rat MAO A, low salt concentration of potassium phosphate buffer is required for the binding of the enzyme to the DEAE Sepharose column. Since proteins are charged molecules, the interaction of proteins with the column resin depends upon the distribution of charges molecules on the surface of the proteins. Furthermore, binding affinity of mobile counter ions bound to the resin should be weaker than that of protein to the resin, so that protein will displace the

		Rat MAO A			Human MAO A		
		k_{cat} (min^{-1})	K_m (mM)	k_{cat}/K_m ($\text{min}^{-1}\text{mM}^{-1}$)	k_{cat} (min^{-1})	K_m (mM)	k_{cat}/K_m ($\text{min}^{-1}\text{mM}^{-1}$)
Substrate	Benzylamine	19.5 ± 0.2	0.21 ± 0.02	92.9 ± 8.9	2.5 $\pm 0.1^a$	1.04 $\pm 0.15^a$	2.4 $\pm 0.4^a$
	Kynuramine	149.1 ± 1.7	0.09 ± 0.01	1656.7 ± 185.0	125.4 $\pm 8.5^b$	0.13 $\pm 0.01^b$	964.6 $\pm 98.9^b$
	Phenylethylamine	85.0 ± 0.7	0.35 ± 0.01	242.9 ± 7.2	53.8 $\pm 1.0^c$	1.48 $\pm 0.08^c$	36.4 $\pm 2.1^c$
	Serotonin	358.7 ± 6.7	0.30 ± 0.02	1195.7 ± 82.8	175.1 $\pm 2.1^c$	0.30 $\pm 0.05^c$	583.7 $\pm 97.5^c$
		K_i (μM)					
Reversible Inhibitor	Isatin	10.5 \pm 1.8			15 ^d		
	Phentermine	625.6 \pm 81.9			498 ^e		
	d-Amphetamine	5.98 \pm 0.46			3.69 \pm 0.45		

Table 4.3 Comparison of steady-state kinetic properties of the purified human and rat MAO A's

^a from Miller *et al.* (Miller *et al.* 1999)

^b from Nandigama *et al.* (Nandigama *et al.* 2001)

^c from Li *et al.* (Li *et al.* 2002)

^d Unpublished data from Min Li, Dr. Edmondson's lab

^e from Nandigama *et al.* (Nandigama *et al.* 2002)

mobile counter ions and bind to the resin. Since DEAE-Sepharose is a weaker anion exchanger, the negative surface charges on MAO could facilitate the binding of enzyme on DEAE-Sepharose. Study on MAO surface charge shows that distribution of negatively charged residues is greater on human MAO A (sum of formal charge is -6) than on rat MAO A (sum of formal charge is +2), resulting in a stronger binding of human MAO A to the positively charged DEAE-Sepharose resin (Figure 4.6). Therefore, the salt

concentration that allows binding of human MAO A (25 mM potassium phosphate) to the resin has to be decreased to 10 mM for binding of rat MAO A to DEAE-Sepharose column.

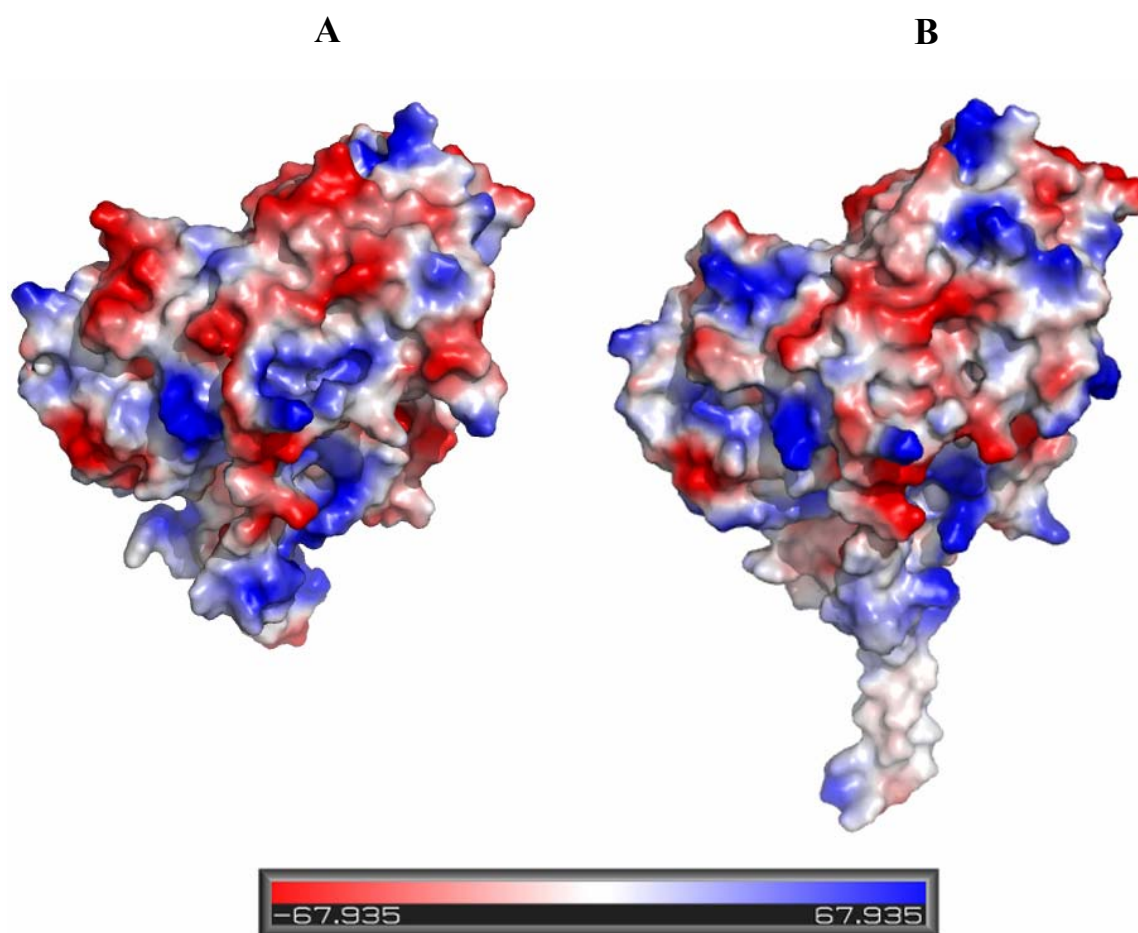


Figure 4.6 Electrostatic features of human MAO A (A) and rat MAO A (B). The figures were prepared with the program Pymol (DeLano Scientific, San Carlos, CA). Electrostatic potential is colored from negative potential (red) to positive potential (blue). Neutral potential is shown in white.

Thermal stability studies show that rat MAO A exhibits a much higher stability than human MAO A. Since MAOs are outer mitochondrial membrane proteins, most of

biochemical studies on the purified enzymes have to be performed in detergent solution. Oligomeric state of MAOs would be a key factor to affect the stability of MAO in detergent solubilized form. Therefore, the different thermal stability between human and rat MAO A's might be explained by the fact that in their detergent solubilized forms, human MAO A is a monomer whereas rat MAO A is dimeric.

Different catalytic efficiencies between rat MAO A and human MAO A in oxidation of the substrates suggest that rat MAO A oxidizes MAO B-specific substrates more rapidly than does human MAO A. The dimeric form of rat MAO A could affect the shape of activity cavity which would be similar to that of dimeric human MAO B to adapt human MAO B's substrates. With regard to inhibitors, rat MAO A does not show significant differences from human MAO A, indicating that other factors rather than the oligomeric state of enzyme affect inhibitor specificities of MAOs.

Chapter 5

Functional Comparison of Human MAO A K151E and Rat

MAO A with WT-human MAO A

5.1 Introduction

Human MAO A is found to be ~90% identical in sequence with rat MAO A. The recent crystallographic and analytical ultracentrifugation data suggest that human MAO A is a monomer (De Colibus *et al.* 2005) whereas rat MAO A is dimeric (Ma *et al.* 2004). According to the comparison of the coding region of the MAO genes among human, chimpanzee, gorilla as well as other mammalian species, Andres *et al.* (Andres *et al.* 2004) found that only one human exclusive non-conservative change is present in the sequence of human MAO A, a Lys at position 151, while MAO A in other mammalian species as well as human MAO B exist as dimer with Glu at the analogous position. Modeling studies show that this human specific substitution may affect protein dimerization since a Glu/Lys mutation at position 151 is expected to destabilize the dimeric structure.

It is of interest to investigate the structural and functional basis for this selection mutation in human MAO A. The Lys151Glu mutant of human MAO A was created and its functional properties were studied. Moreover, the sequence identity of human and rat MAO A is the premise for using rat MAO A as a model for the human enzyme in drug development studies. Therefore, in this chapter, the functional consequences of this selection mutation among human wild-type MAO A, human MAO A K151E mutant and rat MAO A were investigated.

5.2 Materials and Methods

5.2.1 Materials

The plasmid (pPIC3.5K) and strain (KM71) were obtained from Invitrogen Corp. β -Octylglucopyranoside was from Anatrace Inc. Potassium phosphate was from Fisher and reduced Triton X-100 was from Fluka. Glycerol, HEPES, isatin, benzylamine, kynuramine, phenylethylamine, serotonin, d-amphetamine, deprenyl, phentermine and 1,4-diphenyl-2-butene were purchased from Sigma-Aldrich. Rasagiline was a gift from TEVA Pharmaceuticals. 7-(3-Chlorobenzoyloxy)-4-(methylamino)methyl-coumarin and 7-(3-Chlorobenzoyloxy)-4-carboxaldehyde-coumarin were from Angelo Carotti, University of Bari (Bari, Italy). Chlorostyrylcaffeine was a gift from Dr. Neal Castagnoli, Virginia Tech University. Harmane, pirlindole mesylate and tetrindole mesylate were purchased from TOCRIS Bioscience. All benzylamine analogs were synthesized as described previously (Walker *et al.* 1994).

5.2.2 Creation of human MAO A K151E mutant

Human MAO A K151E was created using QuikChange XL Site-Directed Mutagenesis Kit (STRATAGENE). The PCR amplifications and the subsequent cloning steps were carried out according to the manufacturer's instruction. The constructs of human MAO A K151E in pPIC3.5K vector was linearized with *Sal* I to target integration at the AOX1 locus in the *Pichia* genome. The spheroplast transformation of the mutated MAO A genes into the yeast strain KM71 was performed by the method described previously (Li *et al.* 2002).

5.2.3 Expression and purification of human MAO A K151E

Human MAO A K151E was expressed in *Pichia pastoris* strain KM71 and purified as described previously (Li *et al.* 2002). A 1-liter cell culture yielded ~200 mg of purified enzyme with a specific activity of 1.7 units of MAO A/mg of protein. The purified protein was stored in 50 mM potassium phosphate containing 20% glycerol and 0.8% (w/v) octyl β -D-glucopyranoside (pH 7.2). D-Amphetamine, a reversible MAO A inhibitor used for stabilizing the enzyme during purification, was removed prior to all kinetic measurements.

5.2.4 Thermal stability

Solutions of WT-human MAO A (10 μ M), human MAO A K151E (10 μ M) and rat MAO A (10 μ M) were incubated at four different temperatures: 0°C, 15°C, 25°C, 30°C. The loss of enzyme activity was determined over a 2-hour period. Every 10 minutes, 5 μ L aliquots were removed for the determination of catalytic activity. For WT-human MAO A and human MAO A K151E mutant, the rate of 1 mM kynuramine oxidation in 50 mM HEPES with 0.5% reduced Triton X-100 (pH 7.5) was monitored at 316 nm. The rate of oxidation of 1 mM *p*-(trifluoromethyl)benzylamine oxidation in 50 mM HEPES with 0.5% reduced Triton X-100 (pH 7.5) by rat MAO A to *p*-(trifluoromethyl)benzaldehyde was followed spectrophotometrically by monitoring characteristic absorption at 243 nm.

5.2.5 Determination of k_{cat} , K_m and K_i

k_{cat} , and K_m values were obtained by fitting steady state kinetic data to the Michaelis-Menten equation using a nonlinear least-squares fitting routine in Origin software. Competitive K_i values were determined by measuring initial rates of substrate oxidation in the presence of varying concentrations of inhibitor. All assays were performed in air-saturated solutions.

5.2.6 Determination of $K_m(O_2)$

Assays at 25°C in 50 mM potassium phosphate, pH 7.5, containing 0.5% reduced Triton X-100 were followed spectrophotometrically with oxidation of kynuramine at 316 nm. Oxygen concentrations were varied by equilibration of the buffer with 10%, 50% oxygen/nitrogen mixtures in stoppered cuvettes.

5.2.7 Steady state kinetic measurements of *para*-substituted benzylamine analogue oxidation

All steady state kinetic measurements of *para*-substituted benzylamine analog oxidation with rat MAO A were performed in 50 mM HEPES buffer (pH 7.5) containing 0.5% (w/v) reduced Triton X-100 at 25°C. The steady state rate of benzylamine analog oxidation to the corresponding benzaldehyde was measured spectrophotometrically. Monitoring wavelength and molar absorption extinction coefficients for each aldehyde were given by Walker and Edmondson (Walker *et al.* 1994). It is noted that the oxidation rates of *p*-F-BA, *p*-Me-BA, *p*-MeO-BA as well as α,α -[^2H]benzylamine analogs are too low to accurately monitor the formation of the corresponding aldehyde, therefore,

Amplex Red-peroxidase coupled assays ($\epsilon_{560} = 54,000 \text{ M}^{-1}\text{cm}^{-1}$) were used as it has a 5 fold higher level of sensitivity.

5.2.8 Data analysis

Values of substituent parameters σ and V_w were obtained from Hansch *et al.* (Hansch *et al.* 1995) and from Bondi (Bondi 1964), respectively. Binding data for the benzylamine analogs were determined from steady state deuterium kinetic isotope effect data as described by Klinman and Matthews (Klinman *et al.* 1985). Multivariate linear regression analysis of rate and binding data as a function of substituent parameters was performed using the StatView software package (Abacus Concepts)

5.3 Results

5.3.1 Enzyme expression and purification

As described in the experimental section, human MAO A K151E was successfully overexpressed in *P. pastoris*. The purification scheme of rat MAO A (Table 5.1) shows that 1 liter cell culture produced 406 units of human MAO A K151E protein purified from the crude extract.

Step	Total protein (mg)	Total activity (U)	Specific activity (U/mg)	Yield (%)
Cell Lysate	18080	406	0.022	100
Membrane Fraction	5696	358	0.063	88
Phospholipase Digestion	6600	352	0.053	87
Triton X-100 Extraction	2784	319	0.115	78
DEAE Sepharose Elution	106	183	1.734	45

Table 5.1 Purification scheme of human MAO-A K151E expressed in *P. pastoris*

5.3.2 Spectral property of human MAO A K151E

The purified human MAO A K151E shows the absorption of flavin cofactor at 456 nm (Figure 5.1). By adding the acetylenic mechanism based irreversible inhibitor clorgyline, the flavocyanine adduct is formed, exhibiting characteristic absorption at 410 nm.

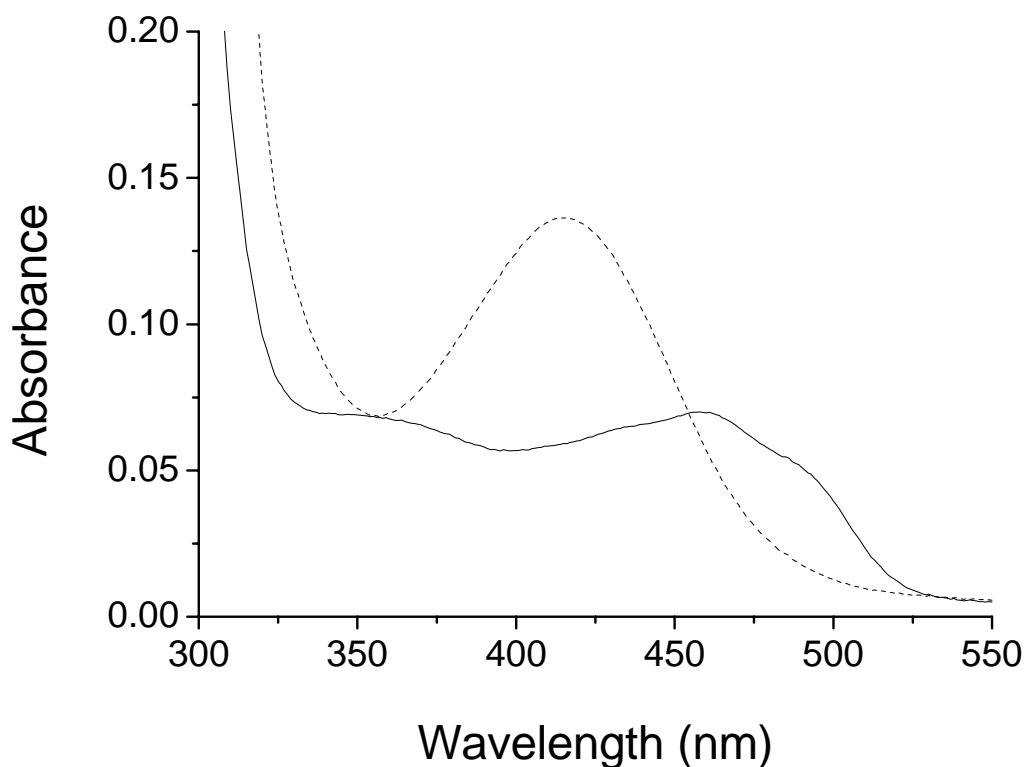
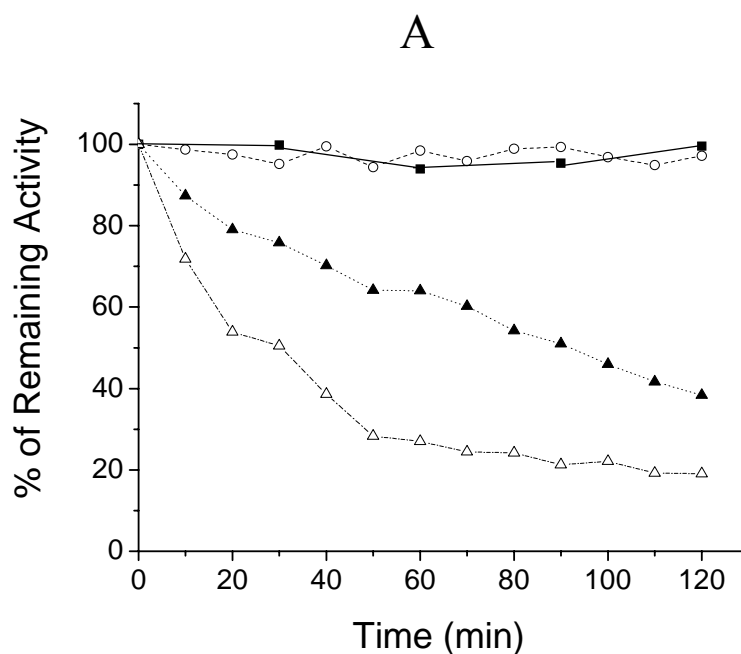


Figure 5.1 UV-Vis spectra of purified human MAO A K151E before (—) and after (---) the addition of 10-fold molar excess of clorgyline. The reaction was performed in 50 mM potassium phosphate buffer (pH 7.2) containing 20% glycerol and 0.8% (w/v) β -octylglucopyranoside.

5.3.3 Thermal stability

Since human MAO B is much more thermally stable than human MAO A, its dimeric structure is thought to confer stabilization of the enzyme. In Figure 5.2, the

thermal stability of WT-human MAO A, human MAO A K151E and rat MAO A are compared at four different temperatures: 0°C, 15°C, 25°C and 30°C. These three enzymes exhibit pronounced stability at 0°C and 15°C, making possible perform stopped flow studies at low temperatures (10°C or below). At 25°C, human MAO A loses ~60% activity in 120 minutes (Figure 5.2 A), whereas human MAO A K151E and rat MAO A remain 80% and 90% activity, respectively (Figure 5.2 B and C). At 30°C, ~80% of human MAO A activity is lost. In contrast, human MAO A K151E loses ~40% of enzyme activity, and rat MAO A still retains 80% catalytic activity. Therefore, the observations on thermal stability show that human MAO A K151E is more thermally stable than monomeric WT-human MAO A but less stable than dimeric rat MAO A.



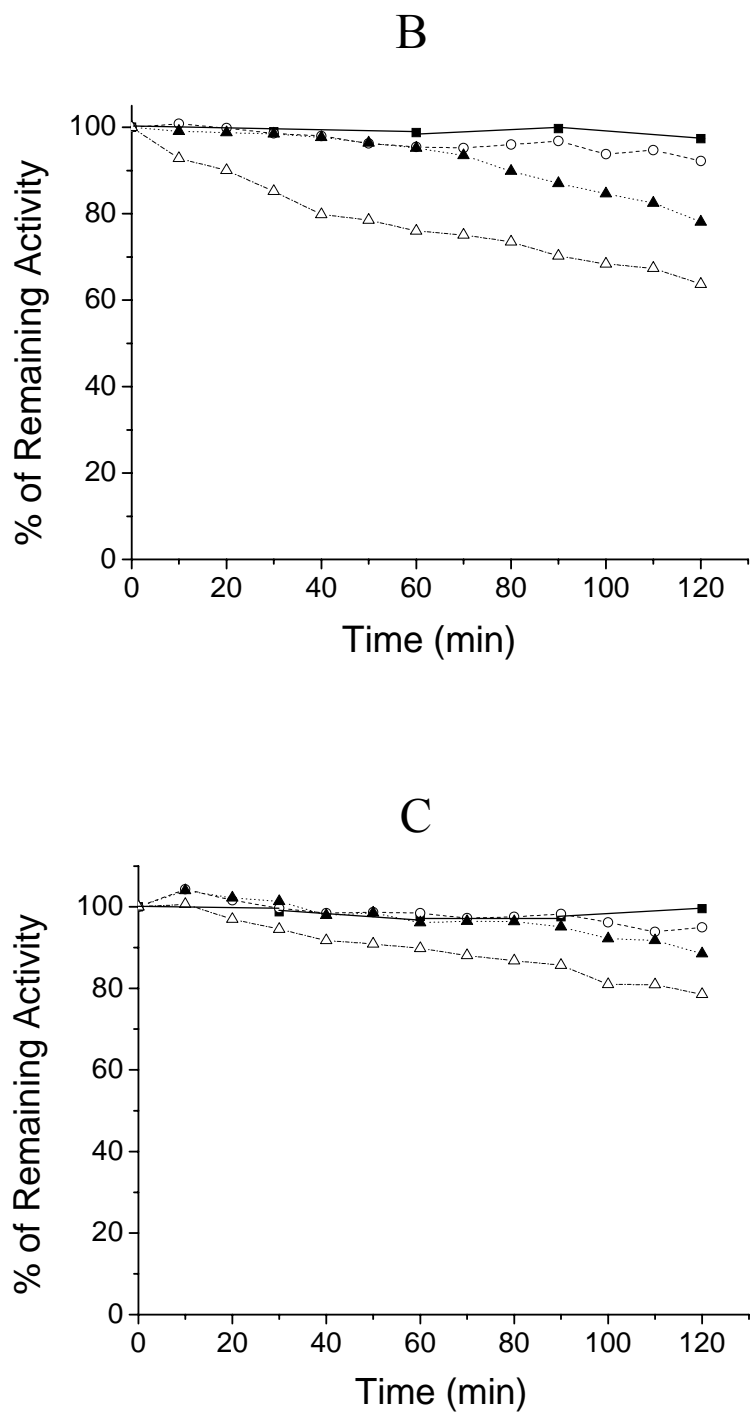


Figure 5.2

Comparison of thermal stability of WT-human MAO A (A), human MAO A K151E mutant (B) and rat MAO A (C). Profiles of remaining enzyme activity versus incubation time at 0°C (— ■), 15°C (--- ○), 25°C (..... ▲) and 30°C (- · - · - · Δ), respectively, are shown.

5.3.4 Steady state kinetic properties and competitive inhibition

The observed kinetic constants for the oxidation of benzylamine (Table 5.2) show that benzylamine is a better substrate for human MAO A K151E and rat MAO A with 3-fold and 40-fold increase, respectively, in catalytic efficiency relative to WT-human MAO A. Both WT-human MAO A and human MAO A K151E oxidize kynuramine with similar catalytic efficiency, whereas rat MAO A shows 2-fold higher catalytic efficiency. Phenylethylamine is oxidized by human MAO A K151E and rat MAO A with 3.3-fold and 6.7-fold higher catalytic efficiency, respectively, than does WT-human MAO A. For serotonin, both human MAO A K151E and rat MAO A exhibit higher catalytic efficiency than WT-human MAO A.

For competitive inhibitors (Table 5.3), only small changes are observed among these three enzymes regarding inhibitor specificity and affinity. The reversible MAO B selective inhibitors 1,4-diphenyl-2-butene and chlorostyrylcaffeine do not exhibit any inhibition of human MAO A, human MAO A K151E mutant or rat MAO A activity.

5.3.5 $K_m(O_2)$

The activities of human MAO A K151E and rat MAO A were measured at different concentrations of oxygen with kynuramine as the amine substrate. The Lineweaver-Burk plots with oxygen as the variable substrate (Figure 5.3 A and Figure 5.4 A) intersect on the y axis, indicating both human MAO A K151E and rat MAO A follow ternary-complex mechanism. The values of $K_m(O_2)$ obtained from Hanes-Woolf plots for human MAO A K151E and rat MAO A (Figure 5.3 B and Figure 5.4 B) are 10.5 μM and 9.3 μM , respectively; very similar to that of WT-human MAO A ($\sim 6 \mu\text{M}$)

(Ramsay 1991). The data calculated from Lineweaver-Burk plots (10.4 μM for human MAO A K151E and 9.0 μM for rat MAO A) are consistent with that from Hanes-Woolf plots.

		Benzylamine	Kynuramine	Phenylethylamine	Serotonin
Human MAO A	k_{cat} (min^{-1})	2.5 \pm 0.1 ^a	125.4 \pm 8.5 ^b	53.8 \pm 1.0 ^c	175.1 \pm 2.1 ^c
	K_{m} (mM)	1.04 \pm 0.15 ^a	0.13 \pm 0.01 ^b	1.48 \pm 0.08 ^c	0.30 \pm 0.05 ^c
	$k_{\text{cat}}/K_{\text{m}}$ ($\text{min}^{-1}\text{mM}^{-1}$)	2.4 \pm 0.4 ^a	964.6 \pm 98.9 ^b	36.4 \pm 2.1 ^c	583.7 \pm 97.5 ^c
Human MAO A K151E	k_{cat} (min^{-1})	4.16 \pm 0.04	67.5 \pm 1.3	42.8 \pm 1.3	178.0 \pm 3.9
	K_{m} (mM)	0.65 \pm 0.02	0.10 \pm 0.01	0.36 \pm 0.03	0.21 \pm 0.02
	$k_{\text{cat}}/K_{\text{m}}$ ($\text{min}^{-1}\text{mM}^{-1}$)	6.37 \pm 0.04	674.7 \pm 50.5	119.4 \pm 10.0	836.6 \pm 68.9
Rat MAO A	k_{cat} (min^{-1})	19.5 \pm 0.2	149.1 \pm 1.7	85.0 \pm 0.7	358.7 \pm 6.7
	K_{m} (mM)	0.21 \pm 0.02	0.09 \pm 0.01	0.35 \pm 0.01	0.30 \pm 0.02
	$k_{\text{cat}}/K_{\text{m}}$ ($\text{min}^{-1}\text{mM}^{-1}$)	92.9 \pm 8.9	1656.7 \pm 185.0	242.9 \pm 7.2	1195.7 \pm 82.8

Table 5.2 Comparison of steady state kinetic properties of WT-human MAO A, human MAO A K151E and rat MAO A.

^a from Miller *et al.* (Miller *et al.* 1999)

^b from Nandigama *et al.* (Nandigama *et al.* 2001)

^c from Li *et al.* (Li *et al.* 2002)

	Human MAO A	Human MAO A K151E K_i (μ M)	Rat MAO A
d-Amphetamine	3.69±0.45	8.99±0.90	5.98±0.46
Deprenyl	N. D.	264.54±21.65	353.84±46.01
Isatin	15 ^a	13.38±0.32	10.54±1.79
Phentermine	498±60 ^b	338.85±25.19	625.58±81.93
7-(3-Chlorobenzoyloxy)-4-(methylamino)methyl-coumarin	15.73±1.99	7.26±0.44	8.65±0.12
7-(3-Chlorobenzoyloxy)-4-carboxaldehyde-coumarin	10.97±0.48	6.37±0.25	9.50±0.81
Rasagiline	9.7 ^c	10.19±0.64	25.63±4.35
Harmane	0.58±0.02	0.42±0.05	0.75±0.04
Pirlindole Mesylate	0.92±0.04	0.77±0.07	0.77±0.02
Tetrindole Mesylate	5.27±0.24	3.25±0.06	3.55±0.34
1,4-Diphenyl-2-butene	No Inhibition	No Inhibition	No Inhibition
Chlorostyrylcaffeine	No Inhibition	No Inhibition	No Inhibition

Table 5.3 Comparison of competitive inhibition constants for WT-human MAO A, human MAO A K151E and rat MAO A. N. D. is not determined.
^a Unpublished data from Franta Hubalek, Dr. Edmondson's lab
^b from Nandigama *et al.* (Nandigama *et al.* 2002)
^c from Hubalek *et al.* (Hubalek *et al.* 2004)

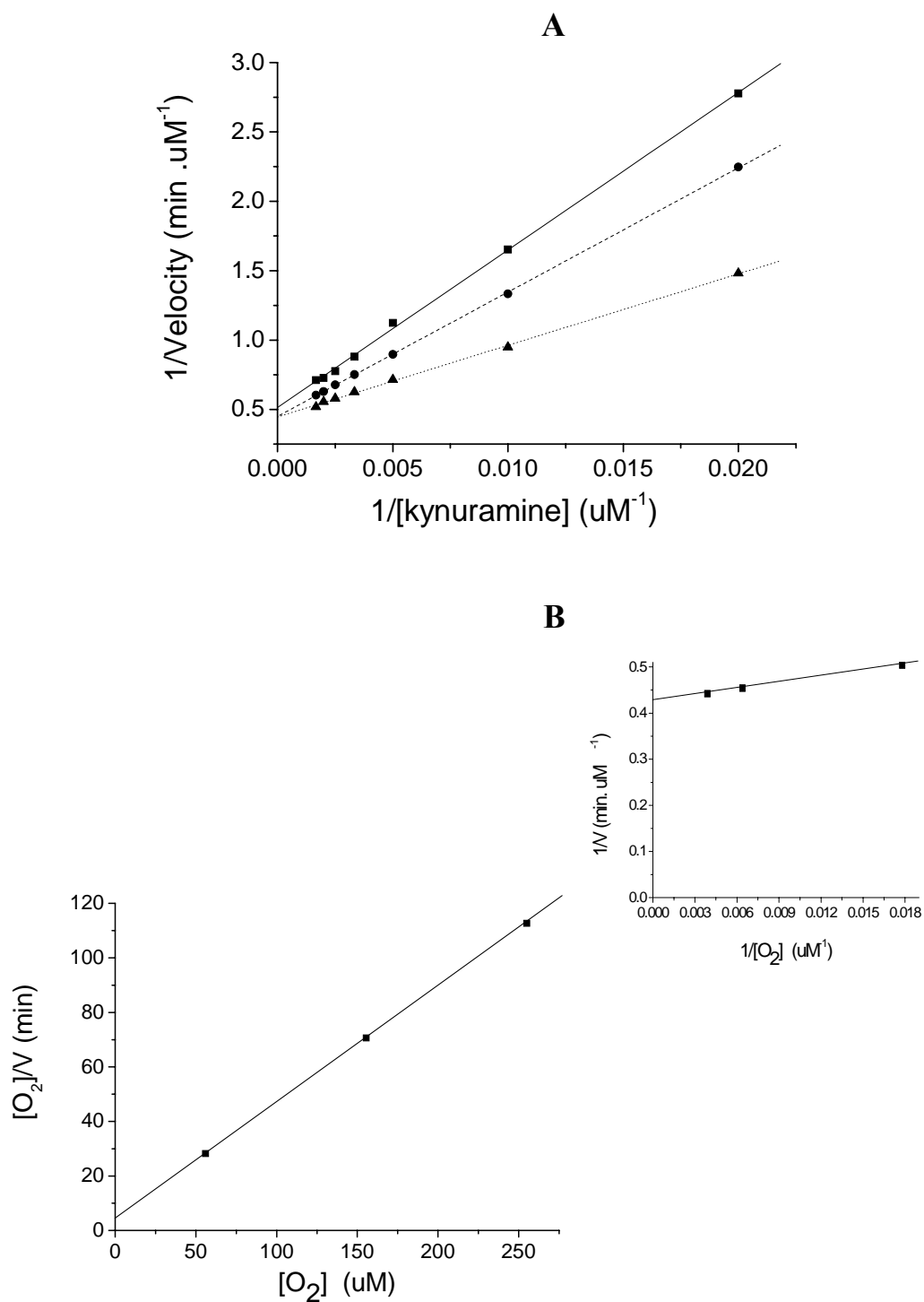


Figure 5.3

Steady-state kinetics for the oxidation of kynuramine by human MAO A K151E with different oxygen concentrations. (A) Effect of the oxygen concentration on the Lineweaver-Burk plots for varying kynuramine. The oxygen concentrations were 56 μM (—■), 155.5 μM (---●) and 255 μM (.....▲), respectively. (B) Hane-Woolf plot for determination of $K_m(\text{O}_2)$. The inset is a Lineweaver-Burk plot for determination of $K_m(\text{O}_2)$.

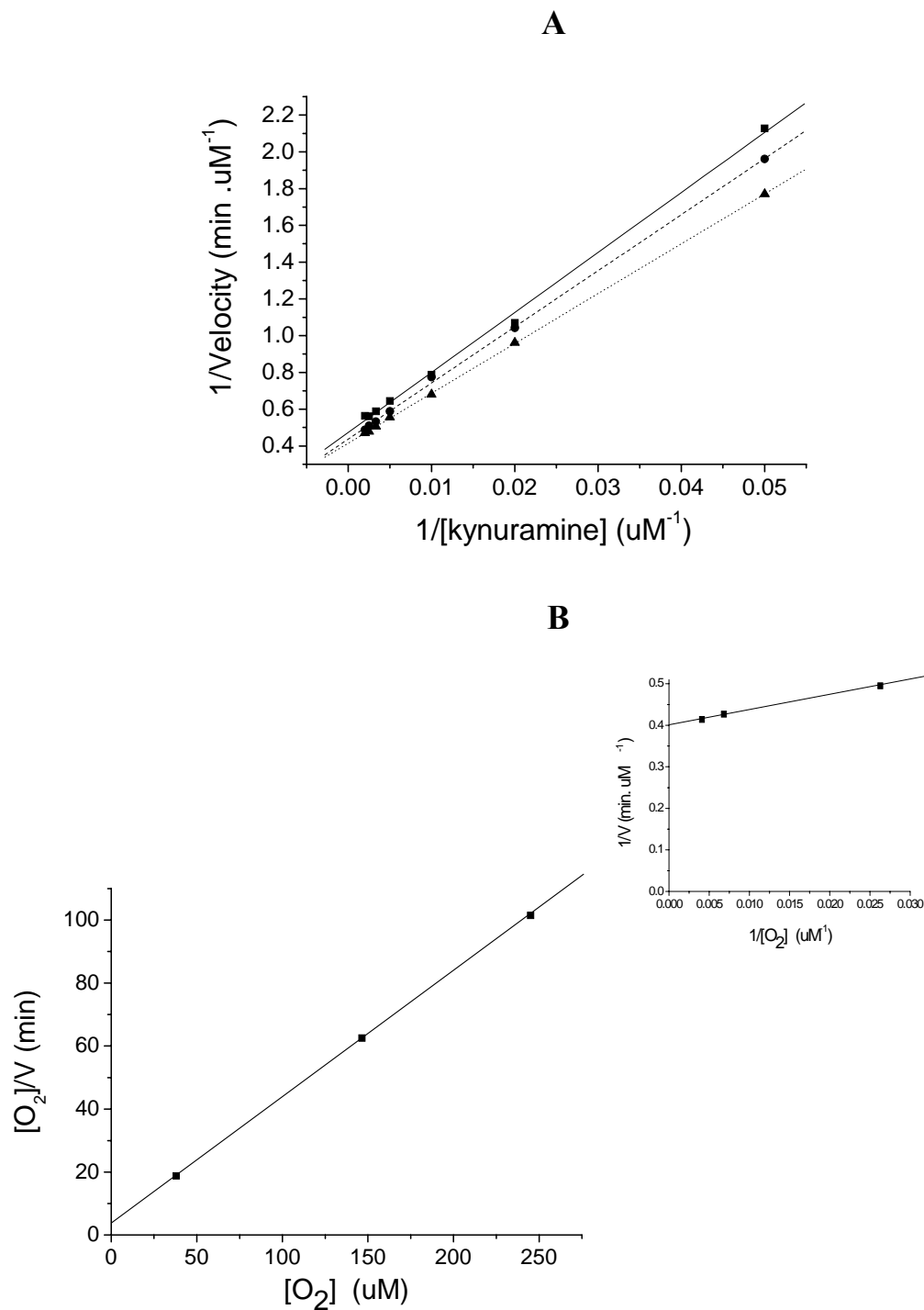


Figure 5.4 Steady-state kinetics for the oxidation of kynuramine by rat MAO A with different oxygen concentrations. (A) Effect of the oxygen concentration on the Lineweaver-Burk plots for varying kynuramine. The oxygen concentrations were 38 μM (—■), 146.5 μM (---●) and 245 μM (.....▲), respectively. (B) Hane-Woolf plot for determination of $K_m(\text{O}_2)$. The inset is a Lineweaver-Burk plot for determination of $K_m(\text{O}_2)$.

5.3.6 Steady state kinetics of the human MAO A K151E and rat MAO A catalyzed oxidation of *para*-substituted benzylamine analogues and the effects of isotopic substitution

The steady-state kinetic parameters for human MAO A K151E mutant and rat MAO A catalyzed oxidation of seven *para*-substituted benzylamine analogues were determined and the respective values for k_{cat} and K_m are shown in Table 5.4 and Table 5.5. Due to the low $K_m(\text{O}_2)$ of human MAO A K151E mutant and rat MAO A, these analogues were tested in air saturated buffer and analyzed by Michaelis-Menten equation. The turnover numbers ($k_{\text{cat}}(\text{H})$) of human MAO A K151E mutant and rat MAO A determined for each substrate show a marked dependence on substituent. The k_{cat} values of human MAO A K151E for the analogues tested range from 4.16 min^{-1} for *p*-H analogue to 166.11 min^{-1} for *p*-CF₃ analogue (Table 5.4), and the k_{cat} values of rat MAO A for the analogues tested range from 9.16 min^{-1} for *p*-MeO analogue to 333.47 min^{-1} for *p*-CF₃ analogue (Table 5.5). Human MAO A K151E mutant oxidation of the benzylamine analogues is characterized by $^{\text{D}}(k_{\text{cat}}/K_m)$ values in the range of 4-8. Examination of the α,α -[²H]benzylamine analogues with rat MAO A showed large isotope effect ($^{\text{D}}(k_{\text{cat}}/K_m)$ ranges from 7-13).

Comparison of the observed rates of *para*-substituted benzylamine oxidation for WT-human MAO A, human MAO A K151E mutant and rat MAO A (Table 5.6) show large isotope effects on k_{cat} , indicating that α -C-H bond cleavage (the reductive half-reaction) is rate limiting in steady state turnover of these enzymes.

<i>para</i> substituent	$k_{\text{cat}}(\text{H})$ (min^{-1})	$K_{\text{m}}(\text{H})$ (μM)	$^{\text{D}}k_{\text{cat}}$	$k_{\text{cat}}(\text{D})$ (min^{-1})	$K_{\text{m}}(\text{D})$ (μM)	$^{\text{D}}(\text{V/K})$
<i>p</i> -H	4.16 ± 0.04	653.36 ± 17.80	7.86 ± 0.14	0.53 ± 0.01	675.87 ± 21.52	8.13 ± 0.04
<i>p</i> -CF ₃	166.11 ± 2.74	228.80 ± 9.94	7.90 ± 0.15	21.01 ± 0.22	145.02 ± 4.96	5.01 ± 0.29
<i>p</i> -Br	44.36 ± 0.46	104.60 ± 4.46	11.52 ± 0.13	3.85 ± 0.02	40.45 ± 1.92	4.46 ± 0.29
<i>p</i> -Cl	26.53 ± 0.44	62.53 ± 4.47	8.64 ± 0.15	3.07 ± 0.01	61.12 ± 1.66	8.44 ± 0.08
<i>p</i> -F	6.64 ± 0.08	184.41 ± 7.71	4.31 ± 0.08	1.54 ± 0.02	181.45 ± 7.34	4.24 ± 0.26
<i>p</i> -Me	14.17 ± 0.07	49.82 ± 1.59	8.24 ± 0.06	1.72 ± 0.01	52.19 ± 1.83	8.63 ± 0.41
<i>p</i> -MeO	5.24 ± 0.02	28.20 ± 0.88	5.35 ± 0.11	0.98 ± 0.02	22.02 ± 0.49	4.18 ± 0.18

Table 5.4 Steady-state kinetic constants for the human MAO A K151E catalyzed oxidation of *p*-substituted benzylamine analogues

<i>para</i> substituent	$k_{\text{cat}}(\text{H})$ (min^{-1})	$K_{\text{m}}(\text{H})$ (μM)	$^{\text{D}}k_{\text{cat}}$	$k_{\text{cat}}(\text{D})$ (min^{-1})	$K_{\text{m}}(\text{D})$ (μM)	$^{\text{D}}(\text{V/K})$
<i>p</i> -H	19.49 ± 0.19	211.13 ± 18.70	6.72 ± 0.17	2.90 ± 0.07	422.8 ± 51.87	13.46 ± 2.06
<i>p</i> -CF ₃	333.47 ± 5.36	194.02 ± 9.87	8.37 ± 0.19	39.86 ± 0.67	273.24 ± 13.69	11.78 ± 0.88
<i>p</i> -Br	62.50 ± 0.98	33.69 ± 3.24	13.24 ± 0.24	4.72 ± 0.04	29.96 ± 1.58	11.78 ± 1.31
<i>p</i> -Cl	43.77 ± 0.96	53.71 ± 6.20	14.26 ± 0.39	3.07 ± 0.05	30.99 ± 3.16	8.23 ± 1.29
<i>p</i> -F	13.96 ± 0.36	174.06 ± 13.56	11.35 ± 0.36	1.23 ± 0.02	109.27 ± 8.70	7.12 ± 0.82
<i>p</i> -Me	16.24 ± 0.14	54.87 ± 2.24	10.61 ± 0.23	1.53 ± 0.03	41.96 ± 3.87	8.11 ± 0.84
<i>p</i> -MeO	9.16 ± 0.24	79.62 ± 9.54	11.17 ± 0.50	0.82 ± 0.03	59.92 ± 10.21	8.41 ± 1.79

Table 5.5 Steady-state kinetic constants for the rat MAO A catalyzed oxidation of *p*-substituted benzylamine analogues

<i>para</i> substituent	Human MAO A ^a		Human MAO A K151E		Rat MAO A	
	$k_{\text{cat}}(\text{H})$ (min^{-1})	$^{\text{D}}k_{\text{cat}}$	$k_{\text{cat}}(\text{H})$ (min^{-1})	$^{\text{D}}k_{\text{cat}}$	$k_{\text{cat}}(\text{H})$ (min^{-1})	$^{\text{D}}k_{\text{cat}}$
<i>p</i> -H	2.54±0.08	11.5±0.6	4.16±0.04	7.86±0.14	19.49±0.19	6.72±0.17
<i>p</i> -CF ₃	85.1±1.7	8.1±0.2	166.11±2.74	7.90±0.15	333.47±5.36	8.37±0.19
<i>p</i> -Br	17.2±0.5	9.6±0.4	44.36±0.46	11.52±0.13	62.50±0.98	13.24±0.24
<i>p</i> -Cl	15.2±0.5	9.8±0.4	26.53±0.44	8.64±0.15	43.77±0.96	14.26±0.39
<i>p</i> -F	7.55±0.38	8.2±0.3	6.64±0.08	4.31±0.08	13.96±0.36	11.35±0.36
<i>p</i> -Me	7.94±0.28	10.0±0.5	14.17±0.07	8.24±0.06	16.24±0.14	10.61±0.23
<i>p</i> -MeO	1.56±0.03	12.9±0.7	5.24±0.02	5.35±0.11	9.16±0.24	11.17±0.50

Table 5.6 Comparison of steady-state rates of human MAO A, human MAO A K151E and rat MAO A catalyzed oxidation of α , α -[¹H]-*p*-substituted benzylamines and deuterium kinetic isotope effects observed with α , α -[²H]-*p*-substituted benzylamines.
^a from Miller *et al.* (Miller & Edmondson, 1999)

5.3.7 Effect of the *para* substituent on the rates of steady state turnover

Linear regression analysis of the rate of steady state turnover of human MAO A K151E and rat MAO A with electronic substituent parameter (σ) was performed using a set of 7 benzylamine substrate analogues (Figure 5.5 and Figure 5.6). A strong correlation of the rate of turnover of enzyme with electronic substituent parameter (σ) was observed, and positive values of the slopes (Figure 5.5 and Figure 5.6) suggest that electron-withdrawing substituents increase the rate of turnover. Moreover, Similar ρ values were

observed in correlations of the steady state oxidation rate of the deuterated substrate analogues and the equations describing the steady state human MAO A K151E mutant and rat MAO A by α, α -[^1H]- and α, α -[^2H]-*p*-substituted benzylamines are

$$\text{Human MAO A K151E} \quad \log k_{\text{cat}} ([^1\text{H}]) = 1.79(\pm 0.50)\sigma + 1.06 (\pm 0.13) \quad \text{Equation 5.1}$$

$$\log k_{\text{cat}} ([^2\text{H}]) = 1.58(\pm 0.45)\sigma + 0.22(\pm 0.12) \quad \text{Equation 5.2}$$

$$\text{Rat MAO A} \quad \log k_{\text{cat}} ([^1\text{H}]) = 1.83(\pm 0.29)\sigma + 1.35(\pm 0.08) \quad \text{Equation 5.3}$$

$$\log k_{\text{cat}} ([^2\text{H}]) = 1.84(\pm 0.38)\sigma + 0.32(\pm 0.10) \quad \text{Equation 5.4}$$

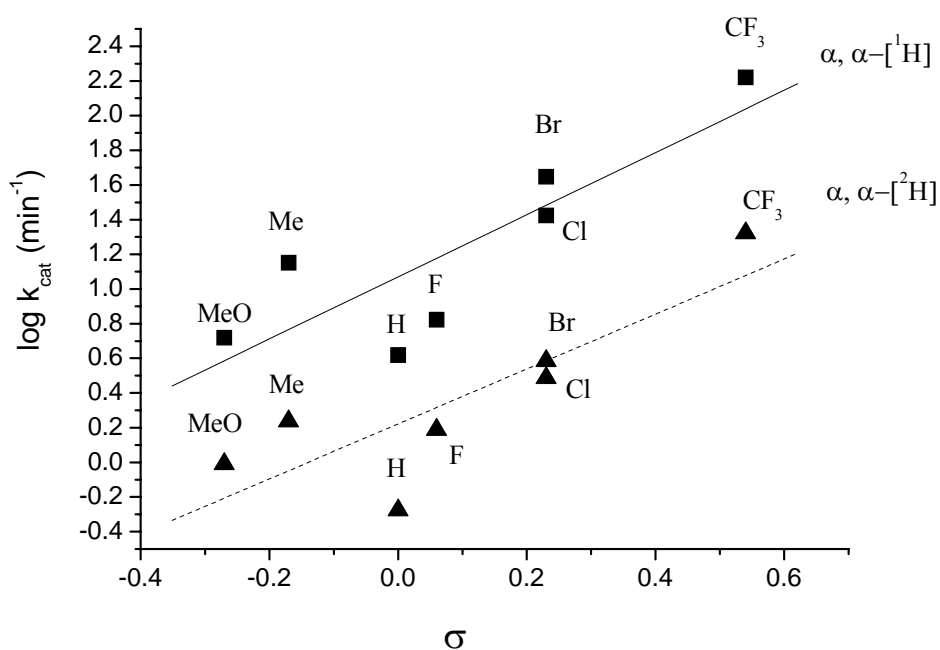


Figure 5.5 Correlation of steady state rates of human MAO A K151E turnover of α, α -[^1H] (—■) and α, α -[^2H]-*p*-substituted benzylamines (---▲) with the substituent electronic parameter (σ).

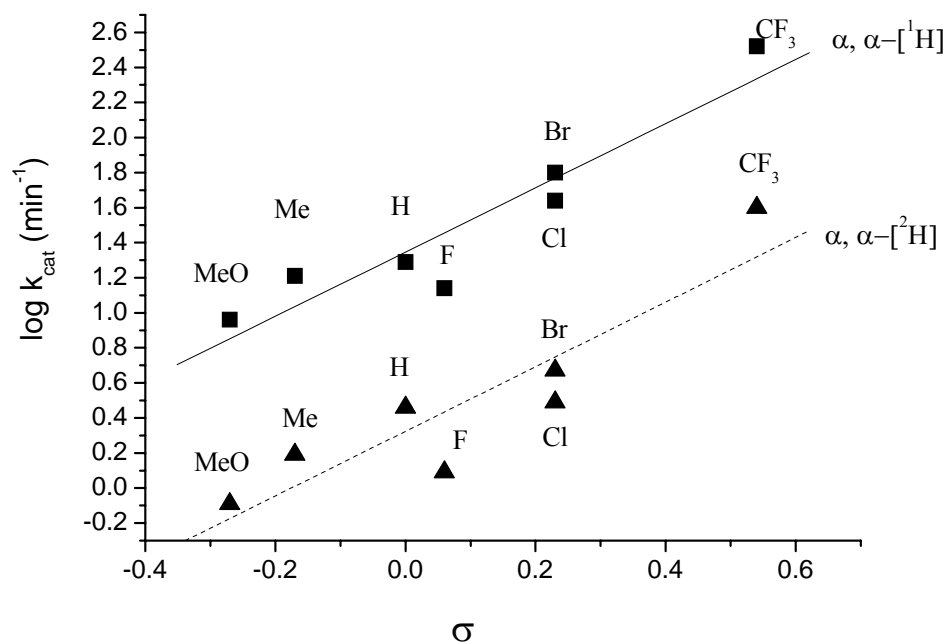


Figure 5.6 Correlation of steady state rates of rat MAO A turnover of $\alpha, \alpha\text{-}[^1\text{H}]$ (—■) and $\alpha, \alpha\text{-}[^2\text{H}]$ -*p*-substituted benzylamines (---▲) with the substituent electronic parameter (σ).

To investigate whether human MAO A K151E mutant and rat MAO A exhibit the same effect of *para* substituents on the rate of turnover of benzylamine oxidation as does WT-human MAO A, the linear regression analysis of $\log k_{\text{cat}}$ of human MAO A K151E mutant and rat MAO A as a function of the electronic parameter σ is compared with the published values of WT-human MAO A (Miller *et al.* 1999). Figure 5.7 shows that the correlations of electronic substituent parameter with rate of turnover of human MAO A K151E mutant and rat MAO A is consistent with the correlation observed with WT-human MAO A. In contrast, there is no correlation of electronic substituent parameter observed in human MAO B enzyme (unpublished data from Li *et al.*).

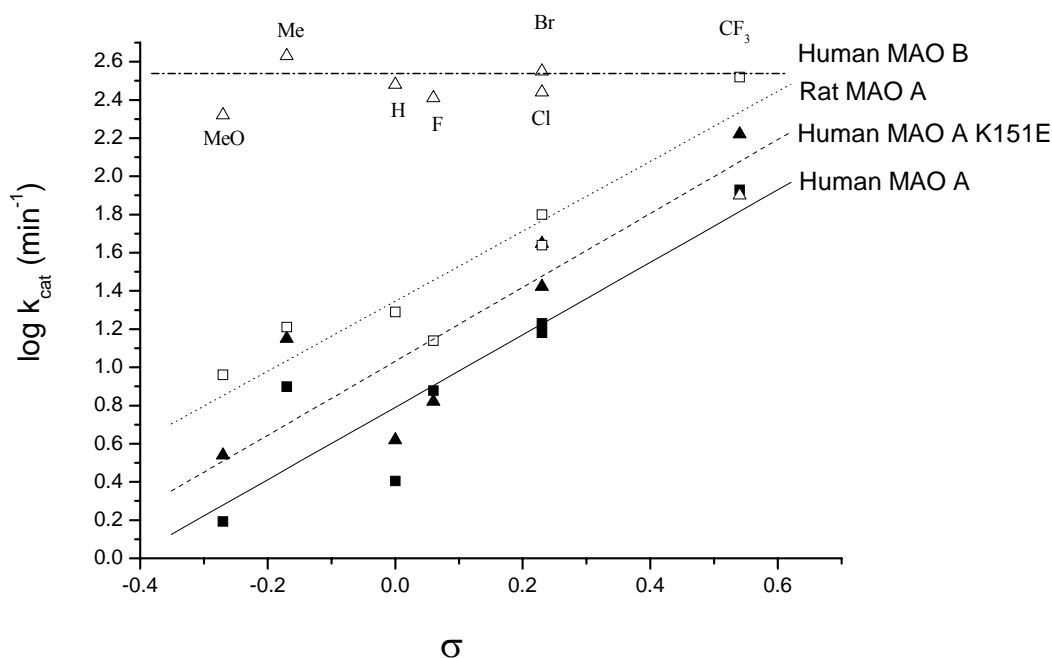


Figure 5.7 Comparison of correlation of steady state rates of human MAO A (—■) (Miller *et al.* 1999), human MAO A K151E (---▲), rat MAO A (····□) and human MAO B (- · - · - Δ) (unpublished data from Li *et al.*) turnover with the substituent electronic parameter (σ).

With regard to WT-human MAO A, both the steady state rate and anaerobic flavin reduction rates of WT-human MAO A catalysis were used to analyze the correlations with the substituent parameters of benzylamine analogues (Miller *et al.* 1999). To better compare QSAR analysis of human MAO A K151E and rat MAO A with WT-human MAO A, the steady state rate correlations of WT-human MAO A oxidation of seven *para*-substituted benzylamines with substituent effects were used (Table 5.7) (Miller *et al.* 1999). The statistical F values offer a means to judge data correlation, showing the higher F value reflects a better correlation of experimental data. A statistical analysis of the turnover rate correlations of human MAO A K151E is shown in Table 5.8. Besides the good correlation of $\log k_{\text{cat}}$ with electronic effect (σ) as shown in Figure 5.5,

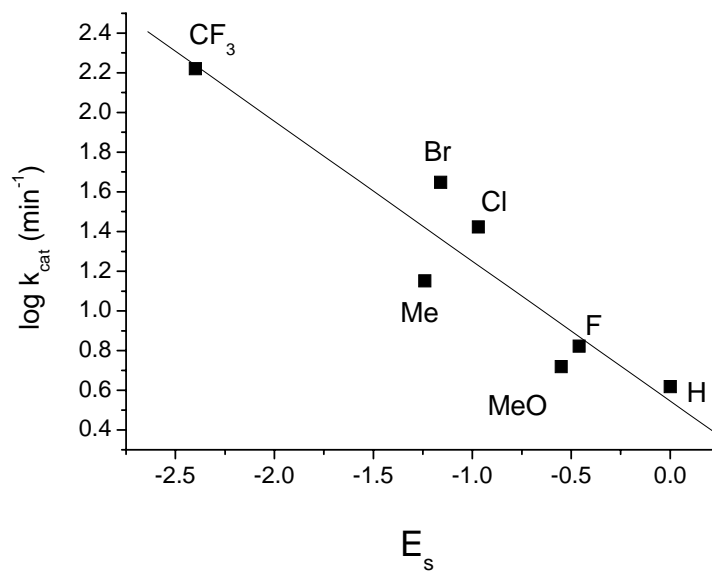
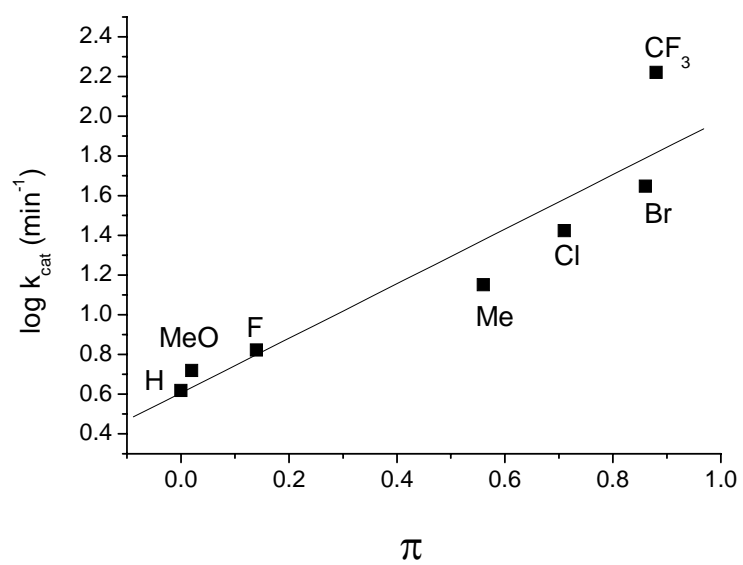
additional correlations of $\log k_{\text{cat}}$ with the hydrophobicity parameter (π) and steric parameter (E_s) are observed with good F values (Figure 5.8 A and B, respectively). The single V_w parameter correlation with $\log k_{\text{cat}}$ shows poor F value. Moreover, the double parameter regression ($\sigma + E_s$, $\sigma + \pi$, $\sigma + V_w$ and $E_s + \pi$) with $\log k_{\text{cat}}$ of human MAO A K151E also gave a meaningful correlation with the increased F values of the fit. (Figure 5.8 C, D, E and F, respectively).

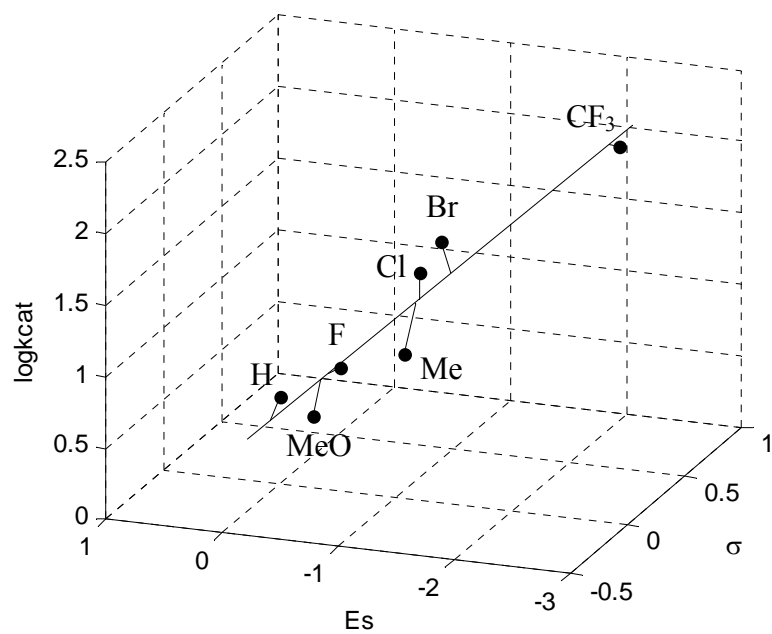
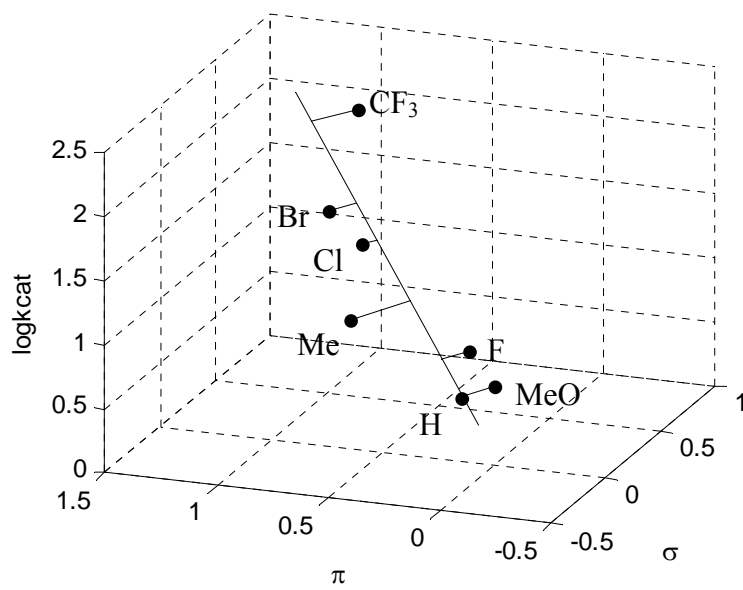
parameter	correlation (slope)	y-intercept	correlation coefficient	F value	significance
σ	1.90±0.40	0.79±0.11	0.90	23	0.005
E_s	-0.66±0.16	0.32±0.19	0.88	17	0.009
V_w	0.47±0.34	0.37±0.46	0.53	2.0	0.218
π	1.29±0.31	0.37±0.18	0.88	17	0.009
$\sigma + E_s$	1.19±0.32 -0.37±0.11	0.50±0.11	0.98	39	0.002
$\sigma + \pi$	1.18±0.41 0.70±±0.29	0.54±0.13	0.96	25	0.006
$\sigma_s + V_w$	1.72±0.38 0.23±0.16	0.52±0.22	0.94	15	0.014
$E_s + \pi$	-0.36±0.26 0.70±0.52	0.29±0.18	0.92	11	0.023

Table 5.7 Correlations of the steady state rate of wild-type human MAO A oxidizing *para*-substituted benzylamine (k_{cat}) with steric, electronic and hydrophobic substituent parameters (Miller *et al.* 1999)

parameter	correlation (slope)	y-intercept	correlation coefficient	F value	significance
σ	1.79±0.50	1.07±0.13	0.85	13	0.016
E_s	-0.71±0.12	0.55±0.14	0.94	36	0.002
V_w	0.65±0.28	0.42±0.38	0.73	5.6	0.064
π	1.38±0.24	0.61±0.14	0.93	32	0.002
$\sigma + E_s$	0.83±0.28 -0.50±0.10	0.67±0.10	0.98	50	0.002
$\sigma + \pi$	0.78±0.40 0.98±0.28	0.72±0.13	0.96	27	0.005
$\sigma + V_w$	1.44±0.26 0.45±0.11	0.54±0.15	0.97	34	0.003
$E_s + \pi$	-0.40±0.15 0.72±0.29	0.52±0.10	0.98	39	0.002

Table 5.8 Correlations of the steady state rate of human MAO A K151E oxidizing *para*-substituted benzylamine (k_{cat}) with steric, electronic and hydrophobic substituent parameters

A**B**

C**D**

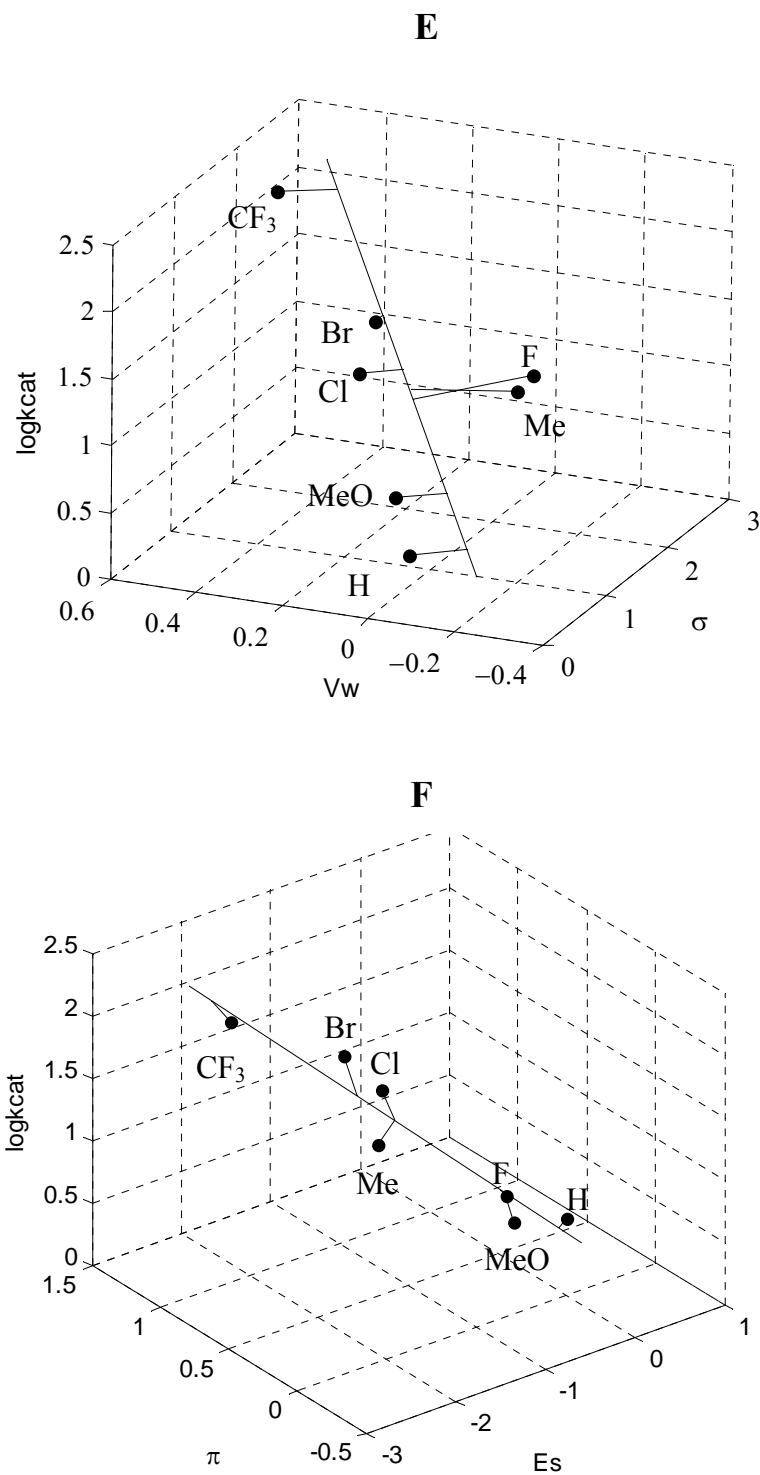


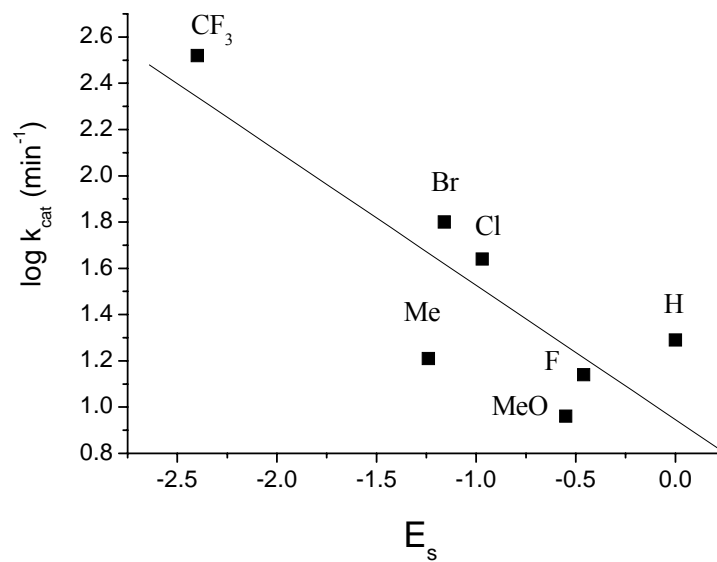
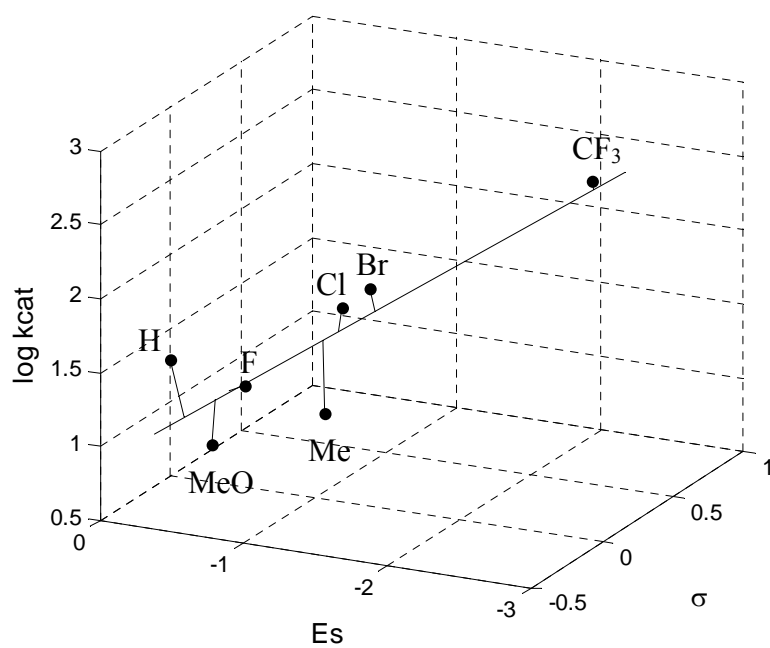
Figure 5.8

Correlation of steady-state rates of human MAO A K151E mutant turnover of *p*-substituted benzylamines with substituent parameters. (A) $\log k_{\text{cat}}$ vs. E_s (B) $\log k_{\text{cat}}$ vs. π (C) $\log k_{\text{cat}}$ vs. $\sigma + E_s$ (D) $\log k_{\text{cat}}$ vs. $\sigma + \pi$ (E) $\log k_{\text{cat}}$ vs. $\sigma + V_w$ (F) $\log k_{\text{cat}}$ vs. $E_s + \pi$.

Statistical analysis of the rat MAO A turnover rate data (Table 5.9) showed that, besides the good correlation with σ (Figure 5.6), steric parameter (E_s) also gives a meaningful correlation with turnover rate (Figure 5.9 A). All other single parameter correlations (π and V_w) showed low F values. Two parameter correlations of $\log k_{cat}$ with both parameters ($\sigma + E_s$, $\sigma + \pi$ and $\sigma + V_w$) improved the statistics of the correlation (Figure 5.9 B, C and D).

parameter	correlation (slope)	y-intercept	correlation coefficient	F value	significance
σ	1.83±0.30	1.35±0.08	0.94	38	0.002
E_s	-0.58±0.17	0.95±0.20	0.84	12	0.019
V_w	0.46±0.31	0.93±0.42	0.56	2.3	0.192
π	1.10±0.36	1.01±0.21	0.80	9.2	0.029
$\sigma + E_s$	1.34±0.27 -0.26±0.10	1.14±0.09	0.98	45	0.002
$\sigma + \pi$	1.46±0.41 0.36±0.28	1.22±0.13	0.96	22	0.007
$\sigma + V_w$	1.65±0.22 0.23±0.09	1.08±0.12	0.98	41	0.002
$E_s + \pi$	-0.38±0.32 0.48±0.63	0.93±0.21	0.86	5.7	0.068

Table 5.9 Correlations of the steady state rate of rat MAO A oxidizing *para*-substituted benzylamine (k_{cat}) with steric, electronic and hydrophobic substituent parameters.

A**B**

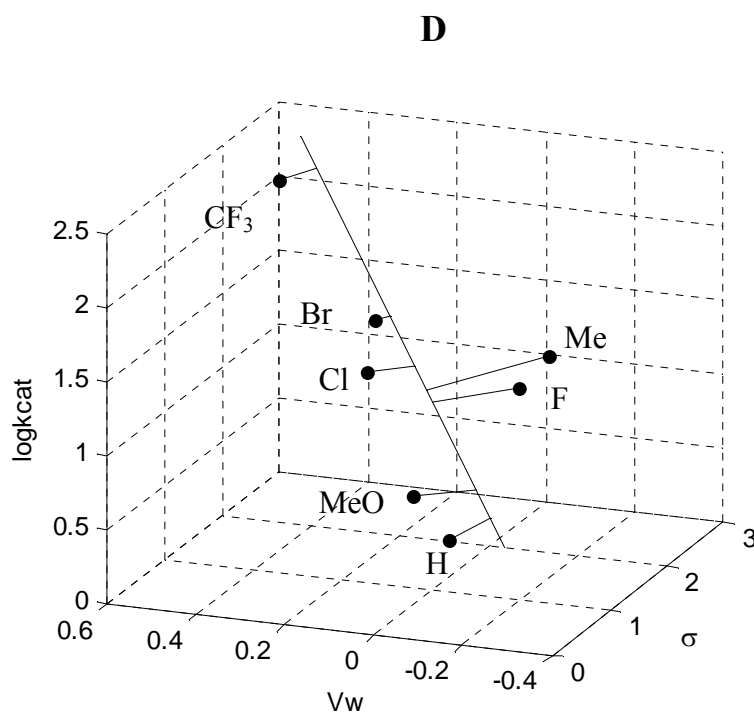
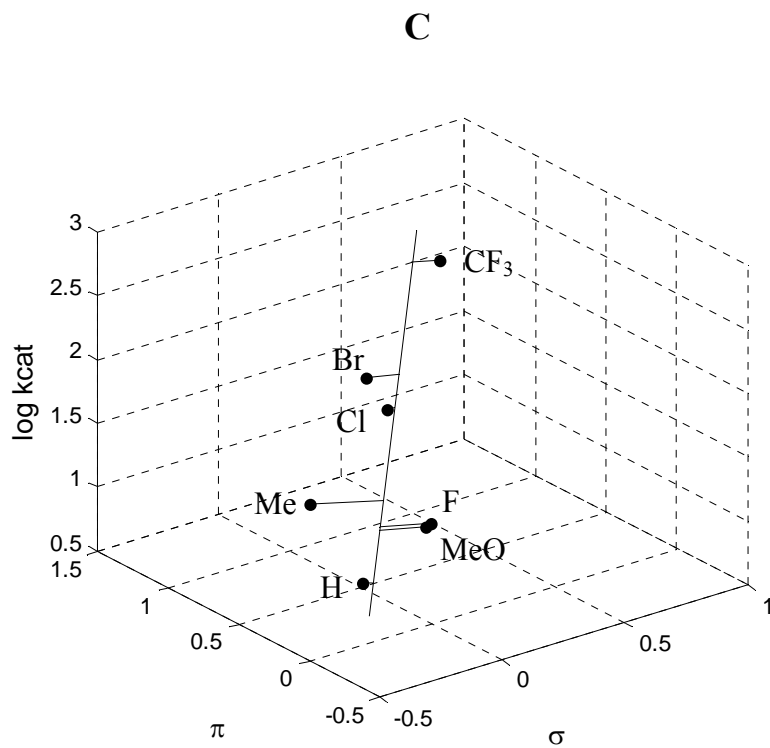


Figure 5.9

Correlation of steady-state rates of rat MAO A turnover of *p*-substituted benzylamines with substituent parameters. (A) $\log k_{\text{cat}}$ vs. E_s (B) $\log k_{\text{cat}}$ vs. $\sigma + E_s$ (C) $\log k_{\text{cat}}$ vs. $\sigma + \pi$ (D) $\log k_{\text{cat}}$ vs. $\sigma + V_w$.

Therefore, according to the comparison of QSAR analysis on the steady state rate of MAO A oxidation of *p*-substituted benzylamine analogues, substituent effects show the similar behaviors on WT-human MAO A, human MAO A K151E and rat MAO A.

5.3.8 Quantitative structure-activity relationships describing the binding of *para*-substituted benzylamine analogues to MAO A's

Large steady state kinetic isotope effects are observed in *para*-substituted benzylamine analogues oxidation by human MAO A K151E mutant and rat MAO A (Table 5.6), permitting the calculation of substrate dissociation constants representing all pre-isotopically sensitive steps. Dissociation constants for each benzylamine analogue were calculated from the data in Table 5.10, according to the following equation described by Klinman and Matthews (Klinman *et al.* 1985):

$$\frac{{}^D k_{cat} - 1}{{}^D (k_{cat} / K_m) - 1} = K_m / K_d \quad \text{Equation 5.5}$$

where K_d is the amine substrate dissociation constant from all complexes prior to the isotope-sensitive step and K_m is the Michaelis constant determined experimentally from steady state data.

Since MAOs only bind the deprotonated form of the amine substrates (McEwen *et al.* 1968; McEwen *et al.* 1969) and pH of enzyme assay buffer used in this study is 7.5, the observed K_d values require correction, with the combination of pK_a , to reflect the real concentration of the deprotonated amine in assay buffer. The Equation 5.6 is used to correct dissociation constants of each deprotonated benzylamine analogue with MAO A's:

$$K_{d(\text{corrected})} = \frac{K_{d(\text{observed})}}{1 + \text{anti log}(pK_a - pH)} \quad \text{Equation 5.6}$$

where pH is that of the assay buffer. The corrected K_d values are summarized in Table 5.10.

Linear regression analysis of *para*-substituted benzylamine binding constants of both human MAO A K151E mutant and rat MAO A with the van der Waals volume (V_w) was performed using the pK_a corrected K_d values. The values of V_w were scaled by a factor of 0.1 to make their magnitudes similar to the other substituent parameters. Within experimental error, the essentially parallel correlations of $\log K_d$ with the van der Waals volume (V_w) of the *para* substituent are observed in WT-human MAO A (Miller *et al.* 1999), human MAO A K151E mutant and rat MAO A (Figure 5.10), suggesting the same influence of *para* substituent on benzylamine analogues binding affinity. These correlations are described by

$$\text{WT-Human MAO A} \quad \log K_d = -0.92(\pm 0.23)(0.1V_w) - 4.36(\pm 0.28) \quad \text{Equation 5.7}$$

$$\text{Human MAO A K151E} \quad \log K_d = -1.04(\pm 0.20)(0.1V_w) - 4.77 (\pm 0.24) \quad \text{Equation 5.8}$$

$$\text{Rat MAO A} \quad \log K_d = -0.76(\pm 0.15)(0.1V_w) - 5.15 (\pm 0.18) \quad \text{Equation 5.9}$$

<i>para</i> substituent	Calculated Amine pK _a ^a	Human MAO A K151E			Rat MAO A		
		Observed K _d (μM)	pK _a corrected K _d (μM) ^b	logK _d (M)	Observed K _d (μM)	pK _a corrected K _d (μM) ^b	logK _d (M)
<i>p</i> -H	9.33	679.08	9.90	-5.01	459.91	6.7	-5.17
<i>p</i> -CF ₃	8.75	393.70	20.96	-4.68	283.79	15.11	-4.82
<i>p</i> -Br	9.08	34.40	0.88	-6.06	29.67	0.76	-6.12
<i>p</i> -Cl	9.08	64.21	1.64	-5.78	29.28	0.75	-6.13
<i>p</i> -F	9.27	180.51	3.01	-5.52	102.92	1.72	-5.76
<i>p</i> -Me	9.52	52.50	0.50	-6.30	40.94	0.39	-6.41
<i>p</i> -MeO	9.63	20.62	0.15	-6.82	58.01	0.43	-6.37

Table 5.10 Correction of *p*-substituted benzylamine human MAO A K151E and rat MAO A binding constants for selective binding of the deprotonated form of the amine substrate.

^a Calculated pK_a values were determined from Miller *et. al.* (Miller *et al.* 1999).

^b pK_a corrected binding constants were calculated using Equation 5.6.

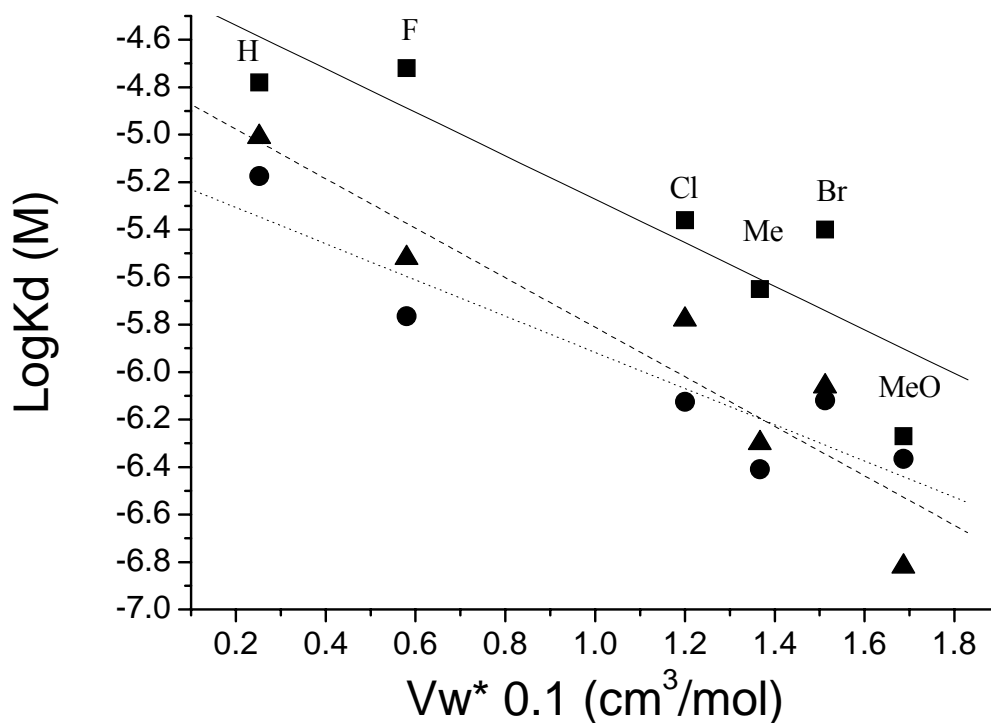


Figure 5.10 Comparison of correlations of the binding of *p*-substituted benzylamine to human MAO A (— ■) (Miller *et al.* 1999), human MAO A K151E (----- ▲) and rat MAO A (..... ●) with the van der Waals volume (V_w) of the *para* substituent. All binding constants are corrected for selective binding of the deprotonated amine.

In the case of WT-human MAO A, 12 substituents were involved in the binding affinities QSAR analysis of *para*-substituted benzylamines for WT-human MAO A (Miller *et al.* 1999). In this dissertation, only 6 substituents (*p*-H, *p*-F, *p*-Br, *p*-Cl, *p*-Me and *p*-MeO) were used to investigate the correlations of binding affinities of *para*-substituted benzylamine analogues for human MAO A K151E mutant and rat MAO A. Therefore, to better understand whether human MAO A K151E mutant and rat MAO A show similar correlations of binding affinities of *para*-substituted benzylamine analogues

with the substituent parameters as does WT-human MAO A, 6 out of 12 substituents were chosen to perform a statistical analysis of the substrate dissociation constant correlation on WT-human MAO A. As shown in Table 5.11, for single parameter correlations, only V_w shows a meaningful correlation which is consistent with data presented in Figure 5.10. Moreover, with double parameters, such as $\pi + V_w$ and $\sigma + V_w$, the reasonable correlations with substrate binding affinities are also observed.

A statistical analysis of the substrate dissociation constant correlations of human MAO A K151E mutant is shown in Table 5.12. Like WT-human MAO A, linear regression analysis of $\log K_d$ of human MAO A K151E mutant as a function of single substituent parameter shows that only steric parameter (V_w) gives a meaningful correlation with the substrate binding data (F value is 27), whereas all other single parameters exhibit very poor statistical correlations. Addition of hydrophobicity parameter (π) or electronic parameter (σ) as a second independent variable result in an improvement in the K_d correlation over V_w alone (F = 52 and F = 71, respectively) (Figure 5.11).

A statistical analysis of the substrate dissociation constant correlations on rat MAO A (Table 5.13) exhibit the similar behaviors to that of both WT-human MAO A and human MAO A K151E mutant, suggesting the van der Waals volume (V_w) is the best descriptor of benzylamine binding interaction in MAO A. However, the correlations of substrate binding with double parameters ($\pi + V_w$ and $\sigma + V_w$) show poorer statistical correlations than WT-human MAO A and human MAO A K151E mutant (Figure 5.12).

parameter	correlation (slope)	y-intercept	correlation coefficient	F value	significance
σ	1.54±1.17	-5.38±0.22	0.55	1.7	0.259
E_s	0.52±0.54	-4.98±0.46	0.43	0.93	0.390
V_w	-0.916±0.23	-4.36±0.28	0.90	16	0.016
π	-0.17±0.76	-5.30±0.39	0.11	0.05	0.837
$\pi + V_w$	0.66±0.24 -1.13±0.16	-4.37±0.17	0.97	25	0.014
$\pi + E_s$	1.79±1.29 1.75±1.02	-4.77±0.44	0.71	1.5	0.349
$\sigma + V_w$	1.08±0.40 -0.84±0.14	-4.46±0.18	0.97	25	0.014
$\sigma + \pi$	2.82±1.26 -1.12±0.69	-4.97±0.31	0.79	2.6	0.225

Table 5.11 Correlations of the binding affinities (K_d) of deprotonated *para*-substituted benzylamine for wild-type human MAO A with steric, electronic and hydrophobic substituent parameters (Miller *et al.* 1999).

parameter	correlation (slope)	y-intercept	correlation coefficient	F value	significance
σ	1.58±1.32	-5.94±0.25	0.51	1.4	0.300
E_s	0.73±0.55	-5.38±0.47	0.55	1.8	0.256
V_w	-1.04±0.20	-4.77±0.25	0.93	27	0.007
π	-0.30±0.82	-5.80±0.42	0.18	0.13	0.739
$\pi + V_w$	0.61±0.19 -1.24±0.12	-4.78±0.13	0.99	52	0.005
$\pi + E_s$	2.22±1.08 2.26±0.84	-5.12±0.37	0.84	3.7	0.150
$\sigma + V_w$	1.04±0.26 -0.97±0.10	-4.87±0.12	0.99	71	0.003
$\sigma + \pi$	3.10±1.32 -1.35±0.72	-5.44±0.33	0.81	2.9	0.199

Table 5.12 Correlations of the binding affinities (K_d) of deprotonated *para*-substituted benzylamine for human MAO A K151E with steric, electronic and hydrophobic substituent parameters.

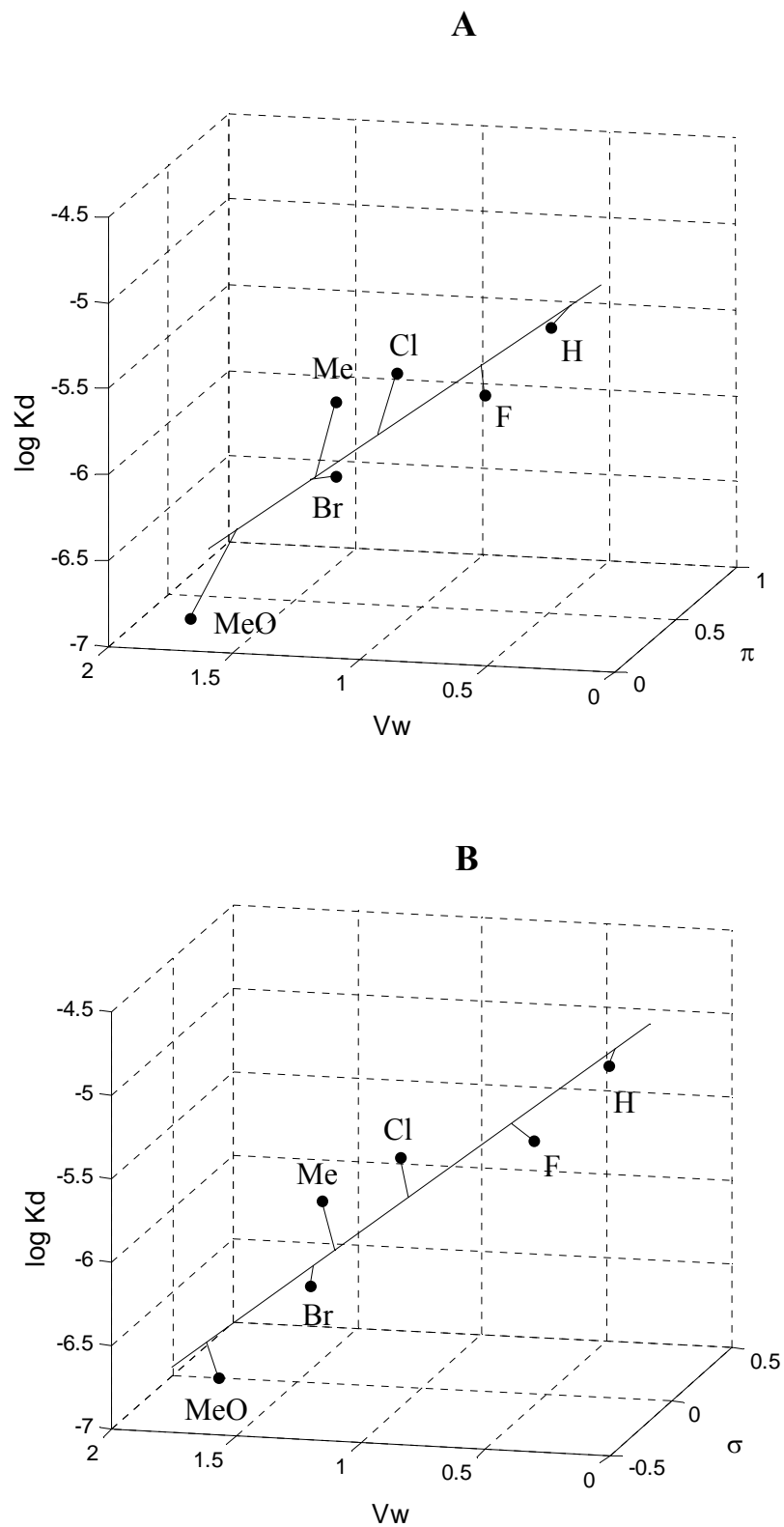


Figure 5.11 Correlation of binding affinity of *p*-substituted benzylamines for human MAO A K151E with substituent parameters. (A) $\log K_d$ vs. $\pi + V_w$ (B) $\log K_d$ vs. $\sigma + V_w$.

parameter	correlation (slope)	y-intercept	correlation coefficient	F value	significance
σ	0.60±1.10	-6.00±0.20	0.26	0.3	0.613
E_s	0.78±0.29	-5.42±0.24	0.81	7.4	0.053
V_w	-0.77±0.15	-5.15±0.18	0.93	25	0.007
π	-0.59±0.55	-5.77±0.28	0.48	1.2	0.342
$\pi + V_w$	-0.04±0.30 -0.76±0.20	-5.15±0.21	0.93	9.6	0.050
$\pi + E_s$	1.23±0.51 1.63±0.40	-5.27±0.18	0.94	11	0.042
$\sigma + V_w$	0.18±0.48 -0.76±0.18	-5.16±0.21	0.93	10	0.047
$\sigma + \pi$	2.06±0.86 -1.29±0.47	-5.53±0.22	0.86	4.1	0.139

Table 5.13 Correlations of the binding affinities (K_d) of deprotonated *para*-substituted benzylamine for rat MAO A with steric, electronic and hydrophobic substituent parameters.

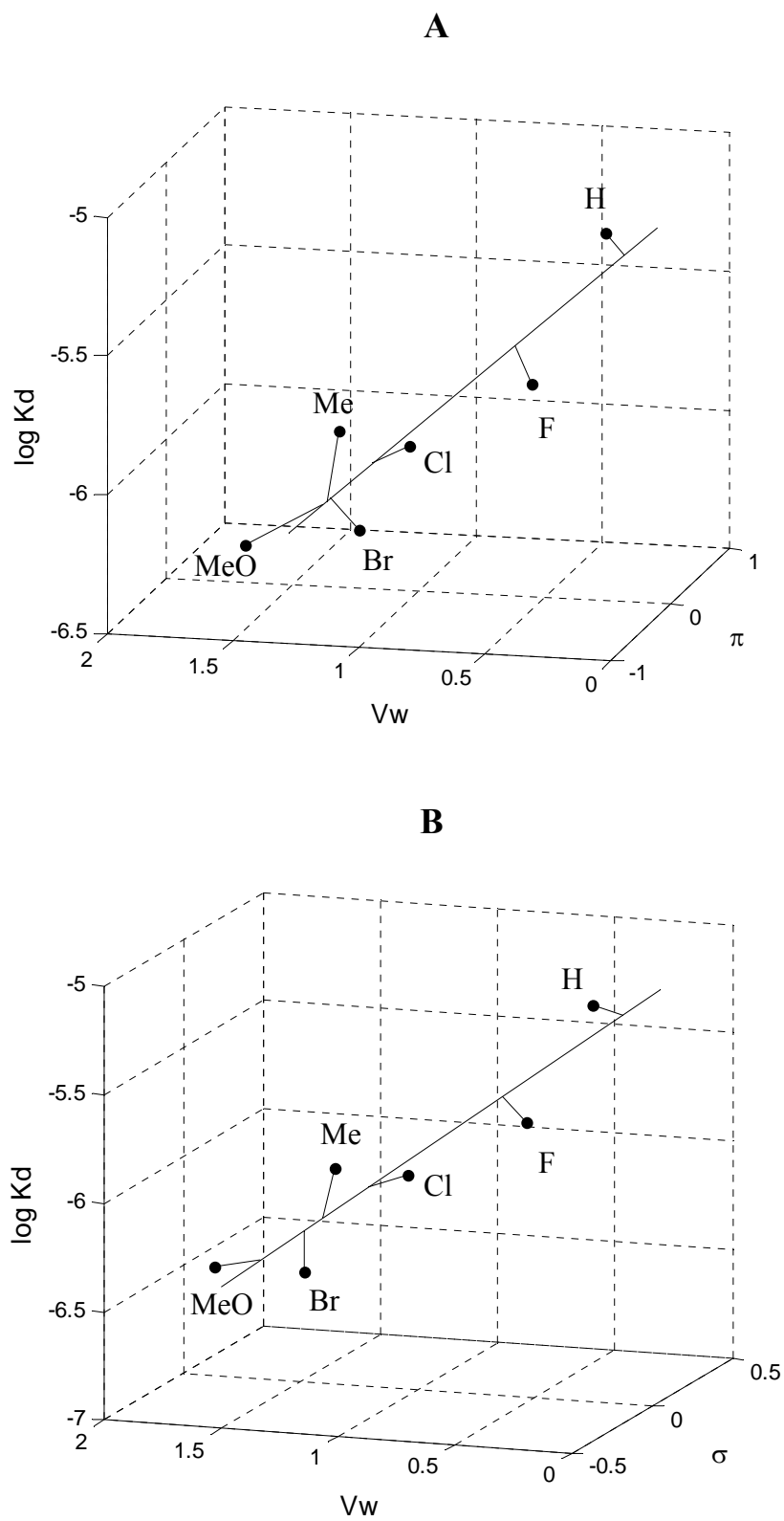


Figure 5.12

Correlation of binding affinity of *p*-substituted benzylamines for rat MAO A with substituent parameters. (A) logK_d vs. π + V_w (B) logK_d vs. σ + V_w.

5.4 Discussion

5.4.1 Thermal stability and substrate/inhibitor specificities

The studies on thermal stability of WT-human MAO A, human MAO A K151E and rat MAO A indicate that the oligomeric state of the enzyme plays a critical role in enzyme stability. Moreover, the mutation of lysine to glutamate in human MAO A confers a marked increase of thermal stability, implying that human MAO A selective mutation might contribute to the enzyme oligomeric state and human MAO A K151E mutant may possess dimeric property since its thermal stability is close to that of the dimeric rat MAO A.

The kinetic data of substrate specificity shows that both human MAO A K151E mutant and rat MAO A are more efficient catalysts than human wild-type MAO A with “MAO B” specific substrates. In competitive inhibitor study, no significant differences are observed between human MAO A’s and rat MAO A, suggesting these enzymes exhibit the similar inhibitory properties.

5.4.2 Mechanistic interpretation of $K_m(O_2)$

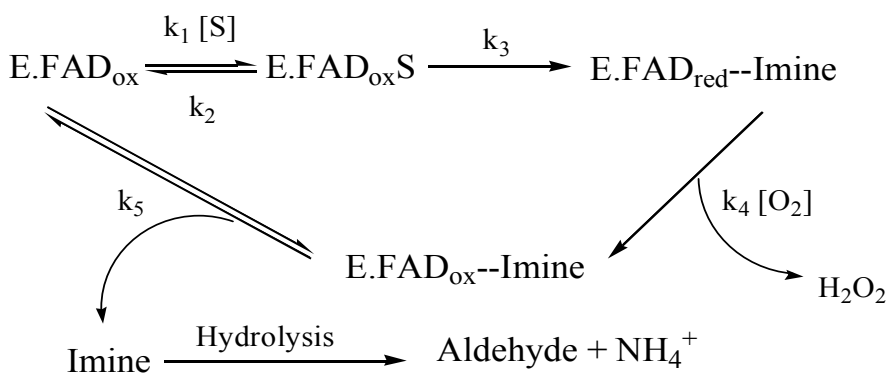
As shown in Figure 5.3 and Figure 5.4, the Hanes-Woolf plots of human MAO A K151E mutant and rat MAO A with oxygen as the variable substrate intersect either on or very close to the y axis which obey the equation 5.10, indicating these enzymes follow a ternary-complex mechanism.

$$v = \frac{Vab}{K_{ia}K_{mb} + K_{mb}a + K_{ma}b + ab}$$

Equation 5.10

where v is observed velocity, V is maximum velocity, a is the concentration of amine, b is the concentration of oxygen, and K_{ma} and K_{mb} are the Michaelis constants for a and b , respectively. K_{ia} is the dissociation constant for a .

Therefore, for human and rat MAO A's, when flavin in oxidation state is reduced by kynuramine, the reduced enzyme-imine complex is formed, directly followed by reoxidation by oxygen. The imine product is released from the resultant reoxidized enzyme and hydrolyzed to produce the corresponding aldehyde and NH_4^+ .



Scheme 5.1 Reaction pathway for the MAO A-catalyzed oxidation of kynuramine

5.4.3 Structure-activity relationships describing the steady-state turnover rate of human MAO A K151E mutant and rat MAO A by *para*-substituted benzylamine analogues

With the comparison of human wild-type MAO A, human MAO A K151E mutant and rat MAO A (Table 5.14), the similarity of the ρ values with both protio and dideuterio substrates and large isotope effect indicate that, in oxidation of benzylamine,

α -C-H bond cleavage is the rate-limiting step. Furthermore, for both α , α -[^1H]-*p*-substituted benzylamines and α , α -[^2H]-*p*-substituted benzylamines, correlations of $\log k_{\text{cat}}$ with the electronic parameter σ show positive ρ values of approximately 2.0 within the experimental error, indicating electron-withdrawing substituents significantly enhance the rate of α -C-H bond cleavage. This is suggested to be due to the stabilization of a developing negative charge at the α -carbon in the transition state, which is consistent with a proposed MAO A catalytic mechanism that α -C-H bond is cleaved by proton abstraction (Miller *et al.* 1999).

parameter	correlation (slope)	y-intercept	correlation coefficient	F value	significance	
	k_{cat} (7 substituents)			(1,6)		
	Human MAO A^a	1.89±0.40	0.79±0.11	0.90	23	0.005
σ	Human MAO A K151E	1.96±0.54	1.01±0.15	0.85	13	0.015
	Rat MAO A	1.83±0.30	1.35±0.08	0.94	38	0.002
	K_{d} (6 substituents)			(1,5)		
	Human MAO A^a	-0.92±0.23	-4.36±0.28	0.90	16	0.016
V_{w}	Human MAO A K151E	-1.04±0.20	-4.77±0.24	0.93	28	0.006
	Rat MAO A	-0.76±0.15	-5.15±0.18	0.935	25	0.007

Table 5.14 Correlations of the steady-state rates of MAO A oxidizing *para*-substituted benzylamines (k_{cat}) and the binding affinities of deprotonated *para*-substituted benzylamines (K_{d}) for MAO A with electronic and steric substituent parameters ^a (Miller & Edmondson, 1999)

In the study of correlations of human MAO A K151E mutant and rat MAO A turnover rate with substituent parameters, besides correlation with electronic parameter (σ), additional correlations of $\log k_{\text{cat}}$ with the steric parameter (E_s) hydrophobicity parameter (π) and the van der Waals volume (V_w) were observed (Figure 5.8 and Figure 5.9). It would be due to a coincidental cross-correlation between σ and π (E_s or V_w) The findings by Miller and Edmondson (Miller *et al.* 1999) have shown that there was no significant correlation observed between anaerobic rates of human wild-type MAO A flavin reduction of *p*-substituted benzylamine analogues with π or E_s parameters, in which a larger set of substituents was involved. Moreover, with comparison of steady state data (k_{cat}) and flavin reduction data (k_{red}), only the correlation with σ showed consistent results. Therefore, for steady state rate of human MAO A K151E mutant and rat MAO A, the improved correlations by inclusion of π , E_s or V_w are likely due to the cross-correlation of these two substituent parameters with this group of analogues.

5.4.4 Structure-activity relationships describing the binding of *para*-substituted benzylamine analogues to human MAO A K151E mutant and rat MAO A

The linear regression analysis of binding constants of *para*-substituted benzylamine analogues to human MAO A K151E mutant and rat MAO A with the size of substituents shows that there is a correlation of $\log K_d$ with the van der Waals volume (V_w) of the *para* substituent. Moreover, within the experimental error, these correlations are parallel to that of human wild-type MAO A (Table 5.14), indicating that increasing the size of the *para* substituent increases the binding strength of *para*-substituted

benzylamine analogues to both human and rat MAO A's. These observations also suggest that these enzymes contain a large binding pocket situated around the *para* position of the bound substrate.

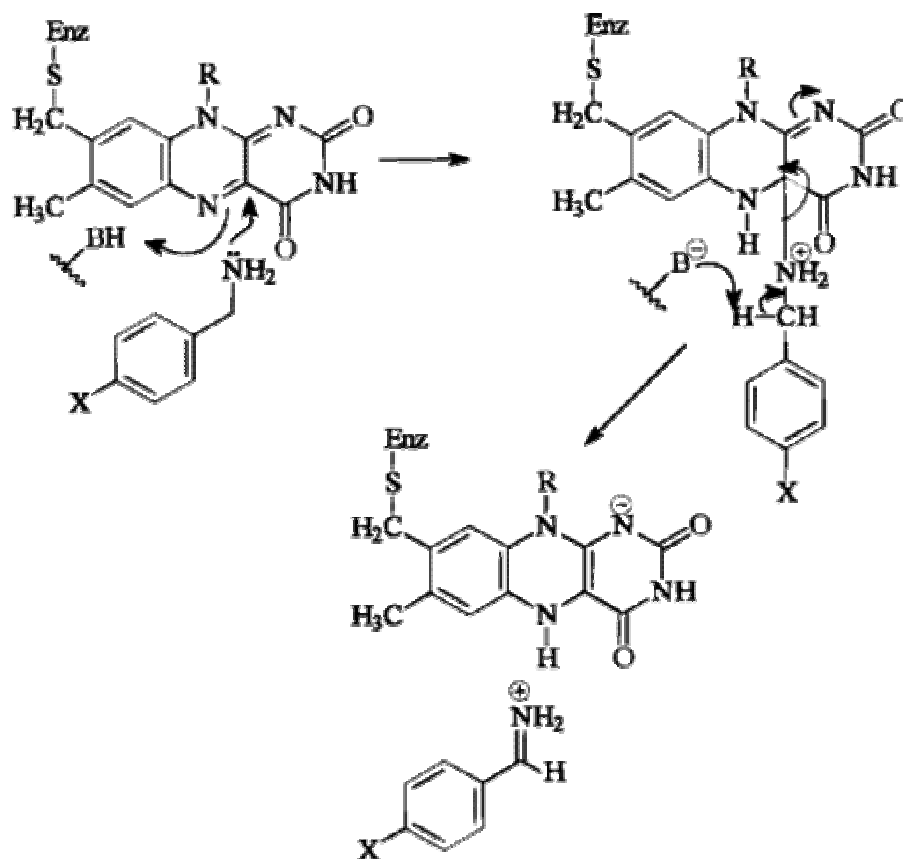
The involvement of σ and π improved the correlation of binding affinities (K_d) with the van der Waals volumes, and the F values and significance values show a better fit (Table 5.12 and Table 5.13). This result would explain that the increased binding affinity with a large substituent would be due to more substituent-protein interactions involved, such as hydrophobic interactions or hydrogen bonding.

The corrected dissociation constants of benzylamine analogues according to their respective pK_a values improved binding correlations of both human MAO A K151E mutant and rat MAO A, further supporting that only deprotonated amines bind to MAOs (McEwen *et al.* 1968; McEwen *et al.* 1969).

5.4.5 Mechanistic interpretation of QSAR results

The observed large kinetic isotope effects on the rate of flavin reduction by all amine substrates and the formation of the protonated imine product suggest that α -C-H bond cleavage is rate-limiting step. Moreover, as shown in QSAR analysis, electron-withdrawing *para* substituents increase the limiting rate of α -C-H bond cleavage for MAO A catalysis. Therefore, both human MAO A K151E mutant and rat MAO A follow the similar concerted nucleophilic mechanism (Scheme 5.2) as WT-human MAO A: the formation of an amine-flavin-C4a adduct results in the transformation of the N(5) to a very basic site ($pK_a \sim 25$), the proton from α -carbon of amine substrate is then abstracted

by the nitrogen at 5 position of the flavin ring with subsequent formation of the protonated imine product released from the reduced flavin.



Scheme 5.2 Proposed concerted polar nucleophilic mechanism for MAO A catalysis (Miller *et al.* 1999).

The previous QSAR results of benzylamine analogues with human wild-type MAO A support α -C-H bond cleavage occurring via proton abstraction in MAO A catalysis. According to the QSAR data obtained for both human MAO A K151E and rat MAO A, these two enzymes also follow the concerted polar nucleophilic mechanism with α -C-H bond cleavage. A strong dependence on the electron-withdrawing properties of the *para* substituent provides the evidence that the negative charges develop on the benzyl ring after proton abstraction in the transition state so that electronic parameter plays a role in

the substrate binding site. Furthermore, as shown in Figure 5.13, overlap of substituent, the π -orbital of benzene ring, α -carbon and allows the electronic effect transmitting from substituent to α -carbon through aromatic ring, resulting in a large ρ value which is also observed in bovine serum amine oxidase (Hartmann *et al.* 1991). This model further explains the steric effect on binding affinity of *para*-substituted benzylamine analogues, that coplanar configuration does not impair the transmission of electronic effect and more interactions are involved with increased size of substituent.

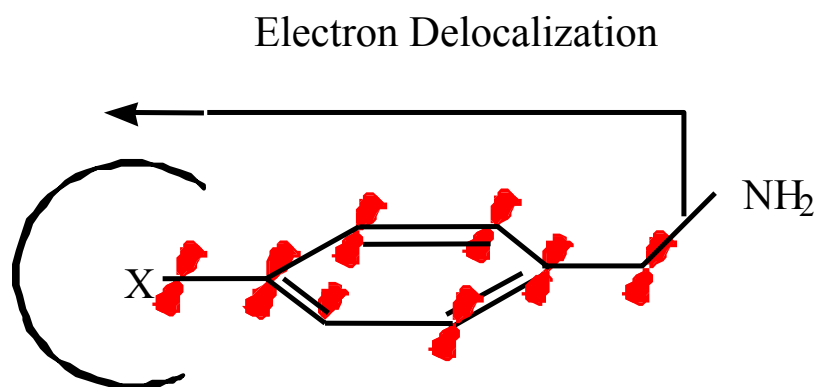


Figure 5.13 Model representation of the relative conformation of *para*-substituted benzylamine analogues bound to human MAO A.

Interestingly, the study of alkylthio-substituted amphetamine derivatives shows that human MAO A and rat MAO A exhibit different behaviors in inhibition by these amphetamine analogues (Fierro *et al.* 2007). Increasing substituent size results in tighter binding of amphetamine derivatives to human MAO A, whereas in the case of rat MAO A, propyl and butylthio analogues exhibit less binding affinity than ethylthio analogue. The molecular modeling further demonstrates the binding modes of all amphetamine derivatives in human MAO A's active site are similar and also consistent with that of

methyl and ethylthio analogues in rat MAO A's active site. Propyl and butylthio analogues bind to rat MAO A in an opposite manner. The amino group is facing the flavin ring, instead of pointing away from the cofactor. Both experimental and computational data suggest that there are some structural differences between human MAO A and rat MAO A, resulting in the different inhibitory potency of alkylthio-substituted amphetamine derivatives.

With regard to the human selective mutation in MAO A, pulsed dipolar electron spin resonance (PDS) studies carried out by Anup Upadhyay (unpublished data) have demonstrated that WT-human MAO A is 100% dimeric in the membrane and ~50% dimeric in detergent solutions. No difference in PDS data and distances for human MAO A K151E mutant and rat MAO A are observed as compared with WT-human MAO A.

The preliminary data on the electron density map of human MAO K151E mutant crystal (unpublished data from Dr. Daniele Bonivento, in Dr. Andrea Mattevi's laboratory) shows that the 209-216 cavity shaping loop is much more similar to that of the rat MAO A (in green) than to that of the human MAO A (in yellow). As stated in Chapter 1, the structure of the rat MAOA cavity-shaping loop is identical with that of human MAOB and they exist as dimer in the crystals. These observations raised the possibility that oligomeric state of MAO would affect the conformation of the cavity-shaping loop. To further confirm this hypothesis, the crystallization of human MAO A K151E mutant has been in progress in Dr. Andrea Mattevi's laboratory (Pavia, Italy).

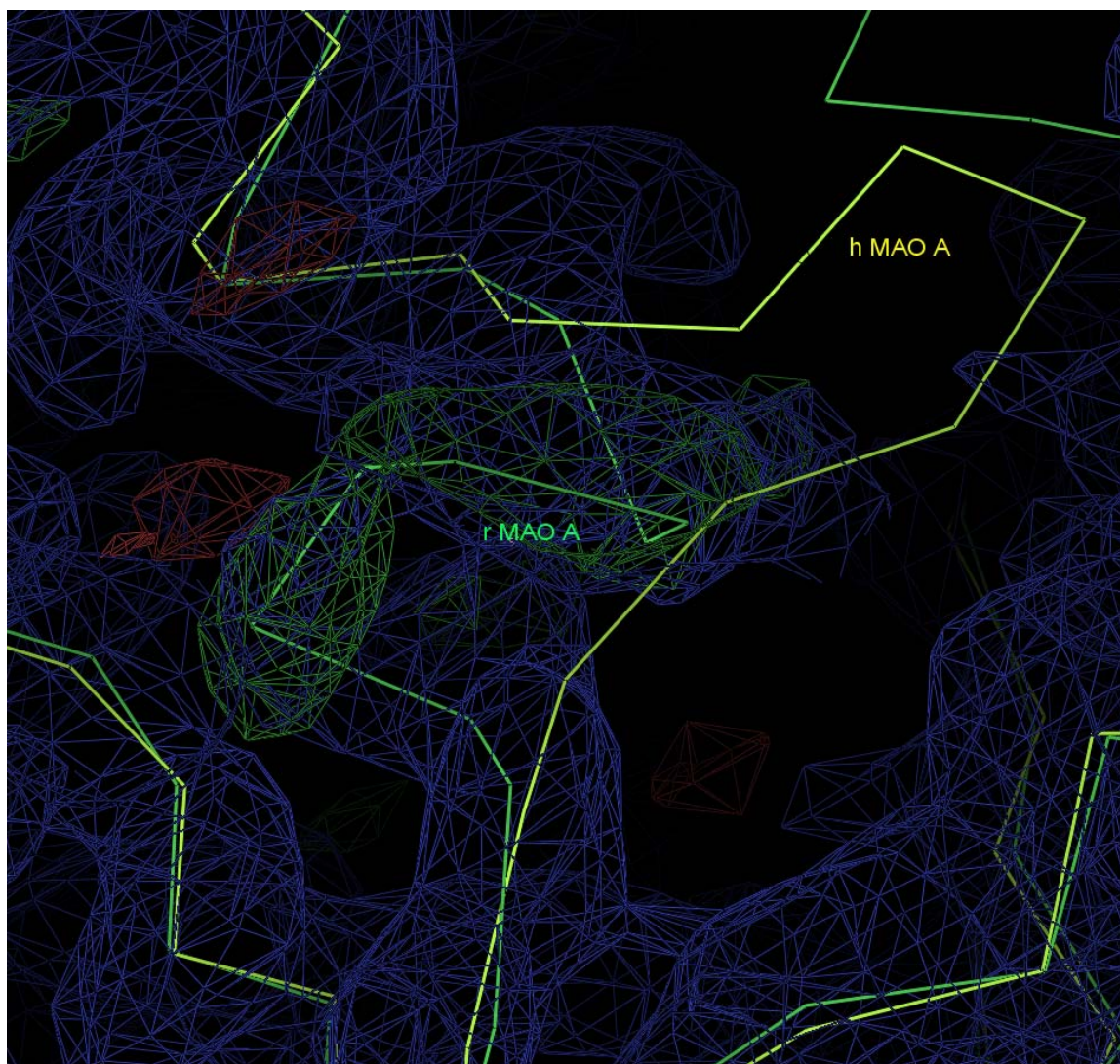


Figure 5.14 Electron density map of human MAO A K151E mutant. The structures of cavity-shaping loop of rat MAO A and WT-human MAO A are shown in green and yellow, respectively.
Unpublished data from Dr. Daniele Bonivento, in Dr. Andrea Mattevi's laboratory

In conclusion, functional comparisons of human wild-type MAO A, human MAO A K151E mutant and rat MAO A discussed in this dissertation show no major changes in catalytic properties between human and rat MAO A's, although both human MAO A K151E mutant and rat MAO A oxidize "MAO B" substrates more efficiently than the

human wild-type MAO A. The major difference observed is the temperature stability of human MAO A K151E mutant and dimeric rat MAO A as compared with the monomeric human MAO A. This observation would result from more labile purified form of WT-human MAO A to in detergent solution. It remains for future work to delineate the functional significance for the selective mutation in human MAO A resulting in formation of its monomeric state.

Dissertation summary

Monoamine oxidases A and B (MAO A and MAO B), being outer mitochondrial membrane proteins, have been important targets for drug therapy over the past 30 years. MAO A plays a major role in the degradative metabolism of neurotransmitters such as serotonin and dopamine. MAO B's functions involve metabolism of dopamine and xenobiotic amines and initiation of apoptosis of neuronal cells. In spite of the over 20,000 papers in the literature on monoamine oxidases, the molecular understanding of these enzymes is still limited. Publication of crystal structure of recombinant human liver MAO B is a breakthrough in monoamine oxidase research, and the sequent structures of human MAO A and rat MAO A also provide insights into understanding the structural and catalytic properties of MAOs. However, crystal data only reveal the structural properties of MAOs in crystalline form, and may not reflect the dynamic conformations of MAOs in their native states. Moreover, the recent structural modeling study has proposed that monomerization of human MAO A is due to a human exclusive Glu151Lys mutation. Therefore, this dissertation work focuses on investigation of structural properties of MAOs in both detergent solubilized and membrane-bound forms, as well as the functional differences between human and rat MAO A's.

The first part of this dissertation describes the structural properties of human MAO A and MAO B in their detergent solubilized form using fluorescence resonance energy transfer (FRET) technique. In this work, a fluorophore labeled MAO irreversible inhibitor (DCP) which is bound to the active site of MAO was synthesized and served as a probe to investigate structural properties of these enzymes. The time course of DCP inhibiting MAO A or MAO B shows that the wider and shorter active site cavity of

human MAO A than human MAO B lead to faster inhibition of MAO A than that of MAO B by DCP. Both iodide quenching data and molecular dynamic modeling data suggest that DCP is exposed outside the active site cavities in both MAO A and MAO B. The fluorescent dansyl group of DCP located in a hydrophobic environment with restricted motion is supported by polarization and anisotropy studies. According to the distances measured by FRET, the distances between DCP and the N-terminus of the protein are consistent with that from the available crystal structures. However, the distances between DCP and the end of C-terminus are shorter than the distances measured from the crystal structures with the modeled C-terminal helices, indicating that C-terminal helices of MAO would be interrupted and turn back toward the membrane surface.

Chapter 3 of this dissertation describes further investigation of the conformation of C-terminal helices of human MAO A and MAO B in their membrane bound forms. The C-terminus of the detergent solubilized MAO was labeled with a hydrophobic fluorophore N-(1-pyrenyl)maleimide and reconstituted into isolated yeast mitochondria. Application of spin-labeled stearic acids (5-FASL and 12-FASL) to paramagnetically quench fluorescence of pyrene provides an approach to locate the depth of membrane-embedded fluorophores since the doxyl groups of these quenchers are assumed to penetrate the membrane with different depth from the head-group interface. Incorporation with lipid bilayer results in the mobility restrictions of C-terminal helices in MAOs, since their fluorescence polarization and anisotropy values are significantly increased when C-terminal helices are located in the membrane. Fluorescence quenching data show that pyrene-labeled human MAO A was quenched by 5-FASL slightly greater than 12-FASL,

suggesting that the end of the C-terminal helix of human MAO A would be almost located in the middle of the headgroup interface and the center of the bilayer with a little bit proximity to membrane surface. In the case of human MAO B, 5-FASL quenches the extrinsic fluorescence of pyrene more efficiently than 12-FASL, thus, the end of the C-terminal helix of human MAO B would be closer to membrane-water interface. It has been shown that transbilayer distributions of phospholipids between mammals and yeast are different (Daum *et al.* 1997) which would cause different topology of membrane protein in mitochondria. Therefore, it would be valuable, in the future, to investigate conformations of the C-termini of MAO in their native membranes.

Chapter 4 describes high-level overexpression of recombinant rat liver MAO A in methanotrophic yeast expression system *Pichia pastoris*. This expression system exhibits high expression level that ~500 mg of purified enzyme are obtained from a 1-L fermentation culture, whereas *Saccharomyces cerevisiae* expression system used by Ma *et al.* can only produce 10 mg of rat MAO A per liter of culture (Ma *et al.* 2004). Although human and rat MAO A share 90% sequence identity, they differ in several aspects: 1) rat MAO A binds to the positively charged DEAE-Sepharose resin less tightly than does human MAO A. It would be due to the fact that distribution of negatively charged residues is greater on human MAO A (sum of formal charge is -6) than on rat MAO A (sum of formal charge is +2); 2) Thermal stability studies show that rat MAO A exhibits a much higher stability than human MAO A. It might be the consequence of their different oligomeric states (human MAO A is monomeric, whereas rat MAO A is dimeric). Both human and rat MAO A do not show significant differences in their

catalytic properties, although rat MAO A oxidizes MAO B-specific substrates, such as benzylamine and phenylethylamine, more rapidly than does human MAO A.

The last chapter of this dissertation describes the effect of selective mutation on human MAO A. Andres *et al.* (Andres *et al.* 2004) found that only one human exclusive non-conservative change is present in the sequence of human MAO A, a Lys at position 151, while MAO A in other mammalian species as well as human MAO B exist as dimer with Glu at the analogous position. In this work, human MAO A Lys151Glu mutant was created and its functional properties were compared with WT-human MAO A and rat MAO A in several aspects: 1) Human MAO A K151E is more thermally stable than monomeric WT-human MAO A but less stable than dimeric rat MAO A; 2) No major changes in catalytic properties between human and rat MAO A's; 3) WT-human MAO A, human MAO A K151E and rat MAO A follow a ternary-complex mechanism during the oxidation of kynuramine with very low $K_m(O_2)$ (6, 10 and 9 μM , respectively); 4) With the comparison of WT-human MAO A, human MAO A K151E mutant and rat MAO A, similar correlations of the steady-state rates of MAO A oxidizing both protio and dideuterio *p*-substituted benzylamine analogues with substituent electronic parameter (σ) suggest that electron-withdrawing substituents significantly enhance the rate of α -C-H bond cleavage. Moreover, large isotope effect indicates that α -C-H bond cleavage is the rate-limiting step in MAO oxidizing benzylamine; 5) These three enzymes exhibit the similar correlation of $\log K_d$ (binding affinity) with the van der Waals volume (V_w) of the *para* substituent, indicating that increasing the size of the *para* substituent increases the binding strength of *para*-substituted benzylamine analogues to MAO A's, 6) Both human MAO A K151E mutant and rat MAO A follow the similar concerted nucleophilic

mechanism (Scheme 5.2) as WT-human MAO A. Taking all these data together, except thermal stability, there is no major functional changes observed among WT-human MAO A, human MAO A K151E mutant and rat MAO A. Therefore, it remains for future work to delineate the functional significance for the selective mutation in human MAO A resulting in formation of its monomeric state. Moreover, as indicated previously, cavity-shaping loop of MAO might play a role in substrate and inhibitor specificities. It would be valuable, in the future, to investigate the functional role of cavity-shaping loop as well as effect of protein oligomeric state on conformation of cavity-shaping loop.

References

- Abeles, R. H. and Tashjian, A. H. (1974) *Biochemical Pharmacology* **23** (15):2205-2207.
- Abell, C. W. and Kwan, S. W. (2001) *Progress in Nucleic Acid Research and Molecular Biology, Vol 65* **65** 129-156.
- Achee, F. M., Gabay, S. and Tipton, K. F. (1977) *Progress in Neurobiology* **8** 325-348.
- Anderson, M. C., Hasan, F., McCrodden, J. M. and Tipton, K. F. (1993) *Neurochemical Research* **18** (11):1145-1149.
- Andres, A. M., Soldevila, M., Navarro, A., Kidd, K. K., Oliva, B. and Bertranpetit, J. (2004) *Human Genetics* **115** (5):377-386.
- Barber, D. J. W., Morris, D. A. N. and Thomas, J. K. (1976) *Chemical Physics Letters* **37** (3):481-484.
- Barber, M. J., Eichler, D. C., Solomonson, L. P. and Ackrell, B. A. (1987) *Biochemical Journal* **242** (1):89-95.
- Barden, J. A. and Dosremedios, C. G. (1987) *European Journal of Biochemistry* **168** (1):103-109.
- Bartholomew, A. A. (1962) *Medical Journal of Australia* **2** (4):151-&.
- Berendsen, H. J. C., Postma, J. P. M., van Gunsteren, W. F. and Hermans, J. (1981). Simple point charge water. In *Intermolecular Forces*. Pullman, B. The Netherlands, Reidel, Dordrecht: 331.
- Berry, M. D., Juorio, A. V. and Paterson, I. A. (1994) *Progress in Neurobiology* **42** (3):375-391.
- Berry, M. D., Juorio, A. V. and Paterson, I. A. (1994) *Progress in Neurobiology* **44** (2):141-161.
- Binda, C., Hubalek, F., Li, M., Edmondson, D. E. and Mattevi, A. (2004) *FEBS Lett* **564** (3):225-228.
- Binda, C., Hubalek, F., Li, M., Herzig, Y., Sterling, J., Edmondson, D. E. and Mattevi, A. (2004) *J Med Chem* **47** (7):1767-1774.
- Binda, C., Li, M., Hubalek, F., Restelli, N., Edmondson, D. E. and Mattevi, A. (2003) *Proc Natl Acad Sci U S A* **100** (17):9750-9755.

- Binda, C., Newton-Vinson, P., Hubalek, F., Edmondson, D. E. and Mattevi, A. (2002) *Nat Struct Biol* **9** (1):22-26.
- Birkmayer, W., Riederer, P., Youdim, M. B. H. and Linauer, W. (1975) *Journal of Neural Transmission* **36** (3-4):303-326.
- Bondi, A. (1964) *Journal of Physical Chemistry* **68** (3):441-&.
- Bordwell, F. G., Cheng, J. P., Satish, A. V. and Twyman, C. L. (1992) *Journal of Organic Chemistry* **57** (24):6542-6546.
- Brodie, B. B. and Shore, P. A. (1957) *Annals of the New York Academy of Sciences* **66** (3):631-642.
- Brown, L. E. and Hamilton, G. A. (1970) *Journal of the American Chemical Society* **92** (24):7225-&.
- Brunner, H. G., Nelen, M., Breakefield, X. O., Ropers, H. H. and Vanoost, B. A. (1993) *Science* **262** (5133):578-580.
- Cases, O., Seif, I., Grimsby, J., Gaspar, P., Chen, K., Pournin, S., Muller, U., Aguet, M., Babinet, C., Shih, J. C. and Demaeyer, E. (1995) *Science* **268** (5218):1763-1766.
- Casey, D. A. (1994) *Southern Medical Journal* **87** (5):559-563.
- Caspi, A., McClay, J., Moffitt, T. E., Mill, J., Martin, J., Craig, I. W., Taylor, A. and Poulton, R. (2002) *Science* **297** (5582):851-854.
- Chan, S. K. and Lester, R. L. (1970) *Biochimica Et Biophysica Acta* **210** (1):180-&.
- Chen, K., Wu, H. F., Grimsby, J. and Shih, J. C. (1994) *Mol Pharmacol* **46** (6):1226-1233.
- Chen, K., Wu, H. F. and Shih, J. C. (1996) *J Neurochem* **66** (2):797-803.
- Chong, P. L. G. and Thompson, T. E. (1985) *Biophysical Journal* **47** (5):613-621.
- Cloninger, C. R., Bohman, M. and Sigvardson, S. (1981) *Archives of General Psychiatry* **38** (8):861-868.
- Collins, M. A. and Neafsey, E. J. (2000). β -Carboline analogues of MPP⁺ as environmental neurotoxins. Neurotoxic factors in Parkinson's disease and related disorders. Storch, A. and Collins, M. A. New York, Kluwer Academic Publisher: 115-130.

- Cregg, J. M., Cereghino, J. L., Shi, J. Y. and Higgins, D. R. (2000) *Molecular Biotechnology* **16** (1):23-52.
- Daneshmend, T. K., Scott, G. L. and Bradfield, J. W. B. (1979) *British Medical Journal* **1** (6179):1679-1679.
- Darden, T., York, D. and Pedersen, L. (1993) *Journal of Chemical Physics* **98** (12):10089-10092.
- Daum, G. and Vance, J. E. (1997) *Progress in Lipid Research* **36** (2-3):103-130.
- De Colibus, L., Li, M., Binda, C., Lustig, A., Edmondson, D. E. and Mattevi, A. (2005) *Proceedings of the National Academy of Sciences of the United States of America* **102** (36):12684-12689.
- Delrio, M. P., Serrano, M. I. and Cuenca, E. (1982) *Journal De Pharmacologie* **13** (1):168-168.
- Demir, B., Ucar, G. and Sevinc, I. (2002) *European Neuropsychopharmacology* **12** S226-S226.
- Denney, R. M., Fritz, R. R., Patel, N. T. and Abell, C. W. (1982) *Science* **215** (4538):1400-1403.
- Deol, S. S., Bond, P. J., Domene, C. and Sansom, M. S. P. (2004) *Biophysical Journal* **87** (6):3737-3749.
- Devor, E. J., Cloninger, C. R., Hoffman, P. L. and Tabakoff, B. (1993) *American Journal of Medical Genetics* **48** (4):209-213.
- Dostert, P. L., Benedetti, M. S. and Tipton, K. F. (1989) *Medicinal Research Reviews* **9** (1):45-89.
- Edmondson, D. E., Bhattacharyya, A. K. and Walker, M. C. (1993) *Biochemistry* **32** (19):5196-5202.
- Edmondson, D. E., Mattevi, A., Binda, C., Li, M. and Hubalek, F. (2004) *Curr Med Chem* **11** (15):1983-1993.
- Edwards, D., Hall, T. R. and Brown, J. A. (1986) *Comparative Biochemistry and Physiology C-Pharmacology Toxicology & Endocrinology* **84** (1):73-77.
- Eklblom, J., Jossan, S. S., Bergstrom, M., Oreland, L., Walum, E. and Aquilonius, S. M. (1993) *Glia* **8** (2):122-132.
- Erwin, V. G. and Hellerman, L. (1967) *Federation Proceedings* **26** (2):843-&.

Erwin, V. G. and Hellerma.L (1967) *Journal of Biological Chemistry* **242** (18):4230-&.

Essman, W. B. (1977) *Journal of Medicine* **8** (2):95-101.

Faraj, B. A., Davis, D. C., Camp, V. M., Mooney, A. J., Holloway, T. and Barika, G. (1994) *Alcoholism-Clinical and Experimental Research* **18** (5):1114-1120.

Feller, S. E. (2000) *Current Opinion in Colloid & Interface Science* **5** (3-4):217-223.

Fierro, A., Osorio-Olivares, M., Cassels, B. K., Edmondson, D. E., Sepúlveda-Boza, S. and Reyes-Parada, M. (2007) *Bioorg Med Chem* **15** 5198-5206.

Filipowicz, C. M. and Mccauley, R. B. (1983) *Biochimica Et Biophysica Acta* **734** (2):373-377.

Forster, T. (1969) *Angewandte Chemie-International Edition* **8** (5):333-&.

Fowler, C. J., Tipton, K. F., Mackay, A. V. P. and Youdim, M. B. H. (1982) *Neuroscience* **7** (7):1577-1594.

Fowler, C. J., Wiberg, A., Oreland, L., Marcusson, J. and Winblad, B. (1980) *Journal of Neural Transmission* **49** (1-2):1-20.

Fowler, J. S., Logan, J., Wang, G. J. and Volkow, N. D. (2003) *Neurotoxicology* **24** (1):75-82.

Fowler, J. S., Volkow, N. D., Wang, G. J., Pappas, N., Logan, J., MacGregor, R., Alexoff, D., Shea, C., Schlyer, D., Wolf, A. P., Warner, D., Zezulkova, I. and Cilento, R. (1996) *Nature* **379** (6567):733-736.

Gaffney, B. J. and Mcconnel.Hm (1974) *Journal of Magnetic Resonance* **16** (1):1-28.

Galla, H. J. and Luisetti, J. (1980) *Biochimica Et Biophysica Acta* **596** (1):108-117.

Galla, H. J. and Sackmann, E. (1974) *Biochimica Et Biophysica Acta* **339** (1):103-115.

Gerlach, M., Youdim, M. B. H. and Riederer, P. (1996) *Neurology* **47** (6):S137-S145.

Ghisla, S. and Massey, V. (1989) *European Journal of Biochemistry* **181** (1):1-17.

Green, J. A., Singer, L. A. and Parks, J. H. (1973) *Journal of Chemical Physics* **58** (7):2690-2695.

Grimsby, J., Toth, M., Chen, K., Kumazawa, T., Klaidman, L., Adams, J. D., Karoum, F., Gal, J. and Shih, J. C. (1997) *Nature Genetics* **17** (2):206-210.

- Hammett, L. P. (1935) *Chemical Reviews* **17** (1):125-136.
- Hansch, C. and Leo, A. (1995). Exploring QSAR-fundamentals and applications in chemistry and biology. Washington DC, ACS
- Hartmann, C. and Klinman, J. P. (1991) *Biochemistry* **30** (18):4605-4611.
- Hauptmann, N. and Shih, J. C. (2001) *Life Sci* **68** (11):1231-1241.
- Heimburg, T. (2000) *Current Opinion in Colloid & Interface Science* **5** (3-4):224-231.
- Herraz, T. and Chaparro, C. (2005) *Biochemical and Biophysical Research Communications* **326** (2):378-386.
- Higgins, D. R. and Cregg, J. M. (1998) *Methods Mol Biol* **103** 1-15.
- Houslay, M. D., Tipton, K. F. and Youdim, M. B. H. (1976) *Life Sciences* **19** (4):467-477.
- Huang, C. H., Lai, W. L., Lee, M. H., Chen, C. J., Vasella, A., Tsai, Y. C. and Liaw, S. H. (2005) *Journal of Biological Chemistry* **280** (46):38831-38838.
- Huang, R. H. (1980) *Molecular Pharmacology* **17** (2):192-198.
- Huang, R. H. and Faulkner, R. (1980) *Molecular Pharmacology* **18** (2):267-273.
- Hubalek, F., Binda, C., Khalil, A., Li, M., Mattevi, A., Castagnoli, N. and Edmondson, D. E. (2005) *Journal of Biological Chemistry* **280** (16):15761-15766.
- Hubalek, F., Binda, C., Li, M., Herzig, Y., Sterling, J., Youdim, M. B. H., Mattevi, A. and Edmondson, D. E. (2004) *Journal of Medicinal Chemistry* **47** (7):1760-1766.
- Hubalek, F., Pohl, J. and Edmondson, D. E. (2003) *J Biol Chem* **278** (31):28612-28618.
- Husain, M., Edmondson, D. E. and Singer, T. P. (1982) *Biochemistry* **21** (3):595-600.
- Ibanez, L., Ballarin, E., Perez, E., Vidal, X., Capella, D. and Laporte, J. R. (2000) *European Journal of Clinical Pharmacology* **55** (10):761-764.
- Jahng, J. W., Houpt, T. A., Wessel, T. C., Chen, K., Shih, J. C. and Joh, T. H. (1997) *Synapse* **25** (1):30-36.
- Jones, T. A., Zou, J. Y., Cowan, S. W. and Kjeldgaard, M. (1991) *Acta Crystallographica Section A* **47** 110-119.
- Jost, P. C. (1980) *Drug and Alcohol Dependence* **6** (1-2):55-55.

- Khalil, A. A., Davies, B. and Castagnoli, N. (2006) *Bioorganic & Medicinal Chemistry* **14** (10):3392-3398.
- Khalil, A. A., Steyn, S. and Castagnoli, N., Jr. (2000) *Chem Res Toxicol* **13** (1):31-35.
- Kim, J. M., Bogdan, M. A. and Mariano, P. S. (1993) *Journal of the American Chemical Society* **115** (23):10591-10595.
- Kitahama, K., Denney, R. M., Maeda, T. and Jouvett, M. (1991) *Neuroscience* **44** (1):185-204.
- Klinman, J. P. and Matthews, R. G. (1985) *Journal of the American Chemical Society* **107** (4):1058-1060.
- Kobayashi, S., Takahara, K. and Kamijo, K. (1981) *Comparative Biochemistry and Physiology C-Pharmacology Toxicology & Endocrinology* **69** (2):179-183.
- Kochersperger, L. M., Parker, E. L., Siciliano, M., Darlington, G. J. and Denney, R. M. (1986) *Journal of Neuroscience Research* **16** (4):601-616.
- Lakowicz, J. R. (1983). Energy Transfer. Principles of fluorescence spectroscopy. Orton, C. G. New York, Plenum Press: 305-336.
- Lakowicz, J. R. (1983). Fluorescence Polarization. Principles of fluorescence spectroscopy. Orton, C. G. New York, Plenum Press: 112-150.
- Lakowicz, J. R. (1983). Quenching of Fluorescence. Principles of fluorescence spectroscopy. Orton, C. G. New York, Plenum Press: 258-295.
- Lee, A. G. (1977) *Trends in Biochemical Sciences* **2** (10):231-233.
- Leonhardt, H. and Weller, A. (1963) *Berichte Der Bunsen-Gesellschaft Fur Physikalische Chemie* **67** (8):791-795.
- Levitt, P., Pintar, J. E. and Breakefield, X. O. (1982) *Proceedings of the National Academy of Sciences of the United States of America-Biological Sciences* **79** (20):6385-6389.
- Li, M., Hubalek, F., Newton-Vinson, P. and Edmondson, D. E. (2002) *Protein Expr Purif* **24** (1):152-162.
- Ma, J., Yoshimura, M., Yamashita, E., Nakagawa, A., Ito, A. and Tsukihara, T. (2004) *J Mol Biol* **338** (1):103-114.
- Mak, I. T., Shrago, E. and Elson, C. E. (1983) *Biochimica Et Biophysica Acta* **722** (2):302-309.

Masinirepiso, A. M., Cabanillas, A. M., Andrada, M. C. and Coleoni, A. H. (1986) *Hormone and Metabolic Research* **18** (11):750-753.

Matsubara, K. (2000). N-Methyl- β -Carbolinium neurotoxins in Parkinson's disease. Neurotoxic factors in Parkinson's disease and related disorders. Storch, A. and Collins, M. A. New York, Kluwer Academic Publisher: 131-143.

May, T., Rommelspacher, H. and Pawlik, M. (1991) *Journal of Neurochemistry* **56** (2):490-499.

McEwen, C. M., Sasaki, G. and Jones, D. C. (1969) *Biochemistry* **8** (10):3952-3962.

McEwen, C. M., Sasaki, G. and Lenz, W. R. (1968) *Journal of Biological Chemistry* **243** (20):5217-5225.

Melnick, R. L., Haspel, H. C., Goldenberg, M., Greenbaum, L. M. and Weinstein, S. (1981) *Biophysical Journal* **34** (3):499-515.

Mewies, M., McIntire, W. S. and Scrutton, N. S. (1998) *Protein Science* **7** (1):7-20.

Miller, J. R. and Edmondson, D. E. (1999) *Biochemistry* **38** (41):13670-13683.

Mitoma, J. and Ito, A. (1992) *Journal of Biochemistry* **111** (1):20-24.

Muller, S., Sandal, T., Kamp-Hansen, P. and Dalboge, H. (1998) *Yeast* **14** (14):1267-1283.

Nagatsu, T. (1997) *Neuroscience Research* **29** (2):99-111.

Nagatsu, T. (2000). Isoquinoline neurotoxins. Neurotoxic factors in Parkinson's disease and related disorders. Storch, A. and Collins, M. A. New York, Kluwer Academic Publisher: 69-76.

Nagatsu, T. (2004) *Neurotoxicology* **25** (1-2):11-20.

Nakamura, S., Kawamata, T., Akiguchi, I., Kameyama, M., Nakamura, N. and Kimura, H. (1990) *Acta Neuropathologica* **80** (4):419-425.

Nandigama, R. K., Miller, J. R. and Edmondson, D. E. (2001) *Biochemistry* **40** (49):14839-14846.

Nandigama, R. K., Miller, J. R. and Edmondson, D. E. (2001) *Biochemistry* **40** (49):14839-14846.

Nandigama, R. K., Newton-Vinson, P. and Edmondson, D. E. (2002) *Biochem Pharmacol* **63** (5):865-869.

- Naoi, M., Maruyama, W., Dostert, P., Hashizume, Y., Nakahara, D., Takahashi, T. and Ota, M. (1996) *Brain Research* **709** (2):285-295.
- Navarrowelch, C. and Mccauley, R. B. (1982) *Journal of Biological Chemistry* **257** (22):3645-3649.
- Newton-Vinson, P., Hubalek, F. and Edmondson, D. E. (2000) *Protein Expr Purif* **20** (2):334-345.
- Nicotra, A. and Naccarato, M. (1982) *International Journal of Invertebrate Reproduction* **5** (2):101-105.
- Ocarroll, A. M., Fowler, C. J., Phillips, J. P., Tobbia, I. and Tipton, K. F. (1983) *Naunyn-Schmiedebergs Archives of Pharmacology* **322** (3):198-202.
- Pearce, L. B. and Roth, J. A. (1985) *Biochemistry* **24** (8):1821-1826.
- Pintar, J. E., Barbosa, J., Francke, U., Castiglione, C. M., Hawkins, M., Jr. and Breakefield, X. O. (1981) *J Neurosci* **1** (2):166-175.
- Pletscher, A. (1991) *Experientia* **47** (1):4-8.
- Quinn, P. J. (1990) *Biochemical Society Transactions* **18** (2):133-136.
- Ramsay, R. R. (1991) *Biochemistry* **30** (18):4624-4629.
- Rando, R. R. (1977) *Molecular Pharmacology* **13** (4):726-734.
- Rebrin, I., Geha, R. M., Chen, K. and Shih, J. C. (2001) *J Biol Chem* **276** (31):29499-29506.
- Riley, L. A., Waguespack, M. A. and Denney, R. M. (1989) *Molecular Pharmacology* **36** (1):54-60.
- Robinson, D. S. and Nies, A. (1980) *Schizophrenia Bulletin* **6** (2):298-307.
- Ryckaert, J. P., Ciccotti, G. and Berendsen, H. J. C. (1977) *Journal of Computational Physics* **23** (3):327-341.
- Salach, J. I. (1979) *Archives of Biochemistry and Biophysics* **192** (1):128-137.
- Salach, J. I. and Weyler, W. (1981) *Arch Biochem Biophys* **212** (1):147-153.
- Schreiermuccillo, S., Marsh, D. and Smith, I. C. P. (1976) *Archives of Biochemistry and Biophysics* **172** (1):1-11.

- Shih, J. C. and Chen, K. (2004) *Current Medicinal Chemistry* **11** (15):1995-2005.
- Shore, G. C., McBride, H. M., Millar, D. G., Steenaart, N. A. E. and Nguyen, M. (1995) *European Journal of Biochemistry* **227** (1-2):9-18.
- Silverman, R. B., Hoffman, S. J. and Catus, W. B. (1980) *Journal of the American Chemical Society* **102** (23):7126-7128.
- Stenstrom, A., Arai, Y. and Oreland, L. (1985) *Journal of Neural Transmission* **61** (1-2):105-113.
- Stryer, L. (1978) *Annual Review of Biochemistry* **47** 819-846.
- Sullivan, J. L., Stanfield, C. N., Schanberg, S. and Cavenar, J. (1978) *Archives of General Psychiatry* **35** (10):1209-1212.
- Swett, L. R., Everett, G. M., Gladish, Y. C., Taylor, J. D., Martin, W. B. and Wykes, A. A. (1963) *Annals of the New York Academy of Sciences* **107** (3):891-&.
- Van der Spoel, D., Lindahl, E., Hess, B., Groenhof, G., Mark, A. E. and Berendsen, H. J. C. (2005) *Journal of Computational Chemistry* **26** (16):1701-1718.
- Vitalis, T., Fouquet, C., Alvarez, C., Seif, I., Price, D., Gaspar, P. and Cases, O. (2002) *Journal of Comparative Neurology* **442** (4):331-347.
- Voges, K. P., Jung, G. and Sawyer, W. H. (1987) *Biochimica Et Biophysica Acta* **896** (1):64-76.
- Vorbeck, M. L., Martin, A. P., Long, J. W., Smith, J. M. and Orr, R. R. (1982) *Archives of Biochemistry and Biophysics* **217** (1):351-361.
- Walker, M. C. and Edmondson, D. E. (1994) *Biochemistry* **33** (23):7088-7098.
- Walker, W. H., Kearney, E. B., Seng, R. and Singer, T. P. (1971) *Biochem Biophys Res Commun* **44** (2):287-292.
- Wallace, A. C., Laskowski, R. A. and Thornton, J. M. (1995) *Protein Engineering* **8** (2):127-134.
- Weiss, S. and McCauley, R. (1979). Proceedings of the Fourth International Catecholamine Symposium. Usdin, E. and Barchas, J. New York, Pergamon Press: 198-202.
- Wessel, K. and Szelenyi, I. (1992) *Clinical Investigator* **70** (5):459-462.

- Westlund, K. N., Denney, R. M., Kochersperger, L. M., Rose, R. M. and Abell, C. W. (1985) *Science* **230** (4722):181-183.
- Weyler, W. (1989) *Biochem J* **260** (3):725-729.
- Weyler, W. (1994) *J Neural Transm Suppl* **41** 3-15.
- Weyler, W., Hsu, Y. P. and Breakefield, X. O. (1990) *Pharmacol Ther* **47** (3):391-417.
- Weyler, W. and Salach, J. I. (1985) *J Biol Chem* **260** (24):13199-13207.
- Weyler, W., Titlow, C. C. and Salach, J. I. (1990) *Biochem Biophys Res Commun* **173** (3):1205-1211.
- Yahr, M. D. (1993) *Acta Neurologica Scandinavica* **87** 22-25.
- Yguerabide, J. (1972) *Methods in Enzymology* **26** 498-578.
- Yue, K. T., Bhattacharyya, A. K., Zhelyaskov, V. R. and Edmondson, D. E. (1993) *Arch Biochem Biophys* **300** (1):178-185.
- Zachariasse, K. A., Vaz, W. L. C., Sotomayor, C. and Kuhnle, W. (1982) *Biochimica Et Biophysica Acta* **688** (2):323-332.
- Zhuang, Z., Hogan, M. and McCauley, R. (1988) *Febs Letters* **238** (1):185-190.
- Zhuang, Z. P., Marks, B. and McCauley, R. B. (1992) *Journal of Biological Chemistry* **267** (1):591-596.
- Zhuang, Z. P. and McCauley, R. (1989) *Journal of Biological Chemistry* **264** (25):14594-14596.